THE GEOLOGY AND GEOCHEMISTRY OF THE ROOI RAND DYKE SWARM

by

Deanna Lorrine Meth

Thesis submitted in fulfilment of the requirements
for the degree of Master of Science

Department of Geology and Applied Geology
University of Natal, Durban
South Africa

December 1996

This is to certify that this thesis has not been submitted to any other University, and that unless specifically acknowledged, the work in this thesis is my own original work.

D.L. Meth

ABSTRACT

The Jurassic Rooi Rand dolerite dyke swarm was emplaced sub-parallel to the Lebombo Monocline during the initial stages of Gondwana breakup. The dykes extend northwards from the southern Lebombo region in northern KwaZulu-Natal, into central Swaziland, spanning a distance of approximately 200 kilometres with a width between 10 and 22 kilometres. Detailed mapping of a 600m-long section on the Pongolo River, established at least eleven phases of intrusion. Each dyke age was systematically sampled and analysed for whole-rock major, trace and rare earth element composition, as well as mineral chemistry. Selected samples were analysed for stable isotopes.

In addition to notable intra-dyke chemical variations, there is also a high degree of inter-dyke mineralogical and geochemical variation, each dyke age bearing distinct geochemical characteristics. The apparent geochemical trend is not one of simple fractionation with time. Dyke chemistries are closely linked to magma genesis and magma volumes with time. Evolution of the magmas may be described in terms of varying degrees of partial melting and fractional crystallization, with a small degree of crustal contamination.

Major, trace and rare earth element data indicate a lithospheric mantle source for the majority of dyke phases, and an asthenospheric source for only two of the eleven ages. Contrary to this, isotopic data (oxygen and radiogenic) indicate an enriched asthenospheric source for all the dolerites. This suggests that all ages may have originally been derived from the asthenosphere, with the majority of ages being intruded into the lithospheric mantle to later undergo partial melting and fractional crystallization, with some contamination. Previous studies assumed an asthenospheric source with depleted MORB-like rare earth element profiles to be representative for the majority of Rooi Rand dolerites.

The Rooi Rand dolerites appear to display a geochemical link with the southern Sabie River Basalt Formation, as well as the Lebombo rhyolites. Magmatic evolution of the dykes was intimately linked to the initial rifting processes of lithospheric stretching and asthenospheric upwelling, which in this case concluded in a classic failed rift situation.

ACKNOWLEDGEMENTS

I wish to acknowledge and thank the following people:

The technical staff at the Department of Geology and Applied Geology, University of Natal, Durban, Department of Geology, University of Natal, Pietermaritzburg and the Department of Geological Sciences, University of Cape Town, for assistance in sample preparation and analysis.

Dick Rickard at the Department of Geological Sciences, University of Cape Town for assistance in the electron microprobe analytical unit.

Dave Cornell for the use of I.C.P.- M.S. analytical equipment at the University of Natal, Durban.

Anton Le Roex and Andy Duncan at the Department of Geological Sciences, University of Cape Town for hosting me in their Honours Igneous Petrology/Geochemistry module during 1992.

Chris Harris at the Department of Geological Sciences, University of Cape Town for stable isotope analyses of my samples.

Richard Armstrong for advice and encouragement during the initial stages of this project.

Everyone in the Department of Geology and Applied Geology, University of Natal, Durban for creating a friendly and supportive workplace.

The Foundation for Research and Development for two years of financial support.

My supervisor, Mike Watkeys for whom I have the utmost respect as a teacher, colleague and friend, for endless hours of patience and academic guidance.

My husband, Ron Uken, without whom none of this would have been possible.

Members of my family and extended family for their most loyal support and endless faith in me.

TABLE OF CONTENTS

CHAPTER 1

INTRODUCTION

Dolerite dykes of the Rooi Rand dyke swarm, which extends from northern Kwazulu-Natal northwards into Swaziland, were intruded during Jurassic times, in association with the initial stages of Gondwana breakup. The swarm has a K-Ar whole-rock age of 188 ± 5Ma (Cleverly, 1977).

The aim of this study is to document several intrusive ages of the Rooi Rand dyke swarm which were mapped in detail at one locality. Petrographical, mineralogical and geochemical characteristics are used in an attempt to establish a petrogenetic model for the evolution of the parent magmas, and the dyke swarm as a whole.

1.1 Previous Geological Work

Prior to this study, studies of the Rooi Rand dyke contacts and chill margins in the dyke swarm had revealed that there were at least four to six phases of intrusion (Armstrong, 1978; Saggerson *et al.*, 1983 and Meth, 1990). Phases were also distinguishable to a small degree on a petrographic basis.

The largest contribution of geological work on the Rooi Rand Dyke Swarm was made by Armstrong (1978). In his concluding remarks regarding the differentiation and emplacement of the Rooi Rand magmas, he states that:

> *"further studies of this subject should include detailed examination and sampling of recognizable phases of dolerite intrusion".*

This thesis is seen as an extension to that work, and seeks to carry out "detailed examination and sampling of recognizable phases" of the dolerites. Not only are phases recognizable however; in this study cross-cutting relationships enable the secular recognition of intrusive events. This provides a vital aid in the geochemical and

petrogenetic assessment of the swarm as a whole. In this regard, the advances since Armstrong's (1978) thesis are:

(1) A systematic method of mapping and sampling a densely intruded area of the swarm, which allowed for the establishment of the order of dyke intrusion, and correlation of whole-rock and mineral microprobe data from dyke to dyke.

(2) Extensive electron microprobe analysis of the constituent dolerite minerals from each age was undertaken, so that even small-scale variations in mineral compositions between intrusive ages could be noted.

(3) The determination of rare earth element values for the dyke ages sampled, in addition to major and trace elements. This has allowed for general comments on the nature and evolution of the Rooi Rand magmas with time, to be made. It has also allowed for the testing of petrogenetic models of fractional crystallisation and partial melting as possible mechanisms for the evolution of the Rooi Rand magmas. This information may be used to constrain models of lithospheric evolution for the area, thus permitting the re-examination of the role of the Rooi Rand dyke swarm in Gondwana break-up.

Detailed grid-scale mapping at the 600 by 40 metre outcrop locality was initially carried out by Watkeys *et al.* (1990), revealing at least 8 phases of dolerite intrusion. Later additional mapping (this study) revealed at least eleven phases of intrusion.

Following this, it was possible to petrographically identify the different dyke phases. In an effort to work out the exact sequence of intrusion events, Watkeys *et al.* (1990) established a dyke-by-dyke dilational history of the dykes, and this aided in correlating dyke ages between different sections of the study area. Exact correlation between separate domains of dykes was not always possible, and whole-rock geochemistry of the dykes provided the final necessary tool for the correlation of different intrusive ages where contact relationships were unavailable. This became especially important where dyke chill margins were obscured by sand and vegetation, and petrographic classification was unclear.

1.2 Sample and Data Collection

Samples for thin section and whole-rock geochemical analysis were taken of each dyke phase, using the detailed grid map compiled by Watkeys *et al.* (1990). Centre of dyke samples were collected for thin section and whole-rock analysis from all dyke phases. All chill margins were sampled for thin section analysis, but because of the difficulty of sampling the chill margins of the dykes, only 3 dyke phases gave material enough for whole-rock analysis.

Thin sections were made in the workshops at the Department of Geology and Applied Geology, of the University of Natal, Durban, and were then examined petrographically, and point-counted for modal analyses.

Electron microprobe sections of each dolerite phase (centre of dyke and chill margin) were also made in the Department of Geology and Applied Geology, at the University of Natal, Durban. Electron microprobe analyses of the main dolerite minerals, namely pyroxene, feldspar and opaques, with some accessory quartz and olivine, were done at the erstwhile Department of Geochemistry, of the University of Cape Town (see Appendix 2 for analytical methods).

Whole-rock major and trace element analyses of the samples were done using the X-Ray fluorescence technique by the Department of Geochemistry, of the University of Cape Town (see Appendix 3 for analytical methods). Samples were analysed for selected additional trace and rare earth elements using the ICP- MS facility in the Department of Geology and Applied Geology at the University of Natal, Durban.

CHAPTER 2

GEOLOGICAL SETTING

2.1 Regional Geological Setting

The Rooi Rand dyke swarm is aligned approximately north-south, being sub-parallel to the axis of the Lebombo "Monocline" (Figure 2.1), and varies from 10 to 22 km in width (Saggerson *et al.*, 1983).

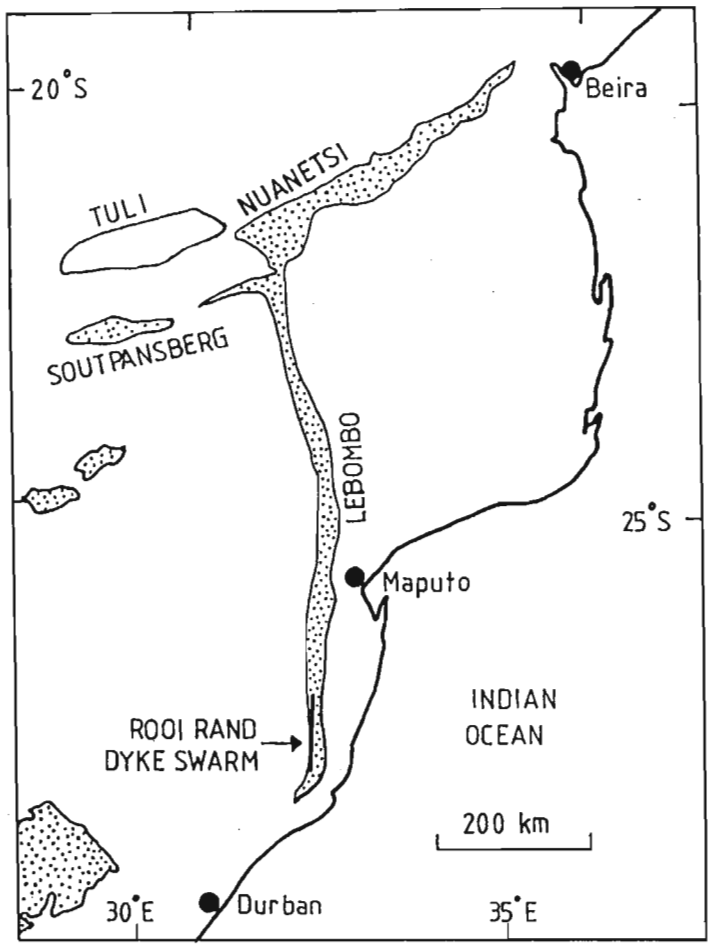

Figure 2.1 Simplified map showing the position of the Rooi Rand dyke swarm relative to other Karoo volcanics (stippled) (after Eales *et al.*, 1984).

The Lebombo represents a faulted monoclinal structure which developed at the western margin of a rift, preceding and eventually associated with the breakup of Gondwana (Armstrong, 1978; Bristow and Saggerson, 1983). From the earliest marine anomaly, the

separation of Antarctica from Africa has been placed at approximately 144 Ma (Martin and Hartnady, 1986). Prior to the 144 Ma break-up, the Karoo flood basalt province in Africa, and the Ferrar flood basalt province in Antarctica were generated (White and McKenzie, 1989). Faulting and tilting would have occurred mainly during the extrusion of the lower basalts, because the overlying rhyolites and upper volcanic rocks were not as strongly affected (Bristow and Saggerson, 1983).

The breakup of Gondwana and associated intrusion of the swarm was controlled by a zone of crustal weakness along the boundary between the stable Archaean Kaapvaal Craton to the west, and the mid to late Proterozoic Mozambique mobile belt to the east (Hunter and Reid, 1987; Saggerson *et al.*, 1983), coupled with tectonic control in the form of tensional east-west stresses (Bristow and Saggerson, 1983). The flood basalt/silicic magmatism/late-stage dyke swarm association seen in the Lebombo, is characteristic of many rift and thinned lithosphere environments (Marsh, 1987).

The swarm extends from northern KwaZulu-Natal into southern and central Swaziland, a length of approximately 200 kilometres. In the south, the dyke swarm intrudes sediments of the Karoo Sequence and the overlying basalts near the base of the Sabie River Basalt Formation (Figure 2.2). In the north in Swaziland however, the dykes intrude the central portion of the Sabie River Basalt Formation (Duncan *et al.*, 1990).

Although K-Ar-dated whole-rock samples from the swarm revealed an age of 188 $\pm$ 5 Ma (Cleverly, 1977), the exact age of the swarm is still uncertain. The main Karoo basalt activity was previously proposed as being episodic over a period of 40 to 50 Ma, starting at 190-195 Ma with a main phase of emplacement at about 175-180 Ma (Fitch and Miller, 1984). Recent $^{39}Ar/^{40}Ar$ age data obtained by Marsh *et al.* (in prep.) shows a far tighter cluster of ages for the majority of volcanic events around 180 Ma. In the same study, Marsh *et al.* conclude an age of ca 177 Ma for the Jozini Formation rhyolites. This is within error of the previous date of 179 $\pm$ 4 Ma obtained by Allsopp *et al.* (1984). Nowhere however, are the Rooi Rand dolerites seen in contact with the Jozini rhyolites.

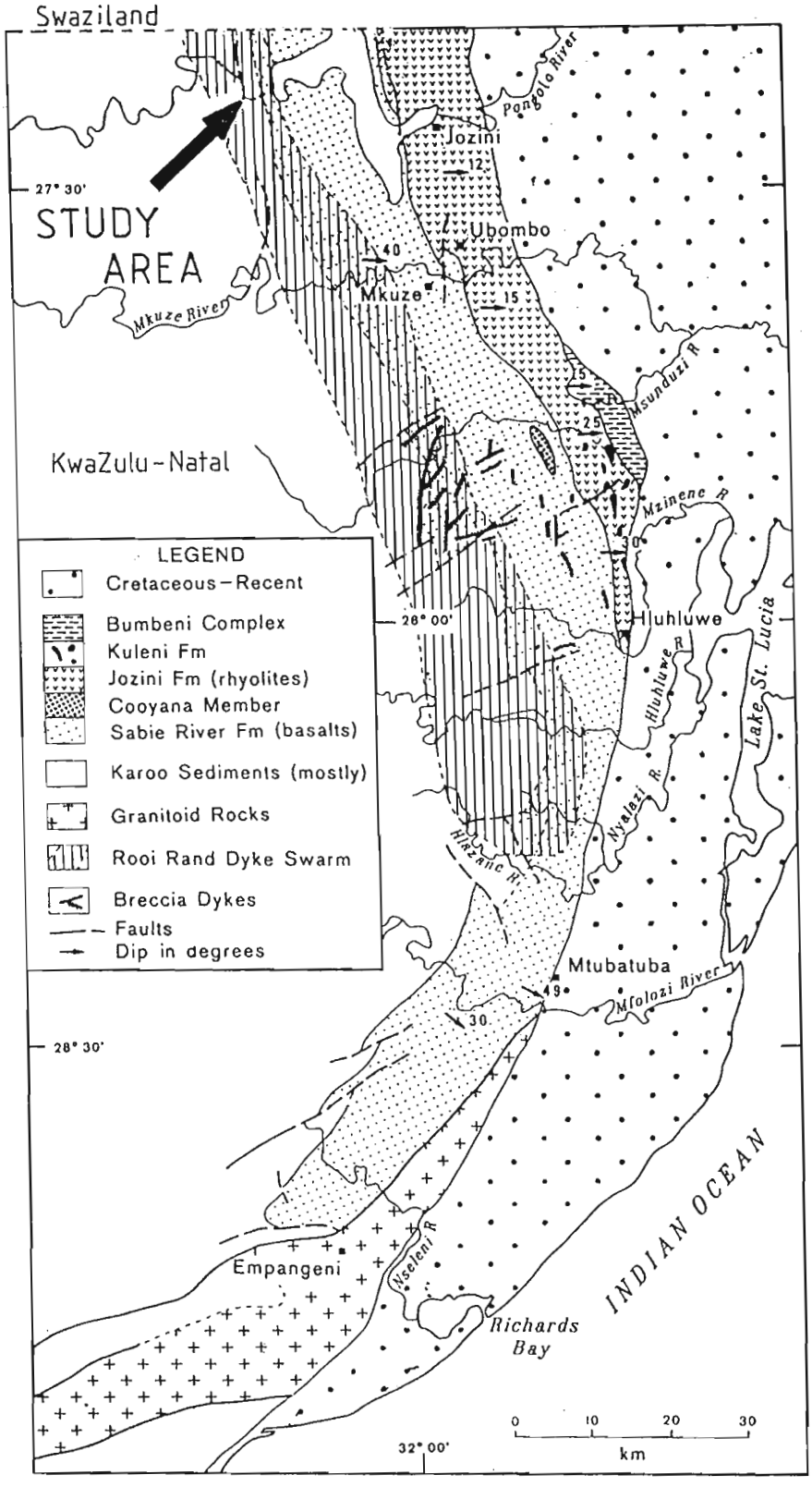

Figure 2.2 Geological Map of the southern Lebombo Region, showing the position of the Rooi Rand Dyke Swarm and study area (from Saggerson *et al.*, 1983).

2.2 Local Geological Setting

The study area lies in the southern portion of the swarm, on the northern bank of the west to east-flowing Pongolo River (Figure 2.2, Figure 2.3). Here the dykes intrude Beaufort Group shales and sandstones, and a Karoo dolerite sill.

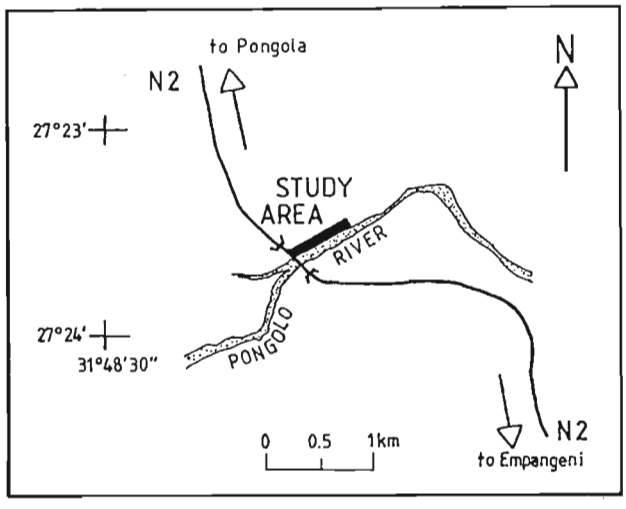

Figure 2.3 Locality Map showing the position of the study area.

Plate 2.1 and Figure 2.4 (overleaf) show the 600m-long by 40m-wide study area, where systematic geological mapping, data collection and sampling took place. The technique of mapping used, allowed for dykes as small as a centimetre wide to be accurately recorded.

Fine-grained or tachylitic chill zones at dyke margins and terminations were used to indicate relative dyke ages. Figure 2.4 is the complete (and updated) map from this study, and shows the 11 discernable dyke phases. At this locality, at least 8 separate intrusive phases were originally identified on the basis of field characteristics, four being porphyritic in texture, and the other four aphyric (Watkeys *et al.*, 1990). Saggerson *et al.* (1983) had previously identified five different types in the field at various localities (the aphyric varieties not being distinguished from one another), with at least six intrusive phases. No correlation was made between phases of intrusion and dolerite types however.

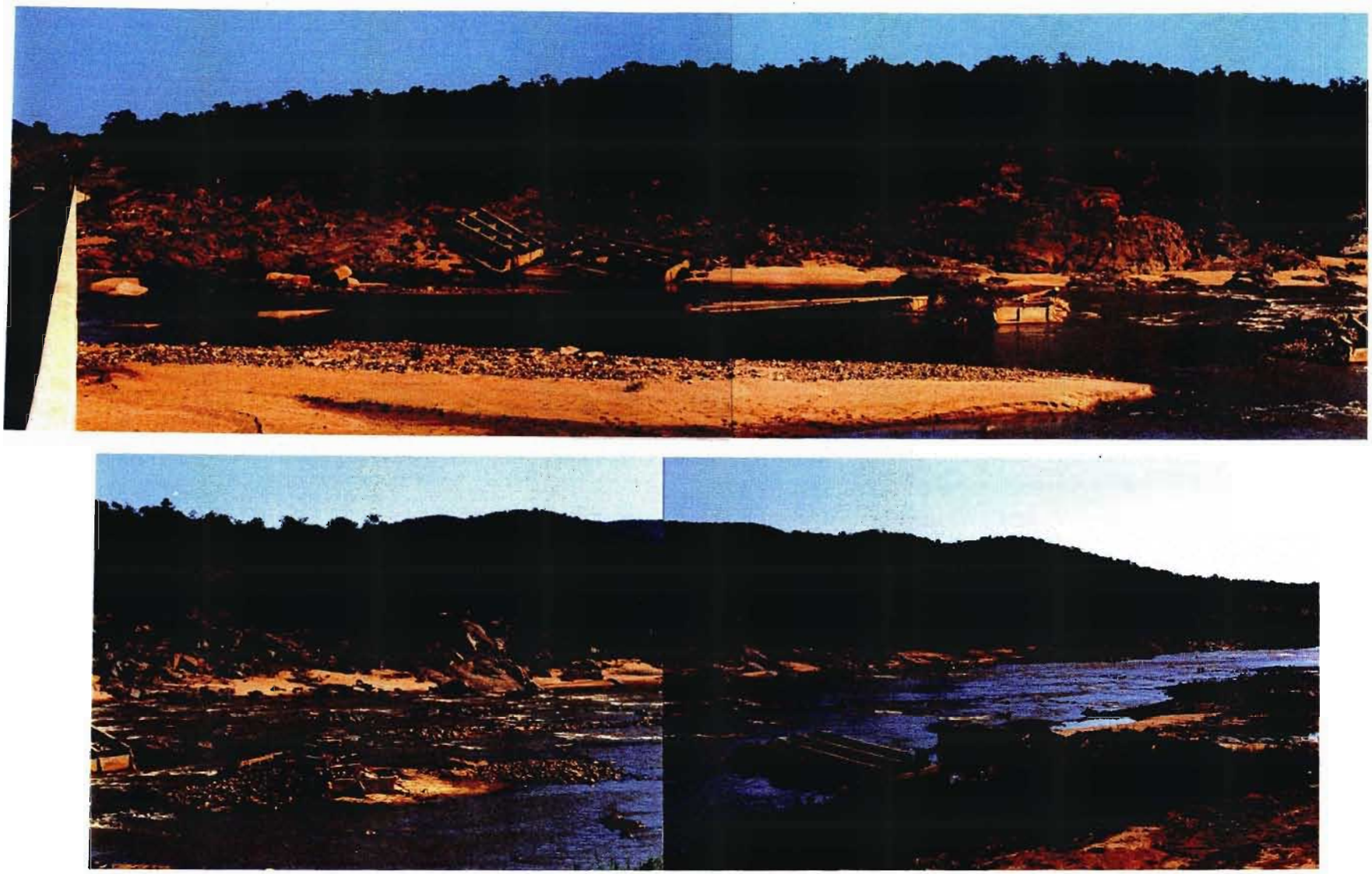

Plate 2.1 Series of photographs of the 600m-wide study area on the northern Pongolo River bank. (Taken facing north on the N2 bridge).

From re-mapping of chill margin relationships, and petrographic, geochemical and structural studies, 11 different intrusive phases were found to be present, each of which is characterised by a particular (and sometimes highly distinguishing) mineralogy and geochemistry. The intrusive phases have been named from H through to A, with H being the oldest phase of intrusion, and A being the youngest.

Dyke thicknesses vary locally from millimetre-scale up to 18.5 metres wide. Figure 2.5 shows the frequency of dyke widths (measured as "restored" dykes based on the dilational history), for 59 dykes at the outcrop locality seen detailed in Figure 2.4. The mean dyke width is 5.26 metres. Dykes with widths above 10 metres are not very common. Although the distribution appears unimodal, with narrow dykes less than 2.5 metres being far more frequent, most of these are only considered to be dykelets or local offshoots. There is a maximum frequency for dykes having widths between 7.5 and 9.9 metres. As may be noted from Figure 2.4, the dykes are clustered as separate "multiple" dykes, averaging about 30 metres in total width, and separated by country rocks of approximately the same width.

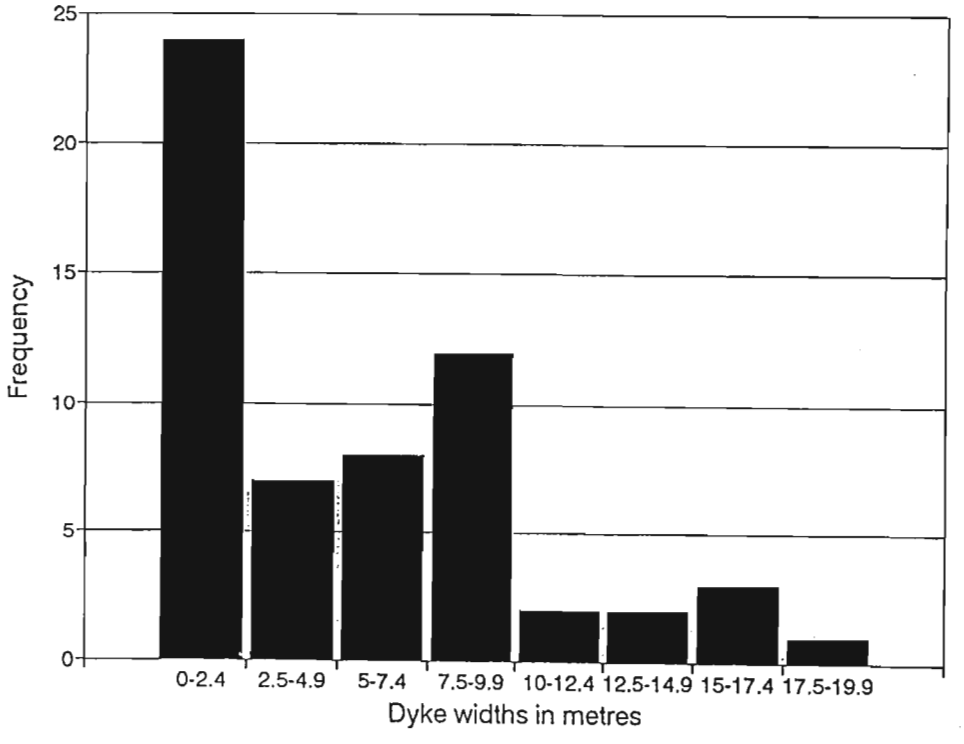

Figure 2.5 Histogram showing the frequency of dyke widths, in 2.5m classes (n=59).

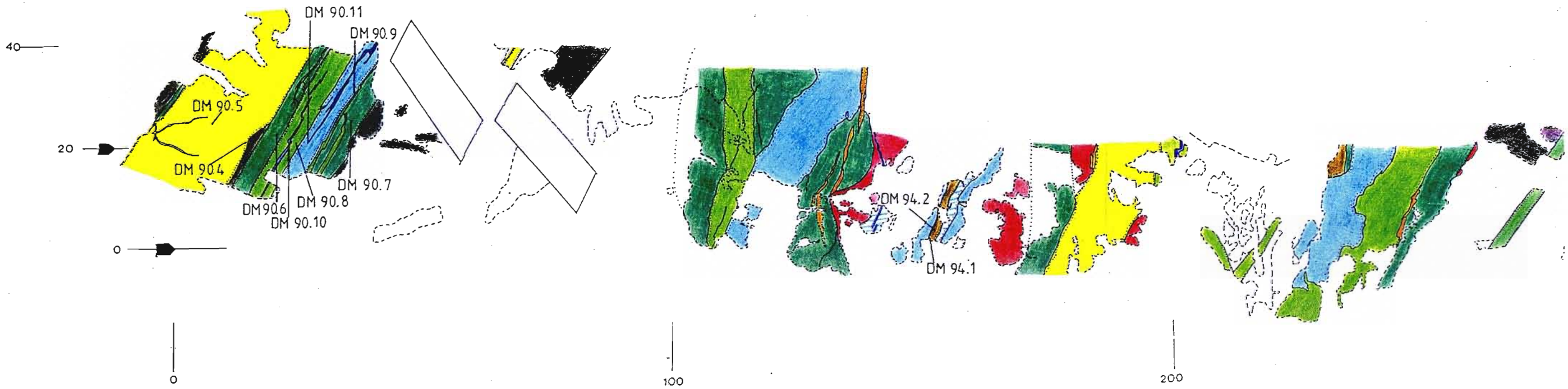

Figure 2.4 Detailed Map of the 600m-wide cross-section of the dykes (after Watkeys *et al.*, 1990). DM **.* are the numbers and positions of samples taken.

From re-mapping of chill margin relationships, and petrographic, geochemical and structural studies, 11 different intrusive phases were found to be present, each of which is characterised by a particular (and sometimes highly distinguishing) mineralogy and geochemistry. The intrusive phases have been named from H through to A, with H being the oldest phase of intrusion, and A being the youngest.

Dyke thicknesses vary locally from millimetre-scale up to 18.5 metres wide. Figure 2.5 shows the frequency of dyke widths (measured as "restored" dykes based on the dilational history), for 59 dykes at the outcrop locality seen detailed in Figure 2.4. The mean dyke width is 5.26 metres. Dykes with widths above 10 metres are not very common. Although the distribution appears unimodal, with narrow dykes less than 2.5 metres being far more frequent, most of these are only considered to be dykelets or local offshoots. There is a maximum frequency for dykes having widths between 7.5 and 9.9 metres. As may be noted from Figure 2.4, the dykes are clustered as separate "multiple" dykes, averaging about 30 metres in total width, and separated by country rocks of approximately the same width.

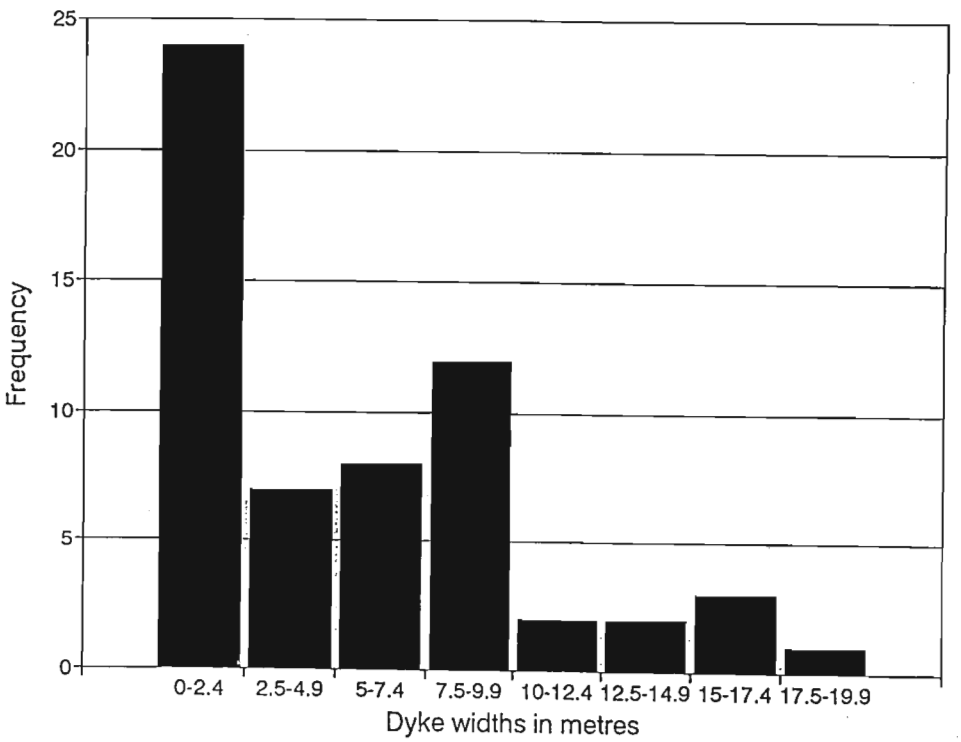

Figure 2.5 Histogram showing the frequency of dyke widths, in 2.5m classes (n=59).

Saggerson *et al.* (1983) noted that the thickest dykes are restricted to the central portion of the swarm, between the Msunduzi and Pongolo rivers. It is here also, that the greatest intensity of dykes may be found.

Locally, the dykes strike approximately north-south (Plate 2.2), with a mean strike value of 357°, having fairly steep dips, with a mean dip of 73.5 degrees to the west (Figure 2.6). Although there is some variation in dip and strike, both measurements display strongly unimodal distributions. Figures 2.7a and 2.7b show the frequencies of dip and strike measurements for the dykes.

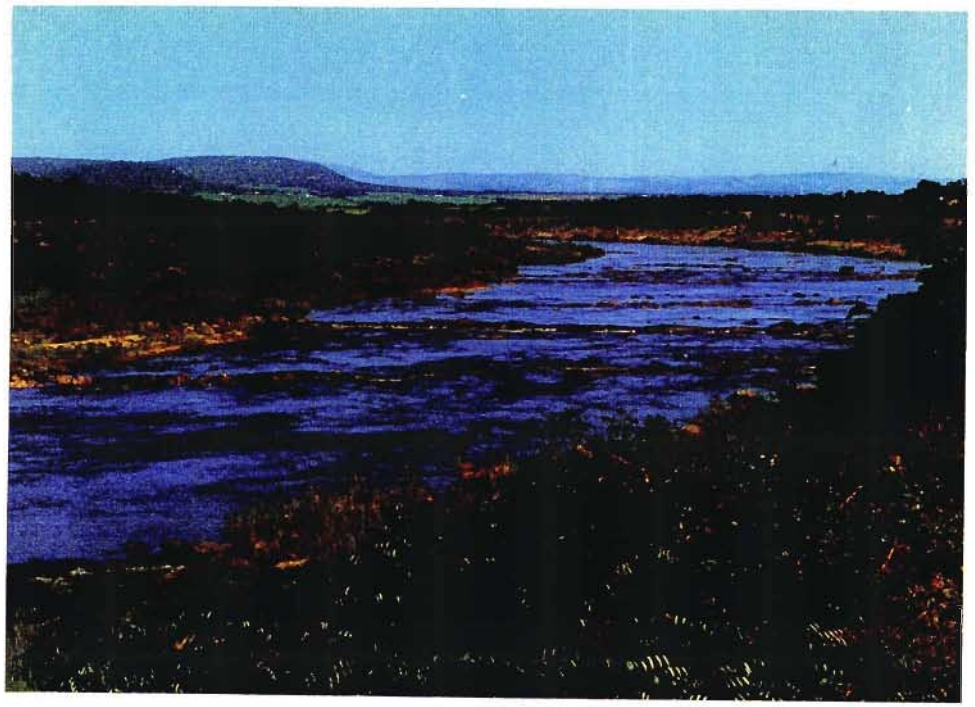

Plate 2.2 Photograph taken looking westwards along the Pongolo River, approximately 5km upstream of the study area. Note the prominent north-south parallel ridges formed by the dolerite dykes.

Armstrong *et al.* (1984) noted a far narrower range of dyke dips, from 65° to 75°, but on a local scale at the study area, dips vary from 90° to an unusually shallow 35°.

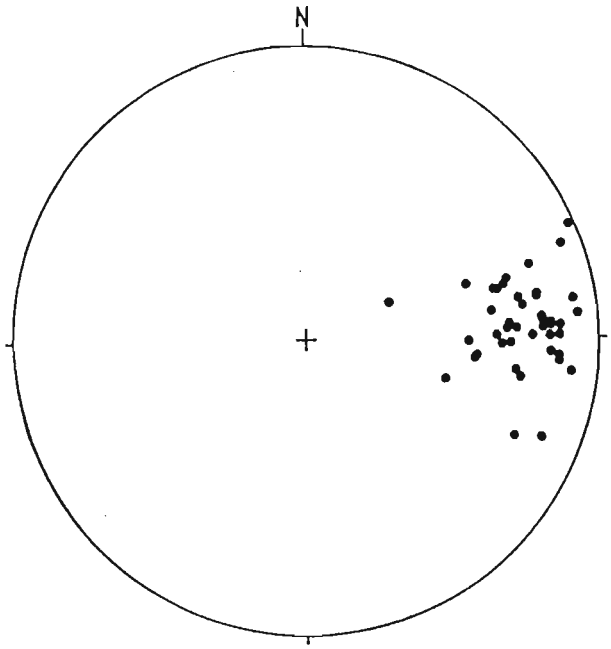

Figure 2.6 Lower hemisphere equal angle stereonet showing the orientations and dips of the dykes (n=47).

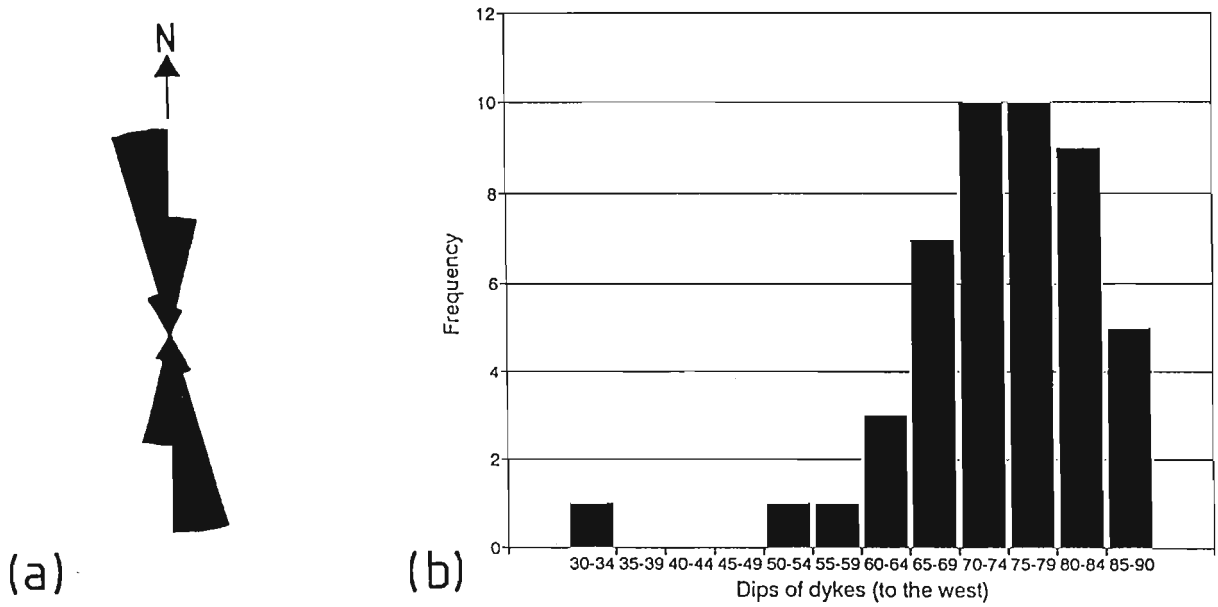

Figure 2.7 **(a)** Rose diagram showing dyke strike orientations, using frequency of angles in 15° classes (n=47) **(b)** Histogram showing the frequency of dips of dykes, using 5° classes (n=47).

Locally, bedding plane dips of the host sediments vary from 27° to 30° to the east. The steep westerly dips of the dykes are thus approximately perpendicular to the sediments, and thus dyke intrusion took place pre-monocline development. This relationship has also been noted regionally by Saggerson *et al.* (1983) using Bristow's (1977) average dip measurements for the basalt flows and basalt-sediment contact.

Gautneb and Gudmundsson (1992) mention that dips which deviate from the vertical are normal for dykes swarms of this nature, where subsequent tilting of the rocks, normally around the magnitude of 10° has taken place.

The dykes are mainly regular with linear margins, but are also irregular in places, swelling and pinching out, or splitting into several veins. Smaller later crosscutting east-west orientated dykes at ninety degrees to the dominant north-south strike, often appear to occupy zones of fracturing or jointing (Plate 2.3).

Plate 2.3 Photograph taken at the study area, showing a narrow dolerite dyke intruding a wider, older dolerite, and exploiting a zone of weakness along a small fault plane (old 5c coin for scale - 17mm diameter).

Locally, the effects of dyke intrusion on the country rocks are mainly mechanical, with igneous and sedimentary host rocks not displaying any evidence of metamorphism. Mechanical effects are noted in the presence of stoped-off material (blocks of wallrock detached and engulfed by the new magma), and in some cases extensive shattering of the host rock.

Stoped-off material is seen on a macro- and micro-scale. In the field, large blocks as big as 30 centimetres have been stoped off into the younger dolerites (Plate 2.4), and in thin section, clumps of crystals are seen "stoped-off" from the older dolerites into the fine-grained chill margin of the younger dolerite (Plate 2.5).

This stoping-off of fragments has been interpreted by Rogers and Bird (1987) as a case where two offset dyke terminations have coalesced, trapping the country rock fragment between them.

The injection, reinjection and propagation of dykes is highly dependent on liquid magma and country rock characteristics. Multiple injections may often occur, and dykes at the Pongolo River locality are often seen splitting into one or more branches. Dykes may be injected into pre-existing joints and fractures (as seen in Plate 2.3), but may also be injected into unfractured rock, fracturing it by the injection (Turcotte *et al.*, 1987). This is termed active, dilatational emplacement (Park, 1983).

The shape of dyke formed will be highly dependent on the elastic deformation of the country rock. The distribution of the intrusions will depend on the value of the boundary stresses around the magma chamber, and the form of the intrusion will depend upon the orientation of the principal stress trajectories around the magma chamber (Roberts, 1970). Ideally, the intrusion plane of dyke emplacement will be perpendicular to σ_3, the minimum compressive stress or direction of maximum extension (Figure 2.8).

Plate 2.4 Photograph taken at the study area showing the intrusion of a narrow dyke into an older more coarse-grained dolerite. Note that the contact is clear, but not straight. A xenolith of older dolerite has been stoped off into the younger dolerite. Note also the fine-grained chill margin, seen as a dark grey zone along the dyke margins (shaft of north arrow 10cm long).

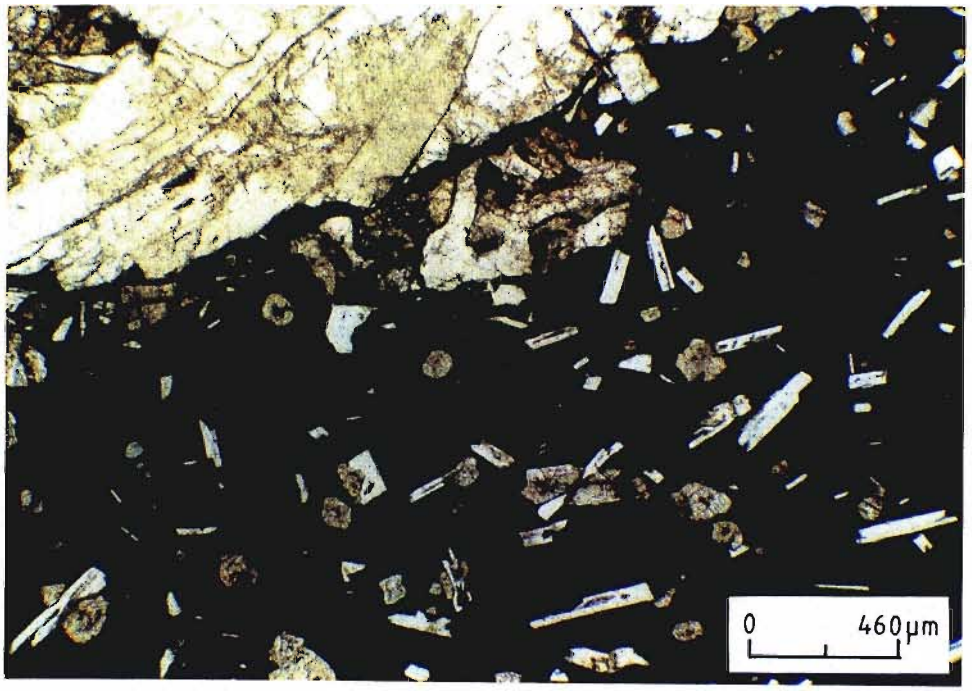

Plate 2.5 Photomicrograph showing a chill margin contact between two dolerite dykes at the study area. Note the stoped-off aggregate of coarser-grained minerals from the older dolerite, which were included as the younger one intruded (magnification = 160; plane-polarised light).

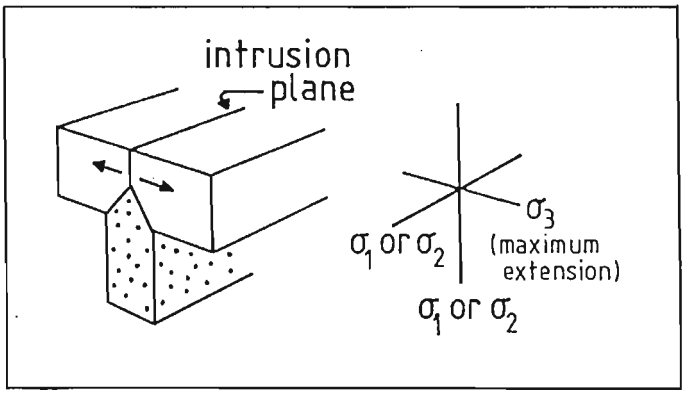

Figure 2.8 Sketch depicting the ideal stress field present during dyke emplacement (after Pollard, 1987).

When intruded into pre-existing crack systems, dyke geometries will vary according to the geometries of the cracks into which they are intruded. Factors such as whether the en echelon fracture system is overlapping or not, and whether the actual fracture propagation path is straight or curved, play a large role. Nicholson and Pollard (1985) describe two end member situations. The first is for cracks which grow along straight propagation paths, and link by the concentration of strain in the bridge of rock between them (Figure 2.9a). Further crack development produces increased dilation, and the formation of a bent bridge. The other situation is for cracks having curved propagation paths, where the fractures link by propagating into the inside edge of the adjacent fracture, which once with further dilation, produces unstrained rotated bridges (Figure 2.9b).

A more detailed examination of the mechanical development of en echelon dykes and multiple offshoots seen at the study area, has been carried out by Kattenhorn and Watkeys (1995). This includes a thorough study of blunt-ended dyke segments observed at the Pongolo River locality.

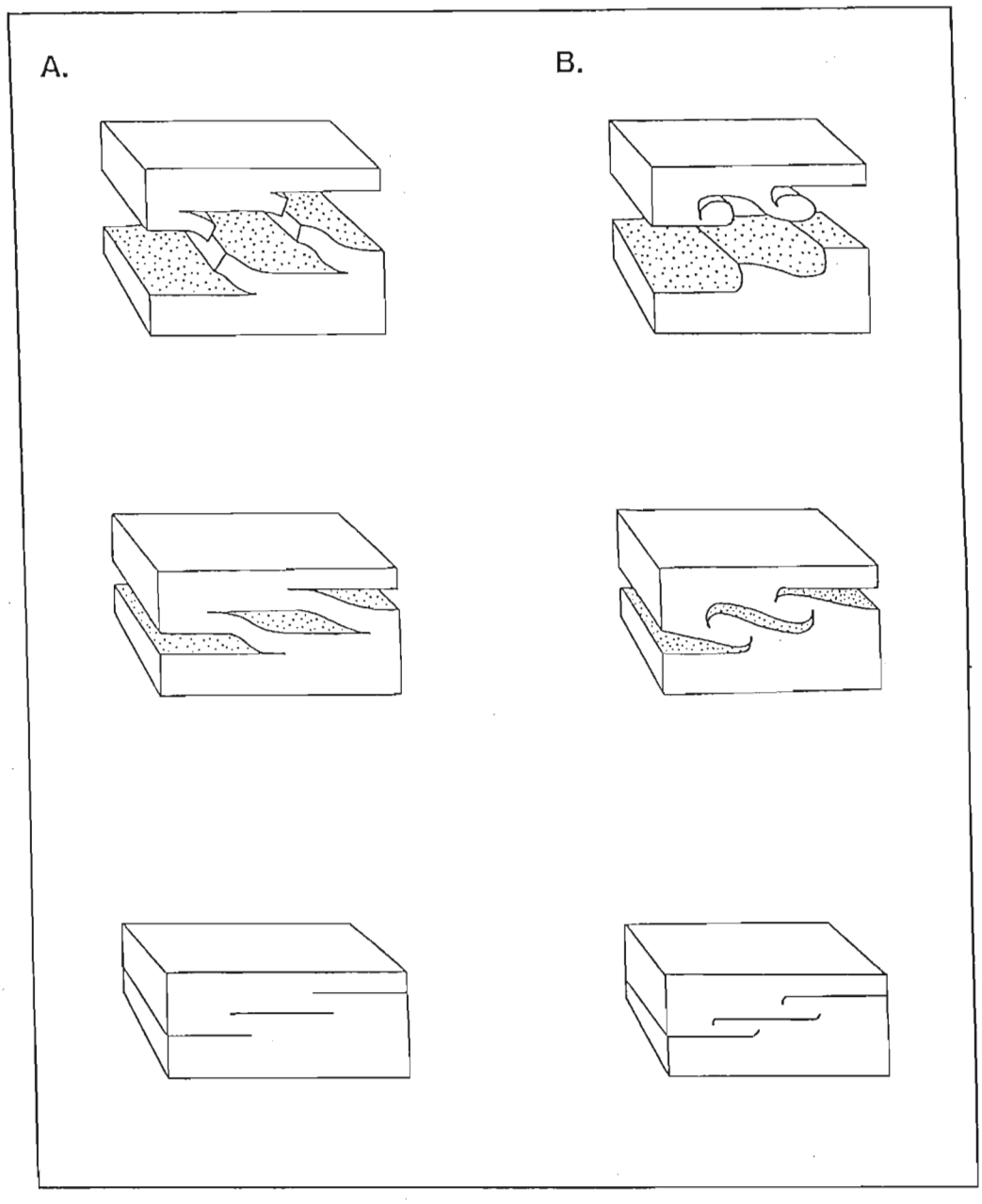

Figure 2.9 Schematic end-member dilation and linkage histories for en echelon cracks which grow along (a) straight propagation paths, and (b) curved propagation paths (from Kattenhorn, 1994; after Nicholson and Pollard, 1985).

Dykes observed at the Pongolo River locality generally show dilation and linkage histories which lie between the two end-member situations put forward by Nicholson and Pollard (1985). The following two examples (Plates 2.6 and 2.7), show dykes from the study area, together with a basic interpretation as to the opening stages of the fractures.

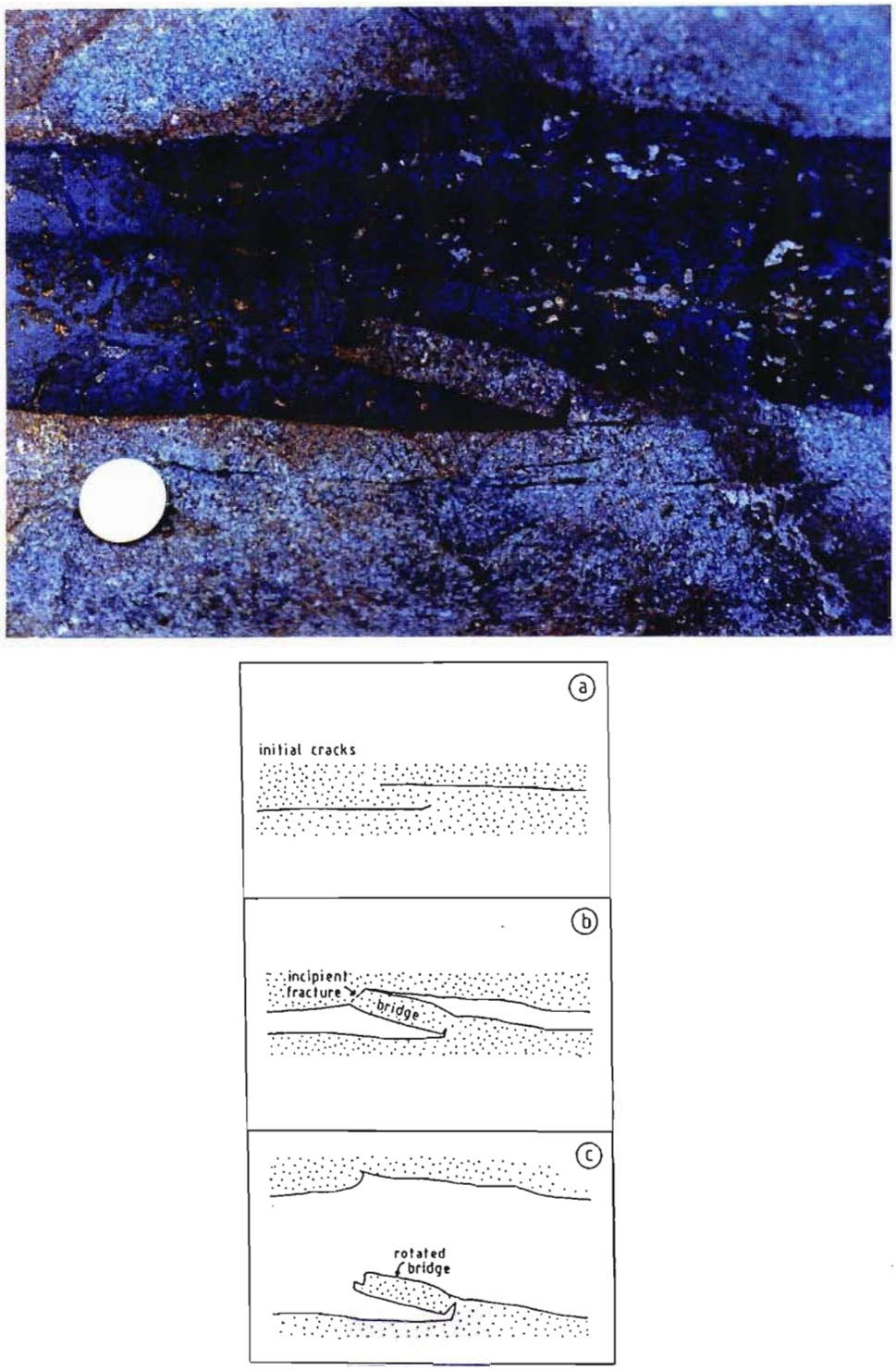

Plate 2.6 Photograph taken at the study area of a fine-grained dolerite dyke, with large plagioclase phenocrysts which has intruded a coarser-grained dolerite. "Bites" out of the dyke and corresponding offset patterns at the chill margin, are as a result of the mechanical interaction of the two dyke segments (old 5c coin scale - 17mm diameter). The adjacent sketch shows an interpretation of the opening stages. a - initial cracks, left-stepping, overstepping straight fractures; b - first stage of intrusion with formation of incipient fracture and development of a bridge; c - as seen in the photograph, matching walls, with a rotated bridge which is very close to being a xenolith.

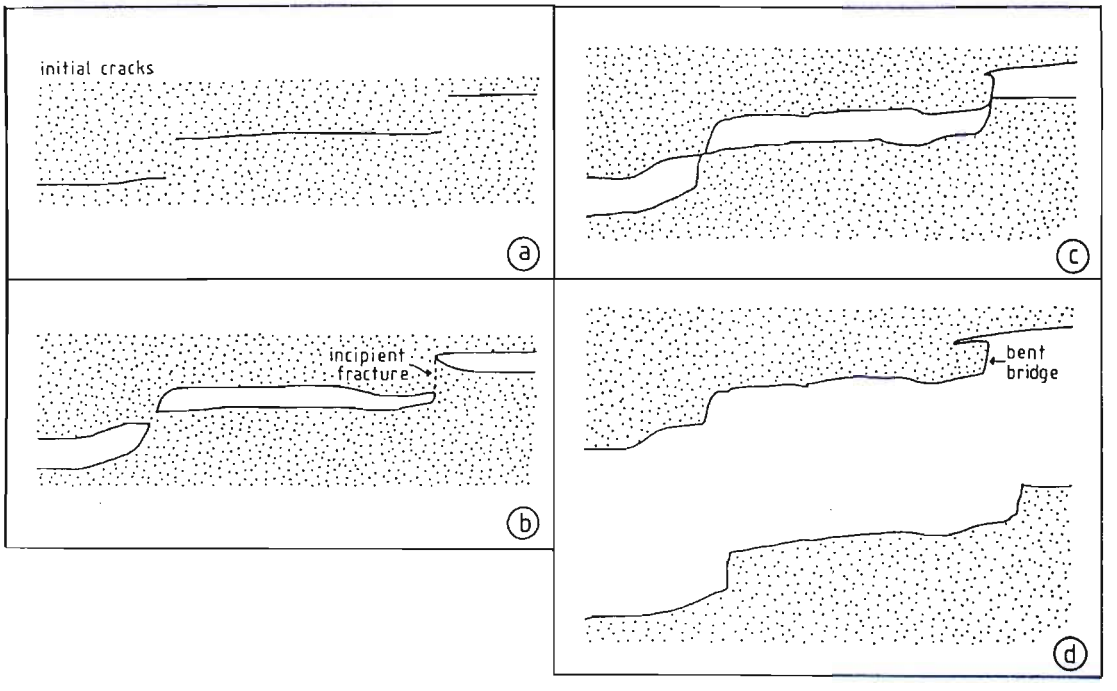

Plate 2.7 Photograph taken at the study area of a fine-grained dolerite dyke intruding a coarser-grained dyke. Note the step-like offsets, and bayonet-shaped horns protruding into the older dolerite dyke. Below is an interpretation of the schematic opening stages of the dyke. a - initial cracks, left-stepping, marginally or not overstepping straight fractures; b - first stage of intrusion, with incipient fracture development; c - further opening; d - matching walls as seen in the photograph, with a bent bridge. Shaft of north arrow 10cm in length.

2.3 General Tectonic Setting

Saggerson *et al.* (1983) are of the opinion that a period of major crustal extension and fracturing took place during the later stages and after emplacement of the Lebombo basalts. During this period, the Rooi Rand dykes were intruded linearly along the zone of fracturing, and parallel to the zone of crustal tension (Du Toit, 1929). This was followed by further rifting, crustal dilation and faulting.

Saggerson *et al.* (1983) give an average estimate of 40% crustal dilation over the whole swarm. The total width of dyke cover over the 600 metre section studied, is 310 metres, suggesting local extension of almost 52%. The intrusion volumes are however, not distributed evenly over the 11 dyke ages.

Figure 2.10 shows the distribution of total dyke widths, and thus indirectly the distribution of magma volumes for these 11 ages, as noted in the field. The observed trend of 3 main magma peaks with time will be commented upon together with geochemical and structural models in later chapters.

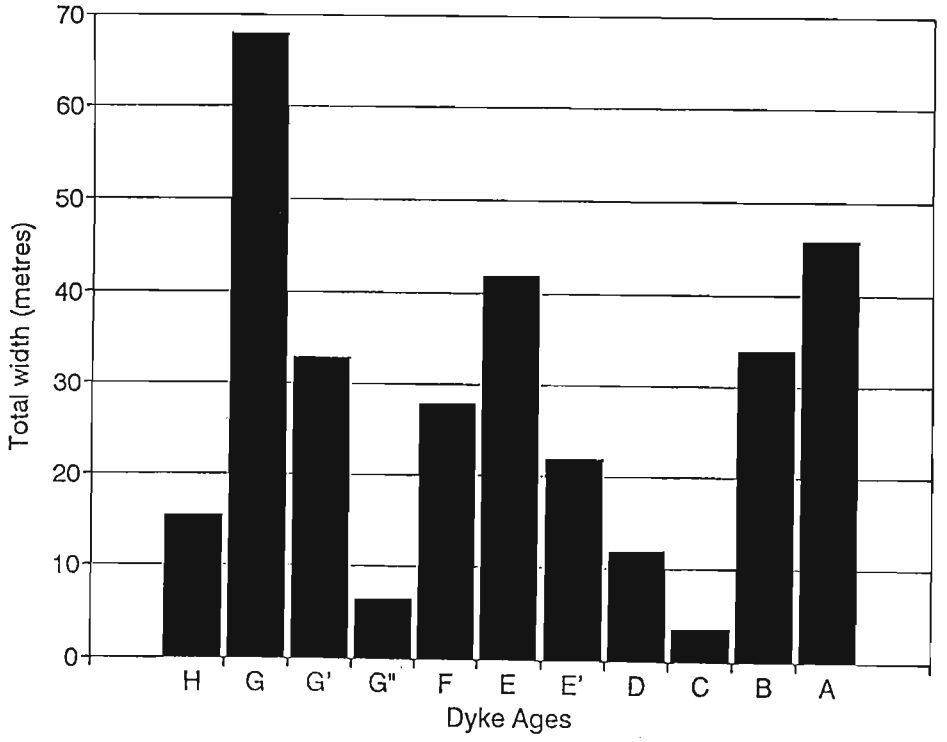

Figure 2.10 Distribution of total dyke widths, and thus relative magma volumes through the eleven dyke ages (H - the oldest, and A - the youngest dyke phase).

Field mapping by Du Toit (1929), Bristow (1977), and Armstrong (1978) showed that the highest dyke density is associated with the steep limb of the Lebombo monoclinal flexure (Saggerson *et al.*, 1983; Hunter and Reid, 1987). Saggerson *et al.* (1983) state that this region of greatest intensity of intrusion occurs at the centre of the swarm in the region of the basalt-sediment contact.

The fact that the dykes represent multiple intrusions, are approximately perpendicular to associated sediments and basalts, and have fairly consistent steep dips to the west is important. Dyke orientation led Du Toit (1929) and later Hunter and Reid (1987), to conclude that the dykes were intruded prior to monoclinal warping. Mohr (1971) studying the Ethiopian Tertiary dyke swarms and associated monoclinal warping, also concluded that perpendicularity between the dykes, and lavas and sediments indicates intrusion prior to warping.

Saggerson *et al.* (1983) state that the basalts, sediments and associated dykes would have undergone tilting, producing the easterly dip, and enhancing the westerly dip of the dykes during the final stages of rifting, crustal dilation and faulting. Karson (1987) comments that dykes and other related extensional structures in these environments are often assumed to be rift-parallel with vertical orientation, but notes that although most dykes probably conform to this, many deviations from this geometry have been noted. They may be the result of initial formation in some other orientation (i.e. not ridge-parallel or vertical), or may be due to post-formation tectonic rotation.

Saggerson *et al.* (1983) and Hunter and Reid (1987) point out that the presence of some near-vertical dykes indicates their post-warping age, and that dykes may also have been intruded during and after warping.

If this is so, a progressive change of dip with relative age of dyke (time) should be noted at the study area. Du Toit (1929) had previously used dyke attitude as conclusive evidence for certain dykes being younger than others in age, because of their "near vertical attitude". In this study there is no correlation between dip and age over the majority of the 600m section. Many dykes which are earlier phases show dips close to

vertical. Only in one small segment, that from 500 to 600 metres, showed a fairly consistent change of dip with age, age B (the youngest) having an average dip of 84°, age E′ one of 81°, age E - 67°, age G′- 62°, and age G one of 60°. These average dips come from widely varying dip values, and it is not thought that any conclusion can or should be made based on this small section, when the others do not provide the same results. No conclusion can thus be reached regarding the timing of dyke intrusion relative to warping.

CHAPTER 3

PETROGRAPHY AND MINERALOGY

3.1 Introduction

3.1.1 *Petrography*

Thin section analysis of the Rooi Rand dolerites reveals the uniform mineral assemblage with augite, plagioclase feldspar (mainly labradorite), and opaque minerals which are predominantly ilmenite and titanomagnetite (Table 3.1; Appendix 1). In some of the dyke phases, olivine or quartz is present in addition to this assemblage.

Table 3.1 Summary of the main mineral assemblages of each centre of dyke age (Appendix 1), and their relative modal percentages (Accessory minerals not included). plag=plagioclase feldspar (generally labradorite); cpx=clinopyroxene (generally augite); ol=olivine; qtz=quartz

RELATIVE AGE	SAMPLE NUMBER	MAJOR MINERALS PRESENT	MODAL %
A (youngest)	DM90.5	plag, cpx, opaques	47 : 46.3 : 5.1
B	DM90.18	plag, cpx, opaques, qtz	50 : 40.2 : 6.6 : 1.2
C	DM94.2	plag, cpx, opaques	45.4 : 43.7 : 8.9
D	DM90.10	plag, cpx, opaques	44.4 : 45.2 : 7.7
E′	DM94.3	plag, cpx, opaques, ol	50 : 42.3 : 3.3 : 2.8
E	DM90.20	plag, cpx, opaques, ol	51.5 : 38.7 : 3.5 : 5.1
F	DM90.27	plag, cpx, opaques, qtz	48 : 42.4 : 7.5 : 0.5
G″	DM90.8	plag, cpx, opaques	42 : 49.1 : 7.2
G′	DM90.25	plag, cpx, opaques	46.1 : 43.4 : 8.2
G	DM90.7	plag, cpx, opaques	50.2 : 40.1 : 7
H (oldest)	DM90.30	plag, cpx, opaques, (ol)	46.3 : 42.3 : 9.4 : 0

Although no pigeonite was identified petrographically, it was observed in small amounts from electron microprobe analyses. Minor pyrite and chalcopyrite were noted in some dyke phases. Accessory minerals include apatite and biotite, with chlorite, biotite and sericite present as alteration products of the constituent dolerite minerals.

In order to determine modal proportions of minerals, point counting was undertaken, counting 2000 points per slide (Table 3.1; Figure 3.1). Only the centre of dyke samples of each age were counted. These are the same samples (except for C and E′) which have been used throughout the project, for petrographic, whole-rock, major, trace and rare earth element analyses.

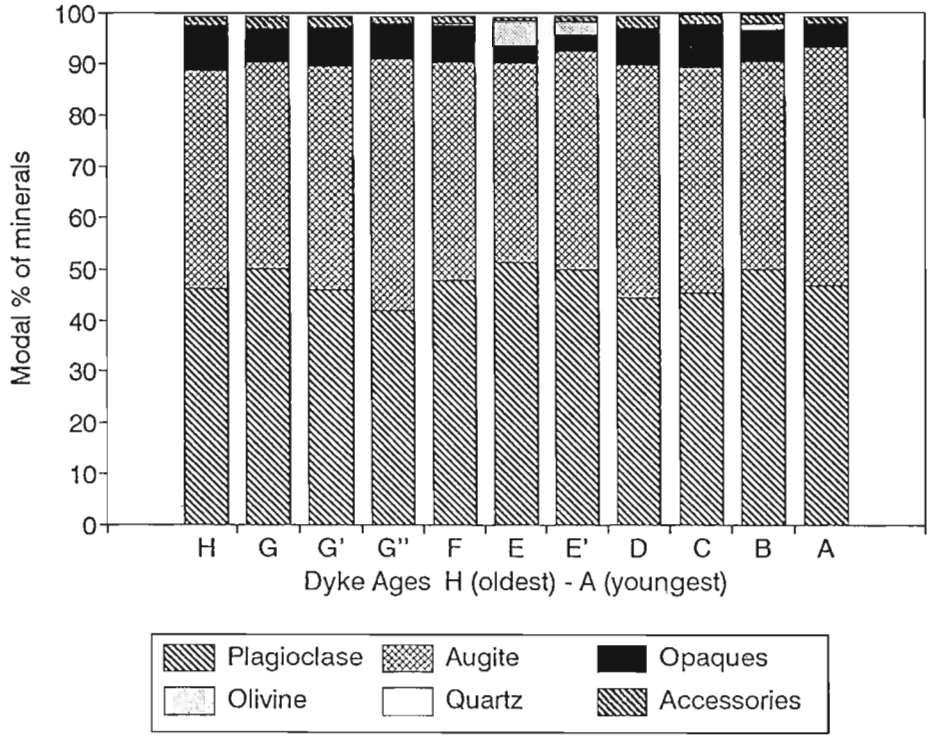

Figure 3.1 Stacked Bar Graph showing the point counting results of the 11 relative ages of Rooi Rand dolerites studied. Note: Accessories include unidentified alteration products and minor minerals. The alteration products of olivine, augite and plagioclase feldspars have been counted as the original minerals.

Grain size and textural variation from one dyke generation to another is noticeable. The dolerites vary from fine- to coarse-grained, and even-grained to porphyritic or glomeroporphyritic (Plate 3.1; Plate 3.2). Where phenocrysts are present, they are most often plagioclase feldspars, occasionally together with augite or olivine (if present). Groundmass plagioclase laths often bear subophitic to ophitic relationships to the pyroxene crystals. Quartz only occurs as anhedral blebs filling the spaces between the crystals.

When considering the order of crystallization, phenocryst phases, in most cases plagioclase feldspar (and occasionally olivine) would have crystallized first. As an interpretation of

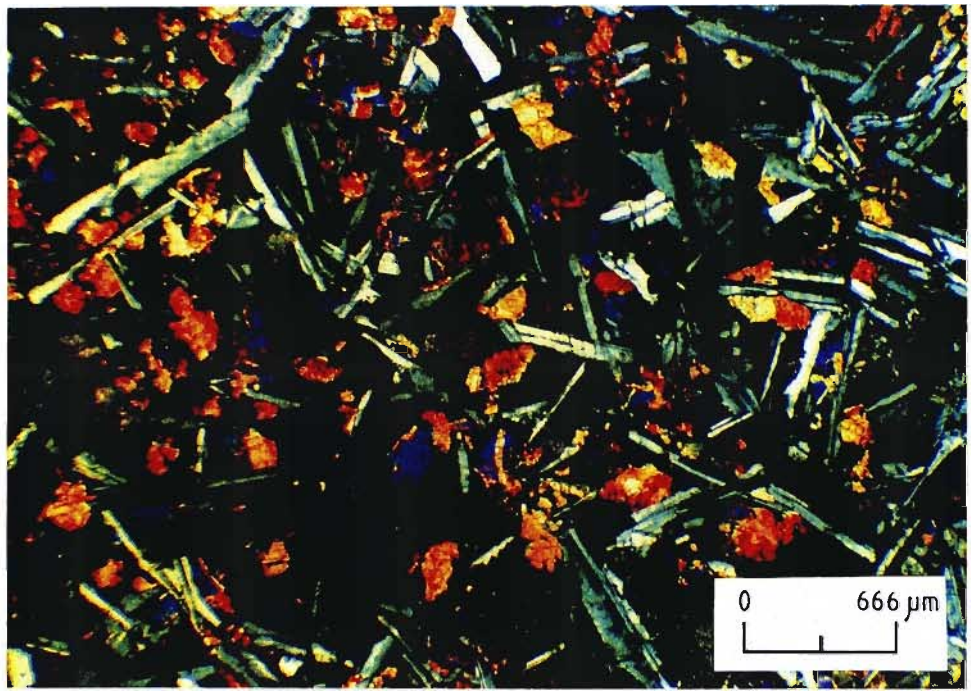

Plate 3.1 Photomicrograph of DM90.8 (Age G″) showing the overall even-grained texture of the dolerite (magnification = 30; cross-polarised light).

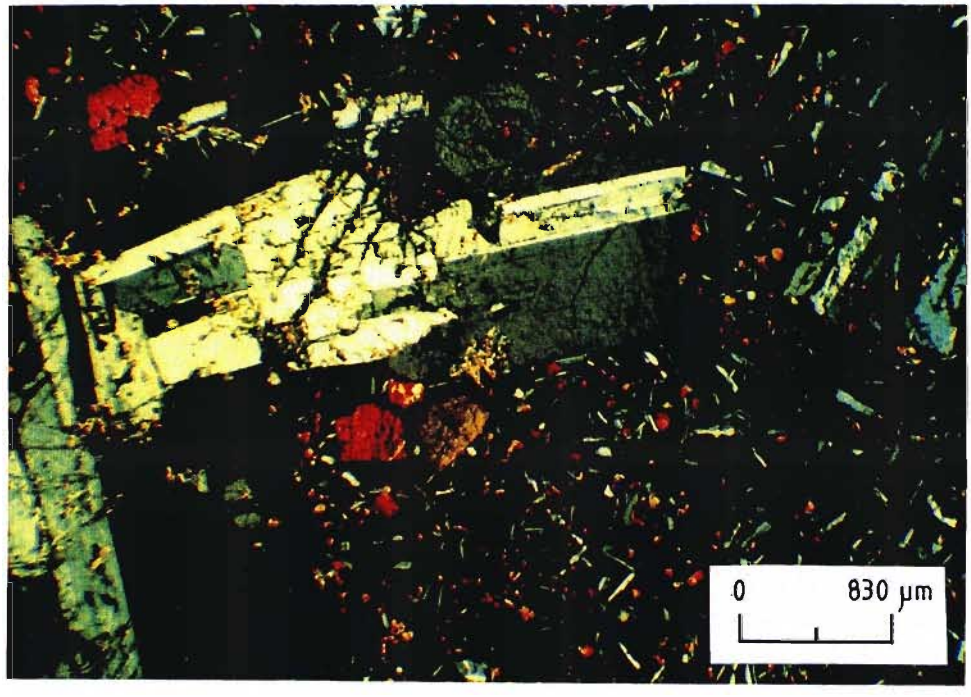

Plate 3.2 Photomicrograph of DM90.10 (Age D), showing glomeroporphyritic aggregates of plagioclase feldspar and augite phenocrysts in a finer-grained groundmass (magnification = 24; cross-polarised light).

the subophitic to ophitic texture between groundmass plagioclase and pyroxene, it is likely that both minerals are liquidus phases which may have crystallized simultaneously. Ophitic textures are the result of a complex interplay of order and ease of nucleation and relative rates of crystal growth and diffusion of elements in the magma. Anhedral quartz infill found in some of the ages would have been the last phase to crystallize.

Chill margins are generally glassy, containing phenocrysts and microphenocrysts of plagioclase, pyroxene and opaques. The variable petrography through the relative dyke ages enabled initial differentiation between the phases of intrusion (Meth, 1990).

3.1.2 *Mineralogy*

The primary minerals listed in Table 3.1 were analyzed chemically for 9 of the 11 ages of sampled dykes using electron probe microanalysis (Appendix 2). In the case of large plagioclase feldspars and pyroxenes, core and rim analyses were obtained.

3.1.3 *Zoning*

For some larger plagioclase and augite crystals (often phenocrysts), rim-core-rim traverses were carried out across the grains to test for the presence of any chemical zonation. Where zoning has been preserved, it reveals information regarding crystal growth processes within the magma, and possible temperature and pressure regimes present at the time of growth.

Zoned crystals may result if they are in a system where fractional crystallization is occurring (such as a magma chamber), and they are not continually being removed, but remain in the system, whilst not equilibrating with the surrounding liquid (Cox *et al.*, 1979). This is because the compositions do not change to the new equilibrium compositions, with changing temperature. The crystals thus have central or core compositions corresponding to the initial temperature of crystallization, and are overgrown to the rims progressively by lower temperature compositions. Post-crystallization diffusion zoning may also occur.

3.2 Plagioclase Feldspar

3.2.1 *Petrography*

On average, plagioclase feldspar (mainly labradorite) is the single-most abundant mineral contributing to the mineral assemblage of the Rooi Rand dolerites (see Figure 3.1). Plagioclase crystals occur as euhedral to anhedral elongate laths, the anhedral nature is often a result of a high degree of sericite and other alteration. In the finer-grained dolerites, plagioclase often occurs as microlites, giving a felted appearance to the dolerite. Where dolerites have a porphyritic texture, plagioclase feldspar is always the dominant phenocryst mineral, often occurring in glomeroporphyritic aggregates, sometimes associated with augite phenocrysts (Plates 3.3, 3.4 & 3.5). In porphyritic-textured dolerites, it also forms a major part of the groundmass. In equigranular dolerites, it occurs as a major constituent together with augite. Plagioclase laths may or may not be ophitically to sub-ophitically enclosed by larger augite crystals.

Plate 3.3 Photograph of DM90.25 (Age G') showing glomeroporphyritic aggregates of plagioclase feldspar in a finer-grained groundmass, giving a "birdsfoot" textured dolerite (shaft of north arrow 10cm in length).

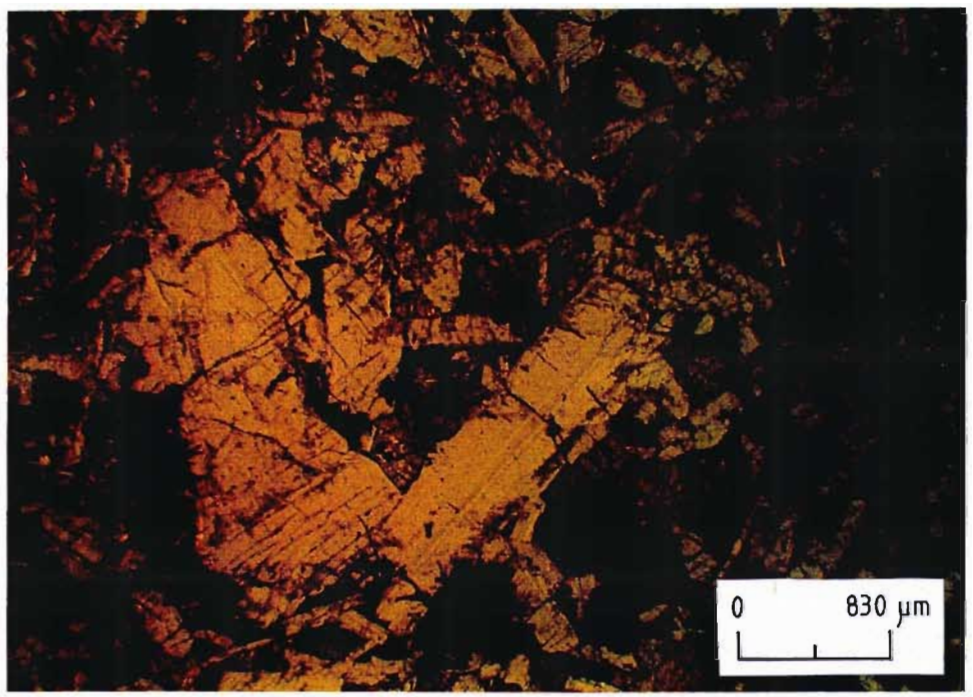

Plate 3.4 Photomicrograph of DM90.7 (Age G) showing glomeroporphyritic aggregates of plagioclase feldspar together with augite, in a finer-grained groundmass of plagioclase laths, augite and opaque minerals (magnification = 24; plane-polarised light).

Albite, Carlsbad-albite and pericline twinning is generally highly developed (Plate 3.5). Plagioclase composition as determined by the Michel-Levy Method (Heinrich, 1965), varies between the groundmass crystals and phenocrysts, with a gradation from $\approx An_{40}$ to $\approx An_{70}$. This compositional variation was also reported by Armstrong *et al.* (1984), but from electron microprobe data, the variation is seen to be slightly larger.

The alteration of plagioclase to sericite, often occurs with the more calcic cores of zoned crystals altering first. This is a common phenomenon resulting directly from the fact that most plagioclase crystals are chemically zoned (Heinrich, 1965), and the higher temperature calcic plagioclase at the crystal core is more unstable than the sodic plagioclase at the rim.

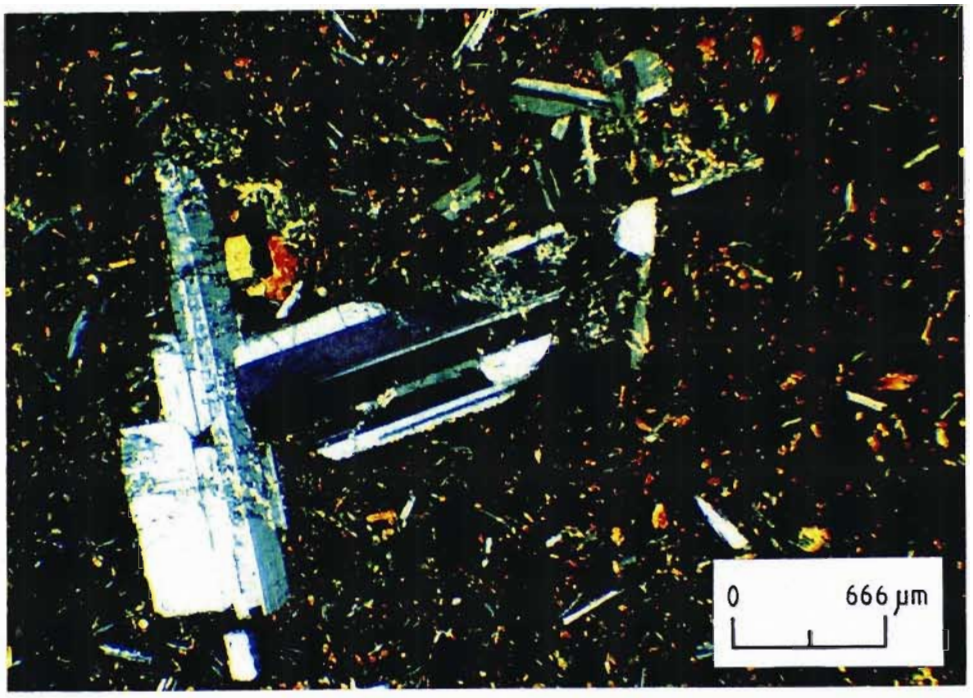

Plate 3.5 Photomicrograph of DM90.29 (Age H), showing glomeroporphyritic aggregates of plagioclase feldspar (labradorite) and some augite phenocrysts, in a finer-grained groundmass. Note the highly developed combined Carlsbad-albite twinning in the plagioclase phenocrysts (magnification = 30; cross-polarised light).

3.2.2 *Mineralogy*

General

Chemical compositions of plagioclases from the 9 sampled dyke ages (Appendix 2a), have been plotted on Albite/Anorthite/Orthoclase ternary diagrams (Figure 3.2). The plagioclases plot mainly in the field of labradorite (An_{50} - An_{70}), i.e. tending towards the more calcic-rich plagioclase and the general composition of plagioclases occurring in tholeiitic dolerites and basalts. Some phenocryst compositions verge slightly into the more calcic field of bytownite (An_{70} - An_{90}), and other more sodic plagioclases fall into the andesine field of composition (An_{30} - An_{50}). A few exceptions to these "average" compositions are for Ages G″ (a phenocryst core composition), D and B (plagioclases in the chill margins) (Figure 3.2), which have a few very sodic plagioclases, and in addition in B's case, some potassic feldspars. These crystals of exceptional composition occur together with more An-rich plagioclases. The significance of these diverse compositions will be discussed in later sections.

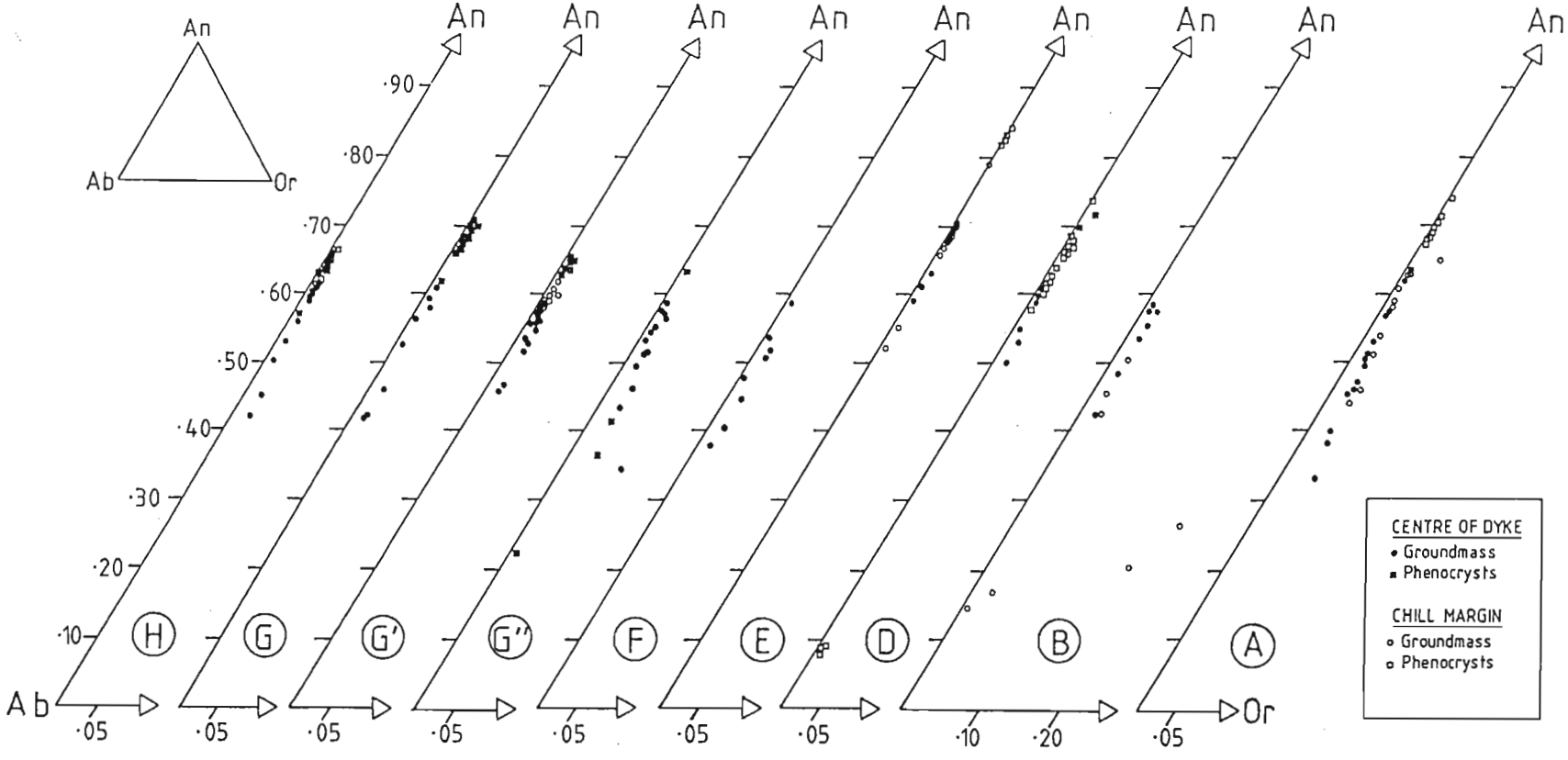

Figure 3.2 Ternary Ab/An/Or diagrams showing plagioclase feldspar compositional variations for several dolerite dykes (Appendix 2a).

Since the solid-solution series varies from pure $NaAlSi_3O_8$ to pure $CaAl_2Si_2O_8$, it is logical that Na and Ca (albite and anorthite components) will have an inverse relationship. But the orthoclase component ($KAlSi_3O_8$) in plagioclases may vary up to 5 mol. percent (Deer *et al.*, 1989). It tends to increase gradually towards the sodic end of the solid solution series of plagioclases. Feldspar compositions plotted for a single dyke age on a diagram of anorthite versus orthoclase components in Figure 3.3 reveal this trend.

All plagioclases have Mg present in small amounts. Most of the Fe reported in feldspar analyses has been said by Deer *et al.* (1989) to be Fe^{3+}, with the small amounts of Fe^{2+} being considered as impurities, or replacing plagioclase. Without seeing evidence of the impurity, the ions are assumed to have replaced Ca in the molecular structure. Fe^{2+} may sometimes replace Ca^{2+}, and this is a possible reason to explain some very high Fe contents (up to 4% in some cases) (Appendix 2a).

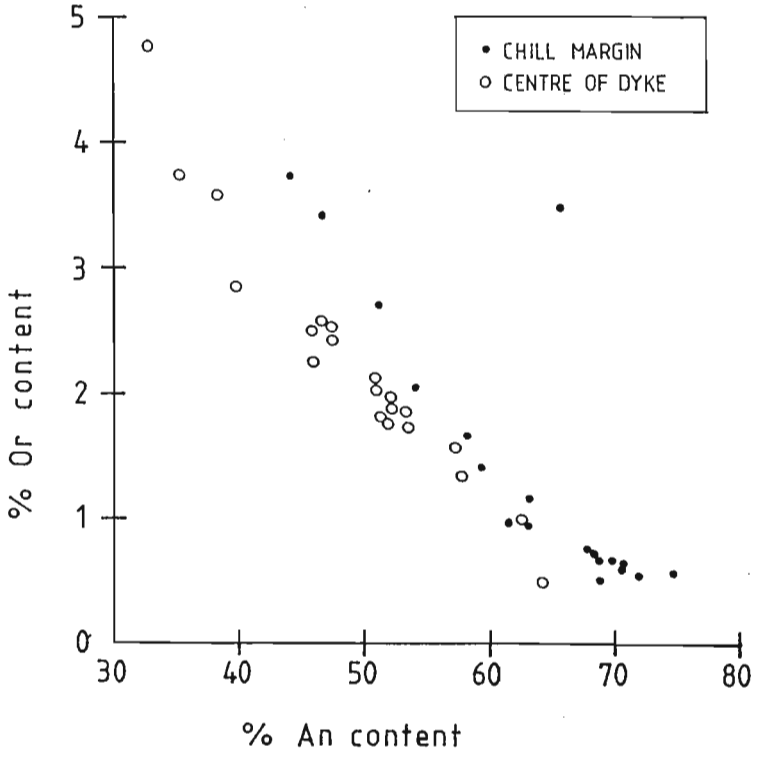

Figure 3.3 Binary diagram of % Anorthite versus % Orthoclase for Age A samples DM90.4 (chill) and DM90.5 (centre) (Appendix 2a).

Plagioclase can be a sensitive indicator of the surrounding magmatic environment. Most larger plagioclases analysed in this study show normal zoning, typical of those grown slowly in a fractionating magma chamber.

Other examples of plagioclase compositions indicating magmatic environment were noted by Stamatelopoulou-Seymour *et al.* (1990), who mention three different types of plagioclase which may arise from different magma mixing processes: inherited, in-situ, and xenocrystic. Pringle *et al.* (1974) infer the crystallization history of basalts from intensive studies of plagioclase feldspar zoning profiles. Many studies have demonstrated that plagioclase zoning is often systematically developed, and is related to systematic changes of environmental conditions during crystallization (Loomis and Welber, 1982).

Observations from Figure 3.2 regarding plagioclase compositional variations relate to:

i) *Chemical variation as a function of crystal size*
    i.e. phenocryst versus groundmass composition
ii) *Intra-dyke compositional variation*
    i.e. chill margin versus centre of dyke composition
iii) *Inter-dyke compositional variation*
    i.e. compositional variation between different dyke ages

3.2.2.i *Chemical variation as a function of crystal size*

Hoffer (1966) noted that the rate of cooling of the magma, determined the composition of the plagioclases. In groundmass crystals which reflect a rapid rate of cooling (i.e. small size of the groundmass plagioclase and some glass present), the anorthite content of these groundmass plagioclases is the direct result of the rapid cooling, and is high. The anorthite content of groundmass plagioclase thus varies inversely with size i.e. the smaller the groundmass crystal, the more An-rich (less Ab-rich) it will be.

In contrast to this, are samples which show crystallization under slower cooling conditions. Early formed groundmass crystals which are not removed from the melt, react with the melt and gradually become converted to more sodic forms. Therefore, the slower the rate of cooling, the more sodic are the final groundmass crystals.

In general, quickly cooled crystals will tend to be small while slowly cooled crystals are larger. No relationship was noted between phenocrysts and cooling rate (correlated to dyke width), but this is to be expected if it is believed that before any significant cooling takes place (i.e. due to intrusion) phenocrysts are already formed.

As can be seen from Figure 3.2, in all ages except G″ and D, phenocrysts are more calcic (i.e. more anorthite-rich) than groundmass crystals. Such compositional variation is typical of basaltic systems. On a study of a basaltic flow from the Columbia River Basalts, Hoffer (1966) noted that the phenocrysts averaged 20% more calcic than corresponding groundmass plagioclases.

Since phenocryst assemblages crystallize earlier than the groundmass assemblage, the variation in composition between groundmass (matrix) and phenocryst plagioclases for the Rooi Rand dolerites is expected. When cooling is accelerated due to intrusion, phenocryst formation (with slow growth at almost constant temperature) is halted. The equilibrium diagram for the plagioclase feldspars by Bowen (1913) shows the change of plagioclase composition with time, as a magma cools and crystallizes. As an example, the compositions of plagioclases from the chill margin of Age A have been plotted onto this diagram (Figure 3.4). Following the solidus line on this binary diagram, it may be clearly seen that with time (i.e. cooling of the magma), the plagioclase compositions become more albite-rich and less anorthite-rich i.e. the phenocrysts should be more An-rich than the groundmass crystals, and this will be the norm in a cooling magma.

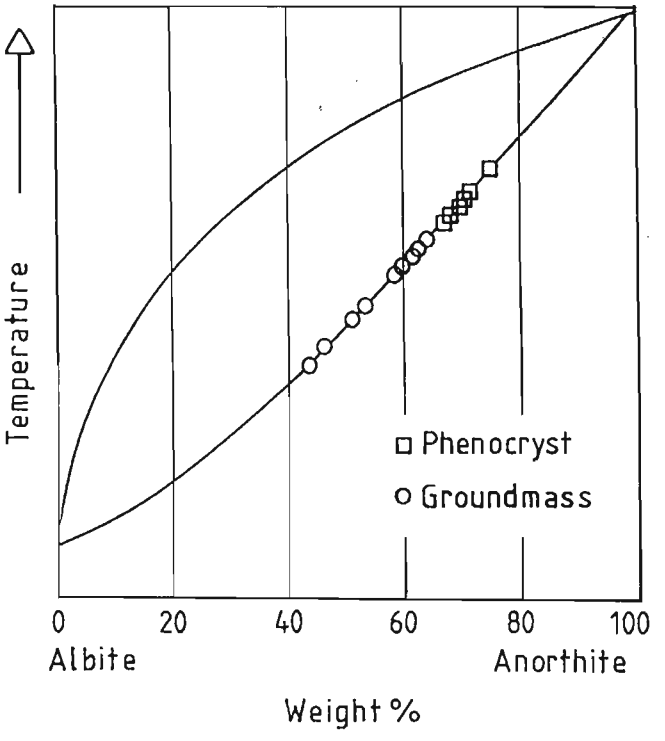

Figure 3.4 Equilibrium diagram of the plagioclase feldspars (after Bowen, 1913), with analyses of plagioclases from sample DM90.4 (Age A) plotted (Appendix 2a).

Although the phenocryst of Age A (DM90.4) is chemically zoned, the rim and core compositions are more anorthite-rich than the groundmass crystals. Some normally zoned phenocrysts may have rims which will continually equilibrate with the surrounding melt, and have similar compositions to later formed groundmass compositions.

The phenocryst analysed in G″ shows the more uncommon reversed zoning, with a very sodic core (An_{23}) (Appendix 2a, analysis fs7z08iv) and a highly calcic rim, which is similar in composition to the groundmass crystals (Appendix 2a, analyses fs7z08).

Also notably different are the three phenocryst analyses from the chill margin of Age D, with less than 10% anorthite component (Figure 3.2, Appendix 2a, analyses fs1r11, fs1c11, fs3r11). The third analysis comes from the rim of a highly zoned phenocryst with a very calcic core, but the first two analyses are rim and core compositions of the same crystal. These two crystals may be xenocrystic, or else possibly represent a late stage alteration which may have taken place at the chill margin of the dyke. Henderson *et al.* (1986) mention unexpected crystal compositions which may arise due to insufficiently fast diffusion rates of some elements in the melt, under conditions of rapid crystallization. These slow diffusion rates cause a boundary layer of a composition very different from that of the bulk melt to form. These phenocrysts may have formed in a situation of extremely rapid crystallization, since the dyke in which they are found is only 8mm wide. Cooling would have taken place very quickly.

3.2.2.ii *Intra-dyke compositional variation*

There is a general trend that chill margin plagioclases (especially phenocrysts) are more anorthite-rich than centre of dyke plagioclases (Figure 3.2). Exceptions to this "norm" are Ages B and D. Age D has 3 phenocryst analyses from the chill margin which are almost pure albite. These have been discussed in the earlier section on phenocrysts versus groundmass crystals. In contrast to Age D's unexpected albite-rich plagioclases, the groundmass chill margin analyses of Age B do not seem strange considering its quartz-rich mineralogy and later evidence in this study which shows that the chemical composition of Age B is very different to the other ages (more Na- and K-rich). They may also however, as was suggested for Age D feldspars, have been affected by late stage alteration of the

rock, possibly promoted by the presence of a high percentage of volatiles.

Chill margin groundmass crystals which sometimes appear to be less anorthite-rich than centre of dyke groundmass crystals, are on average still higher in the anorthite component. Good examples of this are Ages E and G′ (Figure 3.2).

Ross (1983) explains the phenomenon of higher anorthite contents of plagioclases in chill margins as being a primary trend related to the crystallization history of the magma, and not a result of flow mechanics. Phenocrysts in the chill margin would have crystallized from an earlier liquid than those in the dyke centre. After becoming quenched in chill margins, these more calcic phenocrysts were no longer available for further lowering of their anorthite content by reaction with the residual liquid, or to be affected by flow differentiation (Ross, 1986).

Chill margins may represent the bulk composition of an intrusive phase prior to fractionation and differentiation. They may therefore, be more primitive in whole rock composition, i.e. enriched in Mg and Ca relative to the interiors of dykes, and the feldspars could be expected to be more An-rich. However, this interpretation should be treated with caution, because processes, such as flow differentiation, may change the composition of the magma along its margins before nucleation takes place.

3.2.2.iii *Inter-dyke compositional variation*

In general, the variations of plagioclase compositions between each dyke age, reflect the overall chemistry of the dyke phase. Age E is the least evolved magma type, and has plagioclases which are very rich in Ca (i.e. a high An component, Figure 3.2). Ages B and F, which have quartz in their mineral assemblage (Table 3.1) and are chemically the most evolved dolerite phases, have plagioclases all with anorthite contents less than 60% (Figure 3.2) and higher proportions of the sodic end-member, albite.

It is significant that the larger dykes have more primitive feldspars. One possibility is that the greater volumes of magma represented by these dykes have undergone less crystallization, explaining why they are observed as larger dykes.

3.2.3 *Zoning*

Plagioclase shows chemical zonation more obviously than any other minerals (Hatch *et al.*, 1972), and it is a common phenocryst phase. The most common zoning (from Ca-rich cores to Na-rich rims) is termed normal. This was found in most plagioclase feldspar samples analysed (either from core and rim analyses, or from complete zoning profiles) (Appendix 2a). Less frequently observed, was reverse zoning. A phenocryst analysed in Age G″ shows this, with a very sodic core (An_{23}). No oscillatory zoning (normal and reversed) was noted in Rooi Rand dolerite plagioclases.

The equilibrium diagram for plagioclase feldspars shown in Figure 3.4 may also be used to explain the phenomenon of normal zoning in plagioclase feldspars. With progressive cooling, crystals forming will change composition to equilibrate with the melt, unless there is insufficient time for chemical diffusion to take place, in which case, the crystals will be zoned, with calcic cores (crystallizing early out of a Ca-rich melt), and more sodic rims (as cooling and crystallization continues).

Figure 3.5 shows the major element zoning profiles for a plagioclase crystal in the centre of Age A dyke phase. It displays normal zoning. The more calcic cores which are clearly visible as "bell-shaped" profiles, were also identified in the original petrographic study of the plagioclase crystals as being more calcic, by the presence of the alteration product sericite in the feldspar cores. The "u-shaped" Na_2O profile is mimicked by the K_2O profile, reiterating what was stated earlier about plagioclase potassium contents increasing with increasing Na and decreasing Ca. CaO and MgO display bell-shaped profiles, indicating a similar geochemical behaviour.

This zoning is considered to be the original growth zoning of the mineral grain. The broad cores of almost uniform composition tend to indicate a long period of slow crystallization before intrusion and cooling of the magma.

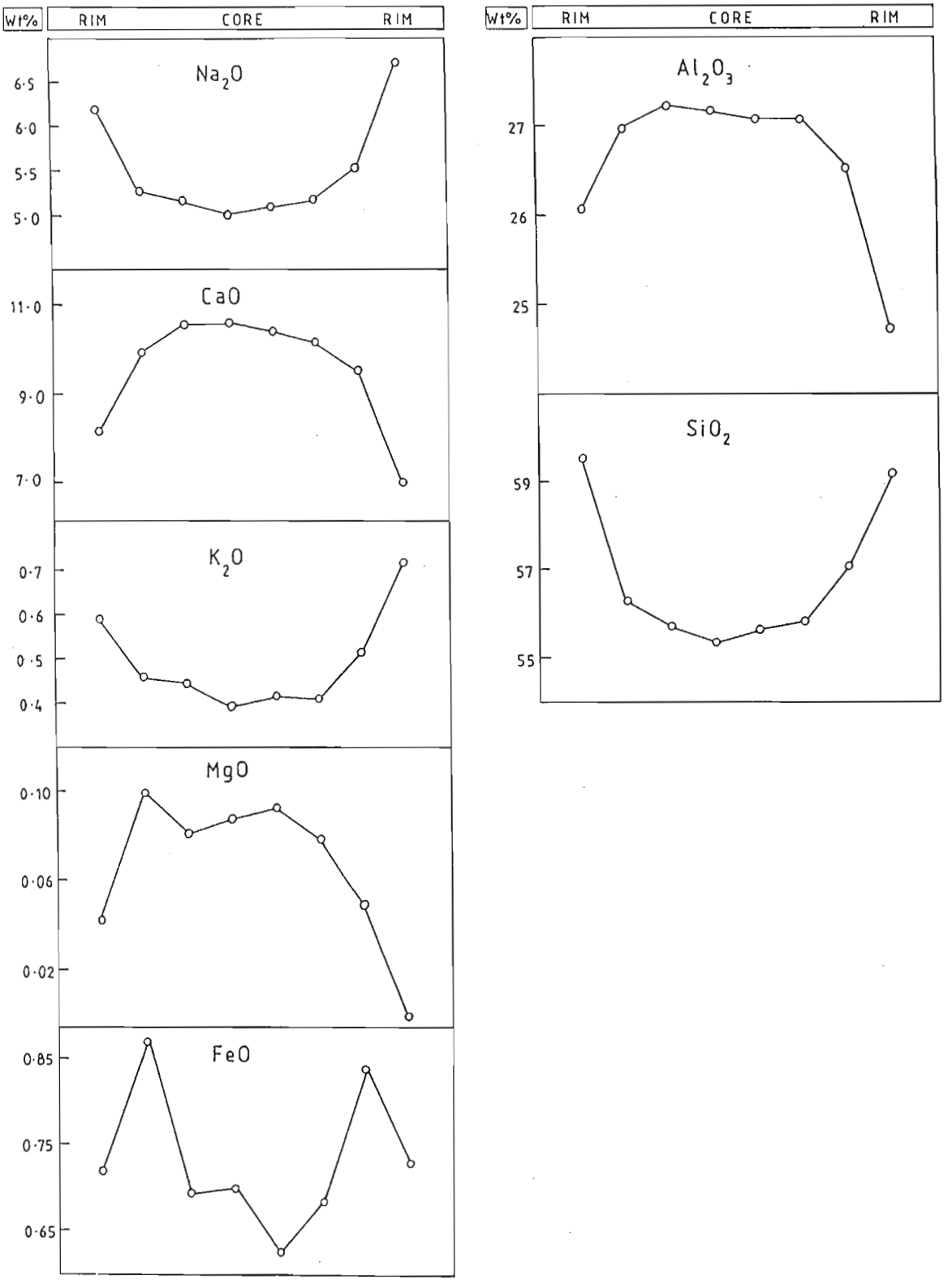

Figure 3.5 Rim-core-rim major element oxide zoning profiles for a plagioclase from the centre of a dyke, Age A (DM90.5), (Appendix 2a, analyses fs1z05). Plagioclase crystal approximately 0.5mm in width.

In contrast to this "normal" case, Figure 3.6 shows chemical zoning in a plagioclase from the chill margin of the same dyke phase. The general shape of the previous zoning profile is still present, but the crystal and thus the profile has been modified at the rims. The Ca content suddenly increases to higher than that of the core, and the Na content decreases. This may reflect a sudden change in composition either towards the end of the crystal's growth period in the form of late-stage diffusion zoning, or later alteration after crystallization ceases. Bottinga *et al.* (1966) consider that magmatic plagioclase growth will be controlled by diffusion at some stage in the crystallization process. This may or may not occur towards the end of the crystal's growth period.

The central part of the profile in Figure 3.6 is not uniform, and this may indicate that some late stage alteration did take place. Whatever the reason for the alteration of the profile, in comparison to the pristine centre of dyke plagioclase zoning profile (Figure 3.5), it may be noted that the chill margin minerals have undergone some process which did not affect the centre of dyke ones. Loomis (1982) states that a combination of both fractionation and disequilibrium processes can produce irregular and reversed zoning such as is seen in the chill margin plagioclase samples.

In Section 3.3.3, it will be shown from pyroxene zoning profiles, that the pyroxenes for the centre of dyke and chill margins vary in a similar manner.

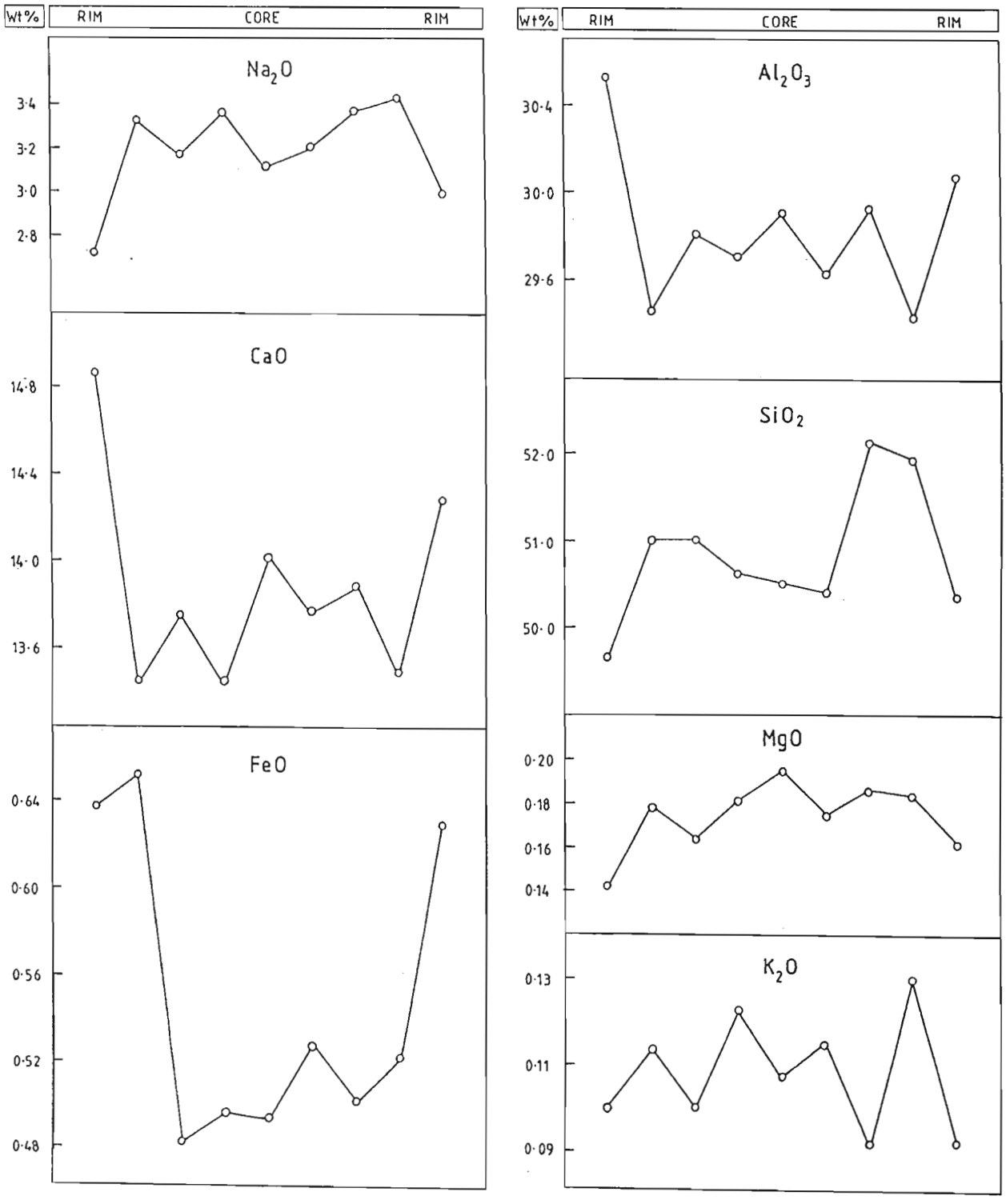

Figure 3.6 Rim-core-rim major element oxide zoning profiles for a plagioclase from the chill margin of a dyke, Age A (DM90.4), (Appendix 2a, analyses fs1z04). Plagioclase crystal approximately 1mm in width.

3.2.4 *Discussion*

Although observations regarding plagioclase compositions have been classed into core versus rim, phenocryst versus groundmass and chill margin versus centre of dyke, a correlation may be drawn between these three criteria. In all cases, the chemical composition of the plagioclase is actually a function of the relative time at which the crystal formed in the history of the melt's crystallization (or remaining melt's evolution). It is therefore not surprising that parallels may be drawn between core, phenocryst and chill margin plagioclase compositions, which in most cases are all more "primitive" (richer in Ca) than the rims, groundmass and centre of dyke plagioclases, simply because they would have crystallized from an earlier higher temperature melt (in the case of cores and phenocrysts), and an earlier stage melt (in the case of the chill margin). It may thus be stated that a link does exist between the time scales of magmatic cooling (thermal history of a magmatic system) and the time scales of differentiation (chemical evolution of a magmatic body).

3.2.5 *Plagioclase alteration by process zone fracturing*

Fluids passing through propagating fractures in minerals may cause alteration in the form of localized chemical changes in mineral composition. Electron microprobe analytical traverses were done across the cores of a plagioclase and pyroxene crystal (Appendix 2a & 2b; fs3t07 & px7t07 respectively) affected by micro-fracture systems.

The fracture system appears to be associated with the intrusion of a subsequent dyke age, both having a north-south orientation. If one refers back to Figure 2.4, it may be noted that the DM90.7 (Age G) was taken almost adjacent to an arrested dyke tip of a later age. In this case, the cracks may represent process zone fractures commonly found in the country rock adjacent to the tip of a propagating dyke (Hoek, 1995).

More consistent results were obtained for the plagioclase traverse than for the pyroxene, and hence only the plagioclase values have been plotted (Figure 3.7). In general, adjacent to cracks the CaO and Al_2O_3 values increase, and the Na_2O, K_2O and SiO_2 values

decrease. The behaviour of iron and magnesium is uncertain. This is not surprising because they occur in such low proportions that any change would be difficult to detect.

From Figure 3.7 it may be seen that the three main cracks of the fracture system did not have equal effects on the mineral composition. The crack which is furthest to the right clearly has the highest degree of accompanying alteration. This may be a function of crack size, and thus the relative proportion of fluids which may have passed through the crack, causing the varying degrees of chemical enrichment or leaching.

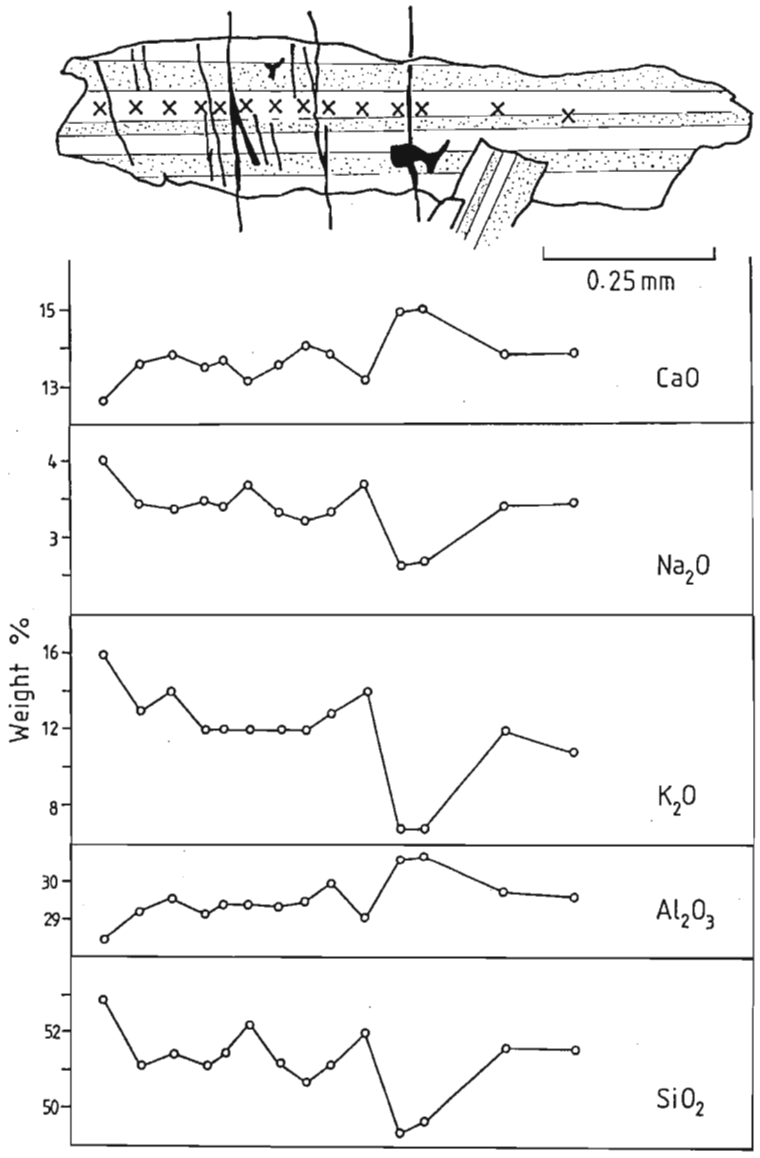

Figure 3.7 Diagrammatic representation of a plagioclase feldspar approximately 1mm in length (analysis points marked with an x), and selected corresponding major element zoning profiles across the core of the crystal (Appendix 2a, fs3t07).

3.3 Pyroxene

3.3.1 *Petrography*

The clinopyroxene augite, is the other major mineral component of the Rooi Rand dolerites, intimately associated with plagioclase (see Figure 3.1). It is most often colourless to pale brown. Rare lamellar twinning was noted. Augite constitutes a large part of the groundmass, and occasionally occurs as phenocrysts (especially in chill margins). Crystals are euhedral to subhedral, and, in very fine-grained samples, are anhedral and often highly altered to chlorite. Augite and plagioclase are interstitially and sub-ophitically (less often ophitically) related (Plates 3.6 & 3.7).

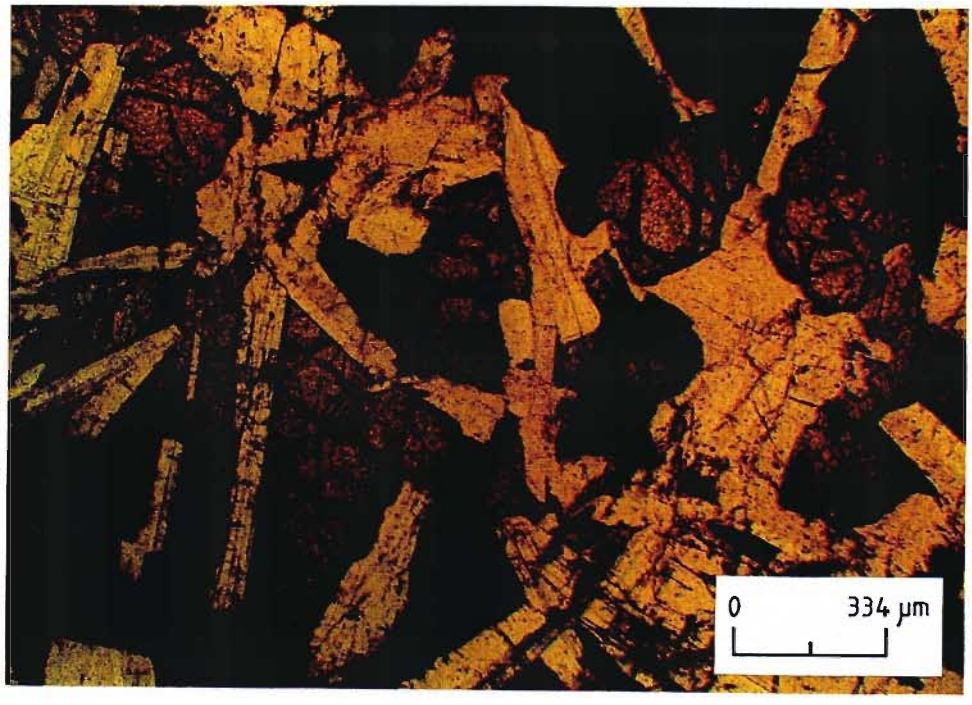

Plate 3.6 Photomicrograph of DM94.3 (Age E′) showing augite crystals (aug) subophitically enclosing plagioclase laths, together with olivine (ol) (magnification = 60; plane-polarised light).

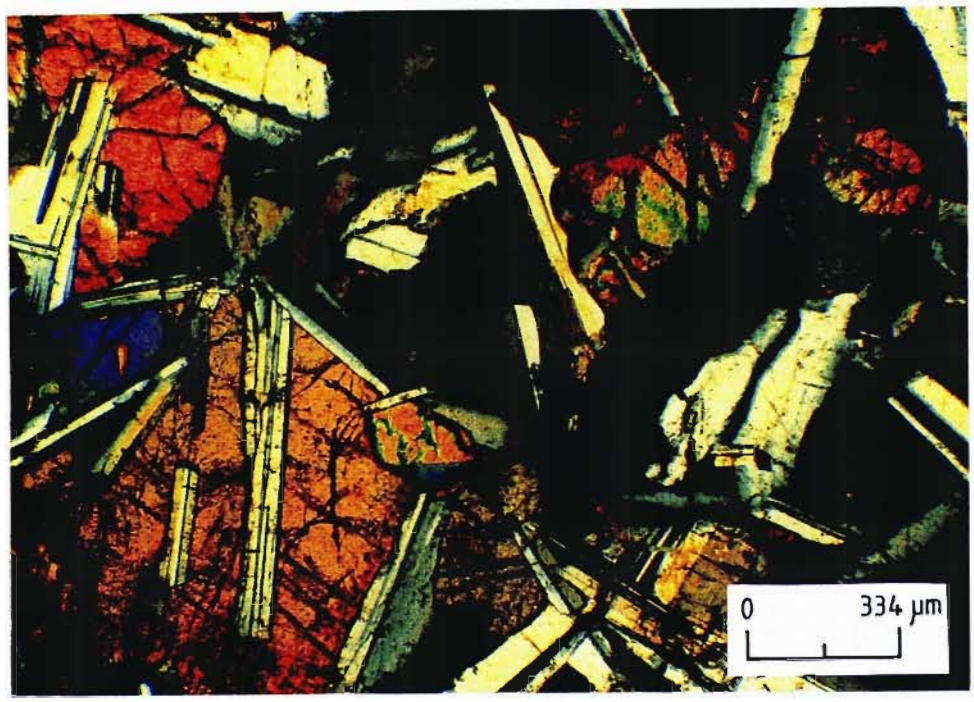

Plate 3.7 Photomicrograph of DM94.3 (Age E') showing augite crystals (aug) subophitically enclosing plagioclase laths, together with olivine (ol) (magnification = 60; cross-polarised light).

3.3.2 *Mineralogy*

General

The chemical compositional fields of pyroxenes for the 9 sampled dyke phases (chill margins and centres) have been plotted on a ternary Wollastonite/Enstatite/Ferrosilite diagram (Figure 3.8).

The pyroxenes are all clinopyroxenes, predominantly augite in composition. The compositional fields verge slightly into ferroaugite, and subcalcic augite compositional ranges, but this is not considered to be the norm. Deer *et al.* (1978) consider subcalcic augite and subcalcic ferroaugite as being characteristic clinopyroxene phases of quickly chilled basic magmas. A minor amount of pigeonite was also identified in one dyke phase.

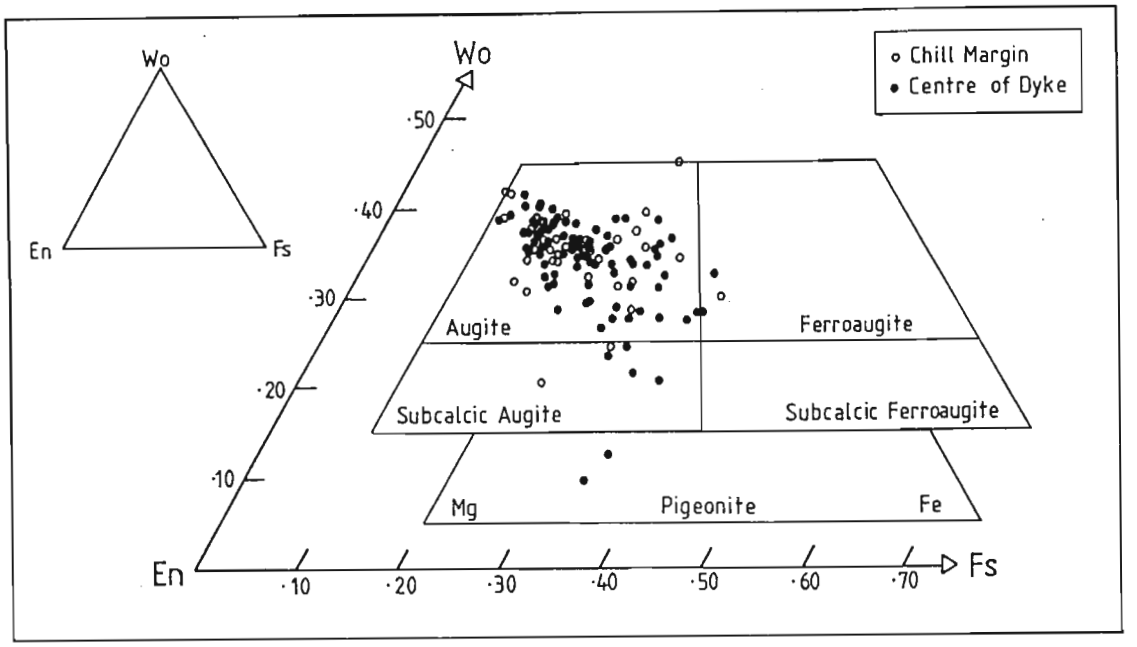

Figure 3.8 Ternary Wo/En/Fs diagram, showing pyroxene compositions for the 9 sampled dyke phases (Appendix 2b). Nomenclature of pyroxene compositional fields after Poldervaart and Hess (1951).

As was done in the plagioclase section, additional observations pertaining to pyroxene compositions, will be made according to certain criteria. They are:

i) *Chemical variation as a function of crystal size*
   i.e. phenocryst versus groundmass composition
ii) *Intra-dyke compositional variation*
   i.e. chill margin versus centre of dyke composition
iii) *Inter-dyke compositional variation*
   i.e. compositional variation between different dyke ages

3.3.2.i *Chemical variation as a function of crystal size*

Phenocryst and groundmass compositions do not show as much variation in the pyroxenes, as for the plagioclase feldspars. This may be a function of the smaller data set accumulated for pyroxene, because the commonest phenocryst phase is plagioclase and not augite. A typical variation is observed in sample DM90.6 (Age G) where the average phenocryst composition is $Wo_{40}En_{45}Fs_{15}$, and the average groundmass crystal composition is $Wo_{37}En_{44}Fs_{19}$. In this case, groundmass crystals are thus more Fe-rich, and less Ca- and Mg-rich than the phenocrysts.

Nakamura and Coombs (1973) compared augite microphenocrysts and groundmass crystals of a chilled margin of a tholeiitic dolerite from Moeraki, New Zealand. Their findings are identical to those in sample DM90.6. The microphenocrysts are approximately $Wo_{38}En_{50}Fs_{12}$ in composition, with low Ti:Al ratios ($\approx$ 1:4), and the groundmass crystals are more Fe-rich having higher Ti:Al ratios ($\approx$ 1:2). DM90.6 phenocrysts have an average Ti:Al ratio of $\approx$1:3.5 and the groundmass crystals have a Ti:Al ratio which is slightly higher ($\approx$1:3.2). Furnes *et al.* (1982), in their study on basaltic dykes at Vestfjella, in Dronning Maud Land, Antarctica, also found that the majority of augite phenocrysts are more Ca- and Mg-rich than groundmass augite in the same dyke phase.

3.3.2.ii *Intra-dyke variation*

The difference in composition between chill margin and centre of dyke pyroxenes is notable. As may be seen from Figure 3.9, chill margin pyroxenes are more Ca-rich, and more Mg-rich in most cases (except for Ages B and H) than pyroxenes in the dyke centres (Appendix 2b). This is expected as dyke chill margins represent a less evolved magma, being generally richer in Ca and Mg than dyke centres. Ernst and Bell (1992) in a study of the Great Abitibi Dyke in Canada, found that Mg:Fe ratios of augite (and olivine) decrease from the dyke chill margins inwards, indicating that the interior rocks are more evolved.

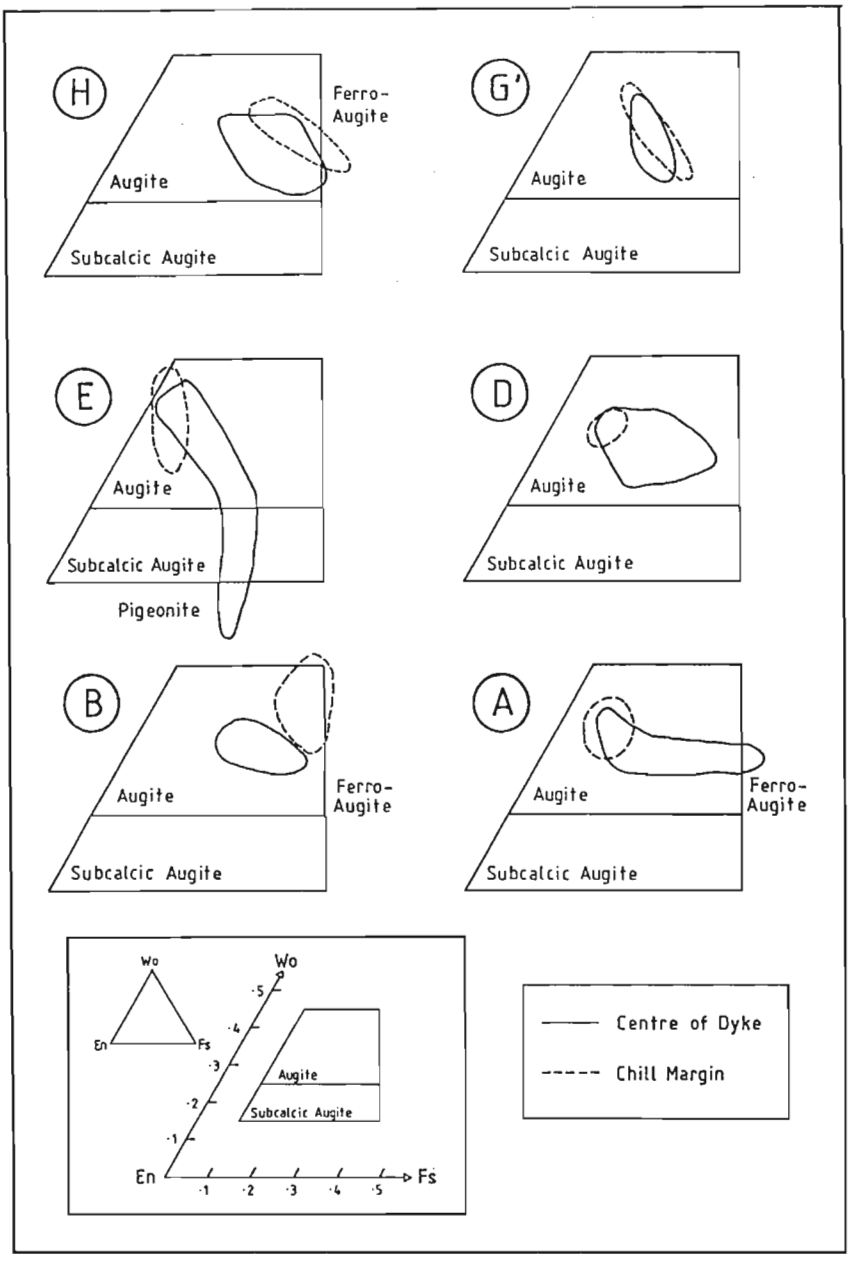

Figure 3.9 Ternary Wo/En/Fs diagrams of pyroxene compositional fields for 6 dyke phases, to show the variation between centre of dyke and chill margin pyroxene compositions.

Compositional variations between chill margin and centre of dyke pyroxenes, may even exist in the minor element compositions, such as Al. Deer *et al.* (1978) noted a variation in Al contents in tholeiitic and related rocks. They found that Al decreases in pyroxenes with increasing fractionation in tholeiitic and related rocks, which may imply that the Al content should decrease with increasing "evolution" of the magma. Since chill margins are said to be more primitive than centre of dyke compositions, one would expect that the Al should be higher in chill margin pyroxene samples.

In addition to the above reasoning, Coish and Taylor (1979), found that the Ti and Al contents in pyroxene increase with increasing cooling rate. This would imply that with the very rapid cooling rate at chill margins, the pyroxenes in chill margins should contain a higher proportion of Al and Ti than those in the centre of dyke.

When Al compositions are plotted on a bar graph for chill margin and centre of dyke pyroxenes (Figure 3.10), this is shown to be the case. Where centre of dyke and chill margin pyroxene Al contents have been plotted, the chill margin pyroxenes are always higher in Al_2O_3. A graph for TiO_2 has not been plotted, but Ti (and also Cr) values are in most cases (although not as noticeably as Al) generally higher in chill margin pyroxenes than centre of dyke ones.

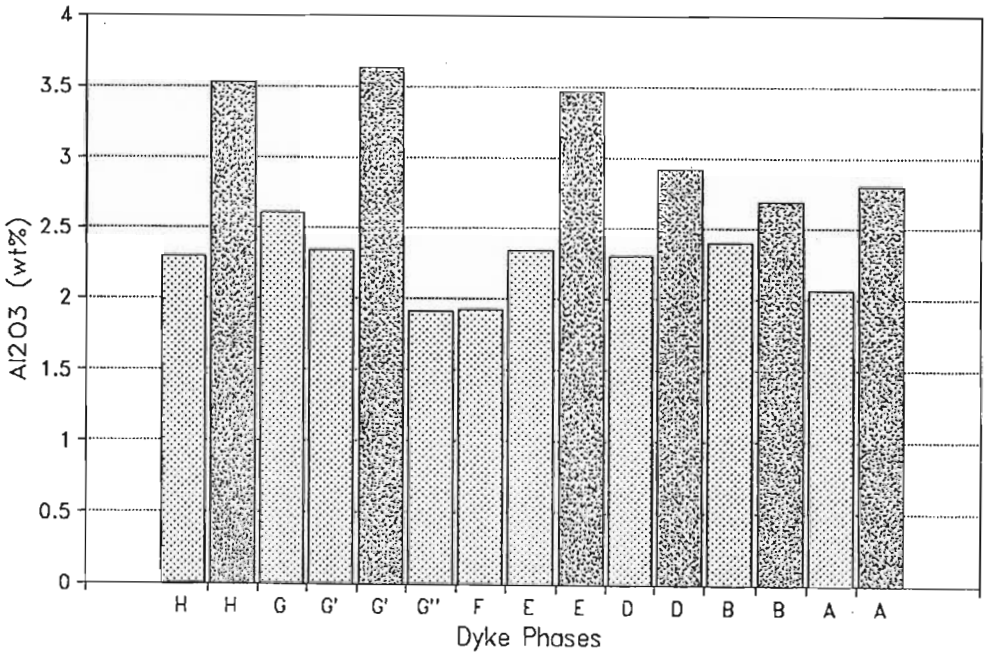

Figure 3.10 Bar graph to show average Al_2O_3 contents of pyroxenes, for centre of dyke (light shading) and chill margin (dark shading) samples (Appendix 2b). Note: Ages G, G" and F have no chill margin analyses.

3.3.2.iii *Inter-dyke variation*

Pyroxene compositions should also reflect the overall chemistry of each dyke phase to some extent. Hall *et al.* (1985 and 1986) in a study of dykes from a tholeiitic dyke swarm in Greenland, found that the pyroxene chemistry parallels the geochemical evolution of the dykes, showing an overall Fe-enrichment trend (Ca and Mg depletion trend). Yoder and Tilley (1962) also state that the pyroxenes of primary basalts will contain more of the

hedenbergite (Ca and Fe) component than the ferrosilite component (Fe), and will become more Fe-rich in derivative basalts. From Figure 3.9, it may be seen clearly that dyke phase E which is the most primitive (Chapter 4 will show it to lie at the least evolved side of the Fe-enrichment trend), has the most Ca- and Mg-rich pyroxene compositions.

3.3.3 *Zoning*

In contrast to the commonly found zoning in most plagioclases, pyroxenes often do not show chemical zoning, especially in groundmass crystals. A reason for this may be that pyroxenes have a far more open crystal structure than plagioclase, and zoning is easily lost through diffusion during subsolidus re-equilibration.

Evolution of the residual liquid chemistry with crystallization (and cooling), will cause a shift of composition in pyroxenes, from Mg-rich to Fe-rich (Hatch *et al.*, 1972). This progressive Fe enrichment may manifest itself in zoned pyroxene crystals, which will thus have Mg-rich cores, and Fe-rich rims. This trend may be seen clearly in the profile of a rim-core traverse across a pyroxene crystal, from the centre of dyke phase Age A (Figure 3.11). The core is also richer in CaO, SiO_2 and Al_2O_3. This zoning may be termed normal. Not all pyroxenes traversed showed this normal zoning.

Figure 3.12 shows a zoning profile for a pyroxene from the chill margin of the same dyke phase. The zoning is almost exactly the reverse of that shown in Figure 3.11. FeO is now at its highest concentration in the core, and CaO and SiO_2 at their lowest. The MgO, Al_2O_3 and MnO profiles are no longer smooth as they were in the previous zoning profile, but appear to have been altered.

It is envisaged that whatever process caused the plagioclase zoning profiles at the chill margins to be irregular (as opposed to "normal" in the dyke centre), must also have affected the pyroxene zoning profiles. Likely processes will be mentioned in section 3.3.4.

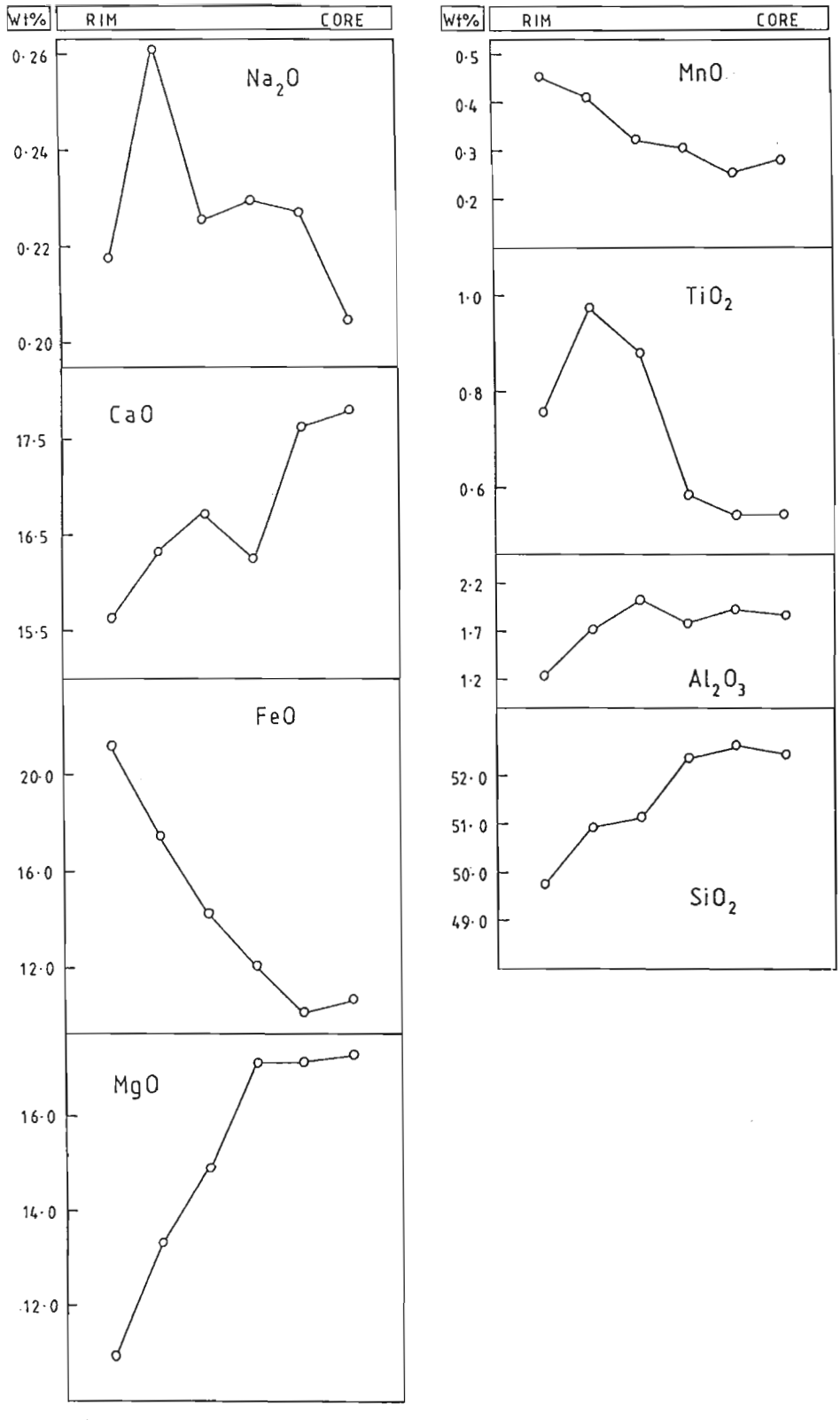

Figure 3.11 Rim-core major element zoning profiles for a pyroxene from the centre of a dyke phase, Age A (DM90.5) (Appendix 2b, analyses px6z05). Augite crystal approximately 0.5mm from rim to core.

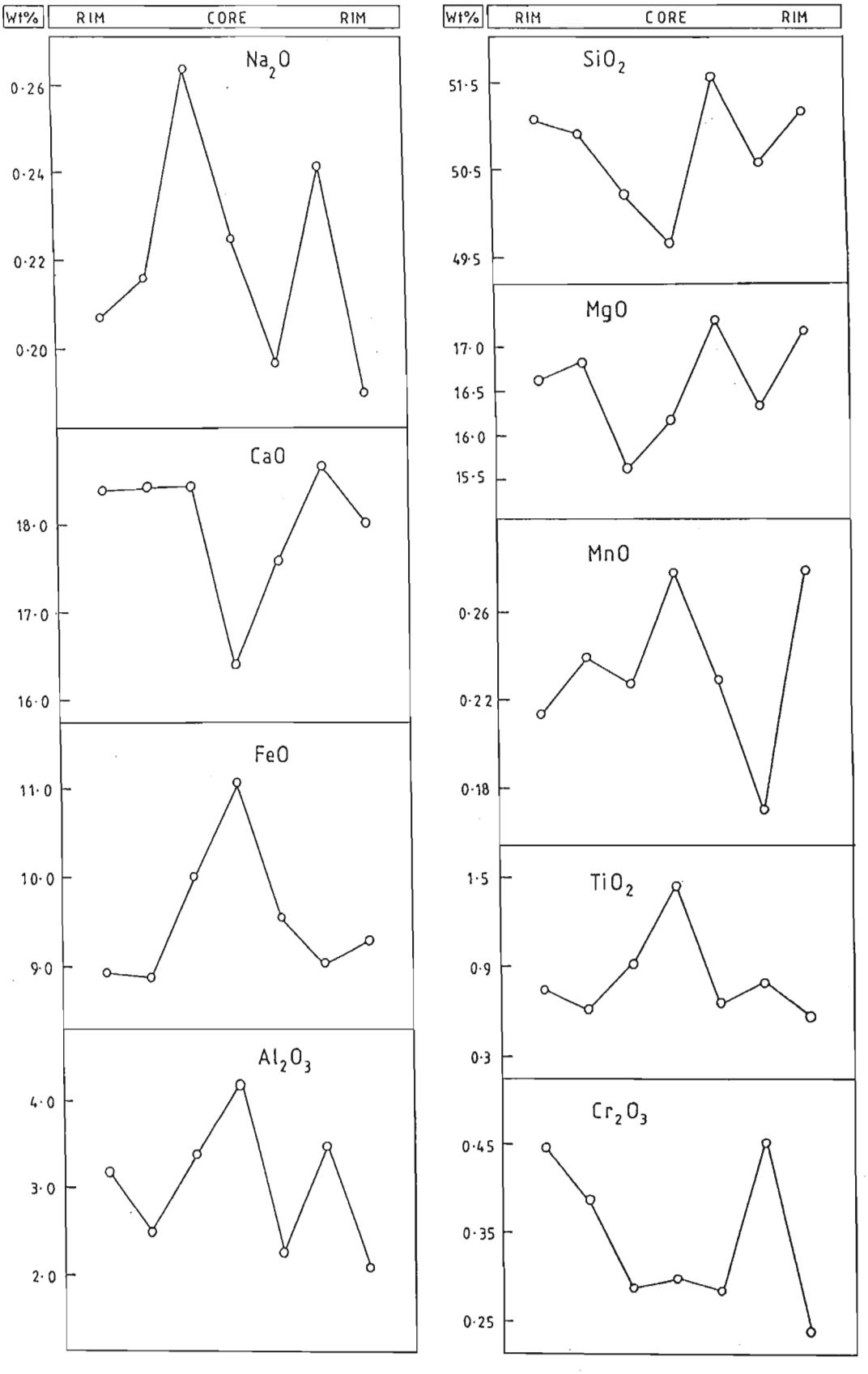

Figure 3.12 Rim-core-rim major element zoning profiles for a pyroxene from the chill margin of a dyke phase, Age A (DM90.4) (Appendix 2b, analyses px5z04). Augite crystal approximately 0.5mm in width.

3.3.4 *Discussion*

Core, phenocryst and chill margin pyroxene compositions, are generally more "primitive" (richer in Ca in all cases and Mg in most cases) than the rims, groundmass and centre of dyke pyroxenes (which have lower Ca and higher Fe contents). These chemical variations are a function of the relative time at which the pyroxenes crystallized from the melt, and to repeat what was stated in the section on plagioclases, cores of crystals will tend to form from higher temperature liquids than rims (normal crystal zoning with decreasing temperature), phenocrysts tend to form at an earlier stage than groundmass crystals (when the melt is still more "primitive"), and chill margins most often represent a more "primitive" melt than centres of dykes.

It must be noted that these correlations are very broad, and may only be said to be the general case in a simple magmatic system. Many other factors may occur which will change these general trends, such as reversed zoning; introduction of a new melt into the system, i.e. magma mixing; phenocrysts which may actually be xenocrysts; turbulence in the flow of magma along the magma conduit, and late-stage alteration processes. Most of these processes are discussed in more detail in Chapter 4, with respect to the detailed chemical zoning of a small dyke (Section 4.5.2). Such factors may have been responsible for the few exceptions, for example Ages B and H having chill margin pyroxenes being more Fe-rich than centre of dyke ones.

Chemical variations in Age B pyroxenes are not unexpected. Age B has a quartz-rich mineralogy which is suspected to have formed in an entirely different manner to the other dyke phases. Age H on the other hand, is the oldest dyke age at the study area, and in addition to the numerous xenoliths it hosts, it is highly altered. This post-intrusion alteration may have had a significant effect on the minerals present. Only once the overall geochemistry of the dykes has been discussed, can inferences be made regarding the origins of each dyke age, and their constituent mineralogies.

3.4 Olivine

3.4.1 *Petrography*

Olivine-bearing assemblages are not very common in the Rooi Rand dolerites, and only Ages E and E′ were found to have olivine present in any significant amount (5.1% and 2.8% respectively; Table 3.1 and Figure 3.1). Some olivine was noted in Age H, but was not present in large enough amounts to feature as a percentage in the 2000-point count modal analysis.

As seen in Age E, a large proportion of the euhedral to subhedral olivines have been replaced by serpentine, biotite and iddingsite. Near-pristine olivines may be distinguished from augites by their higher interference colours and their opaque reaction rims (also referred to as coronas, kelyphitic borders or corrosion mantles), alteration cracks and often partial alteration to serpentine (Plates 3.8 and 3.9).

The olivine in Age H is found associated with the plagioclase feldspar phenocrysts (Plates 3.10 and 3.11). In the chill margin sample, olivine occurs as highly altered microphenocrysts, sometimes together with other phenocrysts, contributing to the glomeroporphyritic texture of the rock in places.

Olivine is very susceptible to hydrothermal alteration, low grade metamorphism and weathering (Deer *et al.*, 1989), and it is thus not surprising that it is mainly observed in the Rooi Rand dolerites in its altered form. Many different types of alteration products may be formed, including serpentine (hydrated magnesium silicate polymorphs eg. chrysotile, antigorite) iddingsite (a silicate component plus goethite or hematite), chlorite (together with a goethite component is called bowlingite), amphibole and iron oxides. These reaction products are normally very fine-grained and difficult to identify petrographically. Neither have electron microprobe analyses been useful, because the alteration products are so fine-grained that only the composite compositions have been determined.

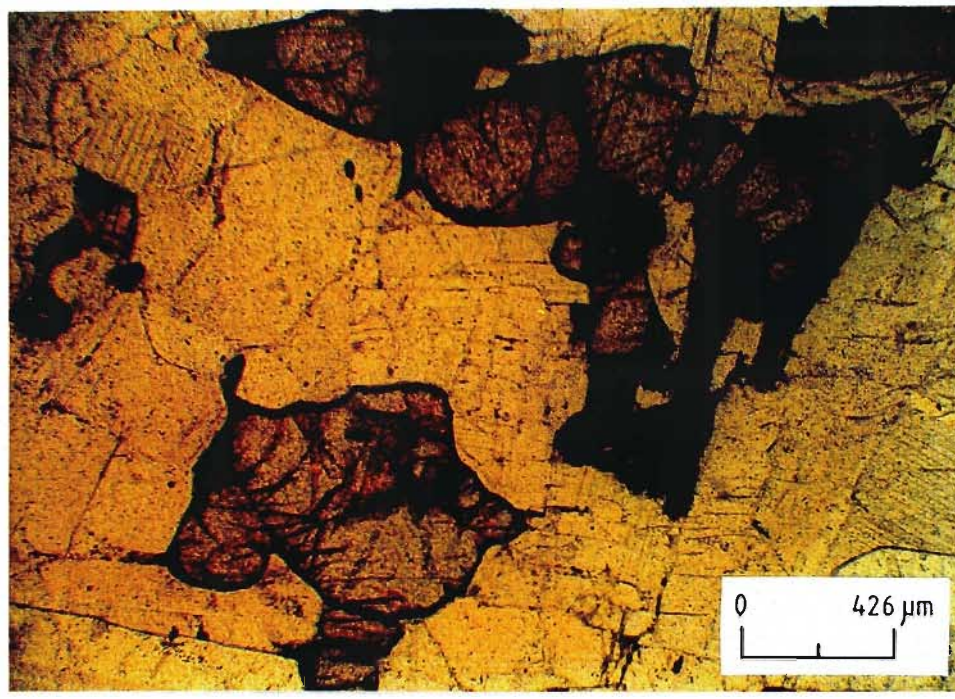

Plate 3.8 Photomicrograph of DM90.20 (Age E) showing subhedral to anhedral olivines (ol) associated with plagioclase feldspars (pl). Note the opaque reaction rims and alteration cracks of the olivine crystals (magnification = 47; plane-polarised light).

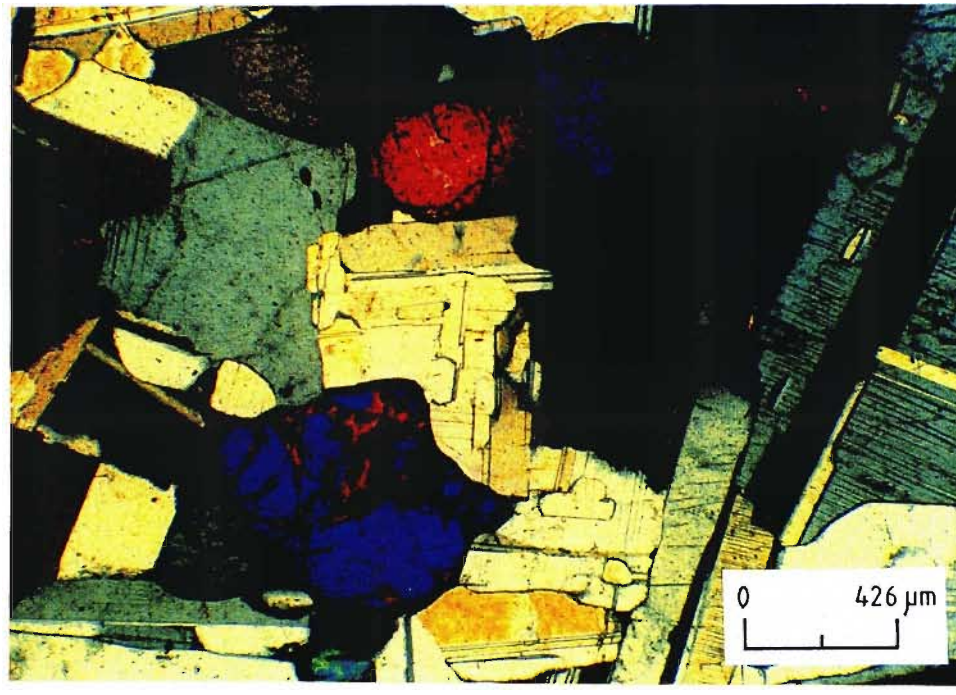

Plate 3.9 Photomicrograph of DM90.20 (Age E) showing subhedral to anhedral olivines (ol) associated with plagioclase feldspars (pl). Note the opaque reaction rims and alteration cracks of the olivine crystals (magnification = 47; cross-polarised light).

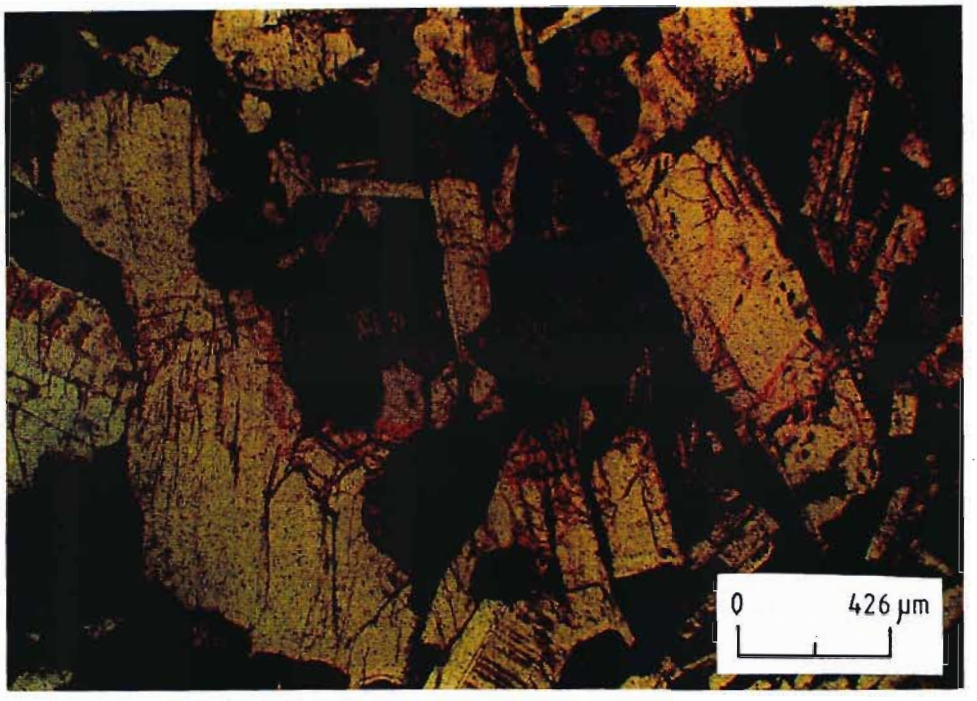

Plate 3.10 Photomicrograph of DM90.30 (Age H) showing olivines (some highly altered) (centre of photograph), associated with plagioclase feldspar phenocrysts (magnification = 47; plane-polarised light).

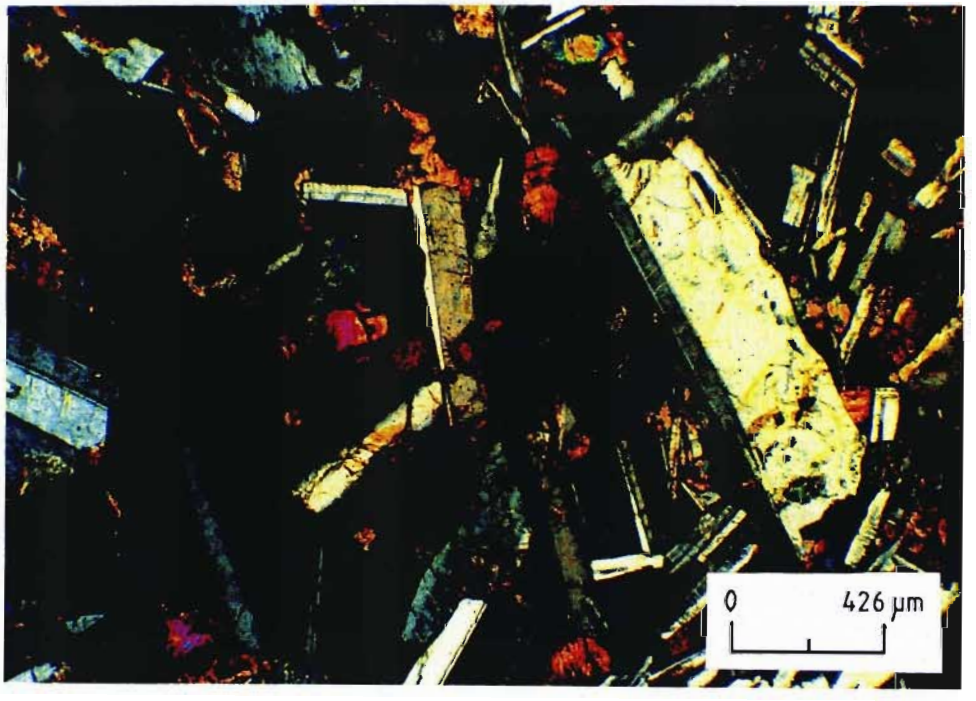

Plate 3.11 Photomicrograph of DM90.30 (Age H) showing olivines (some highly altered) (centre of photograph), associated with plagioclase feldspar phenocrysts (magnification = 47; cross-polarised light).

Muir *et al.* (1957) considered the common opaque reaction rims around olivines as being products of an oxidation reaction:

$$(3Fe_2SiO_4 + 3Mg_2SiO_4) + O_2 \rightarrow 2Fe_3O_4 + 6MgSiO_3$$

olivine — magnetite — enstatite

Kuno (1950) however, has considered this production of an opaque mineral rather to be from a reaction with the liquid and not oxygen.

Iddingsitisation, is a continuous process in the solid state brought about by diffusion of hydrogen atoms into the olivine structure where they become attached to oxygen and release Mg, Fe^{2+} and Si, allowing replacement by Fe^{3+}, Al and Ca ions (Deer *et al.*, 1989).

3.4.2 *Mineralogy*

No olivines from Age H were analysed with the electron microprobe, although petrographic analysis revealed a 2V angle of greater than 80°, suggesting that the olivines are forsteritic in composition i.e. Mg-rich.

Likewise, Age E olivines also showed a very high 2V angle, and the forsteritic composition was confirmed when analysed by electron microprobe. Olivine compositions vary between Fo_{76} and Fo_{78} (Appendix 2c). On the binary diagram by Bowen and Schairer (1935) of the system forsterite-fayalite, at 1 atmosphere pressure, the olivines would have crystallized at 1600°C. Deer *et al.* (1989), find that olivines in the compositional range Fo_{85} to Fo_{40} are very common constituents of gabbros, dolerites and basalts. As previously stated however, olivine is not a common mineral constituent of the Rooi Rand dolerites.

No Ti, Al or Cr were found to be present in the olivines, and only small amounts of CaO (up to 0.41%) and MnO (up to 0.31%) are present. CaO tends to substitute for MgO, and MnO for FeO in the olivine crystal lattice.

Although olivines were only analysed in one sample, for the sake of completion regarding comments on phenocryst versus matrix and chill margin versus centre of dyke crystals, the following relationships have been noted.

Heinrich (1965) noted that in rocks containing phenocryst and matrix or groundmass olivine, the matrix olivines are more Fe-rich (and less Mg-rich). Regarding chill margins and centres, Ernst and Bell (1992) in their study of the great Abitibi Dyke found that centre of dyke olivines are more Fe-rich than those of the chill margins. These statements are in keeping with what was said in the previous sections, with phenocrysts generally representing an earlier, less evolved (Mg-rich) magma, and groundmass crystals forming at a later stage of the magma's chemical evolution. Likewise for the chill margin olivines (the chill margin representing the most primitive magma composition), olivines are less Fe-rich than those of the centre of dyke.

3.5 Opaque Minerals

3.5.1 *Petrography*

The opaque minerals present in all mineral assemblages of sampled dykes are ilmenite and titanomagnetite, with trace amounts of chalcopyrite found in two of the dyke phases. Figure 3.1 of modal mineral proportions in each dyke age shows that a fairly large variation in the opaque mineral contents exists from age to age. The highest proportion of opaque minerals was measured in Age H (9.4%), and the lowest in Age E (3.5%). These reflect the TiO_2 contents of the rock in which they are found i.e. Age E has the lowest Ti whole-rock contents, and Age H has one of the highest Ti contents (Appendix 3a). The ratios of ilmenite to titanomagnetite also vary from age to age.

Magnetites tend to have a more massive tabular appearance than the ilmenites, which are found mainly as skeletal crystals. Ilmenite and titanomagnetite may be seen exsolving one another, and are most frequently found intimately intergrown (Plates 3.12 and 3.13). Ilmenite, titanomagnetite and pyroxene crystals are often intergrown. This often caused problems in the microprobe analyses, and many analyses have low totals, and are combinations of Ti, Fe and Si, sometimes with high Mg and Ca.

Elsdon (1975) noted that many textures of magnetite and ilmenite coexisting, indicate an unmixing process from a single phase Fe-Ti oxide. Microintergrowths of titanomagnetite and ilmenite have been used by Reynolds (1983) to trace variations in oxygen fugacity during the subsolidus cooling histories of rocks.

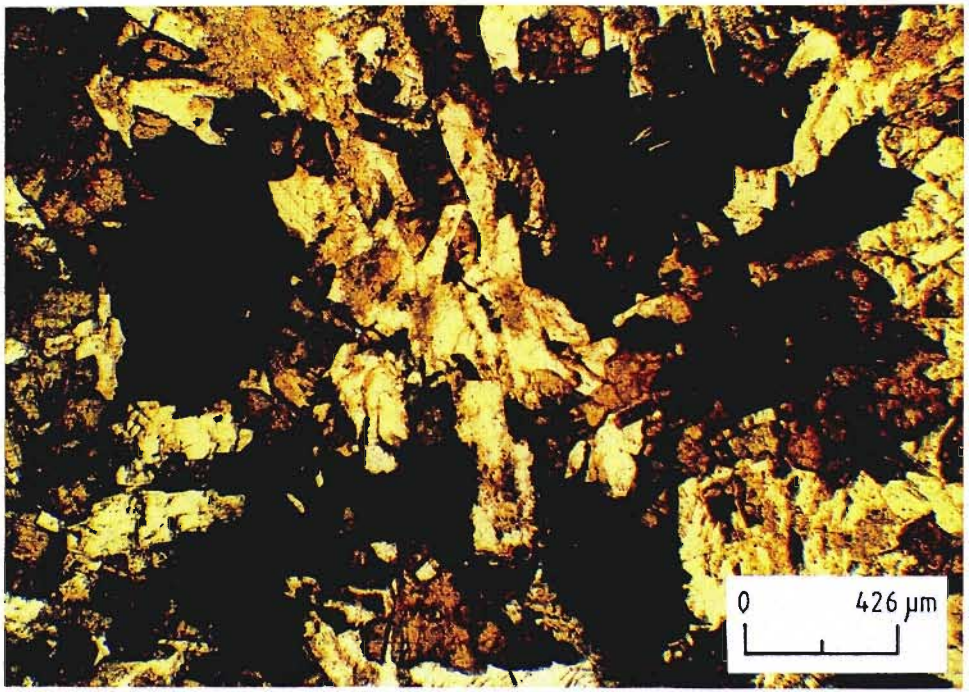

Plate 3.12 Photomicrograph of DM 90.27 (Age F) showing highly intergrown titanomagnetite and ilmenite (opaques) of massive and skeletal habit, surrounded by the major dolerite minerals, augite and plagioclase feldspar (magnification = 47; plane-polarised light).

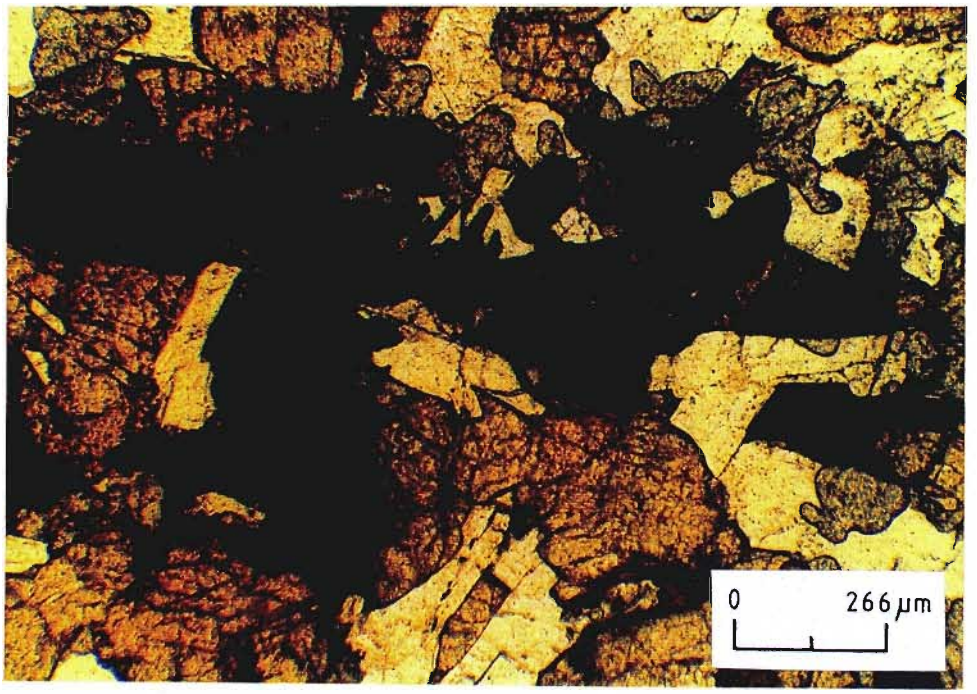

Plate 3.13 Photomicrograph of DM 90.25 (Age G') showing skeletal opaque minerals titanomagnetite and ilmenite intergrown, surrounded by augite and plagioclase feldspar (magnification = 75; plane-polarised light).

3.5.2 *Mineralogy*

Magnetite occurs naturally in solid solution with many spinel components, but the most important is the magnetite-ulvöspinel solid-solution (Waychunas, 1991), $Ti_xFe_{3-x}O_4$ (known as the titanomagnetites) and its oxidation products, the titanomaghemites. In the Rooi Rand dolerites, the titanomagnetites cover almost the entire range of the ulvöspinel-magnetite solid-solution series (Figure 3.13). The variable Ti content of the magnetite may have been caused by subsolidus oxidation-exsolution of ilmenite that partially removed the titanium-bearing components from the magnetite (Reynolds, 1983). Beyond the limits of solid-solution, titanomagnetite shows some compositional variation with minor impurities of Si, Al, Ca, Cr, Mn and MgO being present in small, but variable amounts (Appendix 2d).

On the ilmenite-hematite solid-solution line (Figure 3.13), it may be seen that ilmenite compositions form a tight cluster, near to the theoretical $FeTiO_3$ end member composition, from Il_{90} to Il_{100}. As in the titanomagnetites, ilmenites also contain minor impurities of Si, Al, Ca, Cr, Mn and MgO. Waychunas (1991) found that cation distribution depends strongly on temperature.

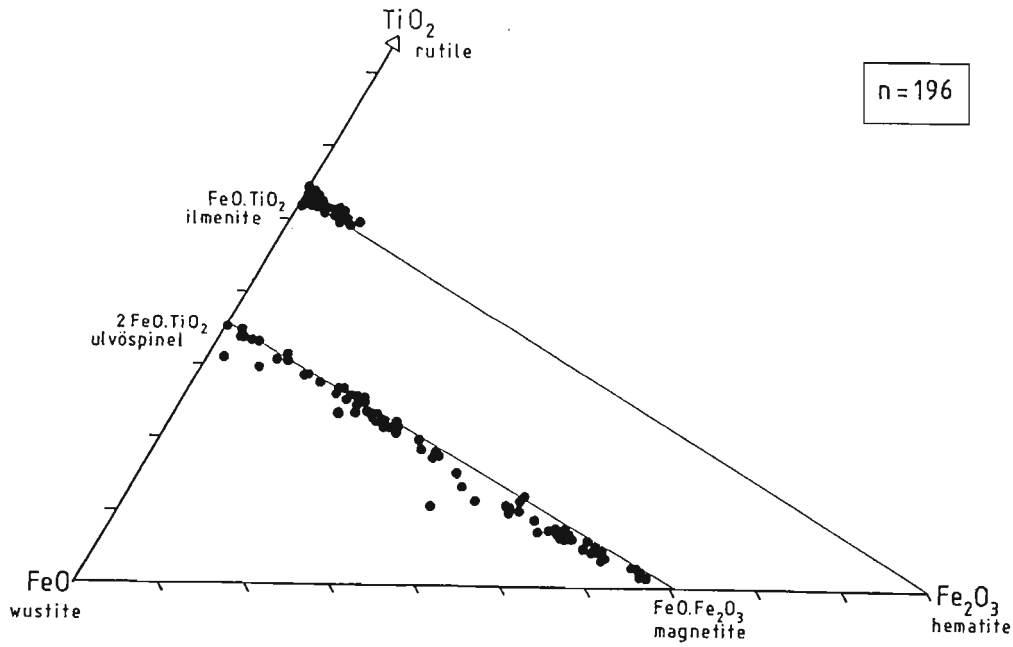

Figure 3.13 Ilmenite and titanomagnetite microprobe analyses (Appendix 2c), plotted on a ternary TiO_2, FeO & Fe_2O_3 diagram (after Oliver, 1978).

Trace amounts of chalcopyrite were noted, most often associated with ilmenite and titanomagnetite.

The Mg and Ti values for the ilmenites plot well into the field of tholeiitic rocks as defined by Haggerty (1976). Tholeiitic rocks should have less than 3% MgO, and minor amounts of MnO or Cr_2O_3 (Cawthorn *et al.*, 1989). Sack and Ghiorso (1991) found that the Cr content of spinels is a sensitive indicator of the degree of fractionation of the host liquids. In the Rooi Rand dolerite ilmenites the Cr_2O_3 contents are negligible, and in the titanomagnetites Cr_2O_3 does not rise above 0.28 wt%. This reflects the generally low Cr levels in the magma at the time of crystallization, and the chemically "evolved" nature of the majority of dyke ages.

Ilmenite may alter in three stages, from patchy ilmenite, to amorphous iron-titanium oxide, to leucoxene. The leucoxene may consist of finely crystalline rutile, or brookite (Deer *et al.*, 1989). This wide variation of alteration products often makes precise identification of the ilmenite alteration product difficult. Titanomagnetite on the other hand, alters to sphene and chlorite (Hugo, 1993). Oxide alteration can also give a good indication of the water present at the time of alteration. Hugo (1993) states that magmatic hydrothermal waters caused most of the Rooi Rand dolerite oxide alteration, which occurred in situ, at a late-stage. This conclusion is however not supported, because there is no evidence in the adjacent Beaufort Group sediments of any hydrothermal alteration.

Neumann (1974) states that Mg and Mn will partition preferentially into ilmenite during crystallization, when it is coexisting with magnetite. A binary diagram of Fe versus Mn contents for a single dyke age (Figure 3.14), shows this to be partly true. MnO tends to increase with decreasing Fe, and increasing Ti.

The proposed relationship by Neumann (1974) regarding Mg and Fe contents cannot be clearly ascertained. This is because the ilmenites and titanomagnetites of the Rooi Rand dolerites contain almost no Mg, but have reasonably high Mn values (up to 3.07 wt% in ilmenite) (Appendix 2d). Reynolds (1983) suggest that a fractional crystallization trend of progressive Mg depletion with time, and Mn enrichment of late stage ilmenite exists.

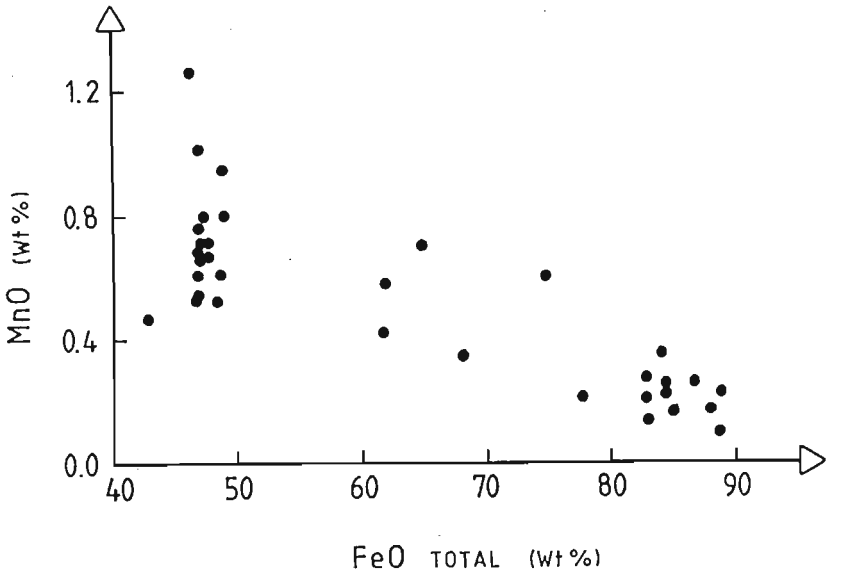

Figure 3.14 Binary diagram of total Fe versus MnO contents for ilmenites and titanomagnetites of sample DM90.25 (Age G') (Appendix 2d).

As with the other dolerite-forming minerals, the opaque minerals also show some chemical variation from chill margin to centre of dyke. Iron oxide variation diagrams have been plotted to illustrate the difference in chemical composition between the chill margin and centre of dyke ilmenites for samples DM90.4 and DM90.5 (Age A) (Figure 3.15). The chill margin ilmenites have far lower Ti and higher Mn values than ilmenites in the centre of the dyke.

In the same dyke phase, SiO2 tends to be at least three times higher in the chill margin ilmenites than those of the centre of dyke (Appendix 2d). This may be due to the fact that the chill margin opaque minerals crystallized very much more rapidly than those of the centre of dyke, and the probability of having silica inclusions and intergrowths will be much higher in the chill margin.

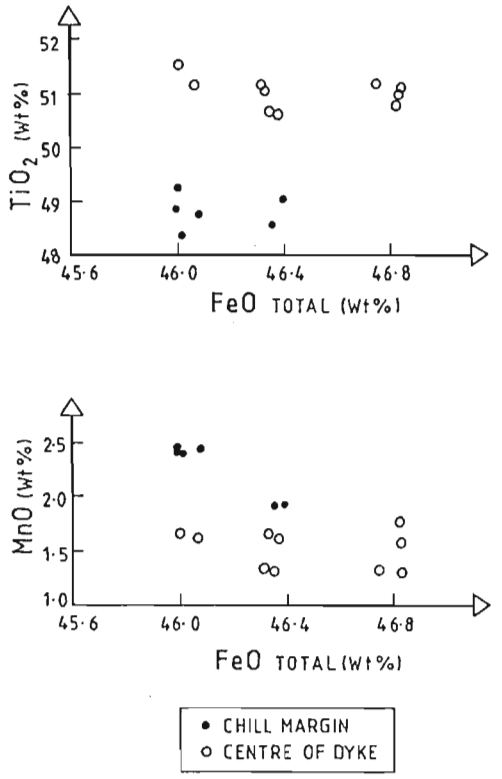

Figure 3.15 FeO variation diagrams for TiO_2 and MnO, for ilmenites of DM90.4 (chill) and DM90.5 (centre) of dyke age A (Appendix 2d).

CHAPTER 4

WHOLE-ROCK GEOCHEMISTRY

4.1 Introduction

The main purposes of gathering whole-rock data are: to classify the rocks geochemically; identify any geochemical trends which might exist; establish whether or not there is a systematic change in dyke composition with age and constrain petrogenetic modelling (Chapter 5).

The centres of 9 of the 11 dyke phases of intrusion were analysed for whole-rock major and trace elements, by means of X-Ray Fluorescence (XRF) Spectrometry, at the erstwhile Department of Geochemistry, University of Cape Town using the techniques described in Duncan *et al.* (1984a) (Appendix 3a). In addition, 3 chill margin samples were analysed. It was not possible to analyse many chill margin phases, due to the difficulty of obtaining sizeable samples, and separating them efficiently enough from the adjoining host rock.

Inductively coupled plasma mass spectrometry techniques were employed at the Department of Geology and Applied Geology, University of Natal, Durban, for the determination of rare earth element (REE) and selected trace element compositions of 8 centre of dyke Rooi Rand dolerite samples (Appendix 3b). For the sake of consistency, only the REE values from the ICP analysis have been plotted. All trace element values used are thus from XRF analysis. To determine the whole-rock composition of a glassy micro-scale dyke, electron microprobe analysis was carried out using a defocussed electron beam. This analysis was done together with the mineral analyses at the erstwhile Department of Geochemistry, University of Cape Town, adopting the same analytical procedure outlined in Appendix 2.

4.1.1 *Chemical Classification*

A weight percent plot of alkalis (Na and K) versus silica, may be used to distinguish alkalic rocks from subalkalic or tholeiitic rocks (MacDonald and Katsura, 1961). Figure 4.1 shows the 13 Rooi Rand samples analysed in this project, as well as those of Armstrong (1978) plotted on this diagram. The dolerites fall clearly within the subalkaline/tholeiitic field, and may thus be classified as tholeiites.

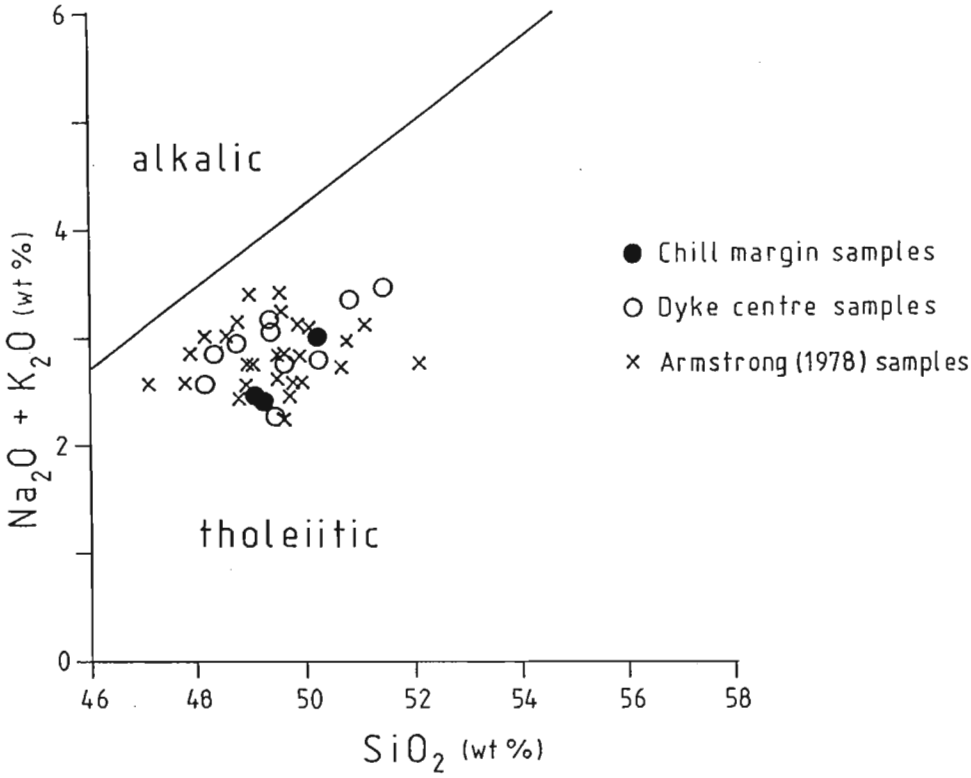

Figure 4.1 SiO_2 vs Na_2O + K_2O diagram after MacDonald & Katsura (1961). All samples are classified as tholeiites.

When the data are plotted on an AFM diagram (Figure 4.2), the dolerites once again fall well into the tholeiitic field defined by Irvine and Baragar (1971). They do not however follow the "main" or "normal" trend of Karoo dolerites, which was given by Nockolds and Allen (1956). Instead, these dolerites show a greater degree of Fe-enrichment than the "main" trend of Karoo dolerites. Nockolds and Allen (1956), and Armstrong (1978), aptly term this as being an "iron-rich" trend.

An alternate definition of tholeiitic rocks, based on petrography, is that of Yoder and Tilley (1962), who define them as consisting of the minerals augite (or subcalcic augite), plagioclase (near An50), and iron oxides. Olivine may be present in small amounts, or absent. Together with the whole-rock data, the mineralogical data from Chapter 3 (which mostly contained the above-mentioned mineral assemblage) indicate that the Rooi Rand dolerites are tholeiites in the mineralogical, as well as geochemical sense.

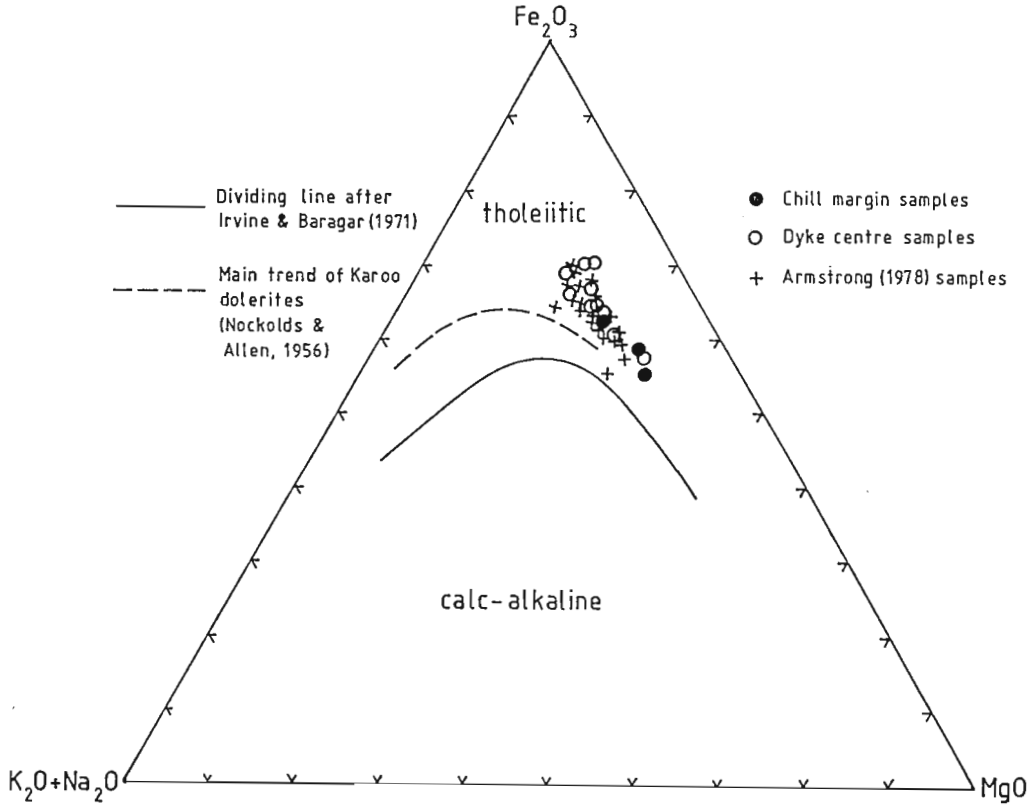

Figure 4.2 AFM diagram for the Rooi Rand Dolerites. The dolerites follow an "iron-rich" trend.

In a MgO vs K_2O diagram for the Lebombo-Nuanetsi-Sabi volcanic rocks, Bristow and Cox (1984) show low-, intermediate-, and high-K fields, superimposed onto rhyolite and mafic (evolved, basaltic and picritic) fields. Most of the Rooi Rand dolerites fall into the low-K basaltic suite, except for Ages B and F (Appendix 3a), which fall into the classification as part of the low- to intermediate-potassium evolved suite.

4.2 Major Elements

Classification parameters for major and trace elements may vary from author to author, and many workers use SiO_2 and sometimes K_2O as a basis for classification (Bristow and Cox, 1984). Petterson and Windley (1992) found only weak correlations for major and trace elements when using traditional fractionation indices such as MgO and SiO_2, and thus used Zr, which showed strong correlations, acting as a very good index of fractionation. The reasonably large variation in Mg values for the Rooi Rand dolerites (4.32 - 7.28 wt%), added to the fact that Mg decreases and Fe increases with increasing fractionation and magma evolution, make MgO a useful parameter against which to plot the Rooi Rand dolerite major and trace elements compositions.

The major element oxides (Appendix 3a), have been plotted against MgO as Harker variation diagrams (Figure 4.3). A distinction has been made between chill margin and centre of dyke samples, although only three chill margin samples were analysed for whole-rock data.

Because a petrographic and mineralogical study was conducted first, much of the noted major element variation between dyke phases is not unexpected. Many of the geochemical differences are reflected in the mineral chemistry. This was also noted by Hall *et al.* (1986) in a study on dykes from the MD tholeiitic dyke swarm, Greenland.

For each oxide plotted, all dyke phases plot in a relatively small field, excepting phase E (chill margin and centre) (Figure 4.3). If decreasing MgO content is a reliable indicator of increasing differentiation, then the following may be noted from Figure 4.3:

1) TiO_2 and Fe_2O_3 both show an increase with increasing differentiation (i.e. decreasing MgO). This increase in Fe content is the normal Fe enrichment trend which any differentiating tholeiitic basic magma should show.
2) Na_2O shows a slight enrichment with increasing differentiation.
3) Al_2O_3 and CaO decrease in concentration with increasing differentiation. CaO is particularly well constrained.

4) K_2O, MnO, and P_2O_5 all show trends of increasing enrichment with increasing differentiation.

5) As Armstrong (1978) notes, SiO_2 behaves fairly erratically, and this may be seen by the poorly defined trend. Nevertheless, the trend is an apparent one of silica-enrichment, or continuous fractionation. As already mentioned, this apparent fractionation trend is noted in most of the major element variation diagrams. **There is however no clear fractionation trend of dyke chemistries changing progressively with the relative ages of the dykes (i.e. with time).** The dykes cannot be said to have formed from a simple process of differentiation in one magma chamber. Their chemistries have resulted from a combination of igneous processes such as partial melting, as well as some fractional crystallization, also with the possibility of having different parent magmas. This observation was not immediately possible for Armstrong (1978) because different dyke ages were not systematically sampled.

6) E stands apart from the other dyke phases in chemistry, and is depleted in Ti, Fe, Na, Mn and P, and enriched in the other major elements, especially Ca and Mg, with respect to all other dolerite phases. Because E has a far higher MgO content than the other phases, it may be thought of as the least evolved of the dolerite phases, at the primitive end of a differentiation trend. Note that E is not the youngest or oldest of the dyke phases.

This is in direct contrast to what Hall *et al.* (1986) found in their study on the MD tholeiitic dyke swarm in Greenland. The swarm has the normal trend of magma evolution with time, the oldest dykes being the most magnesian, and the youngest being the most iron-rich. The oldest dyke has a Mg/(Mg+Fe) ratio of 0.8, and the youngest, one of 0.35.

Cox (1980) pointed out that these major element trends are typical of Fe-enriched continental tholeiitic suites, which are generated by clinopyroxene, plagioclase mineral assemblages (with or without olivine) i.e. gabbroic. These "typical trends" show characteristic strong enrichment in Fe and Ti, with simultaneous depletion in Mg, Ca and Al.

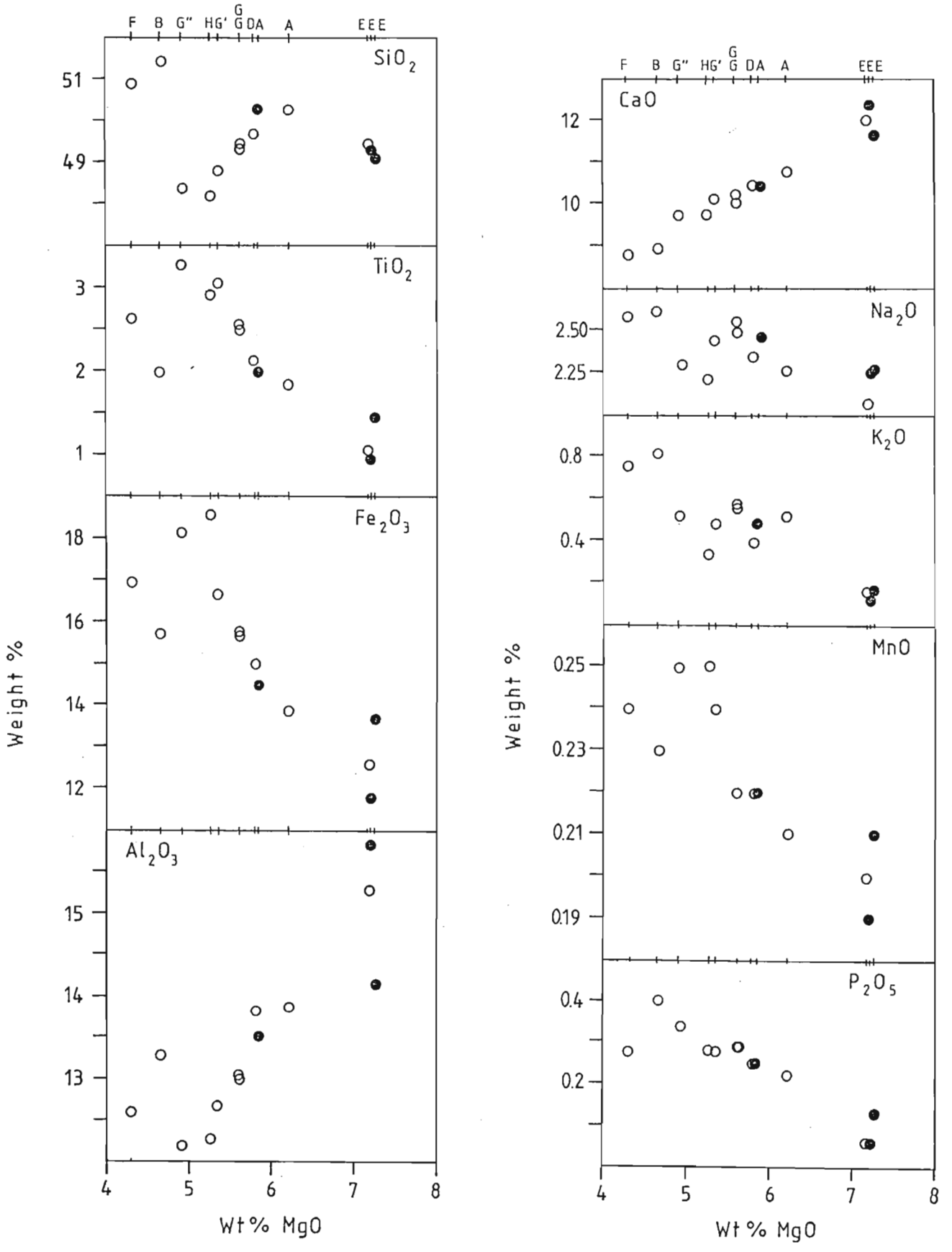

Figure 4.3 Harker-Type Major Element Variation Diagrams for the Rooi Rand dolerites. Oxides versus MgO.
Chill Margin Samples ● Centre of Dyke Samples ○

4.2.1 *CIPW Normative Chemistry*

The CIPW norm enables the determination of the degree of silica-saturation of the rock (Cross *et al.*, 1902). The whole-rock chemical analysis is recalculated into an equivalent assemblage of hypothetical minerals. These are weight percentages of idealized end-members (Table 4.1). They do not necessarily correspond to the mineralogy of the rock. The CIPW norms were calculated using IGPET-II, a GW-BASIC programme (Terra Softa, 1987).

Prior to calculating the norm, a standard Fe_2O_3/FeO ratio must be assumed. The ratio best adopted is debatable, many workers often choosing the ratio of the least oxidised sample of a group and adjusting the others to this value. Alternatively, Brooks (1976) has suggested standardising the analyses of basaltic rocks at an Fe_2O_3/FeO ratio of 0.15. A ratio of 0.2 was chosen so as to be consistent with previous norm data of the Rooi Rand from Armstrong (1978), who did this in order to allow for easier direct comparison with other studies of basalts and dolerites done by Robey (1976) and Bristow (1977).

From Table 4.1, it may be seen that most samples have quartz in the norm. The two samples with very high quartz normative values, Ages B and F, also stand apart on the Harker-type major element variation diagram (Figure 4.3) as being the most silica-rich, and generally the most evolved. Three of the thirteen samples are not quartz normative, but have olivine in the norm. They are those belonging to Age E (chill margin and centre).

According to Yoder and Tilleys' (1962) subdivisions of basalts based on their normative components, the Rooi Rand dolerites vary from oversaturated tholeiites, with normative quartz and hypersthene, to undersaturated olivine tholeiites, with normative hypersthene and olivine. No samples of the intermediate between these two were found, i.e. of a saturated tholeiite, with only normative hypersthene.

Table 4.1 CIPW norms calculated for Rooi Rand dolerite samples. (All samples are centre of dyke unless otherwise stated.)

Q - quartz **or** - orthoclase **ab** - albite **an** - anorthite **di** - diopside **hy** - hypersthene **ol** - olivine
mt - magnetite **il** - ilmenite **ap** - apatite
Plag - Normative Plagioclase (100An/(An+Ab))

	DM90.4	DM90.5	DM90.6	DM90.7	DM90.8	DM90.9	DM90.10
Age	A (chill)	A	G	G	G″	E (chill)	D
Q	2.11	2.18	1.38	1.59	2.89	-	2.07
or	2.90	3.01	3.43	3.25	3.13	1.00	2.36
ab	21.15	19.29	21.58	21.24	19.55	19.29	19.89
an	24.50	26.38	22.34	23.07	21.68	28.15	26.14
di	21.65	21.49	21.23	21.85	20.84	23.82	20.06
hy	19.65	20.10	19.80	19.71	20.30	18.60	20.64
ol	-	-	-	-	-	2.46	-
mt	3.22	3.07	3.49	3.51	4.05	3.03	3.32
il	3.82	3.48	4.82	4.82	6.29	2.75	4.03
ap	0.58	0.53	0.67	0.67	0.79	0.30	0.58
Plag	54	58	51	52	53	59	57

	DM90.18	DM90.19	DM90.20	DM90.25	DM90.27	DM90.30
Age	B	E (chill)	E	G′	F	H
Q	4.63	-	-	1.95	5.06	2.57
or	4.79	0.71	0.95	2.90	4.43	1.95
ab	22.09	19.29	17.60	20.82	21.83	18.95
an	22.16	33.15	32.21	22.36	20.64	23.03
di	16.38	23.51	22.46	21.98	17.87	20.50
hy	20.59	14.72	20.75	19.31	19.48	22.69
ol	-	4.30	0.74	-	-	-
mt	3.47	2.62	2.80	3.71	3.74	4.16
il	3.76	1.80	1.99	5.83	4.96	5.60
ap	0.93	0.14	0.14	0.65	0.65	0.65
Plag	50	63	65	52	49	55

Although normative values should not be expected to correspond to the mineralogy of the rock, they do closely approximate the mode in most cases (Table 3.1, pg 23). For example, Ages B and F have the highest normative proportions of quartz, and were the two ages which have quartz in the mineral assemblage. Opaque mineral proportions are also fairly accurate, with Age H having the highest proportion of total opaque minerals in the norm (mt + il), as shown in the modal analysis, and Age E having the lowest also in both cases. On the major element variation diagram (Figure 4.3), the three Age E samples plotted apart from the others, always being far more Mg-rich, and generally least evolved. Age E is the only sample in which olivine is present in significant amounts in the modal analysis, and it is not surprising that normative calculations showed olivine to be in the norm for this dyke phase only. Although Age E′ was not chemically analysed, it is expected from the petrography that it also has normative olivine present.

It is characteristic of most tholeiites that the percentage olivine in the mode exceeds that in the norm (Yoder and Tilley, 1962). This may due to the fact that olivine normally occurs as phenocrysts and did not attain equilibrium with the groundmass. In Age H, the presence of olivine (although small) is not reflected in the norm calculation. Age E shows 5.1% olivine in the modal analysis, but only 4.3% in the norm.

Yoder and Tilley (1962) also state that most basalts contain less than 1% K_2O and this will contribute at the most, 5.9% Or in the norm. Unless normative Or exceeds 7%, rocks of basaltic composition will rarely contain potash feldspar. DM90.18 (Age B) has almost 1% K_2O, and shows 4.79% normative Or (the highest of all dolerites in this study), also having the most orthoclase-rich feldspars (Appendix 2a).

A diagram of normative plagioclase versus Mg-number has been plotted (Figure 4.4). Normative plagioclase is another well-used classification parameter (Bristow and Cox, 1984). The normative plagioclase value will increase with increasing normative anorthite. The diagram shows a clear positive correlation of increasing normative anorthite, with increasing Mg-number i.e. more primitive rocks will tend to have higher anorthite components in their plagioclases (this has been demonstrated in this study, Chapter 3).

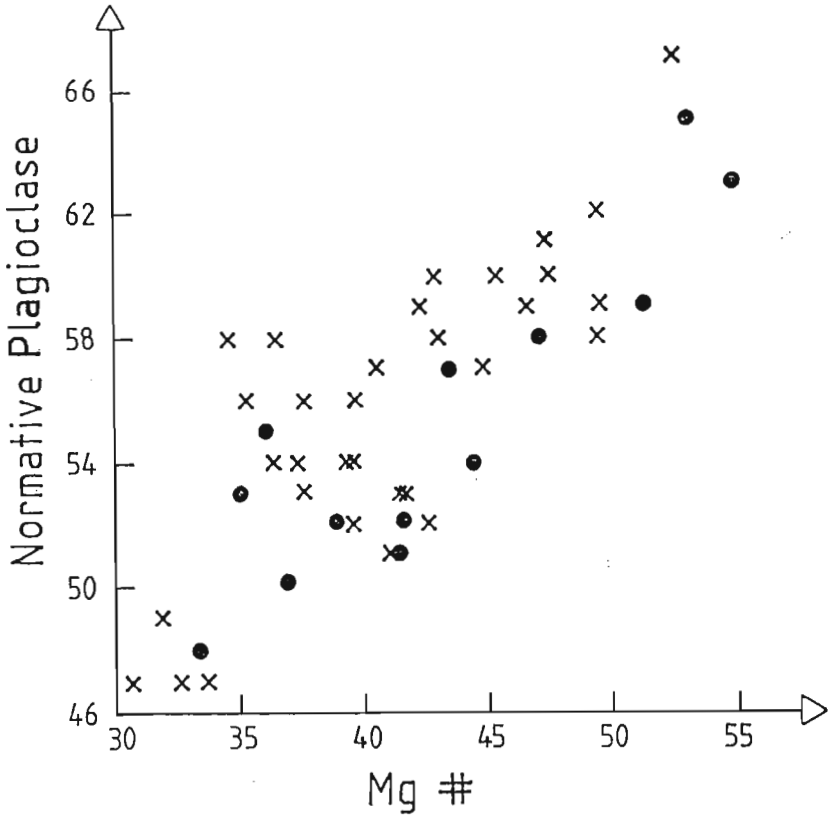

Figure 4.4 Diagram of Normative Plagioclase (100An/(An+Ab)) versus Mg-Number, for Rooi Rand samples from this study and Armstrong (1978).

● samples from this study x Armstrong (1978) samples

4.3 Trace Elements

The trace elements (Appendix 3a), have also been plotted as MgO weight percent variation diagrams. These may be seen in Figure 4.5. As noted with the major elements, dyke phase E is also very chemically different with respect to trace elements. It is greatly enriched in Cr, Ni and Co with respect to the other dyke phases. The only trace element in which it does not show much variation from the main group of dyke phases is Sc.

Using MgO as an index of differentiation, trace elements which show enrichment with increasing differentiation are; Rb, Ba, Sr, Y, Zr, Nb, V, Cu, Zn and Mn. Many of these elements are those which are incompatible with respect to an assemblage of normal peridotitic mantle minerals (olivine, pyroxene, spinel and garnet), and are termed large ion lithophile (LIL) elements. On the other hand, Ni, Co, & Cr (compatible elements which will be preferentially retained in the residual solids during partial melting, and extracted in the crystalline solids during fractional crystallization) become progressively

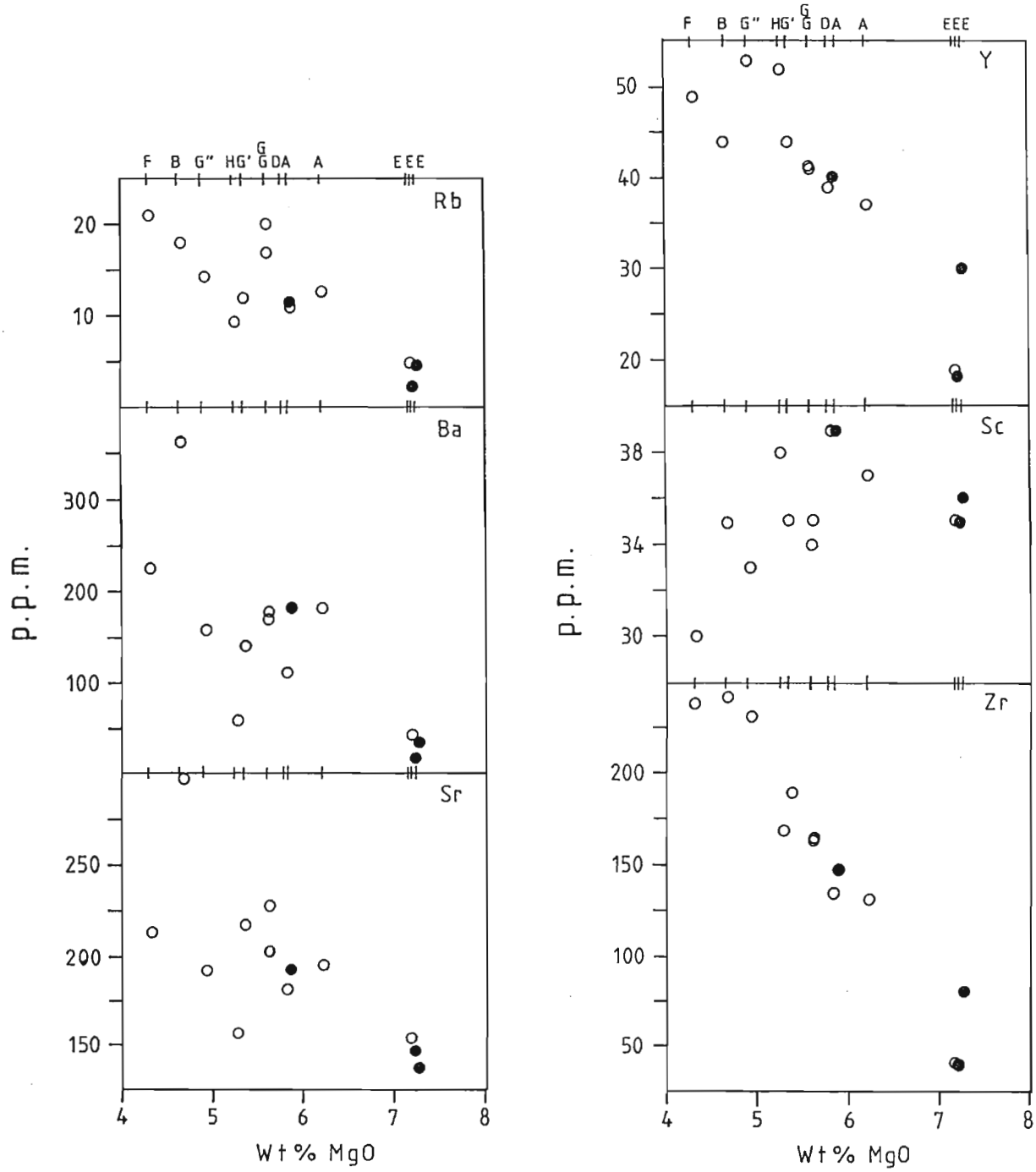

Figure 4.5 Harker-type Trace Element Variation Diagrams for the Rooi Rand dolerites. Trace elements versus MgO
Chill Margin Samples ● Centre of Dyke Samples ○

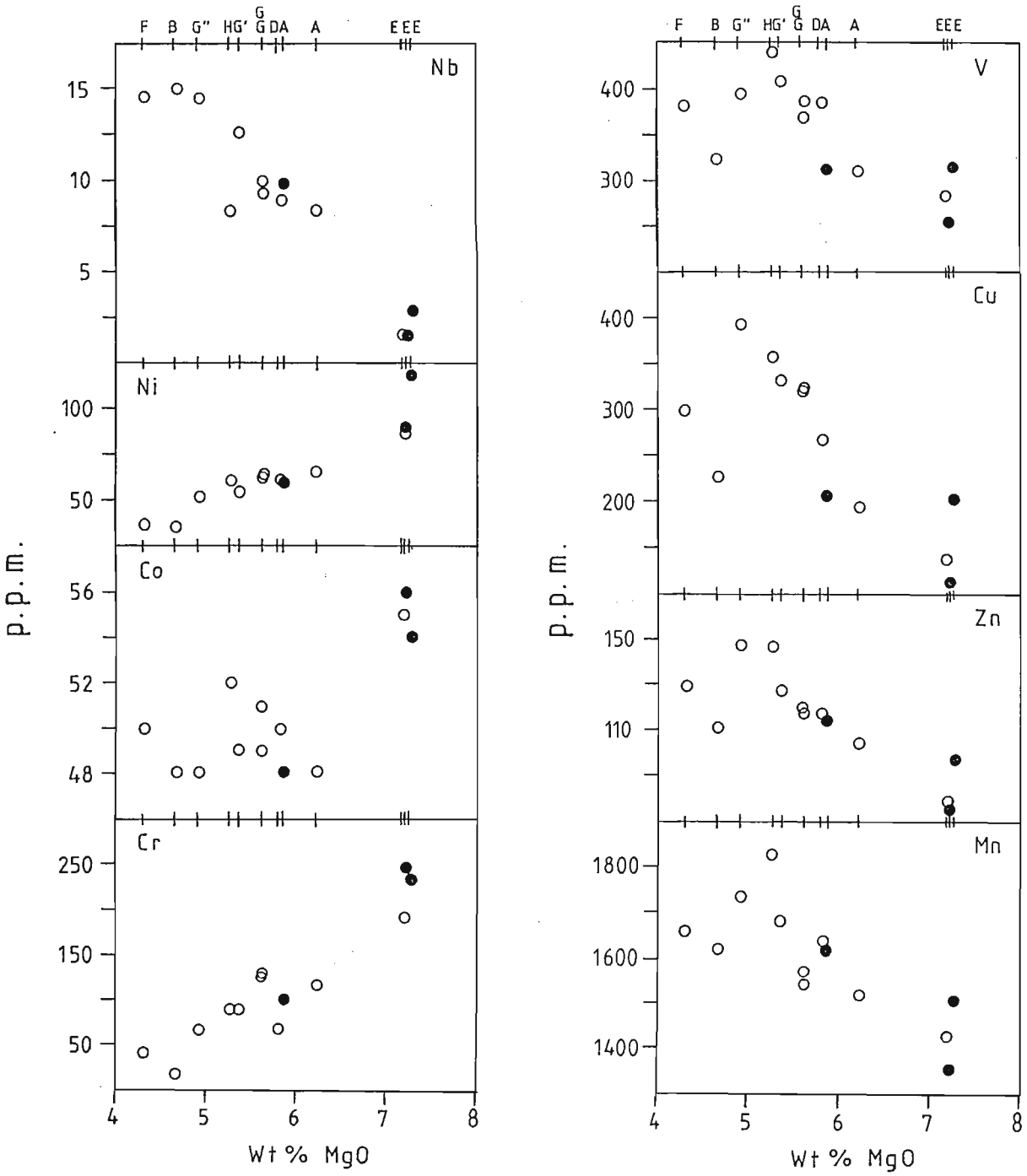

Figure 4.5 (contd.) Harker-type Trace Element Variation Diagrams for the Rooi Rand dolerites. Trace elements vs. MgO
Chill Margin Samples ● Centre of Dyke Samples ○

depleted as differentiation of the magma proceeds. Sc appears to remain relatively constant with increasing differentiation.

With Sc not showing any real trend when plotted against MgO, the use of MgO as a differentiation index was reconsidered. Using Zr as a differentiation index for Sc (Petterson and Windley, 1992) the correlation is only slightly improved, and with increasing Zr (i.e. increasing differentiation), Sc tends to decrease (Figure 4.6). The only samples which do not fit on the clear trend are those of Age E. This would tend to imply a completely different parent magma for Age E. This will be discussed further in Chapter 6. When replotted against Zr, the other trace elements tend to show the same trends as before, so have not been shown.

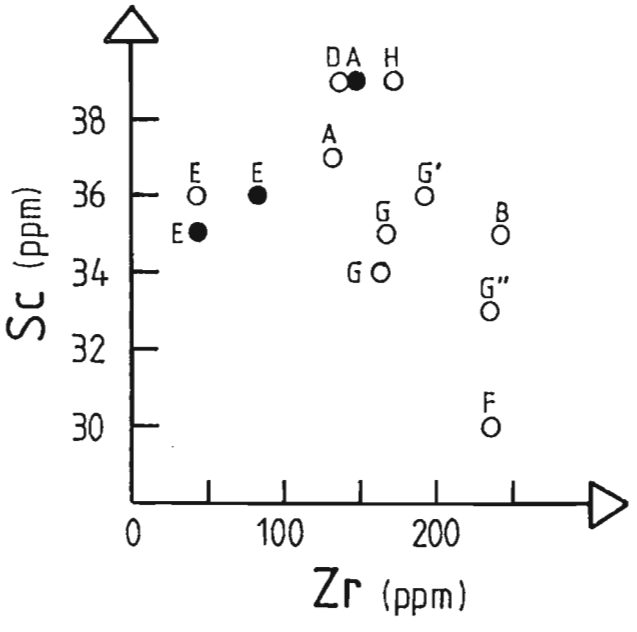

Figure 4.6 Harker-type Trace Element Variation Diagram for the Rooi Rand dolerites. Sc versus Zr (ppm)
Chill Margin Samples ● Centre of Dyke Samples ○

The behaviour of V will parallel that of Ti (Green, 1980), when they have been together as part of the same melting and crystallization process. On Figures 4.4 and 4.5 the Ti and V trends are fairly similar. Similar trends are useful pointers to the fractionation of Fe-Ti oxides, such as ilmenite and titanomagnetite.

4.4 Rare Earth Elements

Results from the rare earth element (REE) analyses obtained using ICP-MS techniques may be seen in Figure 4.7 (Appendix 3b). Concentrations have been normalized to abundances in chondritic meteorites, using the values of Evensen *et al.* (1978) (Appendix 3b). Normalisation allows for easier graphical comparison of REE abundances in rocks, eliminating the Oddo-Harkins effect, which is the existence of higher concentrations of those elements with even atomic numbers compared with those having odd atomic numbers. The chondrite normalized plot (Figure 4.7), shows the REE profiles for the 8 different samples. Tb, Ho and Lu have not been plotted due to the poor working curves obtained during the analytical procedure.

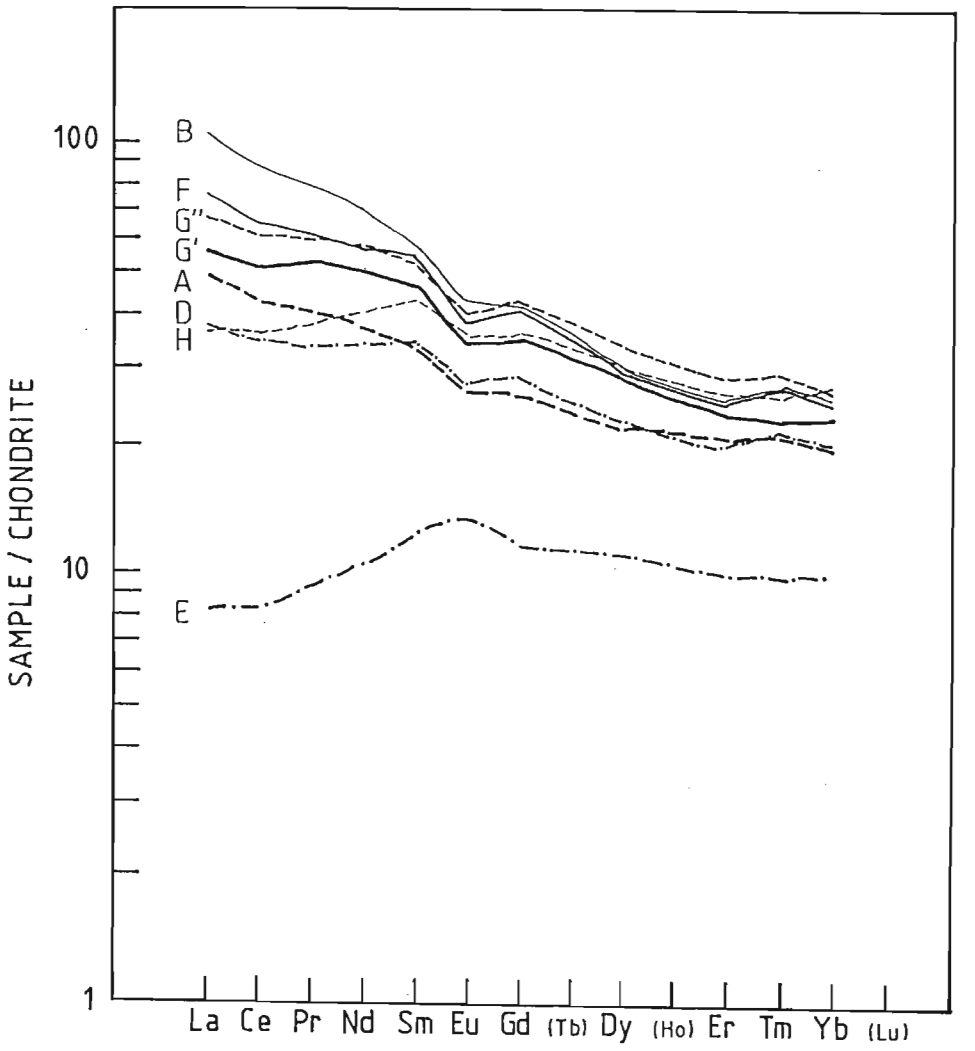

Figure 4.7 Chondrite-normalized REE profiles (Appendix 3b), for the Rooi Rand dolerites.

All profiles, except that for dyke phase E, show slight relative enrichment in the light REE (LREE), and slight depletion in the heavy REE. Dyke phase E is depleted in all REE with respect to the other 7 dyke phases, and is slightly depleted in LREE and HREE. It is not surprising that the REE profile for this age should appear different since it stood apart from the other phases in major and trace element composition (Appendix 3a) being the least evolved dolerite.

The profile of phase E typifies one of a primitive magnesian Mid-Ocean Ridge Basalt-type (MORB) profile. Duncan *et al.* (1990), infer from the slight LREE depletion, an asthenospheric source for this dyke phase. The profiles for the more evolved dyke phases, may be interpreted as similar to continental tholeiite, or similar to enriched MORB-type profiles.

In an earlier assessment regarding the REE character of the Rooi Rand dolerites, Duncan (1987) referred to the "flat" MORB-like Age E profile as being that typical of the Rooi Rand dolerites. It should be noted here that this profile shape was only found in one out of eight dyke phases analysed. (Of the three dyke ages for which there are no REE analyses, G, E′ and C, it is assumed that E′ will have a similar profile to E, because of their similar mineralogies and relative ages. This would then imply that only two of the eleven dyke ages systematically sampled over the 600m-long dyke outcrop in the study area have flat MORB-like profiles).

Consequently it is not considered to be the dominant REE composition for the Rooi Rand dolerites (this also applies to the trace elements, which are also not all considered to be MORB-like in character). Duncan *et al.* (1990) later reported finding Mg-rich and -poor samples in the Rooi Rand dolerites, each exhibiting different REE profiles (i.e. flat and steep profiles). The significance of this MORB-like flat profile being found in only two of the eleven dyke phases will be discussed in the following chapters.

4.5 Intra-dyke whole-rock variation

4.5.1 *Whole-rock variation from chill margin to dyke centre*

Only 3 chill margin samples were analysed for whole-rock data. Chill margin and centre of dyke minerals for most ages were analysed by microprobe, and this data is primary in ascertaining basic chemical trends.

If a dyke is chemically zoned according to a fractionation trend, such as that of the crystallization of plagioclase, augite, olivine and opaques, it is expected that MgO and CaO will decrease towards the dyke centre, and incompatible trace elements will increase. Ransome and Reid (1988) consider the observed fractionation trend towards the dyke centre as representing a cooling profile through the dyke.

In this study, only two dyke ages, A and E have corresponding centre and chill margin whole-rock compositions. Age E shows the expected "normal" variation from chill to centre, with the trace elements showing this more clearly than the major elements.

Age A on the other hand, shows the reverse to this, the chill margin being lower in Mg and Ca, and higher in the incompatible trace elements. Ransome and Reid (1988) when finding this reverse zoning in one of the dykes they studied, attributed it to the mechanical process of flow differentiation, where early fractionating phases such as plagioclase will be concentrated at the dyke centre. In addition, if phenocryst interaction is great, a size sorting may arise, with the largest phenocryst grains preferentially found in the centre of the dyke (Komar, 1972). These mechanical phenocryst redistribution effects, accompanied by geochemical zoning reversals, have also been recognised by Ross (1986). Although dyke Age A shows opposite zoning, the plagioclase compositional variations found in normally zoned dykes, of decreasing anorthite towards the centre of dyke are also present. Ross (1986) however, upon finding this normal change in plagioclase composition from chill margin to centre of dyke, could not attribute it to flow differentiation.

Ernst and Bell (1992) in the study of the Great Abitibi Dyke (GAD), stated that chilled

margins give the composition of the parent magma. The entire range of chemical compositions from the GAD can be produced by fractional crystallization of a magma of similar composition to the chill margin.

4.5.2 Zoning across a micro-scale dyke

Chemical zoning in dykes is a well-known phenomenon. Very few reports have been found where the dyke being traversed is on a micro-scale. A millimetre-scale dyke cools rapidly, and is most often too narrow to consist of anything but a glass phase with phenocrysts. Whole-rock analyses may be obtained by defocussing the electron beam of the electron probe microanalyser on areas which are extremely fine-grained, such as a glassy groundmass, or chill margins of a dyke. It was thus possible to determine whole-rock major element analyses using this method across an entire dyke.

Twenty-three major element whole-rock analyses were obtained from a traverse across an 8mm wide dyke (Appendix 3c). The analyses have been plotted as zoning profiles of the major elements (Figure 4.8), to ascertain whether or not the dyke is chemically zoned.

It was revealed that the dyke, even though only 8mm wide, is chemically zoned, showing relatively symmetrical zoning profiles from the chill margin inwards towards the centre, for almost all major elements.

The dyke has a porphyritic texture, with phenocrysts (mainly plagioclase) in a glassy groundmass (Figure 4.8). It appears to consist of three main zones; the chill margin (which consists of two zones), and the centre.

The chill margin zones may be readily distinguished from the centre, by textural appearance (petrography; Figure 4.8 left), and in the chemical zoning profiles (Figure 4.8 right). All major elements except K_2O show chemical zoning within the chill margin. The most primitive areas are the three chilled samples on the left, and one on the right. Three other chilled margin samples on the right seem to have been chemically modified. This gives a correspondence of petrographic and chemical data on the left, but not on the

right. Possible reasons for this will be explained at a later stage.

Chemical zonation within the centre of the dyke is however, not as clear. What is evident though, is that in most cases, with increasing CaO, FeO and MgO contents, Na_2O, Al_2O_3 and K_2O contents decrease proportionally, and vice versa. The "normal" zoning referred to in the previous section, is present, with CaO and MgO values being highest at the chill margin of the dyke.

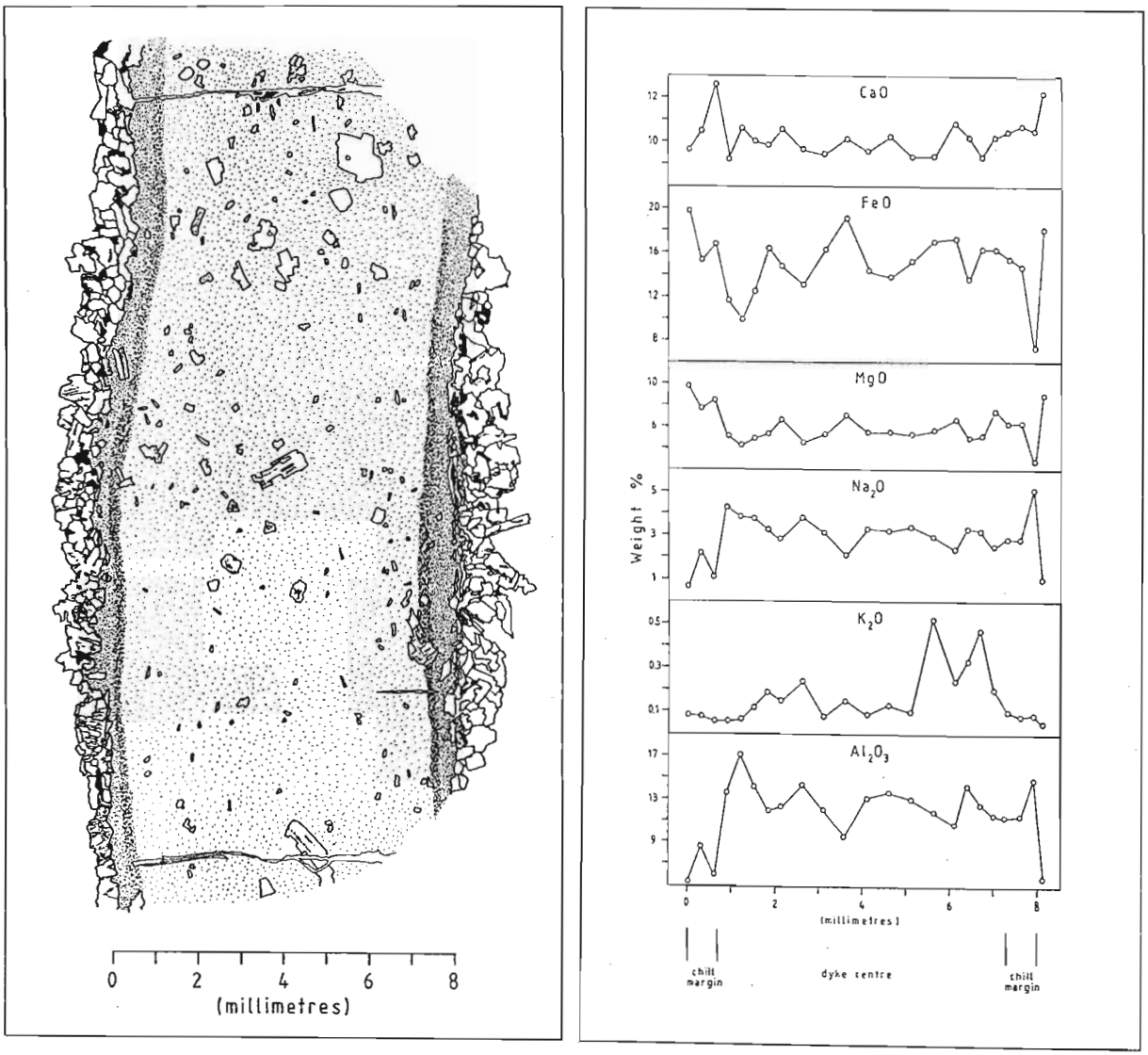

Figure 4.8 Diagrammatic representation of the small dyke (DM90.11) (left), and selected major element zoning profiles thereof (right) (Appendix 3c).

Huppert and Sparks (1989) modelling thermal conditions at a chill margin predict three types of contacts related to the balance between the heat flux of the magma, and the conductive flux of the rock:

(a) If the heat flux of the magma never exceeds the conductive flux, a normal chill margin may be formed, with grain size gradually increasing away from the chilled contact.

(b) If however the heat flux of the magma comes to exceed the conductive flux, the chill margin can be remelted, but some of it will remain as the heat flux drops below the conductive flux once more. This is termed meltback, where the initial chill margin is not completely redissolved. A small internal igneous contact will be observed, and resorbtional textures might be found in the initial chill margin following remelting. Huppert and Sparks (1989) mention that in reality, the internal contact might be gradational. There may also be some change in composition during meltback due to internal differentiation, and the internal contact may thus also be distinguished by a compositional break.

(c) The third type of margin is that where meltback is complete, and country rock may then be melted and assimilated.

The above possibilities may assist in interpreting the profiles in Figure 4.8. For most of the elements, there is an abrupt change in chemical composition at the edges of the inner chill margin, towards the centre of the dyke. This may mark an internal contact, because there is definitely not a gradual change in composition from the edges of the chill margin inwards. The meltback phenomenon, where some of the initial chill margin is preserved aids in explaining why texturally and chemically, there appear to be two zones of chill margin. Taking into account the non-correspondence of textural and chemical data for the right side of the dyke, it also points to the suggestion that this side has suffered more melt-back (or re-equilibration with the centre) perhaps as a result of the dykes orientation from the vertical.

Precisely what was observed at the Rooi Rand was noted by Brouxel (1991), who found

chemical discontinuities and large variation within the chill margin of a dyke 1.5 metres in width. He observed 3 different geochemical zones, two being in the chill margin. He ascribes these differences to several pulses of magma being injected one after the other, and the phenocrysts therein being affected by flow differentiation mechanisms. He did not however consider the phenomenon described by Huppert and Sparks (1989).

It must be remembered however, that what has been said has only been tested on large-scale examples. The feasibility of thermal conditions being identical for such a small dyke is not known.

Ross (1986) states that the concentration of phenocrysts will increase towards the central axis of the dyke as a result of flow differentiation. There may be a large variation in the distribution patterns of phenocrysts. The most common pattern of distribution, is that where phenocrysts progressively increase in concentration and size from the chill margin to the centre of dyke.

There does not seem to be any central concentration of phenocrysts in the dyke being studied, and the dyke appears too narrow to have hosted several magma pulses. The interpretation preferred for this study, is that given by Platten and Watterson (1987). They infer a process of progressive inward growth of marginally accreting material, where the zoning does not represent a pattern developed by flow differentiation (within the flowing magma), but allows the dyke profile to be interpreted as a time profile, thus inferring something about the history of flow in the dyke fissure. The zoning which is present in the dyke being studied would be described by Platten and Watterson as a "wall-parallel layering". This wall crystallization, controlled by heat loss, requires on both walls of the inwardly accreting dyke, inwardly advancing interfaces between accreted rock and the flowing magma. The "meltback" model proposed by Huppert and Sparks (1989) may be combined with this crystallization model, depending on the thermal regime present in the dyke at the time of crystallization.

On a visual estimate, the central portion of the dyke DM90.11 appears geochemically incoherent. This does not however take into account variation which may have been

introduced by the effects of the electron beam sampling, nor the effects of errors or confidence limits for the analyses.

Regarding the unclear zonation within the centre of dyke DM90.11, Ransome and Reid (1988) found a geochemically incoherent zone in a marginal zone (between chill margin and centre), where there were many fluctuations in major and trace element values. They ascribe these to post-crystallization effects resulting from the interaction of the dyke with a hydrothermal system generated in the surrounding granite country rock. They report that the effect on the chill margin is small, and chemical homogeneity is retained there. The marginal zone is adjacent to the chill margin, and is approximately 0.5m and 5m wide in two sections studied (of a 45m-wide dyke). Beyond the marginal zone towards the central portion of the dyke, the altered incoherent geochemistry is not noted, and the profile returns to one signifying closed system fractional crystallization.

It is possible that dyke DM90.11 has been hydrothermally altered, but there is no central unaltered portion of the dyke. It is assumed that this is due to size variations between the dykes under consideration. The dyke studied by Ransome and Reid (1988) was 45m wide as opposed to the 8mm-wide dyke in this study. It is possible in this case therefore, that the entire 8mm-wide dyke should be altered leaving no pristine central portion.

CHAPTER 5

PETROLOGICAL MODELLING

5.1 Introduction

Petrological modelling has not been undertaken in great detail because of the limited data available. This chapter examines models of different igneous processes which may have contributed to the formation of the Rooi Rand magmas, using in most cases, worked examples and ideas from other authors as the foundation. Many inferences have been made based on the small amount of data at hand. It is therefore not considered within the scale of this project to arrive at any one outright conclusion.

In the geochemical modelling, major elements are used to place a constraint on the fractionating phases, and this information is used to constrain trace element models. When carrying out geochemical modelling, close major element matches cannot be solely relied upon. This can be highly unreliable, and almost any model can be made to fit if one manipulates mineral input data and distribution coefficient parameters. It is essential that once the model appears to work for major elements, it is verified against the trace elements, and most importantly, against the rare earth elements (REE's).

This chapter concentrates on two main processes - fractional crystallization and partial melting. Possible contamination processes, and combined contamination and fractional crystallization are also assessed.

Fractional crystallization and partial melting are the two primary petrogenetic processes occurring which may alter a magma's composition (Cox *et al*, 1979). REE profiles from fractional crystallization and partial melting processes tend to differ greatly. Because the Rooi Rand dolerites have been analysed for REE, and the relative ages of the dykes are known, it is possible to examine the profiles and make certain inferences regarding their genesis. Using the standard models and equations for these two processes, the various phases of the dolerites may be geochemically related to one another.

During fractional crystallization, the REE as incompatible elements, become more concentrated in the liquid as crystallization progresses (Cox *et al*, 1979). With increased fractionation, the proportion of REE in the melt increases. The profile slope does not change much from its original value, and the relative concentration of REE's simply becomes greater (Figure 5.1).

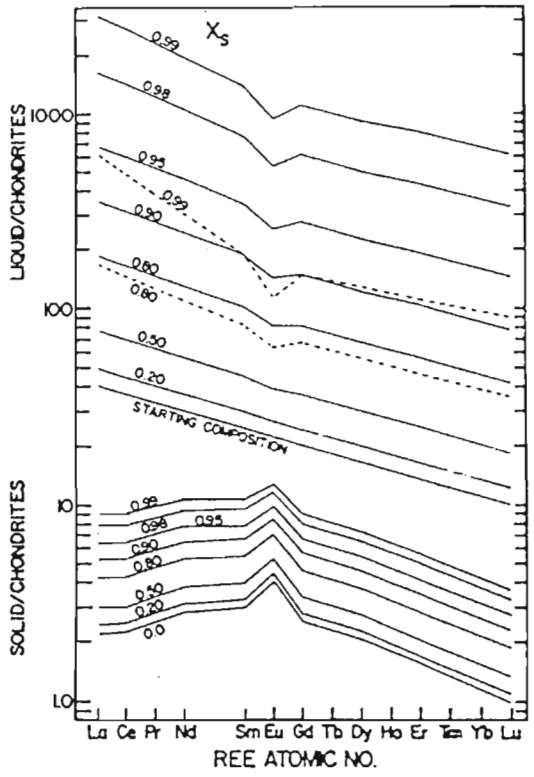

Figure 5.1 Chondrite-normalized REE profiles, showing concentrations in liquid and solid phases after crystallization of a liquid of the starting concentrations shown. Mineralogy of the solid is 20% olivine, 40% plagioclase, and 40% clinopyroxene. Solid lines are for fractional crystallization, dashed lines for equilibrium crystallization. X_s is the fraction of solid (from Haskin, 1984, Figure 4.2).

For partial melting, when only a small proportion of the solid has melted, light REE (LREE) will be most enriched in the liquid, and Eu is most selectively retained by the solid (Hanson, 1989). This is as a result of the higher values of D (the distribution coefficient) for heavy REE (HREE) for clinopyroxene and garnet than for LREE. REE magma profiles related by partial melting processes will change from being very steep for low degrees of partial melting, and flatten out for successively higher degrees of partial melting, as the melt composition becomes closer to that of the source material (Figure 5.2).

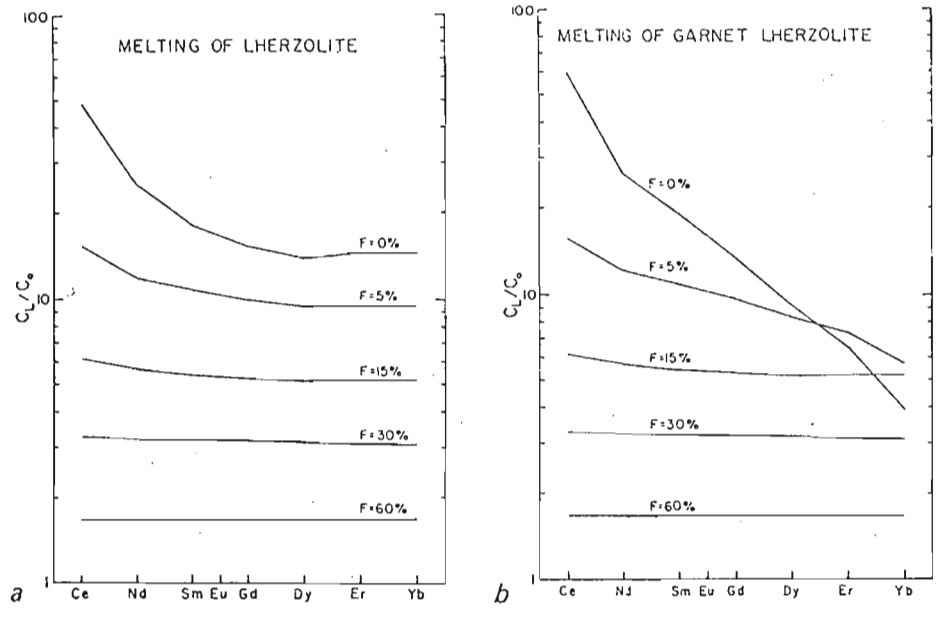

Figure 5.2 Calculated REE patterns for melts derived by batch melting of lherzolite consisting originally of (a) 55% olivine, 25% orthopyroxene and 20% clinopyroxene, (b) 55% olivine, 25% orthopyroxene, 15% clinopyroxene, and 5% garnet (from Hanson, 1980). Data are normalized to the original lherzolite REE composition.

Such explanations for variations in REE profiles can be applied to the Rooi Rand REE profiles (Chapter 4, Figure 4.7). However, before modelling proceeds, it must be remembered that REE analyses were only obtained for 8 of the 11 dyke phases. Age G has no complete REE analysis, and Ages E′ and C have no chemical analyses. These dykes were only sampled at a very late stage in the project, after revised mapping of the area took place. Age G does however have an XRF whole-rock analysis, with some REE, and fits geochemically between the compositions of Ages H and G′ (Appendix 3). This should be remembered when working with models including Ages H and G. It is assumed from very similar mineralogies (Table 3.1, Chapter 3) that Age E′ is very similar in composition to Age E, and likewise, a possible geochemical equivalent for Age C has thus been taken as Age G′.

Separating the REE profiles into different age groupings (Figure 5.3), the following may be noted:

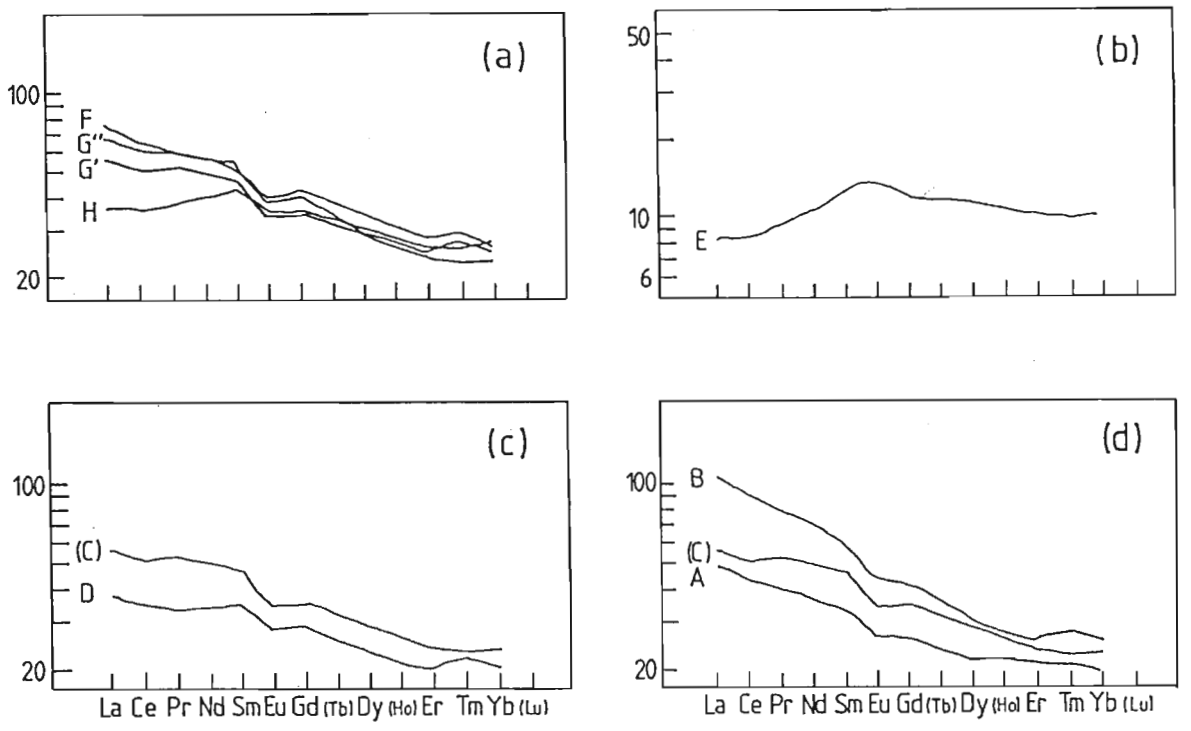

Figure 5.3 Chondrite normalized REE profiles of the Rooi Rand dolerites, divided into possible petrogenetically inter-related suites. a,b,c & d explained below. Age C presented in brackets because it is a hypothetical composition.

(a) Ages H, (G), G′, G″ and F appear to form a consanguineous suite of gradually decreasing degrees of partial melt of the same parent (the changing profile slopes with age would point to this).

(b) As mentioned in the previous chapter, Age E differs greatly from the other profiles, being depleted in all REE's with respect to the other dyke phases, and having a flatter MORB-like profile.

(c) Age C appears slightly steeper than Age D, although they do not cross each other.

(d) Ages C, B and A have similar profile shapes, but varying degrees of REE enrichment, which would suggest that they are genetically related by fractional crystallization.

Because phase E represents an unevolved or depleted magma composition in comparison to the other phases, it provides a suitable model source composition for the other phases, which are more evolved or enriched in composition. In addition, mid-ocean ridge basalt (MORB) and mantle compositions were also used as hypothetical source compositions.

An important point to remember is that each calculation only models a single process or,

if more than one fractionation or melting event has taken place, the net result of several superposed processes.

5.2 Fractional Crystallization

Modelling of fractional crystallization processes, was undertaken to evaluate the possibility of the 9 analysed Rooi Rand dolerite phases (including (C)) representing a consanguineous suite of magmas, related to a parent magma, which may or may not be one of the Rooi Rand phases analysed.

Only models that satisfy the trace element and REE variations, as well as the major element constraints, may be regarded as valid.

5.2.1 *Major Elements*

Major element modelling was undertaken using the least-squares approximation technique of Bryan *et al.* (1969). Based on the program LSPX (written by L. Finger, a co-author of Bryan *et al.* (1969)), a computer-based least-squares mixing program called MIXER, was written by A.R. Duncan at the erstwhile Department of Geochemistry, University of Cape Town.

MIXER was also used by Armstrong *et al.* (1984) to investigate whether the Rooi Rand magmas are related by low pressure crystal fractionation processes. Because analyses used were derived from a wide geographical area, and showed large degrees of scatter on variation diagrams, Armstrong *et al.* (1984) modelled fractionation of the Rooi Rand dolerites using a generalised method. In this study however, the method used by Le Roex and Erlank (1982) is adopted, where specific pairs of rocks are directly related to one another, because they come from adjacent or nearby dyke flows, in this case within the same 600m-long outcrop, where the relative age relationships are known.

The objective of the least-squares analysis is to determine whether an assumed residual liquid might be derived from an assumed parent magma by removal or addition of

components which have the compositions of mineral phases or contaminants (Bryan *et al.*, 1969).

Input data for MIXER consists of parent and daughter compositions, as well as the compositions of fractionating mineral phases. The daughter and mineral compositions are the independent vectors in the calculation, and from these, the parent (dependent vector composition) is calculated and compared with the observed parent composition.

The output data obtained, are values for the observed and calculated oxide values of the parent, the oxide residuals (differences between calculated and observed), the sum of the squares of the oxide residuals, and the calculated proportions of the independent vectors, i.e. daughter and fractionating mineral phases. The F-value, or amount of liquid remaining in crystal removal calculations is given by the daughter mix coefficient.

The validity of the mixing calculations should then be assessed. Wright (1974) mentions vital points to be considered when evaluating output data. The residual values must be below reasonable analytical error, so as to limit the number of possible solutions.

"Reasonable analytical error" allowances vary from author to author. Wright (1974) only considers solutions in which oxide residuals are each < 0.10, as being sufficiently valid. Le Roex (1980) on the other hand, accepted any solutions in which the sum of the squares of residuals was < 0.10, also ensuring that there were no large discrepancies in individual oxide residuals. The standard deviations obtained for individual vectors in the mix should be less than 1%. Large standard deviations indicate a poorly constrained model.

Examples of acceptable and unacceptable data are presented in Tables 5.1 and 5.2.

Table 5.1 An acceptable major element mix obtained using the least squares approximation technique on the program MIXER. Note the low sum of squares of residuals (< 0.10), and the low standard deviations in the mix, all less than 1%.

INPUT DATA

	DAUGHT	CPX	PLAG	ILMEN	TIMGT	PARENT
SiO2	51.49	50.83	55.38	0.01	1.45	49.21
TiO2	1.98	1.10	0.01	51.26	7.18	3.07
Al2O3	13.29	2.77	27.45	0.01	1.23	12.77
FeO	14.14	11.49	0.73	47.30	85.97	15.13
MnO	0.23	0.21	0.01	0.80	0.25	0.24
MgO	4.67	15.07	0.07	0.01	0.51	5.42
CaO	8.93	18.66	11.25	0.01	0.08	10.19
Na2O	2.61	0.27	4.89	0.01	0.01	2.46
K2O	0.81	0.01	0.25	0.01	0.01	0.49

OUTPUT DATA - LEAST SQUARES APPROXIMATION

	OBS.	PARENT CALC.	DIFF.
SiO2	49.21	49.05	-0.16
TiO2	3.07	3.06	-0.01
Al2O3	12.77	12.75	-0.02
FeO	15.13	15.08	-0.05
MnO	0.24	0.22	-0.02
MgO	5.42	5.41	-0.01
CaO	10.19	10.16	-0.03
Na2O	2.46	2.40	-0.06
K2O	0.49	0.58	-0.09

VECTOR	MIX COEFF.	STD-DEV.
DAUGHT	0.6754	0.0099
CPX	0.1482	0.0044
PLAG	0.1211	0.0056
ILMEN	0.0264	0.0012
TIMGT	0.0290	0.0014
TOTALS	1.0000	0.0123

SUM OF SQUARES OF RESIDUALS = 0.04

Table 5.2 An unacceptable major element mix obtained using the least squares approximation technique on the program MIXER. Note the high sum of squares of residuals and standard deviations.

INPUT DATA

	DAUGHT	CPX	PLAG	ILMEN	PARENT
SiO2	51.49	50.65	56.28	0.10	50.93
TiO2	1.98	0.89	0.01	52.07	1.83
Al2O3	13.29	2.15	26.97	0.01	13.97
FeO	14.14	13.43	0.87	46.06	12.54
MnO	0.23	0.32	0.01	1.82	0.22
MgO	4.67	15.12	0.10	0.01	6.27
CaO	8.93	17.05	9.98	0.01	10.86
Na2O	2.61	0.27	5.27	0.01	2.28
K2O	0.81	0.01	0.35	0.01	0.51

OUTPUT DATA - LEAST SQUARES APPROXIMATION

	OBS.	PARENT CALC.	DIFF.
SiO2	50.93	51.34	0.41
TiO2	1.83	2.23	0.40
Al2O3	13.97	13.31	-0.66
FeO	12.54	12.11	-0.43
MnO	0.22	0.23	0.01
MgO	6.27	5.87	-0.40
CaO	10.86	10.61	-0.25
Na2O	2.28	2.58	0.30
K2O	0.51	0.55	0.04

VECTOR	MIX COEFF.	STD-DEV.
DAUGHT	0.5992	0.0769
CPX	0.2019	0.0388
PLAG	0.1823	0.0409
ILMEN	0.0165	0.0103
TOTALS	1.0000	0.0959

SUM OF SQUARES OF RESIDUALS = 1.26

Solutions should then be evaluated for consistency with other petrological and geological information as well as checked against trace and REE data, before the result can be considered to have petrologic significance. The calculated proportions of fractionating minerals should be realistic in terms of the compositions observed in the parent and daughter phases. By attempting to derive the major elements of each dyke phase from the most primitive (phase E), time relationships are not ignored. Phase E is just used to approximate a putative parent to all the phases.

Results

The results of major element modelling are presented in Appendix 4a. These are the best results obtained for the mixes. Parent compositions of Rooi Rand dykes are from Appendix 3b. Many mixing combinations were attempted, varying the mineral compositions and proportions (especially ± olivine and titanomagnetite). Models which gave more satisfactory major element results were those using titanomagnetite in the mineral mix.

In most cases, according to the major elements, it is possible to derive all dyke phases from a depleted Age E-like parent by fractional crystallization, and even Age B was derived from Age C, which was slightly less evolved. Deriving B from C was attempted based on observations of the REE profiles (Figure 5.3), Age B being fairly evolved with respect to the other dolerites, and closest in relative age to C. The major element composition of Age B can be very closely matched by the removal of clinopyroxene (19%), plagioclase (16%) and minor amounts of titanomagnetite and ilmenite (approximately 3% each) from Age C, with 60% of the melt remaining.

Standard deviations for these calculations vary from 1% to 2.6%, and the sums of squares of residuals are mostly below 0.10, the exceptions being for deriving Age F from Age E (0.14) and Age B from Age E (0.19). This is not surprising, when one considers that F and B have the two steepest REE profiles, and remembering what was said in the introduction regarding profile gradient changes with fractionation, it should not really be possible to derive these from a flat E-like profile in this manner.

Modelling of major elements for fractional crystallization of Age E from a mantle source was unsuccessful. The fact that Age E only has 7% MgO suggests that it is not a primary magma, and if derived from a mantle source, would have to have been done so indirectly (through a number of successive fractionation processes). It was not possible to obtain an acceptable mix for deriving Age E from several different mantle and mid-ocean ridge basalt (MORB) compositions. Mantle compositions used were those for "hot" and "cold" mantle xenoliths from Sweeney (1988), and N- and E-MORB values from Humphris *et al.* (1985) (Appendix 4b). It seems far more likely that Age E was derived as a high degree partial melt of one of these parent compositions.

5.2.2 *Trace Elements*

The information derived from the major element fractionation model, i.e. F-values and proportions of fractionating minerals, are used in trace element calculations. Only those models that work for the major elements are carried through to this stage. Using the relevant equations of Rayleigh fractionation, theoretical trace element compositions for the derivative liquid from the parent liquid are calculated. The calculated values are then compared with observed values in the derivative liquid, and the validity of the model is determined.

Trace element behaviour during magma evolution may be thought of in terms of their partitioning between crystalline and liquid phases, expressed as the distribution coefficient D (Table 5.3).

To calculate the trace element concentrations of derivative liquids in this fractional crystallization process, the equation describing Rayleigh fractionation is used.

$$C_L/C_0 = F^{(D-1)} \qquad \text{(Wood and Fraser, 1976)}$$

where C_L = trace element concentration in derivative liquid
C_0 = trace element concentration in parent liquid
F = fraction of liquid remaining
D = bulk distribution coefficient of trace element

and

$$D = \sum_{i=1}^{i=n} w_i.D_i$$

where w_i = weight fraction of phase i in crystallizing assemblage.
D_i = distribution coefficient of trace element in phase i

This equation assumes that either the crystallizing phases are rapidly removed from the magma, or that the rate of crystal growth greatly exceeds solid diffusion rates for the trace elements of interest. In either case, the growing crystals will not have time to re-equilibrate with the derivative liquid and it is only the surface of a growing crystal which is in equilibrium with the current magmatic liquid.

Table 5.3 Trace element distribution coefficients used in fractional crystallization modelling calculations.

	Ol	Cpx	Plag	Ti-Mag	Ilm
Rb	0	0	0.02[5]	0	0.01[17]
Ba	0	0	0.05[5]	0	0.01[17]
Sr	0	0.1[5]	1.5[9]	0	0.01[17]
Y	0.01[1]	0.5[1]	0.2[13]	0.2[1]	0.01[17]
Sc	0.33[2]	2.4[6]	0.15[13]	0.73[2]	7[15]
Zr	0.01[1]	0.1[1]	0.01[1]	0.1[1]	0.3[17]
Nb	0.01[1]	0.1[1]	0.01[1]	2.16[10]	0.8[17]
Ni	20.12[14]	2[4,7]	0	12.2[11]	0.01[17]
Cr	0.6[4]	5[6]	0	21.1[12]	3[15]
V	0.09[3]	0.74[3]	0	5[12]	12[16]
Cu	0.02[2]	0.2[3]	0.004[2]	0.42[2]	1.46[2]
Zn	0.86[3]	0.5[3]	0.13[2]	2.6[2]	2.76[10]
Co	3[3]	2[8]	0	3.4[2]	2[15]

References:
1.Pearce and Norry (1979)
2.Paster *et al.* (1974)
3.Bougault and Hekinian (1974)
4.Lindstrom (1976)
5.Philpotts and Schnetzler (1970)
6.Dale and Henderson (1972)
7.Frey *et al.* (1978)
8.Lindstrom and Weill (1978)
9.Korringa and Noble (1971)
10.Le Roex (1980)
11.Leeman (1974)
12.Leeman *et al.* (1978)
13.Le Roex and Erlank (1982)
14.Hart and Davis (1978)
15.Lemarchand *et al.* (1987)
16.Ringwood (1970)
17.Cox *et al.* (1984)

The calculated values obtained should then be compared with those observed, to assess the

validity of the model. It is important to evaluate whether the calculated and observed trace element concentrations in the two samples are consistent with the model.

If the model is inconsistent with fractional crystallization then other processes, such as magma mixing, partial melting, or even contamination , possibly with the continental crust have to be considered.

Results

Trace element modelling results are presented in Appendix 4c. It is here that large discrepancies between calculated and observed values become evident, and although trace elements can be very unreliable because of some of them being mobile, one can discard many of the attempted models, which not only do not have good trace element matches for the calculated versus the observed, but often do not demonstrate trace element changes in the same direction for progressive fractional crystallization with time.

The most common problem encountered in trace element modelling is that the Rooi Rand dolerites have highly elevated Rb, Ba, Sr, Nb and especially Zr values, and no fractional crystallization modelling can reproduce these high values. The calculated values for these elements are thus too low in every case but one. Armstrong *et al.* (1984) also encountered severe problems when modelling these trace elements in the Rooi Rand dolerites, mentioning the anomalous degrees of enrichment which the dolerites possess. The Zr/Nb ratios vary from 15 to 40 for the Rooi Rand dolerites and Armstrong *et al.* (1984) feel that this high degree of trace element variation cannot be accommodated into a simple fractionation model. The only possible explanation they offer for this enrichment, is source heterogeneity with enrichment in these elements in certain domains of the source. In the words of Cox and Clifford (1982) "the Rooi Rand rocks remain problematic". They also suggest a possible heterogeneous mantle source, but in addition, mention the possibility of contamination, saying that relative to the original magmas, the contaminant must have been enriched in K, Rb, Ba, Sr and Nb, impoverished in Zn, Cu and Y. If contamination did take place, the statement regarding trace element enrichment or depletion may only be considered to hold true for deriving Age B from C and Age F from E. For all the other dyke ages, Zn, Cu and Y are far higher than expected i.e. have not

been depleted. The possibility of contamination having taken place will be discussed in Section 5.4.

The only model that was fairly consistent with these trace elements was deriving Age B from Age C, however, with the exception of the Cu, Zn and Y values. The observed values are far lower than the calculated values. The slight discrepancy between Zr and Nb observed and calculated values is considered acceptable by Le Roex (1980). The diagnostic incompatible element ratio Zr/Nb serves as an excellent indicator for acceptable and unacceptable trace element results. Le Roex (1980), modelling possible fractional crystallization of Atlantic Ocean basalts, considered a discrepancy of 0.4 acceptable, and one of 0.7 unacceptable. In this case the difference is only 0.3. This discrepancy would also have been acceptable to Armstrong *et al.* (1984). Contamination with a source enriched and depleted in those elements suggested by Cox and Clifford (1982) above is a possibility for Age B considering its enriched K, Rb, Ba, Sr, Nb and Zr values, its depleted Zn, Cu and Y values relative to what would be expected from derivation by fractional crystallization, and its LREE enriched REE profile.

5.2.3 *Rare Earth Elements*

It is widely accepted that REE are more reliable indicators than trace elements of the viability of geochemical models. REE are generally immobile and not easily altered except by some magmatic process. In contrast, many trace element abundances are easily changed by alteration.

REE modelling was conducted using the BASIC program REEMDEL written by Geoff Grantham. The REE profile for the starting material in the fractionation process (i.e. the parent used in the major and trace element calculations) is entered as input data, as well as the ideal mineral mix (also calculated in the major element modelling). REE data of the parent were entered into the program, and the ideal mineral mix and melting proportions obtained from the major element modelling were used. Mineral distribution coefficients are presented in Table 5.4.

Table 5.4 Rare earth element distribution coefficients used in fractional crystallization modelling calculations.

	Ol	Cpx	Plag	Ti-Mag	Ilm
La	0.0026[2]	0.08[3]	0.14[3]	0.015[2]	0.098[2]
Ce	0.0008[2]	0.3[3]	0.2[1]	0.0146[2]	0.11[2]
Nd	0.01[1]	0.65[1]	0.14[1]	0.026[2]	0.14[2]
Sm	0.011[1]	0.95[1]	0.11[1]	0.1*	0.15*
Eu	0.01[1]	0.68[1]	0.73[1]	0.1*	0.15*
Gd	0.012[1]	1.35[1]	0.066[1]	0.1*	0.15*
Dy	0.014[1]	1.46[1]	0.055[1]	0.1*	0.15*
Er	0.017[1]	1.33[1]	0.041[1]	0.1*	0.15*
Yb	0.023[1]	1.3[1]	0.031	0.1*	0.15*

Pr and Ho were not analysed, and therefore are excluded from the modelling.

References:
1.Schnetzler and Philpotts (1970)
2.Paster *et al.* (1974)
3.Henderson (1982)
* denotes values assumed for those minerals

The parent was then fractionated by Rayleigh fractionation at 5 and 10% intervals. Profiles for the REE values were then plotted onto a chondrite normalized REE distribution diagram (normalized according to Evensen *et al.*, 1978, Table VI, Appendix 3b). The profiles for the observed end-product (i.e. the observed daughter compositions from major and trace element calculations) as well as the parent composition were also plotted.

Results

Results of REE modelling are shown in Appendix 4d. It was shown that none of the dyke phases could be obtained from an Age E-like source by fractional crystallization alone.

Not only is it fairly clear from a visual examination that the fits are poor, the suggested 90% fractionation of the melt by the REE model is highly implausible, and also does not correspond with fractionation amounts obtained in the major element modelling. Figures 5.4 and 5.5 show examples of poorly- and well-matched profiles respectively. Another possibility to be considered in the future, is relating the other phases to another parent more depleted in the HREE (than Age E), and only slightly LREE depleted.

The only fractional crystallization model which appeared to work for all the elements, including the REE, was that of deriving Age B from Age C (Figure 5.5). Using the ideal mineral mix calculated in the major element modelling, an amount of 35% to 50% fractionation was suggested, thus agreeing closely with the value obtained from major element modelling of approximately 41% fractionation of the parent. Concentrations in the crystalline solid would be expected to be similar in composition to Age A.

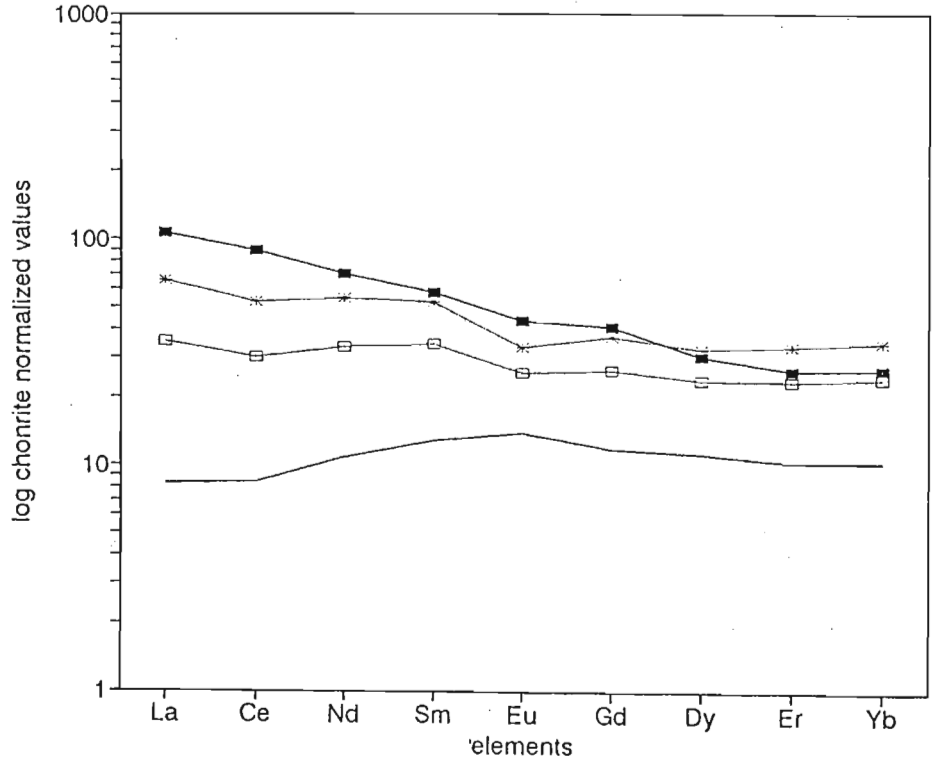

Figure 5.4 Example of a poorly-matched REE profile from fractional crystallization modelling. (solid line=parent, ■ =daughter,..... =profiles obtained from varying degrees of fractional crystallization)

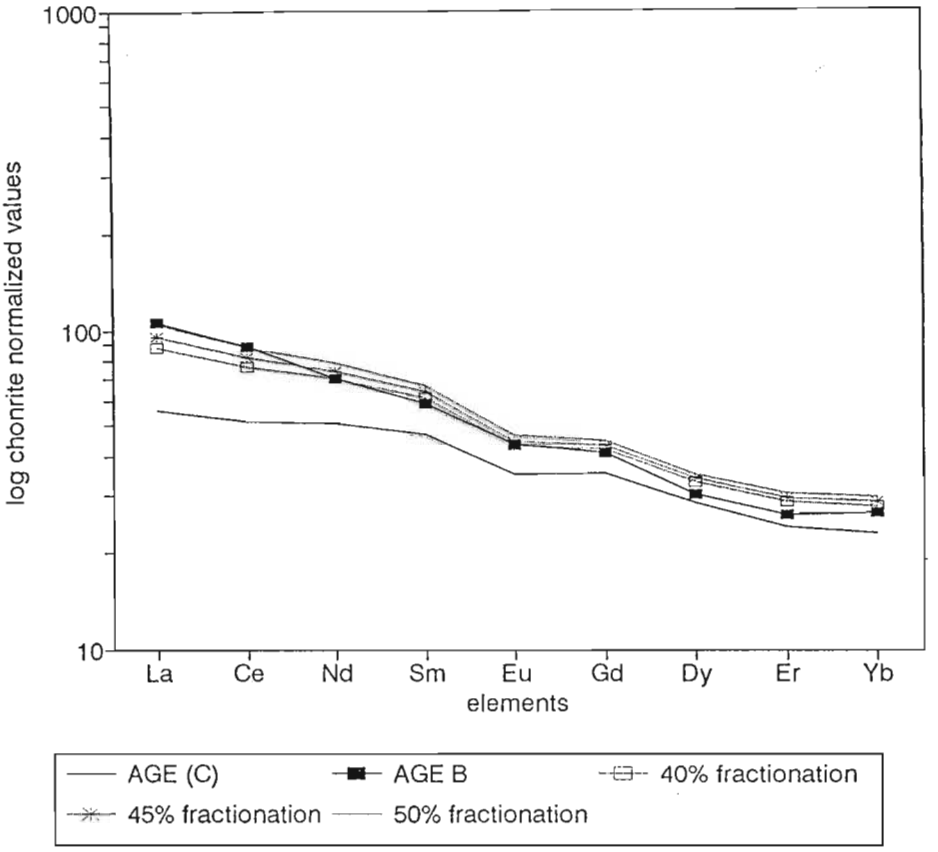

Figure 5.5 Example of a well-matched REE profile for fractional crystallization modelling. The model derives Age B from Age C by the removal of clinopyroxene, plagioclase and minor amounts of titanomagnetite and ilmenite. This model is thus considered viable.

5.2.4 *Discussion*

In most cases, it was possible to account for the major element differences between "parent" and "daughter" magma compositions. In every case but one, it was not possible to do this for trace elements and the REE's. Although the calculated REE profiles may be similar in values, the characteristic shapes they bear, such as gradient, inflection points (points where the slope change) are totally different. This is often a problem with simple crystal fractionation. The relative abundances can almost always be simulated by n% fractionation, but to actually change the anomalous points on the profile, one would require another mechanism to come into play.

Although previous workers (eg. Armstrong, 1978; Armstrong *et al.*, 1984) suggested an origin by fractional crystallization for the Rooi Rand dolerites, with values for the fraction of liquid remaining (F-value) of approximately 0.35, they did so using average chemical compositions for the most and least evolved dolerites, and produced fairly poor trace element results, with no rare earth element modelling. Duncan *et al.* (1990) using newly available Rooi Rand REE data agreed that it is not possible to relate all Rooi Rand dolerites with a simple fractional crystallization model. They attribute the intersecting sets of REE profiles to source heterogeneity, complex melting processes or assimilation.

This would tend to suggest that there were other magmatic fractionation or mixing processes involved in the petrogenesis of the dolerites. i.e. not just simple fractional crystallization.

O'Hara (1977) states that if the concentrations of incompatible elements and REE vary greatly in rocks of comparable major element composition, this variation reflects differences in the extent of partial melting at the source region which gave rise to each magma batch. The possibility of this will be examined in the next section.

5.3 Partial Melting

Modelling of partial melting processes is usually carried out in terms of trace and REE rather than major elements. Since REE are considered to be the most reliable, this study therefore concentrates on REE calculations.

The standard batch melting equation (Wood and Fraser, 1976) was used assuming modal batch melting, because of the small scale of this project, and the poorly constrained distribution coefficients. It is acknowledged that this is a simplification for calculating the concentration of a trace element in a melt because it assumes from modal melting that the proportions of phases entering the melt are the same as those that were originally present in the source rock. Many more complex melting models exist which take into account phase exhaustion and non-modal melting. Hertogen and Gijbels (1976) however, show that when assuming modal melting, fractional melting calculations are far more affected than batch melting calculations. In addition, they conclude that the effects of assuming modal melting are greatly outweighed by the effects of variation in distribution coefficients.

During batch melting, for any given element,

$$C_L/C_0 = 1/(D(1-F)+F) \qquad \text{(Wood and Fraser, 1976)}$$

where F = weight proportion of melt formed
C_0 = initial concentration of element in the source
C_L = concentration of the element in the melt
D = bulk solid-melt distribution coefficient at the time of removal of the melt.

As stated by Consolmagno and Drake (1976), this "simple and assuming" equation may be used in practice if used in the case of generalized and simplified models. The equation is considered adequate in this instance where only minimal sample data and poorly constrained distribution coefficients are used. Modal batch melting has also been used effectively by other Karoo workers (eg. Cleverly *et al.*, 1984)

Once again, a depleted Age E-like source was taken as the parent magma, assuming that potential sources to the more enriched dyke ages would have had LREE-depleted profiles.

Partial melting modelling was also attempted using the mantle and MORB values from Appendix 4b as sources, but no close correlations were obtained for the Rooi Rand profiles.

Table 5.5 REE distribution coefficients used in partial melting modelling calculations

	Oliv[4]	Opx[4]	Cpx[1]	Plag	Ap[2]	Garn[3]
Ce	0.009	0.02	0.3	0.14[4]	16.6	0.35
Nd	0.009	0.05	0.65	0.14[1]	21	0.53
Sm	0.009	0.05	0.95	0.11[1]	20.7	2.66
Eu	0.008	0.05	0.68	0.73[1]	14.5	1.5
Gd	0.012	0.05	1.35	0.066[1]	21.7	10.5
Dy	0.012	0.2	1.46	0.055[1]	16.9	28.6
Er	0.013	0.31	1.33	0.041[1]	14.1	42.8
Yb	0.013	0.34	1.3	0.07[4]	9.4	39.9

1. Schnetzler and Philpotts (1970)
2. Nagasawa and Schnetzler (1971)
3. Shimizu and Kushiro (1975)
4. Henderson (1984)

Bulk distribution coefficients were calculated for each element, assuming a plagioclase peridotite assemblage consisting of 6.5% orthopyroxene, 14.5% clinopyroxene, 48% olivine and 30.5% plagioclase feldspar (or equivalent spinel/garnet), with less than 0.5% total garnet and apatite as minor residual phases. A residue of olivine $\pm$ orthopyroxene $\pm$ clinopyroxene will only have garnet present if melted at great enough depths (Hanson, 1980) (in which case it will be a garnet peridotite, and not a plagioclase peridotite). The presence of garnet leads to less enrichment of the HREE and a significant increase in the Ce/Yb ratio relative to melts derived from an assemblage without garnet. At medium depths it would be termed a spinel peridotite (Hall, 1987). Hanson (1980) mention that it is not the mineralogy of a parent prior to melting that controls the REE patterns. It is rather, the mineralogy of the residue at the time of removal of the melt, which may be drastically different from the parent mineralogy at the onset of melting. Melting of a basalt with a composition similar to that of Age E will lead to a residue depleted in SiO_2 and alkalies, and enriched in Ca, Fe and Mg relative to that of the parent. It is therefore not unlikely that a plagioclase peridotite residue be obtained.

Because of the simplicity of the modal batch melting system, D values have also been kept

constant. Realistically, with increasing degrees of partial melt different minerals will be consumed causing changes in the values of D.

Results

Figures 5.6 and 5.7 show results obtained for the partial melting of an Age E-like source to produce the various other dolerite ages. A fairly good match was obtained to produce all ages except Age B (not shown) and possibly Age H.

Partial melting of an E-like source with successively lower degrees of melting would produce Ages H, (G), G′, G″ and F respectively (Figure 5.6). Age G′ was produced by approximately 5% melting, and Ages G″ and F from between 0 and 2% melting. Remembering the assumption of Age G′ being a geochemical equivalent of Age C, it would also hold true that Age C could be produced by 5% melting of the source. As would be expected because of their notably flatter profiles, it was also possible to produce Ages H and D with slightly higher degrees of melting (5-10% and 15-20% respectively) (Figure 5.7) although the melting of Age H is not as well constrained as that for Age D. A problem with the Ce values may be noted. This may be due to the fact that Ce occurs naturally in two oxidation states, and may present analytical problems (Schreiber *et al.*, 1980) which affect the Ce values reported in this study.

The obvious pattern which has resulted by successively lower degrees of partial melt forming successive dyke ages will be discussed in the concluding statements of Chapter 6.

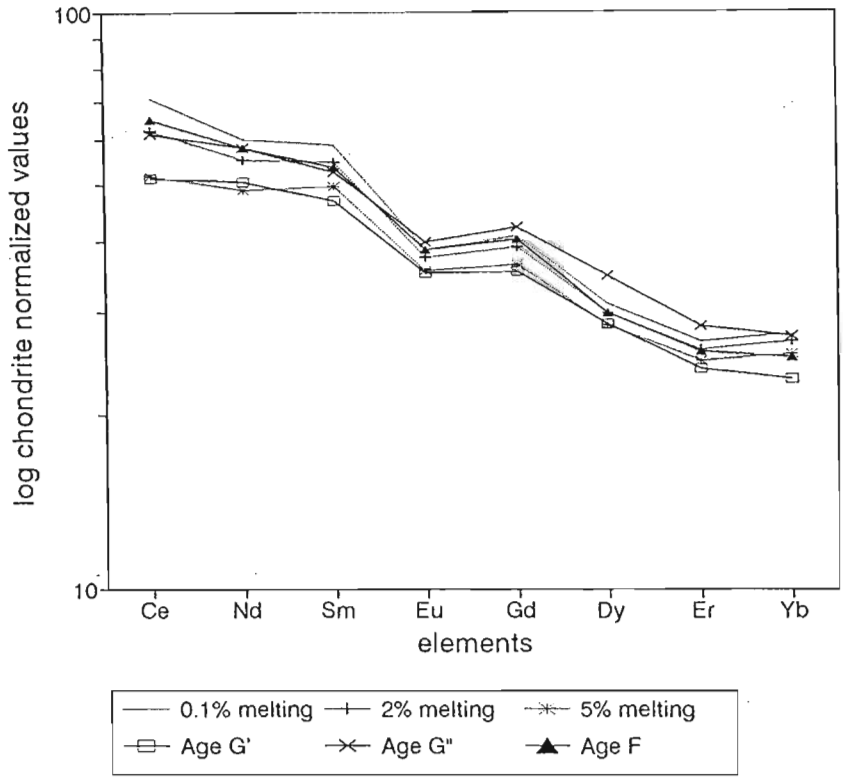

Figure 5.6 Chondrite normalized REE profiles obtained from varying degrees of partial melting of a depleted Age E-like source, leaving a plagioclase peridotite residue. Input data from Appendix 3b.

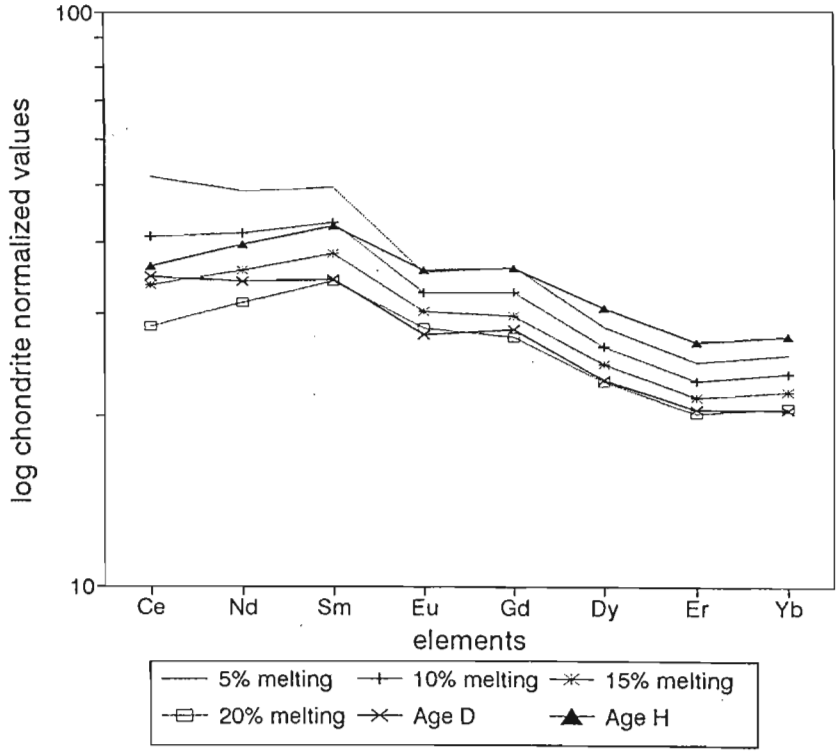

Figure 5.7 Chondrite normalized REE profiles obtained from varying degrees of partial melting of a depleted Age E-like source, leaving a plagioclase peridotite residue. Input data from Appendix 3b.

5.4 Contamination

Sweeney (1988) considered it highly unlikely that large volumes of Lebombo volcanic magmas could pass through approximately 40km of predominantly granitic continental crust without being contaminated. Crustal contamination modifies the composition of the magmas en route to the surface, and it is therefore likely either to generate some broad mixing relation between the original magma and crustal component, and/or to disrupt any pre-existing relationship between isotope and parent/daughter trace element ratios with the result that the two become decoupled (Hawkesworth *et al.*, 1984).

By using simple mass balance calculations and the granite contaminant composition proposed by Sweeney (1988), major element modelling for the possible contamination of Age C to form Age B was attempted. This was done following the methods of Bristow *et al.* (1984) who undertook modelling for the contamination of the Effingham dolerites.

Choice of a contaminant was made following Sweeney (1988), who derived an assimilant composition assuming 20% melting of a granitic source. This was considered to be more realistic than assuming simple bulk contamination. Thus the composition of a hypothetical melt produced at 20% melting from Sweeney (1988) was used. The granitic source was assumed from the basement rocks lying directly to the west of the Sabie River Basalt Formation.

Results

Table 5.6 shows the major element results from the mixing of a granite contaminant with Age C. There is a close match for all major elements with 8.65% granite and 91.35% Age C. When calculations are carried out for trace elements, most calculated values are too low, except for Zr, which corresponds with the observed value. Cr is a factor of 4.5 too high. This implies that fractional crystallization coupled with contamination may have taken place, lowering the Cr value, and enriching the trace and LRE elements.

For this reason, brief modelling of simultaneous assimilation and fractional crystallization must be attempted.

Table 5.6 Major element compositions of granite contaminant (Sweeney, 1988), Rooi Rand dolerite Ages C and B observed, and a calculated value for Age B, using simple mass balance mixing equation for contamination of a dolerite (Age C; 91.35%) with a granite (Sweeney, 1988; 8.65%).

wt%	Granite	Age C	Age B_{obs}	Age B_{calc}
SiO_2	75.57	49.21	51.49	51.49
TiO_2	0.05	3.07	1.98	2.80
Al_2O_3	14.00	12.77	13.29	12.87
FeOt	0.22	16.82	15.74	15.38
MgO	0.13	5.42	4.67	4.96
CaO	1.48	10.19	8.93	9.43
Na_2O	3.09	2.46	2.61	2.51
K_2O	5.46	0.49	0.81	0.91

5.5 Simultaneous Assimilation-Fractional Crystallization (AFC)

AFC modelling was carried out for the Rooi Rand dolerites, because Age B stands apart mineralogically and in major and trace element composition from the other Rooi Rand Ages. Age B has quartz present in its mineral assemblage, and although simple fractional crystallization for Age B appears to work, the trace element modelling presented some problems. It cannot therefore be said with certainty that it was not coupled with assimilation. In AFC modelling, Age C was used as a hypothetical source material, and Age B the resultant composition.

AFC is considered to be the normal mode of contamination, because straight mixing models will be highly unlikely if there are solid components present. Although assimilation and fractional crystallization may be treated as separate processes, heat balance calculations suggest that the two may be combined in AFC (DePaolo, 1981). The heat required for assimilation to take place may be provided by the latent heat of crystallization of the magma. Sweeney (1988) assumes that the prime site where assimilation will occur, will be in that area of the magma chamber where the heat flux is greatest - the roof, while the floor and sides of the chamber will probably be sealed off by the "chilled" magma.

No samples from this study have been analysed for radiogenic isotopes as yet. Two Rooi Rand samples collected by Armstrong (1978) from the same study area are petrographically and geochemically very similar to Ages C (G') and B, and have accompanying radiogenic isotope analyses. Armstrong (1978) details the petrography and major and trace element chemistries of A114 and A117 (used for Ages C and B respectively), and the isotopic data may be found in Bristow *et al.* (1984). Cox and Clifford (1982) suggested that A117 has been contaminated because of its higher isotope ratio.

The trace elements modelled were all those present in the analysis from Sweeney (1988), used in section 5.4. Cox and Clifford (1982) suggested that the source was actually more dioritic than granitic to explain the generally lower Rb/Sr and high Sr, Zr and P values. Sweeney (1988) concluded however that the vast majority of the Archaean crust in the region would have been granitic in composition.

Table 5.7 Trace element data for end-member components used in AFC modelling.

ppm	Granite	Age C	Age B
Rb	152	12	18.1
Ba	371	141	363
Sr	184	219	298
Zr	668	191	243
La	89	15.7	30
Ce	152	39	64
Nd	79	28	38
Cr	13.6	91	18.4
$^{87}Sr/^{86}Sr$	0.709	0.70391	0.70416

DePaolo (1981) provided a mathematical model for the AFC process to calculate trace elements and isotopes. A magma body of mass M_m has assimilated a particular mass of wallrock, M_a and has crystallized simultaneously with M_c (the mass of fractionating phases which have been effectively separated from the magma).

The ratio of mass assimilated to mass fractionated ($r = M_a/M_c$) is very important. On the principle that the latent heat of fusion is approximately equal to the latent heat of crystallization, r would have a maximum reasonable value of 1 (greater than 1 assumes that the magma is superheated because it is crystallizing less than what is being assimilated). It must be remembered when modelling that as a magma moves through the continental crust, r and D values may be changing.

Equations used from DePaolo are as follows:

For r = 1

$$C_m/C^0_m = (C_a/DC^0_m)[1-\exp(-DM_a/M_m)]+\exp(-DM_a/M_m)$$

(Equation 3; DePaolo, 1981)

where C^0_m = original concentration in the magma of an element
C_m = current concentration in the magma of an element
C_a = concentration in assimilated wallrock of element
D = bulk distribution coefficient for an element

In this case, because r=1 (i.e. $M_a=M_c$) the amount of liquid remains the same, and the F-value does not change. The equation is thus controlled by M_a/M_m, which is given values of 0.1, 0.3, 0.5 and 0.7 in the modelling.

For $r \neq 1$

$$C_m/C^0_m = F^{-z}+[r/r-1].[C_a/z.C^0_m].[1-F^{-z}]$$

(Equation 6a; DePaolo, 1981)

where $F = M_m/M^0_m$; fraction of liquid remaining
$z = (r+D-1)/(r-1)$

Calculations were carried out using F-values of 0.9, 0.8, 0.7, 0.6 and 0.5. Values used for r were 0.1 and 0.5.

For calculating radiogenic isotopes,

for r = 1

$$\epsilon_m = \epsilon^0_m+(\epsilon_a-\epsilon^0_m).(1-[C^0_m/C_m].\exp[-D.M_a/M_m])$$

(Equation 13b; DePaolo, 1981)

where ϵ_a = isotope ratio in assimilated material
ϵ_m = current isotope ratio in magma
ϵ^0_m = original isotope ratio in magma

for $r \neq 1$

$$\epsilon_m = \epsilon^0_m + (\epsilon_a - \epsilon^0_m).(1-[C^0_m/C_m].F^{-z}) \quad \text{(Equation 15b; DePaolo, 1981)}$$

Because this work follows the methods of Sweeney (1988), for the sake of completion, distribution coefficients have been taken from that work.

Table 5.8 Distribution Coefficients used in AFC calculations taken from Sweeney (1988, Table 6.2a). Titanomagnetite and ilmenite values taken from Tables 5.3 and 5.4.

	Ol	Cpx	Plag
Rb	0.01	0.03	0.07
Ba	0.02	0.01	0.3
Sr	0.02	0.1	2
Zr	0.035	0.4	0.03
La	0.001	0.04	0.15
Ce	0.001	0.08	0.12
Nd	0.001	0.16	0.08
Cr	0.6	12	0.03

Two fractionating mineral assemblages were assumed. The first was that gained from the results of the fractional crystallization modelling. It consisted of 39% plagioclase, 46% clinopyroxene, 7% ilmenite, and 8% titanomagnetite. The second mineral assemblage was obtained from Nielsen (1985)(used by previous Karoo workers), consisting 10% olivine, 55% plagioclase and 35% clinopyroxene - predicted to occur typically in these proportions for the range of r-values 0.1 to 0.5, for an MgO interval of 7 to 5 weight%. This range of r-values (0.1-0.5) is consistent with the most likely values based on heat budget calculations by DePaolo (1981).

Results

Figure 5.8 shows an example of curves obtained from the results AFC modelling. They are constructed using calculated compositions of the various trace and rare earth elements at various F- and r-values. The complete results of AFC modelling, calculated from a set of graphs similar to Figure 5.8 are presented in Table 5.9. Although a new age of 180 Ma has been established for the Karoo volcanic event (Marsh *et al.*, in prep.), the 190 Ma used in Figure 5.8 is that used by previous workers (Sweeney, 1988; Bristow *et al.*, 1984).

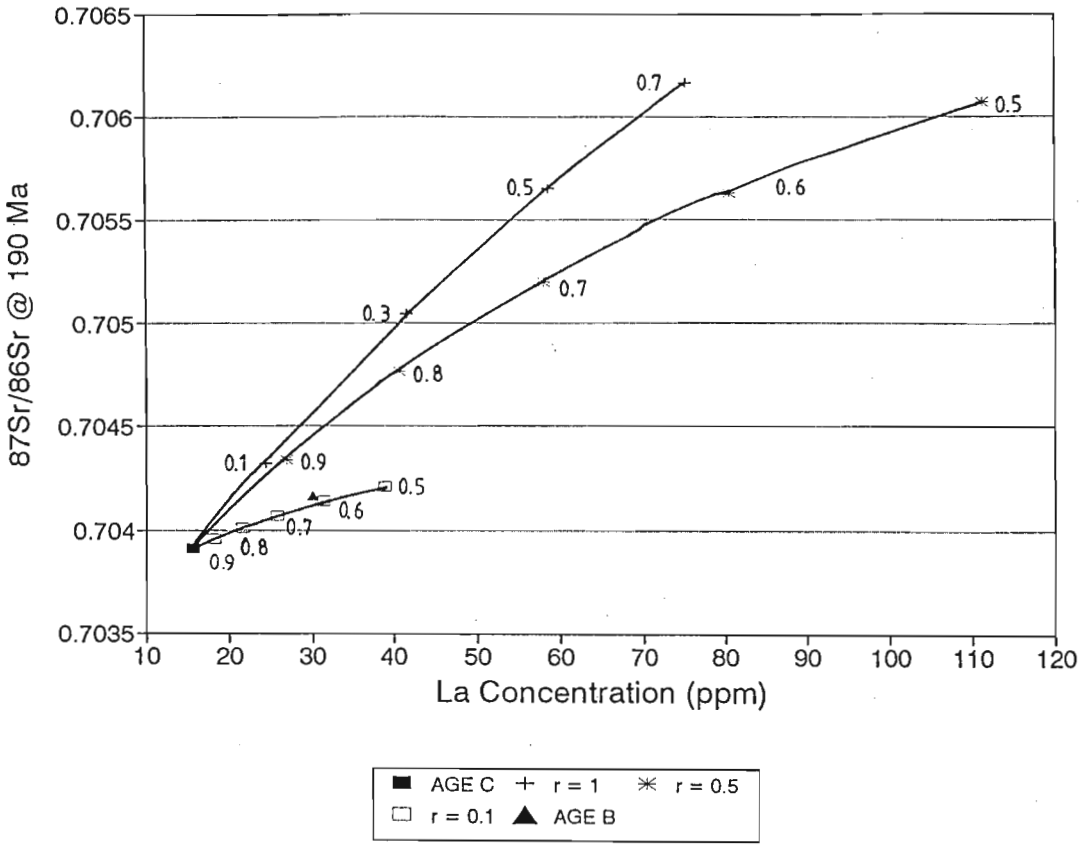

Figure 5.8 Results of AFC modelling of initial $^{87}Sr/^{86}Sr$ ratio versus La for deriving Age B from Age C, with a fractionating mineral assemblage of 39% plagioclase, 46% clinopyroxene, 7% ilmenite, and 8% titanomagnetite. F-values are inserted on the curves. From the graph it may be noted that r=0.2 and F=0.65.

Table 5.9 Calculated r-and F-values for AFC modelling with fractionating assemblage consisting of (1) 39% plagioclase, 46% clinopyroxene, 7% ilmenite and 8% titanomagnetite and (2) 10% olivine, 35% clinopyroxene and 55% plagioclase.

	(1) r	F	(2) r	F
Rb	>1	-	>1	-
Ba	<0.1	-	<0.1	-
Rb/Sr	>1	-	>1	-
Zr	0.4	0.95	0.5	0.94
Cr	0.2	0.82	0.15	0.65
La	0.2	0.65	0.15	0.62
Ce	0.2	0.7	0.2	0.7
Nd	0.3	0.83	0.25	0.83

The greatest problem with the AFC model lies in the trace elements Rb, Ba and Sr. For all the other trace and rare earth elements calculated, r values lie between 0.15 and 0.5, at F-values ranging from 0.62-0.95. These cannot be considered as being very well constrained values, but demonstrate that with some different contaminant, the AFC is a viable model (within the limits of the range in D-values). In the case of Rb, M_a/M_m values of 1 or greater were obtained, implying that the magma as it intrudes represents approximately a 1:1 mix of mantle and crustal materials. Taking heat budget constraints into account, these values are considered highly unlikely. With regards to the heat budget, Nicholls and Stout (1982) point out that in almost every case, the amount of crystallization will exceed that of contamination i.e. r-values will almost always be <1. There was no significant difference between the two mineral assemblages in the calculated values, and it is believed that only by varying the chemical composition of the contaminants, could suitable results be obtained.

The obtained r-values do fall into the range predicted as being most likely for these compositions, taking heat budget considerations during the assimilation process into account (DePaolo, 1981), so the model is still considered viable, even if poorly constrained. If one examines Table 5.9, ignoring Rb, Ba, Sr and Zr, the results for the REE and Cr are reasonable, suggesting contamination of 15 to 30% to generate Age B, requiring a range of 17 to 38% fractional crystallization to take place. This figure is consistent with what was calculated in section 5.2 for straightforward fractional crystallization.

Although a suitable contaminant has not been found, and results are not very well constrained, the possibility of contamination cannot be ruled out when taking into account Age B's higher isotopic and incompatible trace element values.

5.6 Discussion

As Armstrong (1978) pointed out, the strong enrichment of incompatible elements suggests that the dolerites were derived from a number of partial melts, each "batch" of parent magma undergoing limited fractional crystallization. All that was needed was a comprehensive study on exactly how the chemistries of the dykes related to one another with time.

The Rooi Rand dolerites were not formed by one type of igneous mechanism, but rather as a combination of partial melting processes, fractional crystallization and possibly some accompanying contamination.

The chemistry of the majority of the Ages may be explained by partial melting of a depleted Age E-like source. Age B on the other hand appears to have been formed by fractional crystallization of a more evolved Rooi Rand magma (such as Age C). Fractionation may have been accompanied by a small degree of crustal contamination to produce the silica-rich "evolved" Age B. The magmas from these chambers injected as Ages B and A.

With regards to the fractional crystallization of Age B, Green (1980) notes that a decrease of Ni and Co, may indicate that olivine fractionation took place whereas a decrease of Cr implies that clinopyroxene fractionation may have taken place. The trace element data of Ages C and B, shows there is not a very large variation in Ni and Co values, but the variation in Cr is much higher. This implies that the mafic mineral involved in fractional crystallization was clinopyroxene and not olivine. This is in agreement with fractional crystallization calculations for Age B.

In the absence of AFC processes in Rooi Rand dolerites petrogenesis, Armstrong *et al.* (1984) attribute the trace element variations to source heterogeneity where certain domains are enriched in K, Nb and possibly Sr. Erlank *et al.* (1984) working on Etendeka Formation volcanics, also conclude that AFC cannot consistently account for the major, trace element and isotopic variations observed. They prefer a model of fractional

crystallization from isotopically variable parent magmas for the generation of the evolved basalts. They then discuss the development of isotopic heterogeneity. Cox and Clifford (1982) also favour a heterogeneous mantle with domains enriched in K, Rb, Ba and Sr to explain these variations.

Duncan *et al.* (1990) describe more complex melting processes such as those proposed for mid-ocean ridge basalts in the FAMOUS area of the mid-Atlantic ridge, as being a possibility for the derivation of such diverse magma compositions, in addition to source heterogeneity.

Although petrological modelling is not considered to be entirely conclusive, especially when taking into account the simplified manner in which it was carried out, it does aid in suggesting viable mechanisms for the petrogenesis of the Rooi Rand magmas, which have a few distinct compositional types.

CHAPTER 6

DISCUSSION AND CONCLUDING STATEMENTS

6.1 Broad tectonic setting

As discussed in the regional geological setting (Chapter 2), the Lebombo represents a faulted monoclinal structure which developed at the western margin of a rift, preceding and eventually associated with the breakup of Gondwana. White *et al.* (1987) and White and McKenzie (1989) detail the presence of voluminous magmatic activity on some continental margins, producing thick intrusive and extrusive igneous sequences on the rifted margins, often with accompanying extensive flood basalts on the adjacent continents, as seen in the Karoo and Antarctica. Detailed reconstructions show however, that the break did not occur in a single clean episode; there were many small continental fragments involved, and there was probably an abortive period of rifting and possibly transcurrent faulting before a later break to fully oceanic crust occurred in the mid-Jurassic (White and McKenzie, 1989).

As the continental lithosphere is stretched and thinned, so a mid-crustal weakness develops, with a low pressure developing beneath this (Harry and Sawyer, 1992). The asthenosphere passively upwells to fill the space. As it rises, it decompresses and generates partial melt which migrates towards this low pressure region. The amount of partial melt produced depends on the temperature of the asthenosphere, with more melt being produced when the asthenosphere is hotter, and on the amount of decompression that takes place, with more melting occurring where the lithosphere thinning is greatest (White and McKenzie, 1989). Provided the lithosphere thins sufficiently, partial melt can be produced under continental rift zones, even if they do not form new oceanic crust (White and McKenzie, 1989).

White and McKenzie (1989) suggest that continental thinning and accompanying rifting took place above a thermal anomaly in the mantle, most likely in the form of the Karoo

plume (Figure 6.1). They put the most likely location of the thermal plume beneath the coastal region of the Lebombo monocline. A 1000-km radius circle, which is the typical extent of the thermal anomaly created by a plume, encompassing adequately the 1700-km-long offshore volcanically active portion of the continental rift, as well as the volcanics of the Karoo and Antarctica. White and McKenzie (1989) believe that the presence of the plume in this region is indicated by the subsequent generation of the Madagascar Ridge as the plume moved northeastward away from Africa.

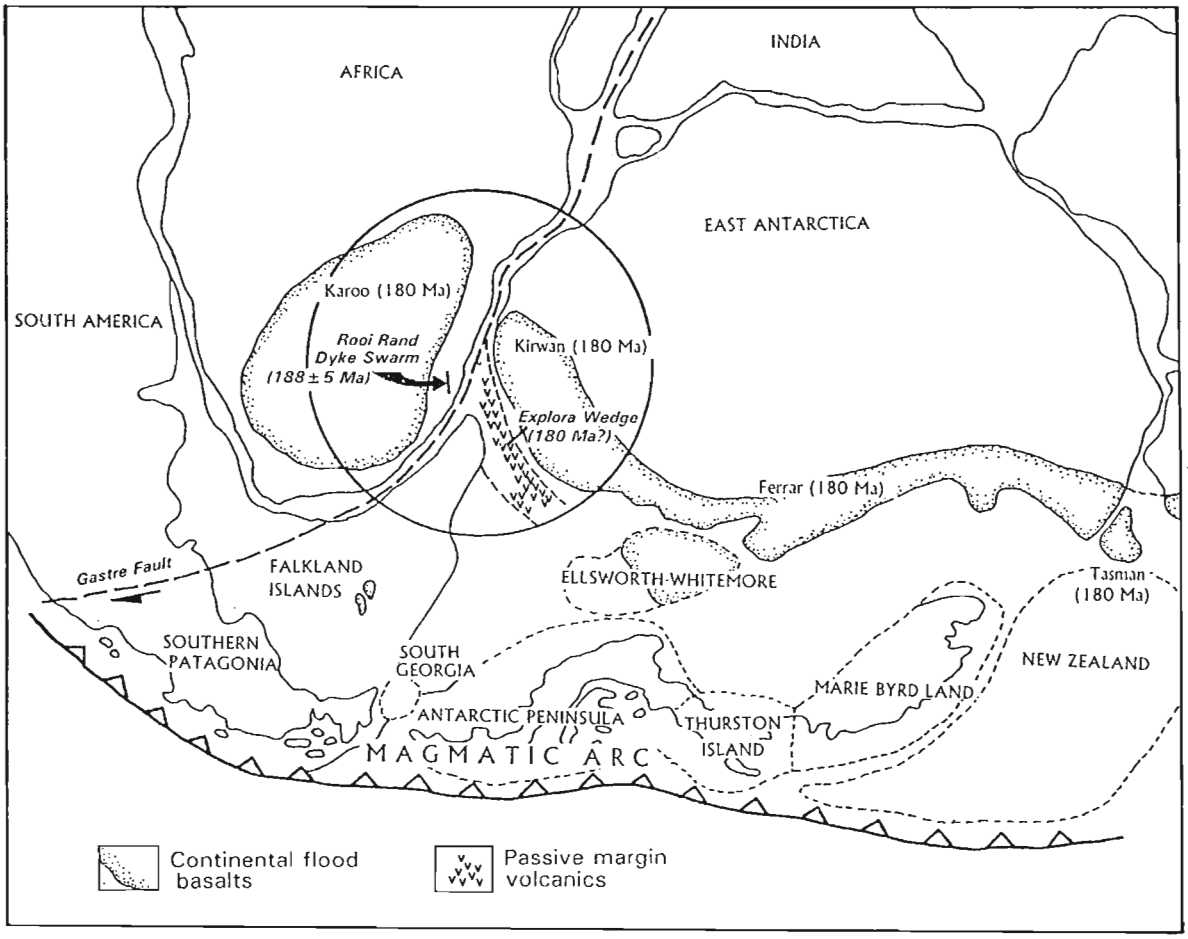

Figure 6.1 Jurassic Gondwana reconstruction illustrating the Karoo plume head (White and McKenzie, 1989) (large circle), the position of the Rooi Rand dykes swarm, the proto-Pacific margin with a subduction-related magmatic arc, within-plate Karoo, Ferrar and Tasman continental flood basalt provinces (approximate dates of intrusion from Marsh *et al.*, in prep; Kyle *et al.*, 1981; and Hergt *et al.*, 1989), and the dipping reflector and failed rift system of the Explora Wedge. The Gastre Fault system and its continuation, may have operated as a transfer fault system on the margin of the broad extensional province (after Storey *et al.*, 1992).

The Explora wedge (Figure 6.1) was identified geophysically by Hinz and Krause (1982) as a major dipping-reflector sequence of volcanics. Elliot (1992) feels that although the age of the Explora Wedge is unknown, it may be correlated with some part of the basalt and rhyolite sequence in the Lebombo Monocline. If one examines Figure 6.1, it appears likely that the Rooi Rand dyke swarm is an on-continent continuation of the Explora Wedge.

The roles of a plume and lithospheric thinning are not considered to be mutually exclusive. It is important to realise the contributions that lithospheric thinning and plume presence make to eventual break-up. White (1992) mentions that the two models of initiating plumes and rifting are not contradictory, often being found occurring together.

Kerr (1994), arguing for a plume model, mentions that the observed degree of lithospheric thinning cannot be explained by extension alone, requiring additional lower lithospheric erosion by the plume head. For the asthenospheric mantle to melt, it must intersect its solidus. It does this by decompression melting during adiabatic upwelling. This passive upwelling may be in response to lithospheric thinning and/or a rising hot mantle plume. These two factors will have a large effect on the amounts of melt generated, and thus the chemistry of the asthenospheric magmas. If there is a plume present, asthenospheric magmas will form larger areas of melting than in the case of passive rifting.

Prior to significant basalt production beneath a continent, Kent *et al.* (1992) suggest that the lithosphere must be sufficiently thinned. This prescribes a period of plume incubation, where the lithosphere will extend with doming, accompanied by the establishment of long-lived palaeodrainage patterns and the intrusion of alkalic magmas. In the plume impact model of Campbell & Griffiths (1990), extension is not a necessary precursor to volcanism, and rifting and uplift commonly follow the main flood basalt event. Kent *et al.* (1992) combine their incubation model with that of White and McKenzie (1989) and White *et al.* (1987), where rift margin igneous provinces form by the decompression melting of the asthenosphere/the presence of a hot plume beneath a region already undergoing extension in response to external plate-driving mechanisms.

White and McKenzie (1989) suggest that the sudden onset of Karoo volcanism during the Jurassic indicates that a mantle plume had only then impinged on the base of the lithosphere. If the plume head cannot readily replace the lowermost mechanical boundary layer (i.e if it occurs beneath a thick craton), it must incubate while thermally and/or mechanically eroding the lithosphere. Kent *et al.* (1992) recognise that this is exactly what occurred in the Karoo Igneous Province. In addition, the incubation period allows for the incorporation of lithospheric mantle into the source region of the erupted basalts.

Many workers argue against the necessity for a plume for the model to work. Storey *et al.* (1992) suggest that a mantle plume below the Karoo province, although not essential to the production of basalt, may have thermally weakened the lithosphere, thereby increasing magma production rates and inducing local rifting. This would have contributed to, but not necessarily caused the eventual separation of east and west Gondwana. Regional tensional forces may have been weak such that sea-floor spreading and continental break-up did not commence until approximately 155 Ma, 25 Ma after the main plume-related event.

Bradshaw *et al.* (1993) argue that the progression from lithosphere to asthenosphere-derived melts with time indicates that extension was a significant factor in their generation. They feel that small volumes of asthenospheric melt constrain the potential temperature at the time of magmatism i.e. had a plume head been present, and the asthenosphere therefore hotter, there would be a greater proportion of asthenosphere-derived magmas. They would therefore find little evidence for a plume in a case such as the Rooi Rand, where the majority of the dyke compositions are influenced by the mantle and crustal lithosphere, and feel that magmatism would therefore have been extension initiated. In the case of the Rooi Rand however, there was probably a failed rift, which implies that there might have been a plume originally present, but for some reason, rifting at that position could not occur - this once again stresses the balance between tectonic rifting forces, and thermal ones.

6.2 Geochemical characterisation of the Rooi Rand dolerites

6.2.1 *Comparison with other Karoo volcanics*

As pointed out in Chapter 4, the Rooi Rand dolerites do not follow the "main" or "normal" trend of Karoo dolerites, which was given by Nockolds and Allen (1956). They show a greater degree of iron-enrichment than the "main" trend of Karoo dolerites.

From previously conducted studies (Armstrong, 1978; Meth, 1990; Meth, 1991), in which the Rooi Rand dolerites were geochemically compared to the Karoo dolerites, the Rooi Rand dolerites have been shown to be geochemically distinct from the Karoo dolerites. The most notable geochemical differences are that the Rooi Rand dolerites are far more enriched in TiO_2 and MnO, than the Karoo dolerites, this being evident from detailed examination of the opaque mineralogy. It was noted that firstly, the Rooi Rand dolerites have far more ilmenite than the Karoo dolerites, and secondly that the ilmenites have an unusually high manganese content. The Karoo dolerites generally have a higher SiO_2 content than the Rooi Rand dolerites. The enrichment in Ti and Mn are expected to accompany the Fe-enrichment (Armstrong *et al.*, 1984).

Geochemical comparisons were made by Armstrong (1978) and Armstrong *et al.* (1984) using average compositions for Rooi Rand dolerites and Sabie River basalts, and this is one possible reason why no equivalent volcanic compositions were ever found in the southern Sabie River Basalt Formation. This thesis has shown that a fairly large diversity in magma compositions exists for the Rooi Rand dolerites, and that one cannot assume an average composition for the dolerites when geochemically characterising them.

The majority of trace element data varies significantly between Karoo volcanics and Rooi Rand dolerites. Armstrong (1978) noted that Zr, Y, Co and V are highly enriched in the Rooi Rand dolerites in comparison to the Karoo igneous rocks, whereas Ba, Rb and Cr values are strongly depleted.

Figures 6.2 to 6.5 are trace element spidergrams of each of the different ages of Rooi Rand dolerites from this study, normalized to average Lesotho Karoo basalt, Zululand Karoo basalt, Swaziland Karoo basalt and southern Lebombo Karoo Basalt (Sabie River Basalt Formation) respectively (data from Duncan *et al.* 1984b).

Figures 6.2 to 6.5 indicate that the trace element observations of Armstrong (1978) may not be correct. In comparison to an average Lesotho, Zululand and Swaziland Karoo basalt, the Rooi Rand dolerites are enriched in Ti, Zr, Nb and Y (except for Age E). Depletion in Ba, Rb and Cr varies greatly between the Rooi Rand dyke ages, some even showing large degrees of enrichment in Ba and Rb relative to the Karoo basalts. This highlights the problem mentioned above of simply comparing averages of the Rooi Rand dolerites, when the dolerites show such diverse chemistry.

The Rooi Rand dolerites bear the strongest trace element resemblance to the southern Lebombo Sabie River Basalt Formation (SRBF) (Figure 6.5). It may be noted that dyke Age A is almost an exact match with the average SRBF basalt. In addition, all other major and trace element data compare well. Previously, no extrusive rocks of equivalent compositional range have been sampled from the Karoo volcanics (Duncan *et al.*, 1984b; Marsh, 1987). It is an interesting match because Age A is the youngest dolerite age in the dyke swarm. As mentioned previously, the Rooi Rand dolerites are seen intruding older Sabie River Basalt Formation flows, and Age A might be a possible feeder to one of the higher basalt flows.

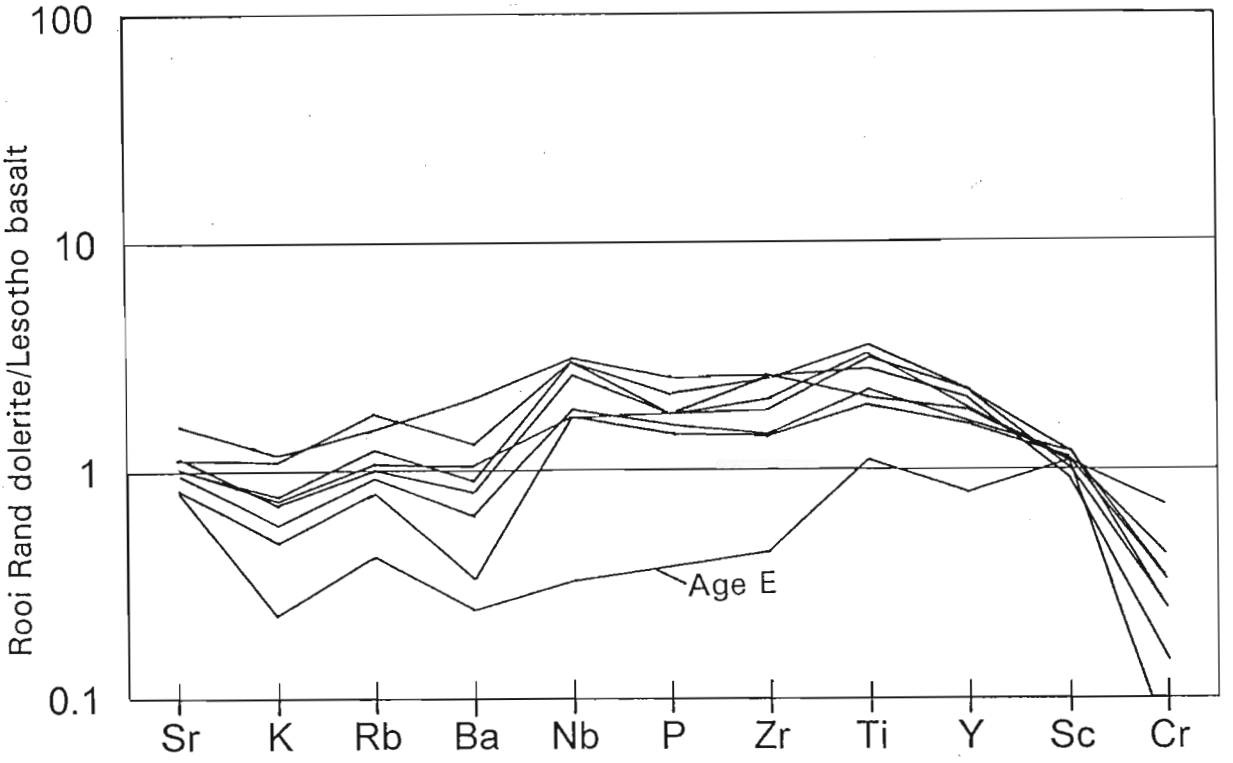

Figure 6.2 Spidergram plot of the Rooi Rand dolerites normalized to an average Lesotho Karoo basalt (data from Duncan *et al.*, 1984b).

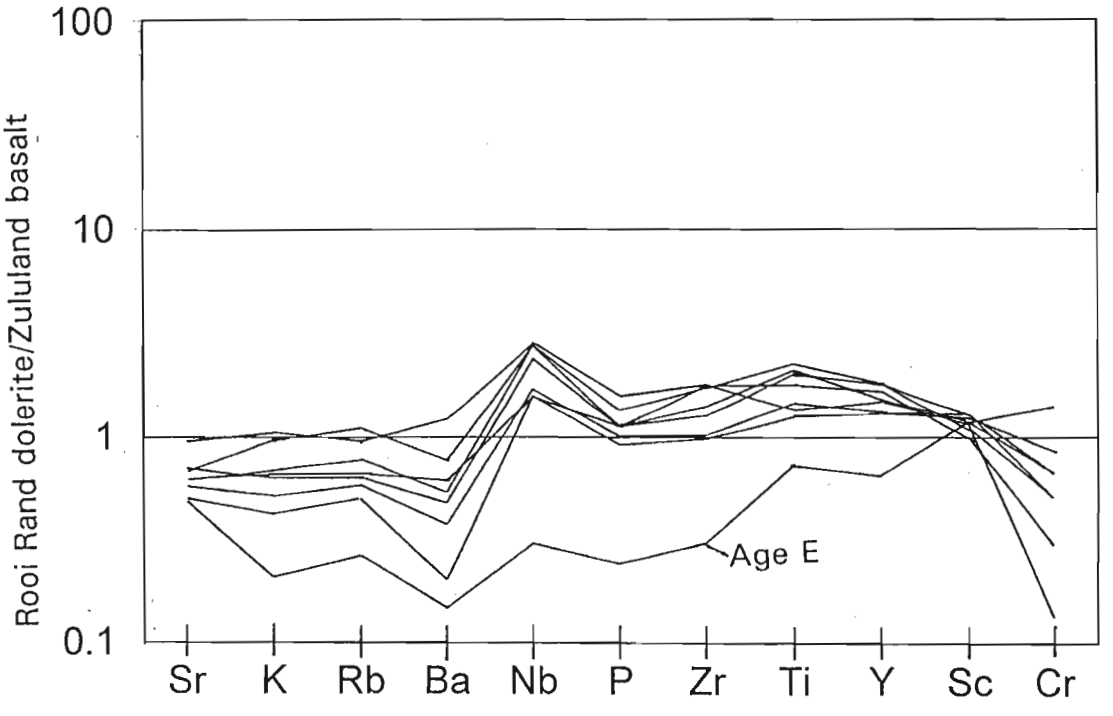

Figure 6.3 Spidergram plot of the Rooi Rand dolerites normalized to an average Zululand Karoo basalt (data from Duncan *et al.*, 1984b).

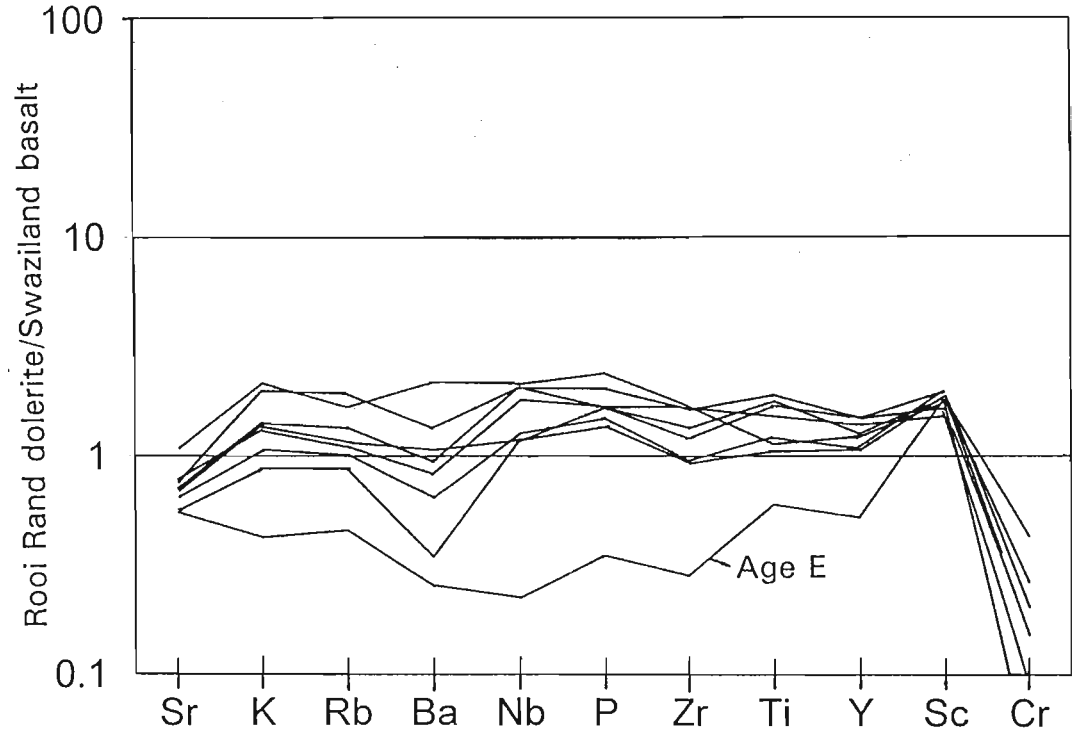

Figure 6.4 Spidergram plot of the Rooi Rand dolerites normalized to an average Swaziland Karoo basalt (data from Duncan *et al.*, 1984b).

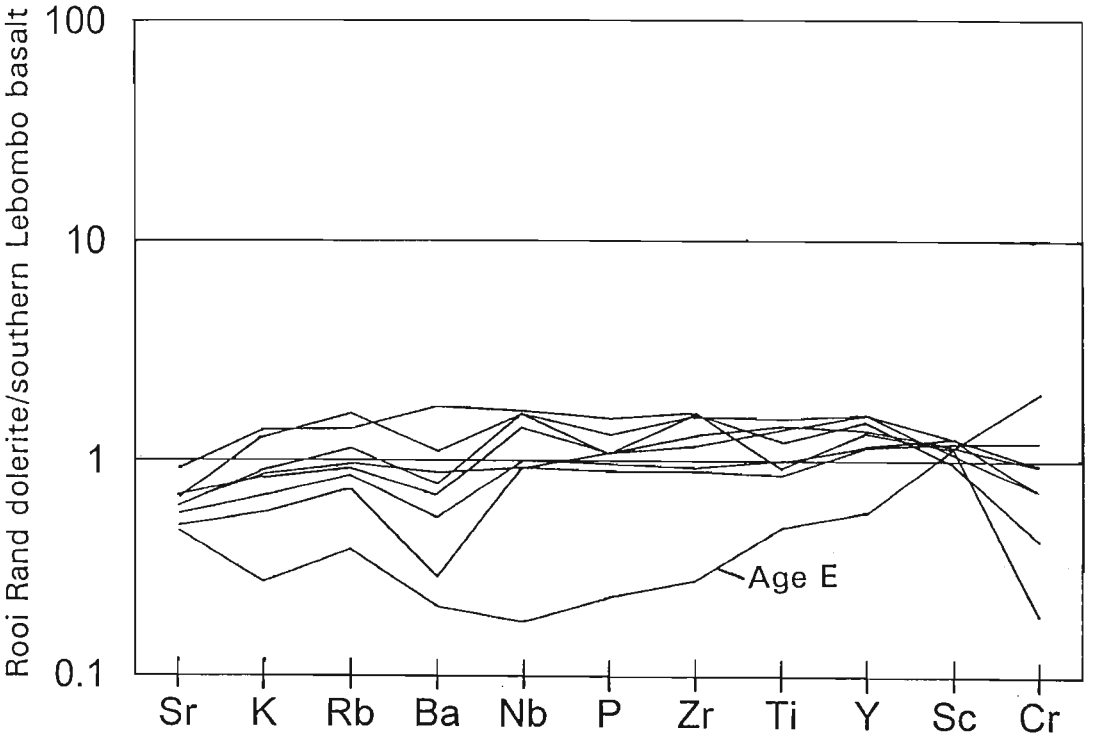

Figure 6.5 Spidergram plot of the Rooi Rand dolerites normalized to an average southern Lebombo Karoo basalt of the Sabie River Basalt Formation (data from Duncan *et al.*, 1984b).

6.2.2 *Oxygen isotopes*

Table 6.1 shows the results of oxygen isotope analyses conducted by Dr. C. Harris (Department of Geological Sciences, University of Cape Town) on samples from this study. For details on analytical methods, errors and duplication of data, the reader is referred to Harris (1995).

Table 6.1 $\delta^{18}O$ values for the Rooi Rand dolerites (Harris, 1995).

Sample Number (relative age)	δmineral (‰)	δmagma (‰)
DM90.7 (Age G)	$5.85_{plagioclase}$	5.65
DM90.25 (Age G')	$5.57_{plagioclase}$	5.37
DM90.20 (Age E)	$5.33_{plagioclase}$	5.13
DM90.20 (Age E)	$6.4_{pyroxene}$	6.9

$\delta^{18}O$ values of the original magmas are estimated from mineral isotope values, based on the assumption that there is not much effect of alteration on the mineral phenocryst $\delta^{18}O$ values. Harris (1995) prefers to base estimates of the $\delta^{18}O$ of the magma on the pyroxene values, because pyroxenes are generally less susceptible to alteration. Postmagmatic hydrothermal alteration frequently results in modification of isotopic ratios, although no evidence for hydrothermal alteration was noted in the Rooi Rand dolerites. It is for this reason that the value used in Harris (1995) for DM90.20 (Age E) was that of the pyroxene.

Figure 6.6 shows oxygen isotopes obtained by Harris (1995) using samples from this study, in addition to the oxygen isotope field for the Lebombo rhyolites, Karoo basalts, Kirwan basalts and MORB. It may be noted that the Rooi Rand dolerites have far lower $\delta^{18}O$ values than the Karoo and Kirwan basalts, indicating their original derivation from a MORB-like source. This is consistent with the fact that the majority of Karoo lavas are considered to represent magmas from lithospheric mantle sources (Duncan *et al.*, 1984b; Duncan *et al.*, 1990), or at least with a greater lithospheric component, whereas the Rooi Rand dolerites tend to have a more asthenospheric signature, although only one age has been shown to be directly asthenospherically-derived. Uncontaminated mantle-derived

basaltic magmas, of which MORB is the main example, have $\delta^{18}O$ values close to 5.7‰ (Harris and Erlank, 1992). Harris (1995) assuming Age E's pyroxene value to be more reliable only plotted this on the original diagram. The plagioclase value for Age E has been added onto Figure 6.6. It is not surprising that Age E had the lowest $\delta^{18}O$ plagioclase value, because it is the most depleted sample in the Rooi Rand dolerites. It plots outside the given MORB field on the diagram.

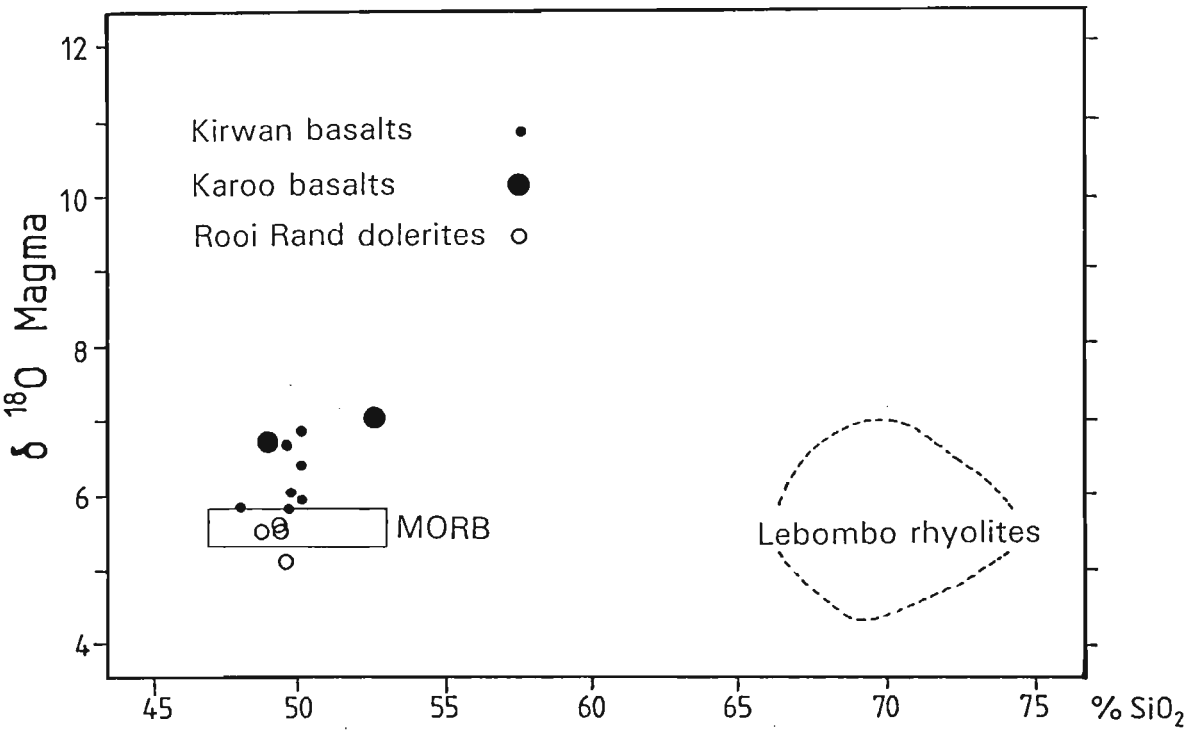

Figure 6.6 The $\delta^{18}O$ values of Karoo magmas calculated from phenocryst $\delta^{18}O$ (‰)values versus SiO_2 content. The range of values for mid-ocean ridge (MORB) is shown (Ito *et al.*, 1987) (after Harris, 1995).

The very similar $\delta^{18}O$ values for the Lebombo rhyolites and Rooi Rand dolerites may be noted. Harris and Erlank (1992) mention that partial melting of a Rooi Rand dolerite, with minor amounts of pre-Karoo crust or Sabie River basalt as contaminant, could produce a rhyolite with an isotopic composition similar to the Lebombo rhyolites. Harris and Erlank (1992) and Harris (1995) then propose that large volumes of water would also have been involved in the production of the low $\delta^{18}O$-rhyolites.

It is interesting to note that the earliest rhyolite flow, the Mkutshane Beds is intercalated with the southern Sabie River Basalts (Cleverly *et al.*, 1984). It has lower silica than the average rhyolite and a trace element composition not dissimilar to Age B of the Rooi Rand

dolerites, at least appearing to form an intermediate composition between Age B (the most evolved Rooi Rand dolerite) and the rhyolites. The Mkutshane Beds are dismissed by Harris (1995), however, as having no genetic relation to the other rhyolites. The suggestion that the bulk of the rhyolites were formed by partial melting is plausible, whereas the earliest manifestations of rhyolite intrusion would have been more contaminated versions of Age B (Rooi Rand), such as the Mkutshane Beds.

6.2.3 *Radiogenic isotopes*

Figure 6.7 shows Nd- and Sr-isotope ratios for the Karoo basalts, together with the Rooi Rand dolerites, calculated at 190 Ma (Hawkesworth *et al.*, 1984). Mantle components were identified by Zindler and Hart (1986) for oceanic basalts.

It may be seen from Figure 6.7, that the Rooi Rand dolerites have negative ϵ_{Sr} and positive ϵ_{Nd} values. In comparison, Karoo basalts have positive ϵ_{Sr} values and negative ϵ_{Nd} values. The Rooi Rand dolerites appear similar in composition to the depleted mantle source, similar to that for enriched MORB. The Karoo on the other hand have a far more enriched mantle signature. It may be noted that some of the southern Lebombo basalt values fall within the same compositional area of the Rooi Rand dolerites. Although no radiogenic isotope data has been obtained in this study, the two Rooi Rand compositions plotted on this diagram are fairly similar to those of Ages B and E, Age E being the more depleted one, with a composition closer to the depleted MORB mantle source, and Age B having a relatively enriched component.

The Rooi Rand dolerites have consistently low $^{87}Sr/^{86}Sr$ R_0 ratios (0.7035-0.70416) (Bristow *et al.*, 1984) despite exhibiting a considerable range in major and trace element compositions. Their R_0 ratios are amongst the lowest measured for any rock type in the Lebombo and contrast sharply with the high R_0 ratios for the basalts. The average initial $^{87}Sr/^{86}Sr$ ratio for all analysed rhyolites is 0.7045 (Harris and Erlank, 1992). The Rooi Rand dolerite Sr-isotopic characteristics are consistent with the overall "depleted" compositional features of the dykes as exhibited by Nd-isotopic composition and low incompatible element abundances (Hawkesworth *et al.*, 1984).

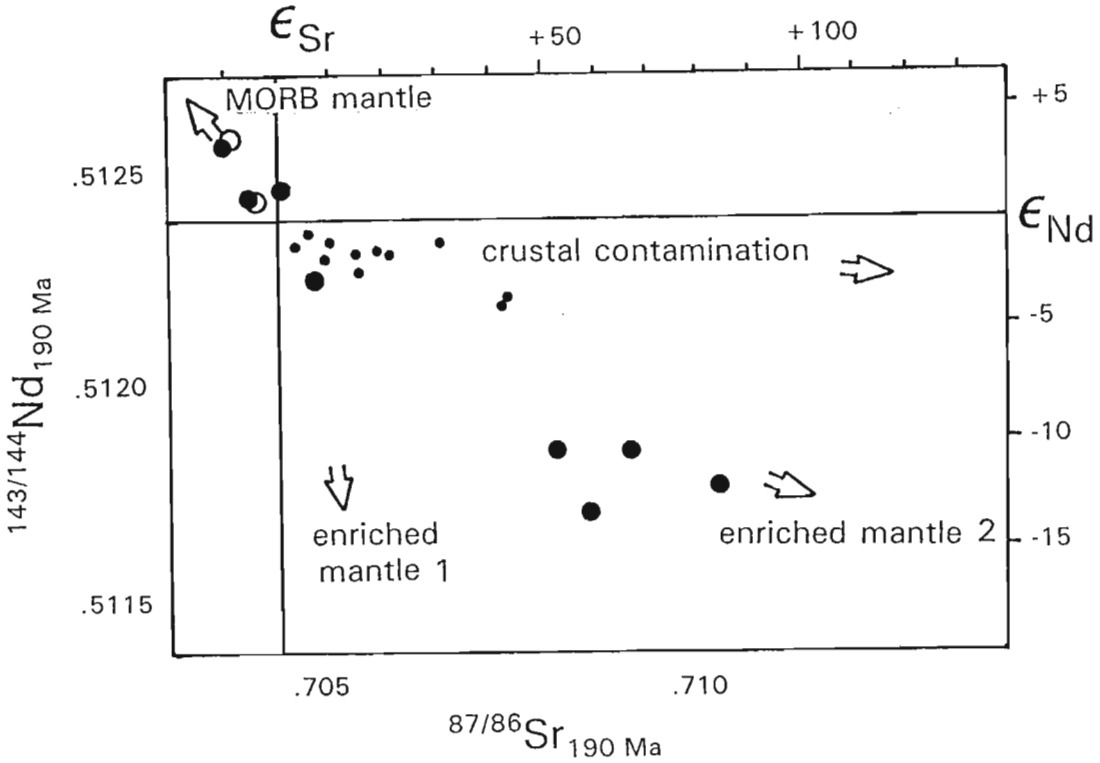

Figure 6.7 Nd- and Sr-isotope ratios for the Karoo basalts, together with the Rooi Rand dolerites, calculated at 190 Ma (after Sweeney and Watkeys, 1990). Data from Hawkesworth *et al.* (1984) and mantle components were identified by Zindler and Hart (1986) for oceanic basalts.

○ Rooi Rand dolerites; ● southern Lebombo basalts; • central Karoo basalts

Overall, oxygen and radiogenic isotope studies indicate a high asthenospheric depleted component, such that even the most enriched Rooi Rand dolerites still appear to fall to the depleted side of the Karoo dolerites, representing relatively uncontaminated magmas. This would tend to indicate that although most ages may have been partial melts from the lithospheric mantle, that material in the lithospheric mantle would originally have formed from a high degree partial melt of asthenospheric composition similar to Age E.

6.2.4 *Tectonomagmatic discrimination of the Rooi Rand dolerites*

Figures 6.7 and 6.8 show the Rooi Rand dolerites from this study as well as those from Armstrong (1978) at the same locality, plotted onto trace element tectonomagmatic discrimination diagrams.

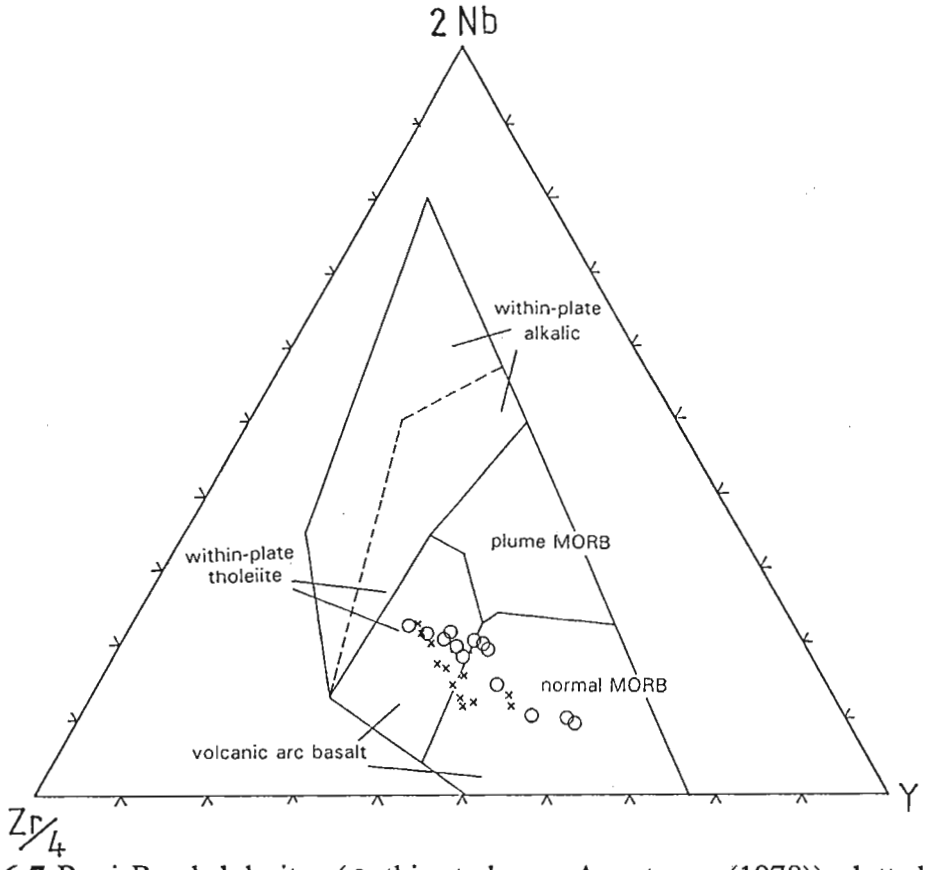

Figure 6.7 Rooi Rand dolerites (○ this study ; x Armstrong (1978)) plotted on a 2Nb-Zr/4-Y tectonomagmatic discrimination diagram for basaltic rocks (Meschede, 1986).

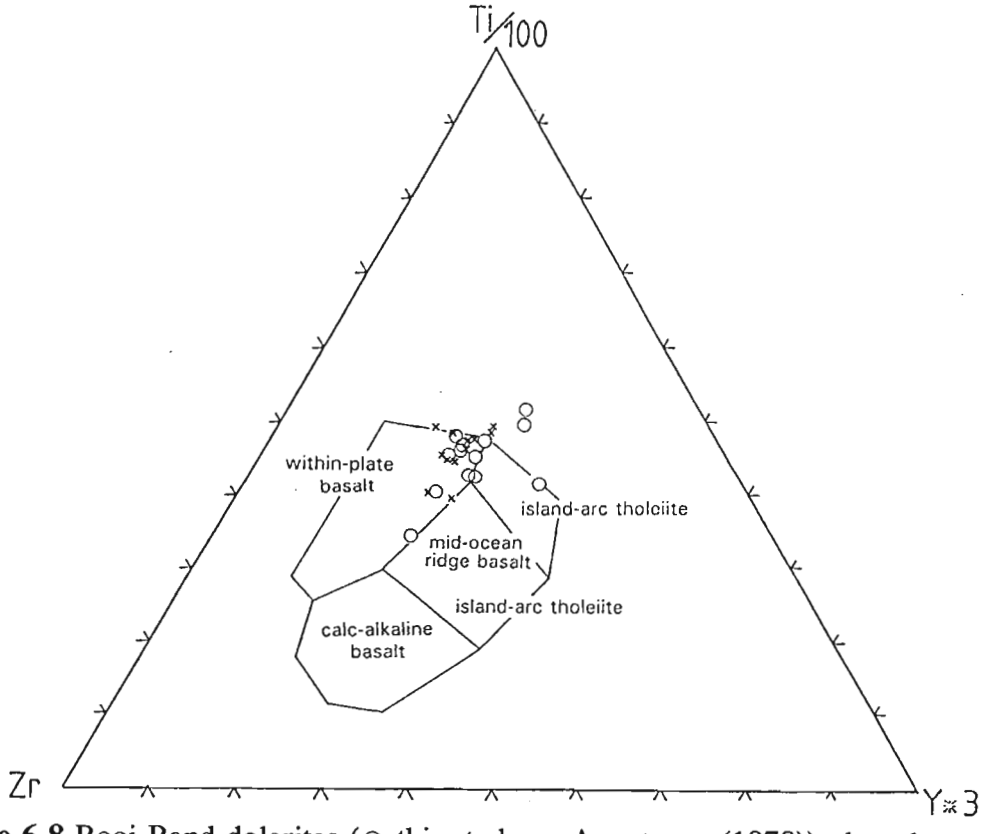

Figure 6.8 Rooi Rand dolerites (○ this study; x Armstrong (1978)) plotted on a Ti/100-Zr-Y*3 tectonomagmatic discrimination diagram for basaltic rocks (Pearce and Cann, 1973).

In Figure 6.7, as would be expected, the Rooi Rand dolerites plot into the within-plate tholeiite and normal mid-ocean ridge basalt (MORB) field, with the highest relative enrichment of Y being for Age E dolerites. The most enriched within-plate dolerite, that which falls closest to the Zr/Nb base line is Age B.

The fields in Figure 6.8 (Ti/100-Zr-Y*3) are not very well constrained. The majority of the dolerites fit within the within-plate basalts, which is expected, with Age E, because of its relative depletion in Zr and Y, and enrichment in Ti, plotting out of the fields. Brewer *et al.* (1992) suggest that fractionation of Ti-magnetite will affect the Ti/Y and Zr/Y ratios. This is one possible reason why all the data plot far too high on the diagram, as opposed to normal Karoo dolerite and basalts (the Rooi Rand dolerites being more enriched in Ti than the Karoo dolerites).

In general, these two tectonic discrimination diagrams serve to confirm the relative enrichment trend already observed in the whole-rock geochemistry and also confirm the fact that the majority of the dolerites have a lithospheric mantle "within-plate basalt"-type chemistry, with Age E standing apart as being more MORB-like.

Figures 6.9 and 6.10 are trace element spidergram plots of the Rooi Rand dolerites normalized to within-plate tholeiites and mid-ocean ridge basalts respectively. Normalization values of Pearce (1982) were chosen for consistency because these have been used by previous workers (Duncan *et al.*, 1990). Ages E and H have been plotted on separate graphs to highlight their distinctive chemistries, Age E representing a different source magma to the other dolerites, and Age H being the earliest partial melt.

Spidergrams of the Rooi Rand dolerites normalized to within-plate tholeiites (Figure 6.9) have a very similar appearance to those in Figures 6.2 to 6.5, which is to be expected, since the Karoo basalts are within-plate basalts.

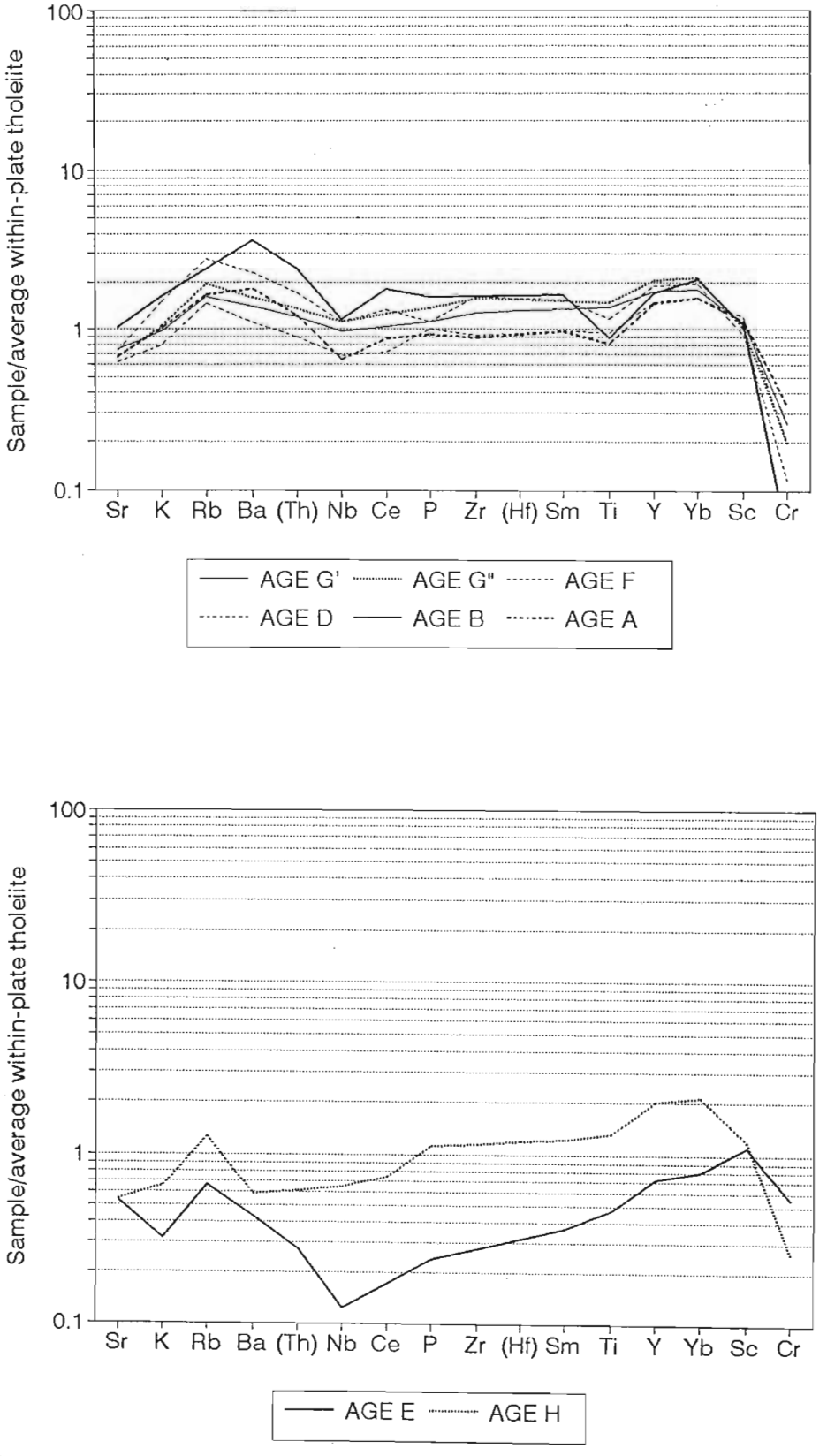

Figure 6.9 Spidergram plot of the Rooi Rand dolerites normalized to an average within-plate tholeiite (data from Pearce, 1982). Top figure, Ages G′, G″, F, D, B and A. Bottom figure, Ages E and H.

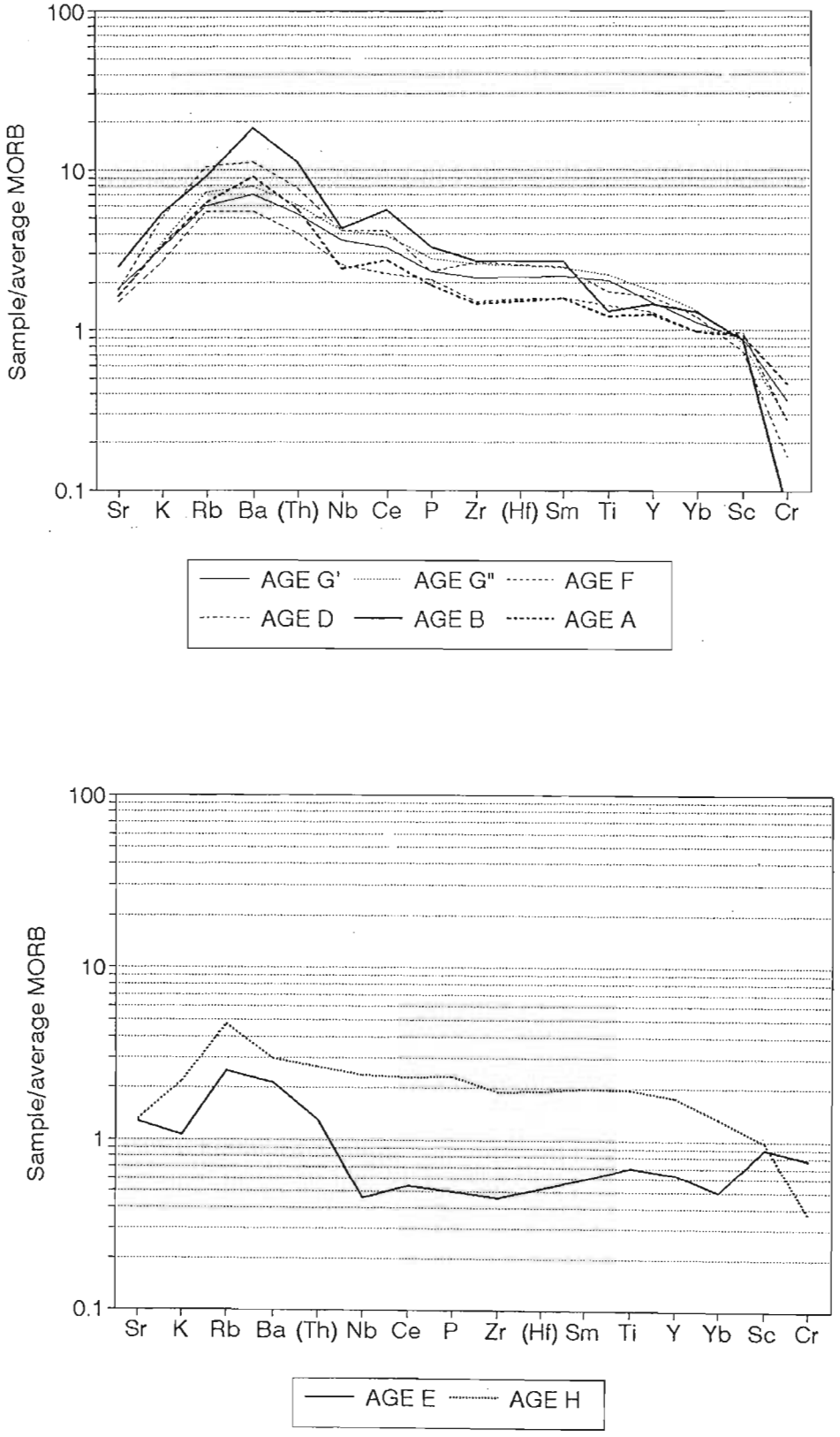

Figure 6.10 Spidergram plot of the Rooi Rand dolerites normalized to an average mid-ocean ridge basalt (data from Pearce, 1982). Top figure, Ages G′, G″, F, D, B and A. Bottom figure, Ages E and H.

Duncan (1987) on a similar spidergram normalized to MORB, state that the Rooi Rand dolerites are all geochemically similar to MORB. It must be stressed that the sample used in Duncan (1987) was the most depleted of Armstrong's (1978) sample set, similar in composition to Age E from this study. In this study, the asthenospheric "depleted" magma type has been shown to be the least common. It cannot be said therefore that all the Rooi Rand dolerites are MORB-like in chemistry, and this may be seen clearly on Figure 6.10. Age E is clearly the most MORB-like, but is enriched in Rb and Ba, and depleted in Ti, Y, Ce, Nb and Zr with respect to MORB.

Duncan *et al.* (1990) state that the Rooi Rand are thought to have been derived from an asthenospheric source, whereas the Karoo basalts are likely to have been generated by decompression melting due to lithospheric thinning associated with mantle plumes and/or the disruption of Gondwana. This study has shown this not to be strictly true, by identifying melts of lithospheric and asthenospheric composition in the Rooi Rand. It is acknowledged however, from isotope data (oxygen and radiogenic), that the dolerites have a depleted signature in comparison to other Karoo volcanics. If one assumes that the majority of the Rooi Rand dolerites and the Karoo basalts come from the lithospheric mantle, the lithospheric mantle must display some degree of heterogeneity, with depleted zones (such as would have originally been derived from the asthenosphere) producing the Rooi Rand dolerites and enriched mantle zones producing the bulk of the Karoo magmas.

Interestingly, White and McKenzie (1995) have since proposed a continental lithospheric source for the Karoo basalts, with melts which were merely remobilised by the thermal anomaly of the plume. In this case, a heterogeneous lithospheric mantle source would then not be required.

6.3 Tectonomagmatic Model

It is necessary to present an overall model of how the dykes may be geochemically inter-related, whilst bearing in mind the fact that only one model of fractional crystallization appeared to work, and several of the partial melt models were viable.

The overall pattern is interpreted as a result of the interaction of lithospheric stretching and asthenospheric upwelling (Watkeys *et al.*, 1995). A schematic diagram combining all the REE profiles and taking the time factor into consideration (Figure 6.11), shows how the dykes are genetically related. Figure 6.11 also shows the relative percentage volumes of magma for each dyke phase.

1) Ages H, G′, G″ and F were produced in the lithospheric mantle (their parent magma originally having been derived from a depleted E-like source) during initial phases of lithospheric stretching. For early magmas to ascend, enough partial melt had to accumulate, hence the higher degree (5-10%) of partial melting for Age H. Once a pathway had formed, successively lower degrees of partial melts - Age G′, 5%; Age G″, 0-2%, Age F, 0-2%, were able to "escape" and intrude. The opening of the pathway is reflected in increasing volumes of melt, corresponding to the decreasing amounts of partial melting.

2) Lithospheric stretching allowed asthenospheric upwelling resulting in asthenospheric-derived magma being injected into the crust - that is Age E. Increased lithospheric stretching above the rising asthenosphere may have assisted with the injection of phases G and F.

3) As the system did not develop into a mid-ocean ridge, but remained as a failed rift, this asthenospheric wedge did not continue to rise. Its presence induced increasingly higher degrees of partial melting in the overlying lithospheric mantle to yield phases D and C. Age D was modelled as having been derived from a 15-20% partial melt from an E-like relatively depleted source. Volumes of melt intruding the crust however, decreased. With the cessation of asthenosphere-assisted stretching, the volume of melt intruding the crust

decreased (see D and C).

4) There is clearly a difference in the way the Ages C, B and A relate to one another. They do not form the classic partial melt sequence, but rather the standard pattern for magmas which have undergone fractional crystallization, C being the source magma, B being derived from C, leaving an A-like residue, which is later melted and intruded. It may be recalled that this was the only model of fractional crystallization which appeared to work. Melts gathered in sub-crustal magma chambers and underwent fractional crystallization dominated by the removal of clinopyroxene (19%) and plagioclase (16%) with 60% (F-value) of the melt remaining. Fractionation may have been accompanied by a small degree of crustal contamination, with r-values (mass assimilated/mass fractionated) between 0.15 and 0.3, and F values of 0.65 to 0.62 to 0.83, to produce the silica-rich, "evolved" Age B. The magmas from these chambers injected as Ages B and A.

Figure 6.12 shows a simplified dilational history for the dykes at the Pongolo River locality (after Watkeys *et al.*, 1995). The colours have been simplified into the sequence of events as listed above, and as shown in Figure 6.11. The four main frames therefore show the sequence of: initial lithospheric stretching, asthenospheric upwelling, failed rift, and melts in subcrustal magma chambers. This interpretation was only made possible through the results of detailed mapping at the outcrop locality.

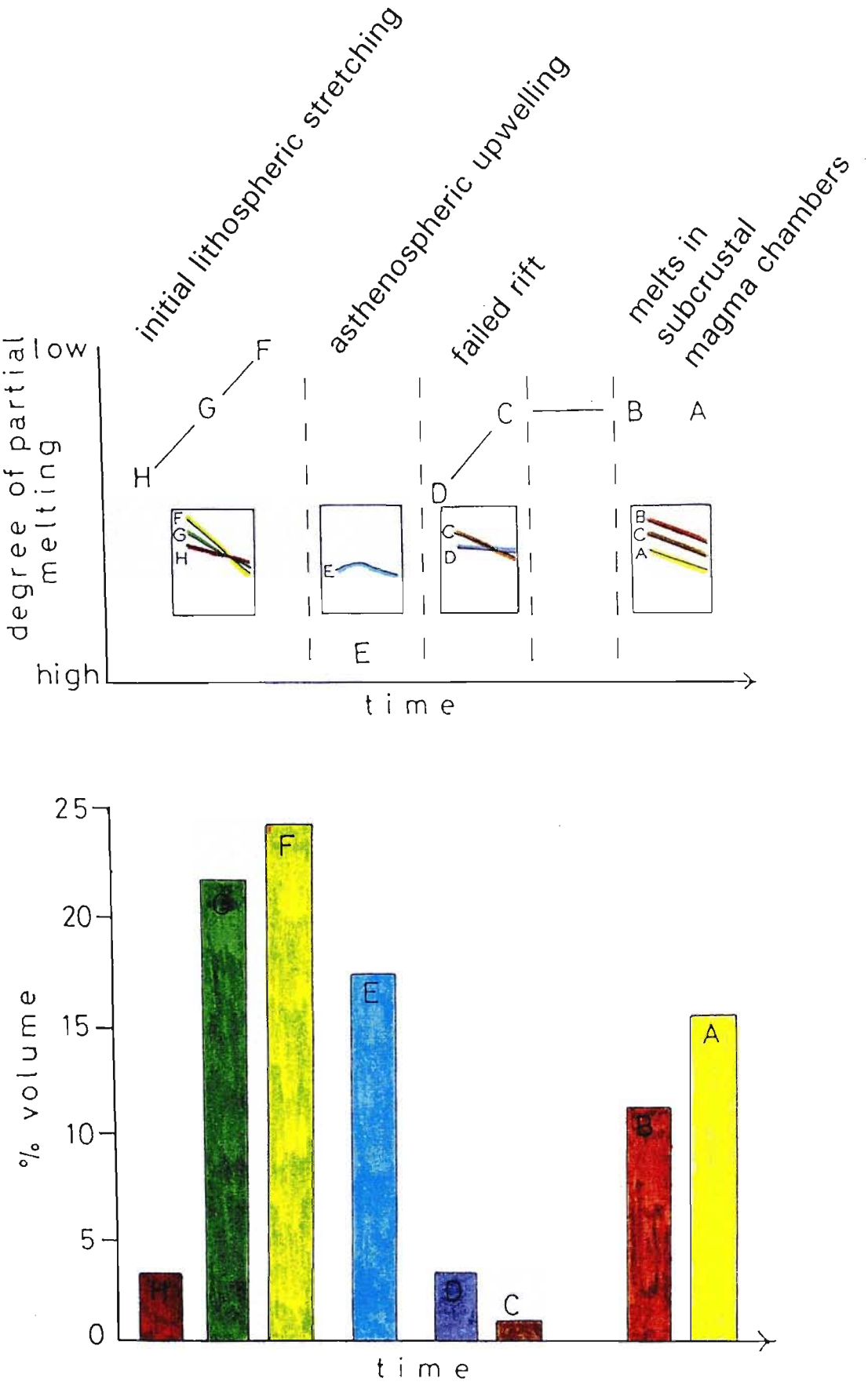

Figure 6.11 (top) Diagram showing the geochemical evolution of the Rooi Rand dykes in terms of time versus the degree of mantle partial melting. The insets are schematic illustrations of the REE profiles for the different ages. (bottom) Diagram showing time versus % volume melt for the Rooi Rand dykes (from Watkeys *et al.*, 1995).

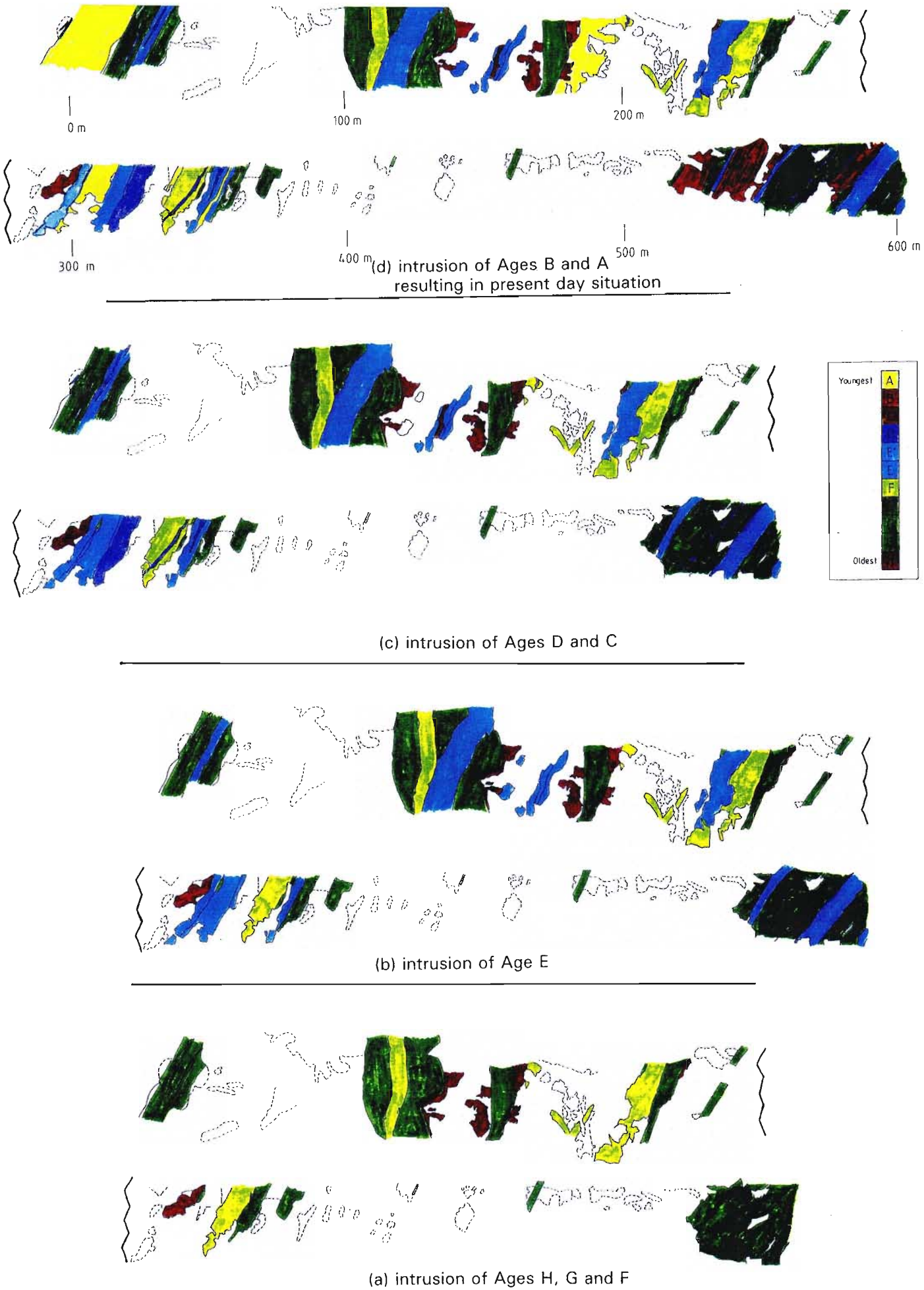

Figure 6.12 Simplified dilational history of the 600m-long outcrop of dykes at the study area (from Watkeys *et al*, 1995).

6.4 Concluding statements

Questions regarding the exact relationship between the Rooi Rand dolerites and the Sabie River basalts may only be answered if similar detailed sampling studies are conducted on the Sabie River Basalt Formation. These may indicate greater variability in the basalts, and a possible genetic link to the Rooi Rand dolerites. A more detailed radiogenic isotope study should also be carried out to further constrain the geochemistry of the dykes, and in the light of the new Karoo ages (determined by Marsh *et al.*, in press), place them in their exact geological position. All Karoo basaltic events have now been placed at 180 Ma, and the Rooi Rand is seen intruding the lower Sabie River basalts in places. This implies that the Rooi Rand is most probably directly related to the basalts which it intrudes as well as those above. Since only a small part of the dyke swarm was covered in this study, similar detailed studies would be encouraged at other outcrop localities in the swarm.

Similarly, the probable relationship between the Rooi Rand dolerites and the Lebombo rhyolites should be further explored. Because the Explora Wedge has been correlated with the Lebombo monocline basalts and rhyolites, and this study has shown that the Rooi Rand is most likely related to those basalts and rhyolites, it is possible to state that the Rooi Rand dolerites may be intimately related to the Explora Wedge volcanics, perhaps being an on-continent expression of them. The possibility of this should be further investigated.

The tectonomagmatic model presented above explains the inter-dyke compositional relationships of the Rooi Rand dyke swarm, which at the study area is represented by a suite of 11 different dyke ages which do not show simple geochemical evolution with time. Contrary to previous assumptions due to poorly constrained sampling, this thesis shows that there is a high degree of variability in Rooi Rand magma compositions. The diverse geochemistry may be linked systematically to relative ages of intrusion and relative volumes with time. The volumes are in turn linked to the tectonic and genetic history. Evolution of the magmas may be described in terms of partial melting, fractional crystallization and crustal contamination processes.

Whole rock major, trace and rare earth element data indicate an enriched lithospheric source for the majority of dyke phases (although magmas may originally have been asthenospherically derived), and a directly asthenospheric (or depleted) source for Age E (and probably Age E'). Contrary to this, isotopic data (oxygen and radiogenic) indicate an "enriched" asthenospheric source for all the dolerites, even the most highly enriched (Age B). This suggests that all ages may have originally been derived from the asthenosphere, with an Age E-like composition being intruded into the lithospheric mantle to later undergo partial melting and fractional crystallization, with some assimilation to form the other dyke phases.

The Rooi Rand dyke swarm represents a failed rift system, with dyke phases derived originally from the asthenosphere being progressively influenced by the lithosphere. The progression from lithospheric- to asthenospheric-source magmas is seen in all major rift settings. In this case however, the rift failed to develop into a mid-ocean ridge, and subsequent magmas underwent fractional crystallization in a sub-crustal magma chamber.

REFERENCES

Allsopp, H.L., Manton, W.I., Bristow, J.W. and Erlank, A.J. (1984). Rb-Sr geochronology of Karoo felsic volcanics. *In*: Erlank, A.J. (ed.). *Spec. Publ. geol. Soc. S. Afr.*, **13**, 273-280.

Armstrong, R.A. (1978). *A Geological and Geochemical Appraisal of the Rooi Rand Dyke Swarm, Lebombo.* MSc. Thesis (unpubl.), Univ. Natal, Durban, 135pp.

Armstrong, R.A., Bristow, J.W. and Cox, K.G. (1984). The Rooi Rand Dyke Swarm, southern Lebombo. *In*: Erlank, A.J. (ed.). *Spec. Publ. geol. Soc. S. Afr.*, **13**, 77-86.

Bence, A.E. and Albee, A.L. (1968). Empirical correction factors for the electron microanalysis of silicates and oxides. *J. Geol.*, **76**,382-483.

Bottinga, Y., Kudo, A., and Weill, D. (1966). Some observations on oscillatory zoning and crystallization of magmatic plagioclase. *American Mineralogist*, **51**, 792-806.

Bougault, H. and Hekinian, R. (1974). Rift valley in the Atlantic Ocean near 36°50'N: Petrology and geochemistry of basaltic rocks. *Earth Planet. Sci. Lett.*, **24**, 249-261.

Bowen, N.L. (1913). The melting phenomena of the plagioclase feldspars, *Am. J. Sci.*, Ser.4, **35**, 577-599.

Bowen, N.L. and Schairer, J.F. (1935). The system MgO-FeO-SiO_2. *Am. J. Sci.*, **29**, 151-217.

Bradshaw, T.K., Hawkesworth, C.J. and Gallagher, K. (1993). Basaltic volcanism in the Southern Basin and Range: no role for a mantle plume. *Earth Planet. Sci. Lett.*, **166**, 45-62.

Brewer, T.S., Hergt, J.M., Hawkesworth, C.J., Rex, D. and Storey, B.C. (1992). Coats Land dolerites and the generation of Antarctic continental flood basalts. *In:* Storey, B.C., Alabaster, T. and Pankhurst, R.J. (eds.), Magmatism and the Causes of Continental Break-up, *Spec. Publ. geol. Soc.*, **68**, 185-208.

Bristow, J.W. (1977). *The Geology and Geochemistry of the Southern Lebombo.* MSc. Thesis (unpubl.), Univ. Natal, Durban, 331pp.

Bristow, J.W., Allsopp, H.L., Erlank, A.J., Marsh, J.S. and Armstrong, R.A. (1984). Strontium isotope characterisation of Karoo volcanic rocks. *In*: Erlank, A.J. (ed.). *Spec. Publ. geol. Soc. S. Afr.*, **13**, 295-329.

Bristow, J.W. and Cox, K.G. (1984). Volcanic rocks of the Lebombo-Nuanetsi-Sabi zone: classification and nomenclature. *In*: Erlank, A.J. (ed.). *Spec. Publ. geol. Soc. S. Afr.*, **13**, 69-75.

Bristow, J.W. and Saggerson, E.P. (1983). A general account of Karoo vulcanicity in southern Africa. *Geologische Rundschau*, **72**, 1015-1060.

Brooks, C.K. (1976). The Fe_2O_3/FeO ratio of basalt analyses: an appeal for a standardised procedure. *Bull. Geol. Soc. Denmark.*, **25**, 117-120.

Brouxel, M. (1991). Geochemical consequences of flow differentiation in a multiple injection dike (trinity ophiolite, N. California). *Lithos*, **26**, 245-252.

Bryan, W.B., Finger, L.W. and Chayes, F. (1969). Estimating proportions in petrographic mixing equations by least squares approximation. *Science*, **163**, 926-927.

Campbell, I.H. and Griffiths, R.W. (1990). Implications of mantle plume structure for the evolution of flood basalts. *Earth Planet. Sci. Lett.*, **99**, 79-93.

Cawthorn, R.G., Bristow, J.W. and Groves, D.I. (1989). Magnesian ilmenite in picritic basalts from the Karoo Province, South Africa. *Min. Mag.*, **53**, 245-252.

Cleverly, R.W. (1977). *The structural and magmatic evolution of the Lebombo monocline, southern Africa, with particular reference to Swaziland.* Unpubl. D. Phil. Thesis, Oxford University, 316pp.

Cleverly, R.W., Betton, P.J. and Bristow, J.W. (1984). Geochemistry and petrogenesis of the Lebombo rhyolites. *In*: Erlank, A.J. (ed.). *Spec. Publ. geol. Soc. S. Afr.*, **13**, 171-194.

Coish, R.A. and Taylor, L.A. (1979). The effects of cooling rate on textural and pyroxene chemistry in DSDP LEG 34 basalts: a microprobe study. *Earth Planet. Sci. Lett.*, **42**, 389-398.

Consolmagno, G.J. and Drake, M.J. (1976). Equivalence of equations describing trace element distribution during equilibrium partial melting. *Geochim. Cosmochim. Acta.*, **40**, 1421-1422.

Cox, K.G. (1980). A model for flood basalt vulcanism. *J. Petrology*, **21**, 629-650.

Cox, K.G., Bell, J.D. and Pankhurst, R.J. (1979). *The Interpretation of Igneous Rocks.* George Allen & Unwin, Great Britain, 450pp.

Cox, K.G. and Clifford, P. (1982). Correlation coefficient patterns and their interpretation in three basaltic suites. *Contrib. Mineral. Petrol.*, 268-278.

Cox, K.G., Duncan, A.R., Bristow, J.W., Taylor, S.R. and Erlank, A.J. (1984). Petrogenesis of the basic rocks of the Lebombo. *In*: Erlank, A.J. (ed.). *Spec. Publ. geol. Soc. S. Afr.*, **13**, 149-169.

Cross, W., Iddings, J.P., Pirsson, L.V. and Washington, H.S. (1902). A quantitative chemico-mineralogical classification and nomenclature of igneous rocks. *J. Geol.*, **10**, 555-690.

Dale, I.M. and Henderson, P. (1972). The partitioning of transition elements in phenocryst-bearing basalts and their implications about melt structure. *24th Int. Geol. Cong. Sect.*, **10**, 105-111.

Deer, W.A., Howie, R.A. and Zussman, J. (1989). *An Introduction to the Rock Forming Minerals.* Longman Scientific & Technical, Essex, 528pp.

Deer, W.A., Howie, R.A. and Zussman, J. (1978). *Rock-Forming Minerals*, Volume 2A, Single-Chain Silicates. Longman, London, 668pp.

DePaolo, D.J. (1981). Trace element and isotopic effects of combined wallrock assimilation and fractional crystallization. *Earth Planet. Sci. Lett.*, **53**, 189-202.

Duncan, A.R. (1987). The Karoo Igneous Province - a problem area for inferring tectonic setting from basalt geochemistry. *J. Volcan. Geotherm. Res.*, **32**, 13-34.

Duncan, A.R., Armstrong, R.A., Erlank, A.J., Marsh, J.S. and Watkins, R.T. (1990). MORB-related dolerites associated with the final phases of Karoo flood basalt volcanism in southern Africa. *In:* Parker, A.J., Rickwood, P.C. and Tucker, D.H. (eds.) *Mafic Dykes and Emplacement Mechanisms*, A.A. Balkema, Rotterdam, 119-129.

Duncan, A.R., Erlank, A.J. and Betton, P.J. (1984a). Appendix 1: Analytical techniques and database descriptions. *In*: Erlank, A.J. (ed.). *Spec. Publ. geol. Soc. S. Afr.*, **13**, 389-395.

Duncan, A.R., Erlank, A.J. and Marsh, J.S. (1984b). Regional geochemistry of the Karoo Igneous Province. *In*: Erlank, A.J. (ed.). *Spec. Publ. geol. Soc. S. Afr.*, **13**, 355-388.

Du Toit, A.L. (1929). The volcanic belt of the Lebombo - a region of tension. *Trans. Royal. Soc. S. Afr.* **18**, 189-218.

Eales, H.V., Marsh, J.S. and Cox, K.G. (1984). The Karoo Igneous Province: an introduction. *In*: Erlank, A.J. (ed.). *Spec. Publ. geol. Soc. S. Afr.*, **13**, 1-26.

Elliot, D.H. (1992). Jurassic magmatism and tectonism associated with Gondwanaland break-up: an Antarctic perspective. *In:* Storey, B.C., Alabaster, T. and Pankhurst, R.J. (eds.), Magmatism and the Causes of Continental Break-up, *Spec. Publ. geol. Soc.*, **68**, 165-184.

Elsdon, R. (1975). Iron-titanium oxide minerals in igneous and metamorphic rocks. *Min. Sci. Eng.*, **7**, 48-70.

Erlank, A.J., Marsh, J.S., Duncan, A.R., Miller, R.McG., Hawkesworth, C.J., Betton, P.J. and Rex, D.C. (1984). Geochemistry and petrogenesis of the Etendeka volcanic rocks from SWA/Namibia. *In*: Erlank, A.J. (ed.). *Spec. Publ. geol. Soc. S. Afr.*, **13**, 195-245.

Ernst, R.E. and Bell, K. (1992). Petrology of the Great Abitibi Dyke, Superior Province, Canada. *J. Petrology*, **33**, 423-469.

Evensen, N.M., Hamilton, P.J. and O'Nions, R.K. (1978). Rare-earth abundances in chondritic meteorites. *Geochim. Cosmochim. Acta*, **42**, 1199-1212.

Fitch, F.J. and Miller, J.A. (1984). Dating Karoo igneous rocks by the conventional K-Ar and $^{40}Ar/^{39}Ar$ age spectrum methods. *In*: Erlank, A.J. (ed.). *Spec. Publ. geol. Soc. S. Afr.*, **13**, 247-266.

Frey, F.A., Green, D.H. and Roy, S.D. (1978). Integrated models of basalt petrogenesis: A study of quartz tholeiites to olivine melilitites from south-eastern Australia utilizing geochemical and experimental petrological data. *J. Petrology*, **19**, 463-513.

Furnes, H., Neumann, E-R and Sundvoll, B. (1982). Petrology and geochemistry of Jurassic basalt dykes from Vestfjella, Dronning Maud Land, Antarctica. *Lithos*, **15**, 295-304.

Gautneb, H. and Gudmundsson, A. (1992). Effect of local and regional stress fields on sheet emplacement in West Iceland. *J. Volcan. Geotherm. Res.*, **51**, 339-356.

Green, T.H. (1980). Island arc and continent-building magmatism: a review of petrogenetic models based on experimental petrology and geochemistry. *Tectonophysics*, **63**, 367-385.

Haggerty, S.E. (1976). Opaque oxide mineral oxides in terrestrial igneous rocks. *In*: Rumble, D., (ed.), *Oxide Minerals*. Min. Soc. Amer. Short Course Notes, Hg. 101-300.

Hall, A. (1987). *Igneous Petrology*, Longman Group, England, 573pp.

Hall, R.P., Hughes, D.J. and Friend, C.R.L. (1985). Geochemical evolution and unusual pyroxene chemistry of the MD tholeiite dyke swarm from the Archaean craton of southern west Greenland. *J. Petrology*, **26**, 253-282.

Hall, R.P., Hughes, D.J. and Friend, C.R.L. (1986). Complex sequential pyroxene growth in tholeiitic hypabyssal rocks from southern West Greenland, *Min. Mag.*, **50**, 491-502.

Hanson, G.N. (1980). Rare earth elements in petrogenetic studies of igneous systems. *Ann. Rev. Earth. Planet. Sci. Lett.*, **8**, 371-406.

Hanson, G.N. (1989). An approach to trace element modelling using a simple igneous system as an example. *In*: Lipin, B. and McKay, G. (eds.), *Geochemistry and Mineralogy of Rare Earth Elements*, Reviews

in Mineralogy, **21**, Mineralogical Society of America, 79-97.

Harris, C. (1995). The oxygen isotope geochemistry of the Karoo and Etendeka Volcanic Provinces of southern Africa. *S. Afr. J. Geol.*, **98**, 126-139.

Harris, C. and Erlank, A.J. (1992). The production of large-volume, low-$\delta^{18}O$ rhyolites during the rifting of Africa and Antarctica: The Lebombo Monocline, southern Africa. *Geochim. Cosmochim. Acta*, **56**, 3561-3570.

Harry, D.L. and Sawyer, D.S. (1992). Basaltic volcanism, mantle plumes, and the mechanics of rifting: The Paraná flood basalt province of South America. *Geology*, **20**, 207-210.

Hart, S.R. and Davis, K.E. (1978). Nickel partitioning between olivine and silicate melt. *Earth Planet. Sci. Lett.*, **40**, 203-219.

Haskin, L.A. (1984). Petrogenetic modelling - Use of rare earth elements, Chapter 4. *In:* Henderson, P. (ed.), *Rare Earth Element Geochemistry*, Elsevier Science Publishing Company, New York, 510pp.

Hatch, F.H., Wells, A.K. and Wells, M.K. (1972). *Petrology of the Igneous Rocks*, Textbook of Petrology, Vol. 1. George Allen & Unwin, London, 551pp.

Hawkesworth, C.J., Marsh, J.S., Duncan, A.R., Erlank, A.J. and Norry, M.J. (1984). The role of continental lithosphere in the generation of the Karoo volcanic rocks: evidence from combined Nd- and Sr-isotope studies. *In*: Erlank, A.J. (ed.). *Spec. Publ. geol. Soc. S. Afr.*, **13**, 341-354.

Heinrich, E. W. (1965). *Microscopic Identification of Minerals*. McGraw Hill, New York, 414pp.

Heinrich, K.F.J. (1981). *Electron Beam X-Ray Microanalysis*. Van Nostrand Reinhold Company, New York, 578pp.

Henderson, P. (1982). *Inorganic Chemistry*, Pergamon Press, Oxford, England, 353pp.

Henderson, P. (1984). General geochemical properties and abundances of the rare earth elements, Chapter 1. *In*: Henderson, P. (ed.), *Rare Earth Element Geochemistry*, Elsevier Science Publishing Company, New York, 510pp.

Henderson, P., Sélo, M. and Storzer, D. (1986). An investigation of olivine crystal growth in a picrite dyke, using the fission track method. *Min. Mag.*, **50**, 27-31.

Hergt, J.M., Chappell, B.W., McCullock, M.T., McDougall, I. and Chivas, A.R. (1989). Geochemical and isotopic constraints on the origin of the Jurassic dolerites of Tasmania. *J. Petrology*, **30**, 841-883.

Hertogen, J. and Gijbels, R. (1976). Calculation of trace element fractionation during partial melting. *Geochim. Cosmochim. Acta*, **40**, 313-322.

Hinz, R. and Krause, W. (1982) The continental margin of Queen Maud Land/Antarctica: seismic sequences, structural elements and geological development. Geologisches Jahrbuch, Reihe E, 23, 17-41. *In:* White, R. and McKenzie, D. (1989). Magmatism at rift zones: The generation of volcanic continental margins and flood basalts. *J. Geophys. Res.*, **94**, 7685-7729.

Hoek, J.D. (1995). Dyke propagation and arrest in Proterozoic tholeiitic dyke swarms, Vestfold Hills, East Antarctica. *In*: Baer, G. and Heimann, A. (eds.), *Physics and Chemistry of Dykes*, Balkema, Rotterdam, 79-93.

Hoffer, J.M. (1966). Compositional variations of plagioclase feldspar from a basaltic lava flow. *American*

Mineral., **51**, 807-813.

Hugo, V.E. (1993). *A study of titanium-bearing oxides in heavy mineral deposits along the east coast of South Africa*. Ph. D. Thesis (unpubl.), University of Natal, Durban, 357pp.

Humphris, S.E., Thompson, G., Schilling, J.G. & Kingsley, R.A. (1985). Petrological and geochemical variations along the Mid-Atlantic Ridge between 46°S and 32°S: influence of the Tristan da Cunha mantle plume. *Geochim. Cosmochim. Acta.*, **49**, 1445-1464.

Hunter, D.R. and Reid, D.L. (1987). Mafic dyke swarms in southern Africa. *In*: Halls, H.C. and Fahrig, W.F. (eds.), *Mafic Dyke Swarms*, Geol. Assoc. Spec. Pap. **34**, 445-456.

Huppert, H.E. and Sparks, S.J. (1989). Chilled margins in igneous rocks. *Earth Planet. Sci. Lett.*, **92**, 397-405.

Irvine, T.N. and Baragar, W.R.A. (1971). A guide to the chemical classification of the common volcanic rocks. *Can. J. Earth Sci.*, **8**, 523-548.

Ito, E., White, W.M. and Göpel, C. (1987). The O, Sr, Nd and Pb isotope geochemistry of MORB. *Chemical Geology*, **62**, 157-176.

Jarvis, K.E. (1989). Determination of rare earth elements in geological samples by inductively coupled plasma mass spectrometry. *J. Analytical Atomic Spectrometry*, **4**, 563-570.

Karson, J.A. (1987). Factors controlling the orientation of dykes in ophiolites and oceanic crust. *In:* Halls, H.C. and Fahrig, W.F. (eds.), *Mafic Dyke Swarms*, Geological Assoc. Canada, Spec. Pap., **34**, 229-241.

Kattenhorn, S.A. (1994). *Mechanisms of sill and dyke intrusion*, MSc. Thesis (unpubl.), Univ. Natal, Durban, 152pp.

Kattenhorn, S.A. and Watkeys, M.K. (1995). Blunt-ended dyke segments. *J. Struct. Geol.*, **17**, 1535-1542.

Kent, R.W., Storey, M. and Saunders, A.D. (1992). Large igneous provinces: sites of plume impact or plume incubation? *Geology*, **20**, 891-894.

Kerr, A.C. (1994). Lithospheric thinning during the evolution of continental large igneous provinces: A case study from the North Atlantic Tertiary province. *Geology*, **22**, 1027-1030.

Komar, P.D. (1972). Flow differentiation in igneous dikes and sills: profiles of velocity and phenocryst concentration. *Geol. Soc. Am. Bull.*, **83**, 3443-3448.

Korringa, M.K. and Noble, D.C. (1971). Distribution of Sr between natural feldspar and igneous melt. *Earth Planet. Sci. Lett.*, **11**, 147-151.

Kuno, H. (1950). Petrology of Hakone Volcano and the adjacent areas, Japan. *Bull. geol. Soc. Amer.*, **61**, 957-1020.

Kyle, P.R., Elliot, D.H. and Sutter, J.F. (1981). Jurassic Ferrar Supergroup tholeiites from the Transantarctic Mountains, Antarctica, and their relation to the initial fragmentation of Gondwana. *In:* Cresswell, M.M and Vella, P. (eds.), *Gondwana Five, Proceedings of the Fifth International Gondwana Symposium, Wellington, New Zealand*. A.A. Balkema, Rotterdam, 283-287.

Leeman, W.P. (1974). *Experimental determination of partitioning of divalent cations between olivine and basaltic liquid*. Ph. D. Thesis (unpubl.), Univ. Oregon, 303pp.

Leeman, W.P., Ma, M.-S., Murali, A.V. and Schmitt, R.A. (1978). Empirical estimation of magnetite/liquid distribution coefficients for some transition elements. *Contrib. Mineral. Petrology*, **65**, 269-272.

Lemarchand, F., Villemant, B. and Calas, G. (1987). Trace element distribution coefficients in alkaline series. *Geochim. Cosmochim. Acta*, **51**, 1071-1081.

Le Roex, A.P. (1980). *Geochemistry and mineralogy of selected Atlantic Ocean basalts*. Ph. D. Thesis (unpubl.), Univ. Cape Town, 281pp.

Le Roex, A.P. and Erlank, A.J. (1982). Quantitative evaluation of fractional crystallization in Bouvet Island lavas. *J. Volcan. Geotherm. Res.*, **13**, 309-338.

Lindstrom, D.J. (1976). *Experimental study of the partitioning of the transition metals between clinopyroxene and coexisting silicate liquids*. Ph. D. Thesis (unpubl.), Univ. Oregon, 188pp.

Lindstrom, D.J. and Weill, D.F. (1978). Partitioning of transition metals between diopside and coexisting silicate liquids. I:Nickel, cobalt and manganese. *Geochim. Cosmochim. Acta*, **42**, 817-831.

Loomis, T.P. (1982). Numerical simulations of crystallization processes of plagioclase in complex melts: the origin of major and oscillatory zoning in plagioclase. *Contrib. Mineral. Petrol.*, **81**, 219-229.

Loomis, T.P. and Welber, P.W. (1982). Crystallization processes in the Rocky Hill granodiorite pluton, California: an interpretation based on compositional zoning of plagioclase. *Contrib. Mineral. Petrol.*, **81**, 230-239.

MacDonald, G.A. and Katsura, T. (1961). Chemical composition of Hawaiian lavas. *J. Petrol.*, **5**, 82-113.

Marsh, J.S. (1987). Basalt geochemistry and tectonic discrimination within continental flood basalt provinces. *J. Volcan. Geotherm. Res.*, **32**, 35-49.

Marsh, J.S., Hooper, P.R., Rehacek, J., Duncan, R.A. and Duncan, A.R. (in prep.). Stratigraphy and age of Karoo basalts of Lesotho and implications for correlations within the Karoo igneous province. *In:* Mahoney, J. (ed.), *Large Igneous Provinces*, AGU press.

Martin, A.K. and Hartnady, C.J.H. (1986). Plate-tectonic development of the south-west Indian Ocean: a revised construction of East Antarctica and Africa. *J. Geophys. Res.*, **91**, 4767-4786

Meschede, M. (1986). A method of discriminating between different types of mid-ocean ridge basalts and continental tholeiites with the Nb-Zr-Y diagram. *Chem. Geol.*, **56**, 207-218.

Meth, D.L. (1990). *A study of some northern Natal Jurassic dolerite suites*. Third Year Project (unpubl.), Univ. Natal, Durban, 33pp.

Meth, D.L. (1991). The Rooi Rand dyke swarm: classification and intra/inter-dyke geochemical relationships. B.Sc. Hons. Thesis (unpubl.), Univ. Natal, Durban, 30pp.

Mohr, P. (1971). Ethiopian Tertiary dyke swarms. *Smithsonian Astrophys. Observ. Spec. Rep.* **339**.

Muir, I.D., Tilley, C.E. and Scoon, J.H. (1957). Contributions to the petrology of Hawaiian basalts. 1. The picrite basalts of Kilauea. *Amer. J. Sci.*, **255**, 241 -253.

Nagasawa, H. and Schnetzler, C.C. (1971). Partitioning of rare earth, alkali and alkaline earth elements between phenocryst and acidic igneous magma. *Geochim. Cosmochim. Acta*, **40**, 1539-1551.

Nakamura, Y. and Coombs, D.S. (1973). Clinopyroxenes in the Tawhiroko tholeiitic dolerite at Moeraki,

north-eastern Otago, New Zealand. *Contrib. Mineral. Petrol.*, **42**, 213-228.

Neumann, E.R. (1974). The distribution of Mn^{2+} and Fe^{2+} between ilmenites and magnetites in igneous rocks. *Amer. J. Sci.*, **274**, 1074-1088.

Nicholls, J. and Stout, M.Z. (1982). Heat affects of assimilation, crystallization and vesiculation in magmas. *Contrib. Mineral. Petrol.*, **81**, 328-339.

Nicholson, R. and Pollard, D.D. (1985). Dilation and linkage of en echelon cracks. *J. Struct. Geol.*, **7**, 583-590.

Nielsen, R.L. (1985). EQUIL: a program for the modelling of low-pressure differentiation processes in natural mafic magma bodies. *Comp. and Geosci.*, **11**, 531-546.

Nockolds, S.R. and Allen, R. (1956). The geochemistry of some igneous rock series: Part 3. *Geochim. Cosmochim. Acta*, **9**, 34-77.

O'Hara, M.J. (1977). Geochemical evolution during fractional crystallization of a periodically refilled magma chamber. *Nature*, **266**, 503-507.

Oliver, G.J.H. (1978). Ilmenite - magnetite geothermometry and oxygen barometry in granulite and amphibolite facies gneisses from Doubtful Sound, Fiordland, New Zealand. *Lithos*, **11**, 147-153.

Park, R.G. (1983). *Foundations of Structural Geology*, Blackie & Son Ltd., Glasgow, 135pp.

Paster, T.P., Schauwecker, D.S. and Haskin, L.A. (1974). The behaviour of some trace elements during solidification of the Skaergaard layered series. *Geochim. Cosmochim. Acta*, **38**, 1549-1577.

Pearce, J.A. (1982). Trace element characteristics of lavas from destructive plate margins. *In:* Thorpe, R.S. (ed.). *Andesites*. John Wiley & Sons, New York, 525-548.

Pearce, J.A. and Cann, J.R. (1973). Tectonic setting of basic volcanic rocks determined using trace element analysis. *Earth Planet. Sci. Lett.*, **19**, 290-300.

Pearce, J.A. and Norry, M.J. (1979). Petrogenetic implication of Ti, Zr, Y and Nb variations in volcanic rocks. *Contrib. Mineral. Petrol.*, **69**, 33-47.

Petterson, M.G. and Windley, B.F. (1992). Field relations, geochemistry and petrogenesis of the Cretaceous basaltic Jutal dykes, Kohistan, northern Pakistan. *J. Geol. Soc. London*, **149**, 107-114.

Philpotts, J.A. and Schnetzler, C.C. (1970). Phenocryst-matrix partitioning coefficients for K, Rb, Sr and Ba with application to anorthosite and basalt genesis. *Geochim. Cosmochim. Acta*, **34**, 307-322.

Platten, I.M. and Watterson, J. (1987). Magma flow and crystallization in dyke fissures. *In:* Halls, H.C. and Fahrig, W.F. (eds.), *Mafic Dyke Swarms*, Geol. Assoc. Can., Spec. Pap. **34**, 65-73.

Poldervaart, A. and Hess, H.H. (1951). Pyroxenes in the crystallization of basaltic magmas. *J. Geol.*, **59**, 472-489.

Pollard, D.D. (1987). Elementary fracture mechanics applied to the structural interpretation of dykes. *In*: Halls, H.C. and Fahrig, W.F. (eds.), *Mafic dyke swarms*, Geol. Assoc. Spec. Pap. **34**, 5-24.

Pringle, G.J., Trembath, L.T. and Pajari, G.E. (1974). Crystallization history of a zoned plagioclase. *Min. Mag.*, **39**, 867-877.

Ransome, I.G.D. and Reid, D.L. (1988). Geochemistry of a late Precambrian mafic dyke in the Vioolsdrif area, north-west Cape. Extended Abstracts. *22nd Earth Science Congress, Geol. Soc. S. Afr.*, 487-489.

Reynolds, I.M. (1983). The iron-titanium oxide mineralogy of Karoo dolerite in the Eastern Cape and southern Orange Free State. *Trans. geol. Soc. S. Afr.*, **86**, 211-220.

Ringwood, A.E. (1970). Petrogenesis of Apollo II basalts and implications for lunar origin. *J. Geophys. Res.*, **75**, 6453-6479.

Roberts, J.L. (1970). The intrusion of magma into brittle rocks. *In*: Newall, G. and Rast, N. (eds.) *Mechanisms of Igneous Intrusion*, Gallery Press, Liverpool, 287-338.

Robey, J. vA. (1976). *Aspects of the geochemistry of the Karroo dolerites and basalts of the north-eastern Cape Province, South Africa.* MSc. Thesis (unpubl.), Rhodes University, Grahamstown, 118pp.

Rogers, R.D. and Bird, D.K. (1987). Fracture propagation associated with dike emplacement at the Skaergaard intrusion, East Greenland. *J. Struct. Geol.*, **9**, 71-86.

Ross, M.E. (1986). Flow differentiation, phenocryst alignment, and compositional trends within a dolerite dike at Rockport, Massachusetts. *Bull. geol. Soc. Amer.*, **97**, 232-240.

Sack, R.O. and Ghiorso, M.S. (1991). Chromite as a petrogenetic indicator. Chapter 9. *In:* Lindsley, D.H. (ed.), *Oxide Minerals: Petrologic and Magnetic Significance*, Reviews in Mineralogy, **25**, Mineralogical Society of America, 323-416.

Saggerson, E.P., Bristow, J.W., and Armstrong, R.A. (1983). The Rooi Rand dyke swarm. *S. Afr. J. Sci.*, **79**, 365-369.

Schnetzler, C.C. and Philpotts, J.A. (1970). Partition coefficients of rare-earth elements between igneous matrix material and rock-forming mineral phenocrysts -II. *Geochim. Cosmochim. Acta*, **34**, 331-340.

Schreiber, H.D., Lauer, H.V. and Thanyasir, T. (1980). The redox state of cerium in basaltic magmas: An experimental study of iron-cerium interaction in silicate melts. *Geochim. Cosmochim. Acta*, **44**, 1599-1612.

Shimizu, N. and Kushiro, I. (1975). Partitioning of rare earth elements between garnet and liquid at high pressures: preliminary experiments. *Geophys. Res. Lett.*, **2**, 413-416.

Stamatelopoulou-Seymour, K., Vlassopoulos, D., Pearce, T. and Rice, C. (1990). The record of magma chamber processes in plagioclase phenocrysts at Thera Volcano, Aegean Volcanic Arc, Greece. *Contrib. Mineral. Petrol.*, **104**, 73-84.

Storey, B.C., Alabaster, T., Hole, M.J., Pankhurst, R.J. and Wever, H.E. (1992). Role of subduction-plate boundary forces during the initial stages of Gondwana break-up: evidence from the proto-Pacific margin of Antarctica. *In:* Storey, B.C., Alabaster, T. and Pankhurst, R.J. (eds.), Magmatism and the Causes of Continental Break-up, *Spec. Publ. geol. Soc.*, **68**, 149-163.

Stormer, J.C. (1983). The effects of recalculation on estimates of temperature and oxygen fugacity from analyses of multicomponent iron-titanium oxides. *Amer. Mineral.*, **68**, 586-594.

Sweeney, R.J. (1988). *Geochemistry of the Sabie River Basalt Formation in the central Lebombo, Karoo Igneous Province.* Ph. D. Thesis (unpubl.), Univ. Cape Town, 416pp (2 volumes).

Sweeney, R.J. and Watkeys, M.K. (1990). A possible link between Mesozoic lithospheric architecture and Gondwana flood basalts. *J. Afr. Earth Sci.*, **10**, 707-716.

Turcotte, D.L., Emerman, S.H. and Spence, D.A. (1987). Mechanics of dyke injection, *In:* Halls, H.C. and Fahrig, W.F. (eds.), *Mafic Dyke Swarms*, Geological Assoc. Canada, Spec. Pap., **34**, 25-29.

Watkeys, M.K. (1991). A short introduction to the Rooi Rand dyke swarm. *Excursion Guide, 6/91*, Natal Branch, Geological Society of South Africa, 5pp.

Watkeys, M.K., Botes, A., Muir, D., Pietersen, K., Reddy, V., Robertson, J. and Turner, A. (1990). Grid-scale map of the Rooi Rand dyke swarm, at the Pongolo River cutting. Unpublished data, Univ. Natal, Durban.

Watkeys, M.K., Meth, D.L. & Kattenhorn, S.A. (1995). The Rooi Rand dyke swarm, southern Africa: vertical expressions of a horizontal desire, Abstracts, *Third International Dyke Conference*, 4-8 September, Jerusalem, Israel.

Waychunas, G.A. (1991). Crystal chemistry of oxides and oxyhydroxides. Chapter 2 *In:* Lindsley, D.H. (ed.), *Oxide Minerals: Petrologic and Magmatic Significance*, Reviews in Mineralogy, **25**, Mineralogical Society of America, 11-68.

White, R.S. (1992). Magmatism during and after continental break-up. *In:* Storey, B.C., Alabaster, T. and Pankhurst, R.J. (eds.), Magmatism and the Causes of Continental Break-up, *Spec. Publ. geol. Soc.*, **68**, 1-16.

White, R.S. and McKenzie, D.P. (1989). Magmatism at rift zones: The generation of volcanic continental margins and flood basalts. *J. Geophys. Res.*, **94**, 7685-7729.

White, R.S. and McKenzie, D.P. (1995). Mantle plumes and flood basalts. *J. Geophys. Res.*, **100**, 17543-17585.

White, R., Spence, G.D., Fowler, S.R., McKenzie, D.P., Westbrook, G.K. and Bowen, A.N. (1987). Magmatism at rifted continental margins. *Nature*, **330**, 439-444.

Wood, B.J. and Fraser, D.G. (1976). *Elementary Thermodynamics for Geologists*, Oxford University Press, London, 303pp.

Wright, T.L. (1974). Presentation and interpretation of chemical data for igneous rocks. *Contrib. Mineral. Petrol.*, **48**, 233-248.

Yoder, H.S. and Tilley, C.E. (1962). Origin of basalt magmas: an experimental study of natural and synthetic rock systems. *J. Petrology*, **3**, 342-532.

Zindler, A. and Hart, S. (1986). Chemical geodynamics. *Ann. Rev. Earth Plan. Sci.*, **14**, 493-571.

POSTER AND PAPER PRESENTATIONS ARISING FROM THIS WORK

Watkeys, M.K., Bullock, A., Pearman, C. and Meth, D. (1990). Why did Gondwana crack-up? *Geol. Soc. S. Afr.*, (Natal Branch) 10th Anniversary, Celebration Colloquium, October 1990.

Watkeys, M.K. and Meth, D.L. (1994). Tectonomagmatic pulses of the Rooi Rand dyke swarm, northern Natal. Abstracts, *Tectonics Division of the Geol. Soc. S .Afr.*, 10th Anniversary Conference, University of Pretoria.

Meth, D.L. and Watkeys, M.K. (1995). The Rooi Rand dyke swarm revisited, *Petros*, **14**, Univ. Natal. Dbn, 15-27.

Watkeys, M.K., Meth, D.L. and Kattenhorn, S.A. (1995). The Rooi Rand dyke swarm, southern Africa: vertical expressions of a horizontal desire. Abstracts, *Third International Dyke Conference*, 4-8 September, 1995, Jerusalem, Israel.

APPENDIX 1

PETROGRAPHY

Introduction

All Rooi Rand dolerites tend to display a uniform mineralogy of plagioclase feldspar, augite and opaque minerals (ilmenite and titanomagnetite identified by electron microprobe analysis). Quartz or olivine are occasionally added to this assemblage. The following petrographic descriptions concentrate on all 11 ages of dykes that were mapped and studied. There are thin section textural descriptions for the centre of dyke samples and chill margins of each dyke age. Modal percentages (excluding accessory minerals) are given for centre of dyke samples (from Table 3.1, page 23). The approximate position on the 600m outcrop at which the sample was taken at the study area is given (refer to Figure 2.4 for exact position on the map, page 9).

Electron microprobe analyses of the minerals may be found in Appendix 2, and whole-rock major, trace and rare-earth element analyses of the samples may be found in Appendix 3.

Petrographic Descriptions

Age H
DM90.30 (Centre of dyke) 290m
Plagioclase feldspar (labradorite-andesine)
Augite
Opaque minerals
(Olivine)

plag:cpx:opaques:ol 46.3:42.3:9.4:0

This is a medium-grained inequigranular porphyritic dolerite, with tabular phenocrysts of plagioclase feldspar up to 3mm in length in a groundmass of plagioclase feldspar, augite, opaque minerals, and some olivine. In general, the groundmass texture is equigranular, but in places, it becomes ophitic, with augite completely enclosing smaller feldspar laths.

The few olivine crystals present occur as aggregates together with the plagioclase feldspar phenocrysts. Although the feldspar laths are generally euhedral, the augite crystals are not, and tend to be anhedral. A large proportion of the groundmass is highly altered, forming an amorphous mass of a greenish-brown alteration product.

DM90.29 (Chill margin) 297m
Plagioclase feldspar (labradorite)
Augite
Opaque minerals
Olivine

A very fine-grained porphyritic dolerite. There are two phenocryst generations. The larger phenocrysts are mainly plagioclase feldspar and laths may be up to 3mm in length. There are microphenocrysts of plagioclase feldspar, augite, completely serpentinised augite, and altered olivine. Some of the phenocrysts occur in aggregates, giving a glomeroporphyritic texture to the rock in places.

The groundmass minerals are not able to be clearly distinguished, and there also appear to be small areas of interstitial glass, implying that this sample (as with many chill margin samples) is not holocrystalline.

Age G
DM90.7 (Centre of Dyke) 35m
Plagioclase feldspar (labradorite-andesine)
Augite
Opaque minerals

plag:cpx:opaques 50.2:40.1:7

This is a medium-grained dolerite, which is generally equigranular, but becomes porphyritic in places with occasional plagioclase feldspar and augite phenocrysts which may be up to 3mm in length.

The clinopyroxenes are subhedral to anhedral, and occasionally sub-ophitically enclose plagioclase feldspar laths. The plagioclase crystals are euhedral to subhedral. Opaque minerals do not occur as massive angular or euhedral crystals, but rather as scattered blebs throughout the rock. This sample is highly altered in places, with a few completely serpentinised pyroxenes, and many pyroxenes with altered greenish-coloured rims. A few grains of possible olivine or orthopyroxene have been totally replaced by biotite.

Age G'
DM90.25 (Centre of dyke) 555m
Plagioclase feldspar (labradorite)
Augite
Opaque Minerals

plag:cpx:opaques 46.1:43.4:8.2

This is a fine- to medium-grained dolerite with a few plagioclase feldspar phenocrysts which occur in glomeroporphyritic aggregates, rendering a birds-foot texture to the rock. The groundmass, which constitutes the greater part of the rock, has an intergranular texture, occasionally becoming sub-ophitic and even ophitic.

Plagioclase feldspar phenocryst laths (generally euhedral) may be up to 4mm in length. Augite crystals are subhedral to anhedral and often altered around the rims to a greenish hydrated mafic silicate. This is seen especially when the pyroxenes are adjacent to opaque minerals. Opaque minerals have a skeletal appearance.

DM90.24 (Chill margin) 550m
Plagioclase feldspar (labradorite)
Augite
Opaques
(possible olivine)
Glassy groundmass

The texture ranges from a totally glassy groundmass with phenocrysts (hypocrystalline) at the chilled contact to a cryptocrystalline groundmass with phenocrysts approximately 5mm away from the chilled contact.

The phenocryst population consists of euhedral plagioclase feldspar laths, and subhedral to anhedral augite crystals. These may occur singly or in aggregates. There is a trace amount of possible altered olivine crystals, which are surrounded by brownish-coloured reaction rims (possibly iddingsite).

Plagioclase feldspar phenocryst laths are aligned parallel to the chilled contact, representing a flow direction, but at a distance of approximately 18mm away from the chilled contact, the feldspar laths have a random orientation once again.

Age G"
DM90.8 (Centre of dyke) 25m
Plagioclase feldspar (labradorite-andesine-oligoclase)
Augite
Opaque minerals

plag:cpx:opaques 42:49.1:7.2

A fine- to medium-grained dolerite. The overall texture is equigranular. The augite crystals are subhedral to anhedral, and some crystals show twinning. Plagioclase feldspars occur as euhedral to subhedral laths, and are occasionally sub-ophitically related to the pyroxene crystals.

Some opaque minerals enclose smaller plagioclase laths, which suggests that they grew later, around the plagioclase feldspar crystals.

The sample has a fair degree of alteration, with many of the augite crystals being rimmed by a reaction halo of greenish-brown biotite-like material. The plagioclase feldspars are not as altered as the pyroxenes, and show only a minor degree of sericite alteration.

Age F
DM90.27 (Centre of dyke) 347m
Plagioclase feldspar (labradorite-andesine)
Augite
Opaque minerals
Quartz

plag:cpx:opaques:qtz 48:42.4:7.5:0.5

A medium-grained equigranular dolerite. Euhedral to anhedral augite crystals are very brown and often altered to biotite. Likewise, there are large areas where plagioclase laths are completely sericitised. The opaque minerals are either massive or skeletal. Quartz occurs as anhedral blebs filling the interstices between the other minerals.

Note: No representative sample for the chill margin

Age E
DM90.20 (Centre of dyke) 355m
Plagioclase feldspar (labradorite)
Augite
Opaque minerals
Olivine

plag:cpx:opaques:ol 51.5:38.7:3.5:5.1

A medium-grained inequigranular seriate-textured dolerite. In general, plagioclase feldspar is sub-ophitically related to augite, but in some places, the texture is ophitic.

Plagioclase feldspar occurs as euhedral laths. The augite crystals are subhedral to anhedral. The very low proportion of opaque minerals is clearly visible.

A large proportion of the euhedral to subhedral olivines have been replaced by biotite and other hydrous alteration products, but almost pristine olivines may be recognised by their higher interference colours, and opaque reaction rims and alteration cracks.

The rock is altered, with a large proportion of greenish-brown alteration products and opaque mineral

reaction products. Surprisingly however, plagioclase feldspars are not very highly altered.

DM90.19 (Chill margin) 358m
Plagioclase feldspar (labradorite-bytownite)
Augite
Opaque minerals
Olivine

This chill margin sample is very fine-grained and displays a porphyritic texture, with phenocrysts of plagioclase feldspar (up to 3mm in length), euhedral to subhedral augite and serpentinised olivines. There is a range of sizes in the phenocryst population.

The fine-grained groundmass has an equigranular texture, with euhedral laths of plagioclase feldspar, and anhedral augites, some of which are altered to chlorite. The opaque minerals are scattered evenly throughout the groundmass.

An interesting feature to note, is that many of the plagioclase feldspar, augite and olivine phenocrysts have scalloped uneven crystal edges, indicative of some kind of resorption having taken place, possibly due to an inequilibrium of the phenocrysts in the remaining melt, or due to undergoing greater pressure changes during transport than other magmas.

DM90.9 (Chill margin) 37m
Plagioclase feldspar (labradorite)
Augite
Opaque minerals

Very fine- to fine-grained. The texture is generally equigranular, with euhedral plagioclase laths and subhedral to anhedral augite. Scattered blebs of opaque minerals occur throughout the slide. There are a few larger plagioclase laths which are not really distinct enough to be termed phenocrysts. Some alteration of pyroxenes to chlorite is visible.

Age E'
DM94.3 (Centre of dyke) 310m
Plagioclase feldspar (labradorite)
Augite
Opaque minerals
Olivine

plag:cpx:opaques:ol 50:42.3:3.3:2.8

A medium-grained, seriate-textured dolerite. Euhedral plagioclase laths are subophitically to ophitically enclosed by subhedral to anhedral augite crystals. Slightly finer-grained subhedral olivine occurs in clusters, which are often unaltered, but may also be completely replaced by magnetite and chlorite. The very low proportion of opaque minerals is immediately notable in thin section, and where they occur, they are massive, with a high degree of alteration to a greenish iron oxide alteration product and biotite.

DM94.4 (Chill Margin) 310m
Plagioclase feldspar
Augite
Opaque minerals
Olivine

A holocrystalline dolerite, with many euhedral phenocrysts of plagioclase feldspar, augite and olivine in a fine-grained groundmass of plagioclase feldspar, augite, olivine and opaque minerals. Some of the plagioclase laths appear to be highly sericitised. A few of the olivines are also highly altered to serpentine.

Plagioclase lath microphenocrysts are aligned parallel to the chill margin for 4mm, becoming randomly orientated further inwards towards the dyke centre. Microphenocryst size increases away from the chill margin. Some of the phenocrysts appear to be xenocrysts, derived from the adjacent dyke (Age E).

Age D
DM90.10 (Centre of dyke) 20m
Plagioclase feldspar (labradorite)
Augite
(Sub-calcic Augite)
Opaque minerals

plag:cpx:opaques 44.4:45.2:7.7

This is a fine-grained porphyritic dolerite. In places the phenocryst phases, plagioclase feldspar and clinopyroxene (augite), become glomeroporphyritic. The groundmass texture is equigranular, consisting of euhedral to subhedral plagioclase feldspar laths, subhedral to anhedral augite crystals, and scattered blebs of opaque minerals. Also noted in the groundmass, are small areas between the crystals, which appear to have been quenched during the final stage of solidification. This is seen by the presence of crystallite-like crystals.

A greenish-coloured alteration product is noted forming along cracks in the plagioclase phenocrysts. Altered pyroxene phenocrysts are completely enveloped by plagioclase phenocrysts, which suggests that the feldspar phenocrysts grew later around the pyroxene phenocrysts. Some pyroxene phenocrysts have been highly altered to biotite.

DM90.11 (Chill margin) 28m
Plagioclase feldspar (labradorite/some albite)
Augite
Glassy groundmass

This is a typical cryptocrystalline porphyritic texture of a rapidly chilled zone in a dolerite, with a totally glassy groundmass, containing phenocrysts (in some cases possibly xenocrysts from the host rock) and microphenocrysts of predominantly plagioclase feldspar, with some augite.

The plagioclase phenocrysts are highly altered, showing much sericitisation, but the euhedral to subhedral augite phenocrysts are still fairly pristine. Microphenocrysts have undergone far less alteration.

Electron microprobe whole-rock analyses of this rock may be found in Appendix 3c, and a detailed drawing and discussion of chemical composition in Chapter 4.5.2.

Age C
DM94.2 (Centre of dyke) 150m
Plagioclase feldspar
Augite
Opaque minerals

plag:cpx:opaques 45.4:43.7:8.9

A medium- to fine-grained phanerocrystalline dolerite, which is slightly inequigranular, with sparse glomeroporphyritic aggregates of plagioclase feldspar (up to 4mm in length) and a few augite phenocrysts. Euhedral laths of plagioclase are slightly larger than the anhedral augite crystals. The typical sub-ophitic/ophitic relationship is not exhibited, suggesting that the plagioclase feldspars crystallized first. The dolerite has a fairly altered appearance, with many of the clinopyroxene altered to chlorite, and the majority of the plagioclase phenocrysts being highly sericitised. The opaque minerals are scattered evenly throughout the rock.

DM94.1 (Chill Margin) 150m
Plagioclase feldspar
Augite
Opaque Minerals

A very fine-grained dolerite, with euhedral plagioclase feldspar microlaths rendering a microscopic felted appearance (they are randomly oriented). A few euhedral to subhedral plagioclase feldspar and augite microphenocrysts are present. There is a high proportion of fine-grained scattered opaque minerals, as noted in the centre of dyke sample.

Age B
DM90.18 (Centre of dyke) 542m
Plagioclase feldspar (labradorite-andesine)
Augite
Opaque Minerals
Quartz

plag:cpx:opaques:qtz 50:40.2:6.6:1.2

A fine-grained generally equigranular dolerite showing much alteration. The texture is mainly intergranular, with many small pyroxene crystals and some quartz occurring between the feldspar laths. In places however, the texture becomes sub-ophitic.

Feldspar laths are euhedral to subhedral, sometimes appearing to be resorbed along the margins. Augite grains are all anhedral, and are often altered to a hydrous brownish-green alteration product. The quartz appears as totally anhedral crystals infilling spaces between crystals. Opaque minerals have a massive sometimes tabular appearance, but may also be skeletal. Feldspars are highly altered to sericite. There is also much alteration of Fe-Mg minerals to biotite.

DM90.17 (Chill margin) 547m
Plagioclase feldspar (oligoclase-andesine)
Augite
Opaque minerals
Quartz

This dolerite exhibits an aphanitic texture, becoming glassy in places. This chill margin sample is generally microcrystalline, often bordering on cryptocrystalline, where positive identification of minerals by the microscope is sometimes difficult.

In contrast to the centre of dyke sample, the opaque minerals are scattered as many tiny specks throughout the rock, giving a speckled appearance to the thin-section. There is a fairly large amount of alteration of the pyroxenes to chlorite.

Age A
DM90.5 (Centre of dyke) 7m
Plagioclase feldspar (labradorite-andesine)
Augite
Minor Pigeonite
Opaque Minerals

plag:cpx:opaques 47:46.3:5.1

Medium-grained massive dolerite. This rock is generally equigranular, with occasional plagioclase feldspar phenocrysts. Pyroxenes are subhedral to anhedral and appear to have crystallized between the plagioclase laths, giving an intergranular texture. Only a few pyroxenes sub-ophitically enclose plagioclase laths.

Some pyroxenes show twinning, whilst others appear to be zoned. Biotite and chlorite are present as alteration minerals.

DM90.4 (Chill margin) 13m
Plagioclase feldspar (labradorite-andesine)
Augite
Minor Pigeonite
Opaque minerals

Very fine-grained porphyritic, with phenocrysts of plagioclase feldspar and pyroxene. Plagioclase is the more dominant phenocryst generation. Pyroxene phenocrysts are often concentrated together with one another, and other plagioclase phenocrysts giving a glomeroporphyritic texture in some instances. Plagioclase appears to have 3 generations:

1) very large phenocrysts (up to 2.5mm)
2) smaller phenocrysts
3) very small groundmass laths
In all cases, it occurs as euhedral to anhedral laths.

Pyroxene phenocrysts are euhedral to anhedral. Most of the pigeonite appears to have altered to a strongly pleochroic, green to brown alteration mineral, which is most likely biotite. Chlorite is also present. Other than these, the rock is still fairly fresh.

APPENDIX 2

ELECTRON MICROPROBE MINERAL ANALYSIS

Introduction: Microprobe Analytical Procedure

Carbon-coated polished thin-sections were analysed for major elements using the wave-length dispersive automated Cameca Camebax electron probe microanalyser at the erstwhile Department of Geochemistry, University of Cape Town, following the techniques stated in Duncan *et al.* (1984a).

Instrumental conditions were: A normal acceleration voltage of 15kV; a specimen current which varied between 0.50 and 0.10 microamps; integrating time of 10 seconds and an electron beam diameter of 1 to 2 microns. Anhydrous multi-element silicates and oxides were used as standards. Data corrections for atomic number, fluorescence and adsorption were made using the methods of ZAF and Bence and Albee (1968).

Prior to use for microprobe analysis, the sections must be washed thoroughly with soapy water, distilled water, and ethanol. This will ensure the removal of any dirt or grease on the slide, which may adversely affect the chemical analyses.

Specimens which are non-conducting (such as dolerites in this instance), must be coated with a thin layer of conducting material (C, Al, Cu or Au), so as to prevent charge build-up from the electron beam. This maintains a stable regime of excitation, and the negative charge transferred by the electron beam to the specimen is thus removed (Heinrich 1981). The specimen surface must therefore be electrically conductive. Any nonconductive regions on the specimen may charge up accidentally, if located too close to the intended target. Such charged regions may produce deflection and distortion of the beam, or intermittent discharge. If the surface is coated with a conductive layer, these problems may be avoided.

The usual method is the evaporation of a 100 to 200 angstrom thick layer of the conducting material onto the specimen The layer must be thin enough to permit the passage of primary beam electrons. Carbon is preferred where the transparency of the layer is essential in allowing easy orientation and microscopic observation of the specimen surface to the analyst. It was therefore used in this instance.

It is essential that the thin section specimen is flat, because the materials transferred during coating in a good vacuum will move in a straight line from the source to the target. In specimens which are not flat, the coating will not be uniform.

Before placing the sample into the microprobe unit, a conductive path must be created in the sample holder. This is done by painting all four corners of the specimen slide and holder with a conductive silver paint.

Other sample properties which might give rise to serious errors in the analysis, are the degree of polish, relief, flatness, tilt, and the thickness of the conductive coating. Combinations of soft and hard materials often give rise to serious relief problems.

Table I Precision and detection limits for major oxide analysis of minerals by electron microprobe (from Duncan *et al.*, 1984a).

Oxide	% Concentration	S.D.	Precision	L.L.D.
SiO_2	41.97	0.08	0.08	0.06
TiO_2	3.92	0.08	0.10	0.07
Al_2O_3	13.51	0.06	0.06	0.04
Cr_2O_3	0.78	0.02	0.02	0.03
FeO	6.82	0.15	0.16	0.10
MnO	0.26	0.01	0.01	0.03
MgO	16.34	0.07	0.10	0.05
CaO	12.10	0.07	0.08	0.05
Na_2O	2.71	0.12	0.14	0.09
K_2O	1.18	0.06	0.10	0.07

The concentration of each oxide is the mean of 10 replicate analyses of the same spot within a pargasitic hornblende except for Cr_2O_3 and MnO data which are from 12 replicate analyses of a garnet. S.D. values are the standard deviation calculated from the replicate data. Precision is expressed as an absolute error in % oxide (2 sigma counting error) and L.L.D. is the lower limit of detection (in % oxide) at the 99 % confidence limit. Data in this table are from Reid (1977) and Shee (1978).

	fs1-30	fs2r30	fs2c30	fs3r30	fs3c30	fs4r30	fs4c30	fs5r30	fs5c30	fs6r30	fs6c30
Na2O	4.44	4.77	4.15	5.25	3.66	5.77	4.20	5.43	4.23	5.68	4.33
K2O	0.11	0.17	0.05	0.08	0.11	0.29	0.16	0.22	0.13	0.35	0.11
SiO2	54.09	53.93	53.50	55.65	52.63	59.70	54.85	57.61	54.51	60.51	53.59
Al2O3	27.93	26.95	28.80	27.21	28.33	26.06	28.54	26.89	28.51	25.29	28.51
FeO	0.76	1.06	0.94	1.09	2.71	0.90	1.13	0.83	0.92	1.01	0.93
MgO	0.13	0.10	0.16	0.11	0.26	-	0.14	0.08	0.14	-	0.16
CaO	11.76	11.20	12.89	10.84	12.22	8.99	12.22	9.99	12.27	7.63	12.73
TOTAL	99.22	98.18	100.49	100.23	99.92	101.71	101.24	101.05	100.71	100.47	100.36
AB	0.40	0.43	0.37	0.46	0.35	0.53	0.38	0.49	0.38	0.56	0.38
OR	0.01	0.01	-	0.01	0.01	0.02	0.01	0.01	0.01	0.02	0.01
AN	0.59	0.56	0.63	0.53	0.64	0.45	0.61	0.50	0.61	0.42	0.61

	fs7z30	fs7z30	fs7z30	fs7z30	fs7z30	fs7z30	fs7z30	fs7z30	fs1-29	fs2-29
Na2O	4.74	3.74	3.91	3.79	3.90	3.75	3.83	4.03	4.30	4.06
K2O	0.16	0.08	0.10	0.09	0.13	0.10	0.11	0.09	0.16	0.11
SiO2	55.26	53.23	53.19	52.65	53.69	52.46	52.88	53.24	55.00	52.50
Al2O3	27.83	29.40	28.79	28.94	29.06	28.83	28.73	28.87	27.31	27.61
FeO	1.04	0.72	0.81	0.66	0.63	0.74	0.76	0.79	1.23	1.05
MgO	0.09	0.15	0.16	0.15	0.14	0.17	0.14	0.14	0.18	0.17
CaO	11.61	13.46	12.98	13.09	13.20	13.21	12.91	12.87	11.85	12.45
TOTAL	100.73	100.78	99.94	99.37	100.75	99.26	99.36	100.03	100.03	97.95
AB	0.42	0.33	0.35	0.34	0.34	0.34	0.34	0.36	0.39	0.37
OR	0.01	0.01	0.01	0.01	0.01	0.01	0.01	0.01	0.01	0.01
AN	0.57	0.66	0.64	0.65	0.65	0.65	0.65	0.63	0.60	0.62

	fs3r29	fs3c29	fs4r29	fs4c29	fs5-29	fs6-29	fs7-29	fs8-29	fs9r29	fs9r29	fs1029	fs1129
Na2O	3.92	3.75	3.61	3.77	4.33	4.34	4.21	3.92	4.01	3.72	3.98	3.85
K2O	0.09	0.09	0.09	0.11	0.14	0.12	0.11	0.10	0.10	0.08	0.09	0.11
SiO2	52.37	51.48	51.37	51.53	53.17	53.19	52.79	51.93	52.65	52.00	53.15	52.12
Al2O3	28.20	27.90	28.53	28.13	26.59	27.54	26.85	27.98	27.59	28.19	28.21	28.32
FeO	0.82	0.82	0.78	0.65	1.12	0.83	1.07	0.74	0.87	0.69	0.72	0.76
MgO	0.13	0.14	0.14	0.13	0.17	0.16	0.18	0.14	0.17	0.14	0.16	0.15
CaO	12.97	13.04	13.35	13.02	11.76	12.15	12.09	12.99	12.73	13.00	12.85	13.03
TOTAL	98.50	97.22	97.87	97.34	97.28	98.33	97.30	97.80	98.12	97.82	99.16	98.34
AB	0.35	0.34	0.33	0.34	0.39	0.39	0.38	0.35	0.36	0.34	0.36	0.35
OR	0.01	0.01	0.01	0.01	0.01	0.01	0.01	0.01	0.01	0.01	0.01	0.01
AN	0.64	0.65	0.66	0.65	0.60	0.60	0.61	0.64	0.63	0.65	0.63	0.64

(a) Feldspar Analyses DM90.30 (centre); DM90.29 (chill) - AGE H

fs=feldspar; r=rim; c=core; z=zoning across a single grain
left hand number=number of mineral grain in slide
right hand number=sample number preceded by DM90.

DM90.30	**DM90.29**
fs1-6: groundmass	fs1,2,5,6,7 : groundmass
fs7: phenocryst	fs3,4,8,9,10,11 : phenocryst

	fs1z06	fs1z06	fs1z06	fs1z06	fs1z06	fs1z06	fs1z06	fs1z06
Na2O	3.22	3.65	3.52	3.56	3.69	3.68	3.60	3.49
K2O	0.11	0.13	0.11	0.12	0.14	0.14	0.12	0.11
SiO2	53.67	53.23	52.65	52.45	52.50	52.10	52.12	51.47
Al2O3	30.58	29.59	29.17	29.21	29.27	28.93	29.24	29.36
FeO	0.65	0.63	0.74	0.65	0.66	0.65	0.68	0.65
MgO	0.16	0.17	0.19	0.15	0.17	0.18	0.19	0.17
CaO	13.65	13.11	13.01	13.23	13.11	13.07	13.11	13.72
TOTAL	102.03	100.52	99.39	99.38	99.54	98.75	99.06	98.96
AB	0.30	0.33	0.33	0.32	0.33	0.33	0.33	0.31
OR	0.01	0.01	0.01	0.01	0.01	0.01	0.01	0.01
AN	0.70	0.66	0.67	0.67	0.66	0.66	0.66	0.68

	fs1z06	fs1z06	fs2r06	fs2c06	fs3r06	fs3c06	fs4r06	fs4c06	fs5r06	fs5c06
Na2O	3.19	3.35	4.41	3.34	5.01	3.40	3.48	3.30	5.74	4.67
K2O	0.05	0.13	0.21	0.13	0.34	0.10	0.11	0.12	0.28	0.22
SiO2	50.34	51.71	53.86	51.52	55.55	51.91	51.98	51.21	56.65	54.24
Al2O3	29.99	29.68	27.88	29.46	26.77	29.70	29.53	29.63	26.29	27.40
FeO	0.68	0.82	0.77	0.62	0.94	0.72	0.85	0.66	0.72	0.70
MgO	0.14	0.13	0.12	0.17	0.08	0.18	0.17	0.17	0.08	0.09
CaO	13.93	13.78	11.91	13.46	10.16	13.64	13.58	13.72	9.28	11.07
TOTAL	98.31	99.59	99.15	98.71	98.85	99.65	99.71	98.79	99.04	98.39
AB	0.29	0.30	0.40	0.31	0.46	0.31	0.31	0.30	0.52	0.43
OR	0.00	0.01	0.01	0.01	0.02	0.01	0.01	0.01	0.02	0.01
AN	0.70	0.69	0.59	0.68	0.52	0.69	0.68	0.69	0.46	0.56

	fs6r06	fs6c06	fs1z07	fs1z07	fs1z07	fs1z07	fs1z07	fs1z07	fs1z07	fs1z07
Na2O	6.07	4.16	5.09	4.62	4.47	4.06	3.21	3.44	3.25	3.29
K2O	0.28	0.17	0.23	0.26	0.27	0.21	0.11	0.12	0.12	0.13
SiO2	58.63	53.10	60.12	54.80	54.23	53.04	51.11	51.61	51.41	51.28
Al2O3	25.85	28.51	24.81	27.75	27.47	28.41	29.56	29.48	29.82	29.80
FeO	0.80	0.84	0.56	0.82	0.72	0.69	0.65	0.64	0.69	0.64
MgO	0.04	0.12	-	0.11	0.11	0.11	0.18	0.17	0.17	0.17
CaO	8.28	12.28	6.94	11.54	11.23	12.24	13.82	13.68	13.91	13.90
TOTAL	99.95	99.19	97.73	99.90	98.50	98.77	98.64	99.14	99.36	99.19
AB	0.56	0.38	0.56	0.41	0.41	0.37	0.29	0.31	0.30	0.30
OR	0.02	0.01	0.02	0.02	0.02	0.01	0.01	0.01	0.01	0.01
AN	0.42	0.61	0.42	0.57	0.57	0.62	0.70	0.68	0.70	0.70

	fs1z07	fs1z07	fs1z07	fs1z07	fs1z07	fs1z07	fs1z07	fs1z07	fs1z07	fs1z07
Na2O	3.13	3.21	3.42	3.55	3.43	3.48	3.36	3.36	3.54	3.41
K2O	0.09	0.10	0.11	0.12	0.09	0.11	0.12	0.11	0.11	0.14
SiO2	49.86	50.91	51.18	51.08	50.91	51.62	51.27	51.10	51.54	51.41
Al2O3	29.55	29.85	29.43	29.16	29.29	29.46	29.23	29.28	29.45	29.32
FeO	0.65	0.68	0.70	0.70	0.63	0.65	0.65	0.66	0.60	0.66
MgO	0.15	0.18	0.16	0.15	0.19	0.17	0.17	0.17	0.17	0.19
CaO	13.93	13.99	13.50	13.34	13.50	13.62	13.48	13.54	13.54	13.61
TOTAL	97.37	98.93	98.52	98.09	98.04	99.11	98.27	98.21	98.96	98.74
AB	0.29	0.29	0.31	0.32	0.31	0.31	0.31	0.31	0.32	0.31
OR	0.01	0.01	0.01	0.01	0.01	0.01	0.01	0.01	0.01	0.01
AN	0.71	0.70	0.68	0.67	0.68	0.68	0.68	0.69	0.67	0.68

(a) **Feldspar Analyses** DM90.6 & DM90.7 (centre) - AGE G

fs=feldspar; r=rim; c=core; z=zoning across a single grain
left hand number=number of mineral grain in slide
right hand number=sample number preceded by DM90.

DM90.6
fs1,2 : phenocryst
fs3-6 : groundmass

DM90.7
fs1 : phenocryst

	fs1z07	fs1z07	fs1z07	fs2r07	fs2c07	fs3t07	fs3t07	fs3t07	fs3t07	fs3t07
Na2O	3.40	3.36	3.11	3.08	3.30	4.03	3.48	3.38	3.50	3.44
K2O	0.10	0.12	0.13	0.11	0.12	0.16	0.13	0.14	0.12	0.12
SiO2	51.42	51.24	50.74	50.71	51.12	52.90	51.17	51.44	51.16	51.44
Al2O3	29.34	29.33	30.09	30.24	29.53	28.44	29.17	29.53	29.15	29.36
FeO	0.64	0.69	0.79	0.97	0.69	0.80	0.67	0.56	0.71	0.92
MgO	0.17	0.16	0.11	0.09	0.16	0.16	0.17	0.17	0.19	0.19
CaO	13.68	13.61	14.21	14.19	13.78	12.62	13.60	13.85	13.52	13.70
TOTAL	98.75	98.52	99.17	99.39	98.69	99.11	98.39	99.07	98.36	99.17
AB	0.31	0.31	0.28	0.28	0.30	0.36	0.31	0.30	0.32	0.31
OR	0.01	0.01	0.01	0.01	0.01	0.01	0.01	0.01	0.01	0.01
AN	0.69	0.69	0.71	0.71	0.69	0.63	0.68	0.69	0.68	0.68

	fs3t07	fs3t07	fs3t07	fs3t07	fs3t07	fs3t07	fs3t07	fs3t07	fs3t07	fs4r07
Na2O	3.70	3.34	3.24	3.36	3.71	2.63	2.69	3.41	3.46	5.82
K2O	0.12	0.12	0.12	0.13	0.14	0.07	0.07	0.12	0.11	0.34
SiO2	52.20	51.20	50.63	51.12	51.97	49.40	49.68	51.60	51.54	59.40
Al2O3	29.40	29.32	29.43	29.95	29.08	30.60	30.70	29.75	29.57	25.43
FeO	0.71	0.65	0.89	0.75	0.85	0.74	0.77	0.71	0.73	0.61
MgO	0.16	0.16	0.15	0.16	0.20	0.14	0.14	0.15	0.15	0.04
CaO	13.13	13.54	14.01	13.87	13.12	14.98	15.00	13.84	13.87	7.56
TOTAL	99.41	98.33	98.46	99.35	99.08	98.56	99.06	99.57	99.43	99.20
AB	0.34	0.31	0.29	0.30	0.34	0.24	0.24	0.31	0.31	0.57
OR	0.01	0.01	0.01	0.01	0.01	0.00	0.00	0.01	0.01	0.02
AN	0.66	0.69	0.70	0.69	0.66	0.76	0.75	0.69	0.68	0.41

	fs4c07	fs5r07	fs5c07	fs6r07	fs6c07
Na2O	4.68	4.43	3.44	5.14	4.89
K2O	0.29	0.21	0.11	0.33	0.27
SiO2	54.35	53.64	51.89	55.63	55.06
Al2O3	27.39	27.77	29.64	26.65	27.01
FeO	0.76	0.79	0.65	0.80	0.69
MgO	0.11	0.15	0.18	0.09	0.12
CaO	11.14	11.90	13.56	10.17	10.86
TOTAL	98.72	98.89	99.48	98.81	98.88
AB	0.42	0.40	0.31	0.47	0.44
OR	0.02	0.01	0.01	0.02	0.02
AN	0.56	0.59	0.68	0.51	0.54

(a) Feldspar Analyses DM90.7 (contd.) - AGE G

fs=feldspar; r=rim; c=core; z=zoning across a single grain
t=traverse across a crack system
left hand number=number of mineral grain in slide
right hand number=sample number preceded by DM90.

DM90,7
fs1,2,3 : phenocryst fs4,5,6 : groundmass

	fs1r25	fs1c25	fs2r25	fs2c25	fs3r25	fs3c25	fs4z25	fs4z25
Na2O	5.13	4.64	4.89	4.82	5.79	4.86	5.05	3.82
K2O	0.29	0.17	0.25	0.24	0.30	0.20	0.25	0.11
SiO2	56.12	53.57	53.38	55.86	57.47	54.59	56.17	52.40
Al2O3	27.24	27.76	27.45	27.69	26.41	27.71	26.99	29.22
FeO	0.62	0.76	0.73	0.72	0.84	0.58	1.24	0.59
MgO	0.09	0.14	0.07	0.11	0.07	0.11	0.26	0.16
CaO	10.62	11.86	11.25	11.31	9.77	11.48	10.74	13.05
TOTAL	100.11	98.90	98.02	100.75	100.65	99.53	100.70	99.35
AB	0.46	0.41	0.43	0.43	0.51	0.43	0.45	0.34
OR	0.02	0.01	0.02	0.01	0.02	0.01	0.02	0.01
AN	0.52	0.58	0.55	0.56	0.47	0.56	0.53	0.65

	fs4z25	fs4z25	fs4z25	fs4z25	fs4z25	fs5r25	fs5c25	fs6r25	fs6c25	fs7r25
Na2O	3.93	3.93	3.76	3.92	3.95	5.91	4.57	4.45	4.67	5.18
K2O	0.13	0.13	0.14	0.13	0.11	0.38	0.18	0.22	0.15	0.28
SiO2	52.37	52.88	52.77	52.65	51.67	58.07	53.99	54.60	54.82	55.67
Al2O3	28.80	29.07	29.04	29.30	28.55	26.17	27.89	27.69	27.85	27.11
FeO	0.61	0.58	0.63	0.59	0.64	0.57	0.64	1.27	0.67	0.80
MgO	0.15	0.16	0.13	0.18	0.19	0.07	0.14	0.21	0.13	0.11
CaO	13.07	13.10	12.97	13.11	13.46	9.53	11.79	11.75	11.66	10.86
TOTAL	99.06	99.85	99.44	99.88	98.57	100.70	99.20	100.19	99.95	100.01
AB	0.35	0.35	0.34	0.35	0.34	0.52	0.41	0.40	0.42	0.45
OR	0.01	0.01	0.01	0.01	0.01	0.02	0.01	0.01	0.01	0.02
AN	0.64	0.64	0.65	0.64	0.65	0.46	0.58	0.59	0.57	0.53

	fs7c25	fs1c24	fs2c24	fs3c24	fs3r24	fs4c24	fs5c24	fs6c24	fs7c24	fs1r08	fs1c08	fs2r08	fs2c08	fs3-08
Na2O	4.58	4.16	3.84	4.54	4.40	4.21	4.40	4.70	4.35	6.14	4.64	4.91	5.00	4.73
K2O	0.20	0.24	0.16	0.21	0.20	0.17	0.21	0.21	0.14	1.37	0.27	0.22	0.24	0.24
SiO2	53.34	53.57	52.64	54.92	54.10	53.68	53.59	54.68	53.47	59.11	54.49	55.09	55.85	54.95
Al2O3	27.77	27.64	27.39	27.79	28.18	28.55	28.07	27.53	28.33	24.45	27.49	27.24	27.06	27.34
FeO	0.76	1.71	3.18	0.89	0.82	0.96	0.92	0.86	0.74	1.58	0.76	0.98	0.80	0.93
MgO	0.11	0.14	0.44	0.17	0.16	0.15	0.12	0.16	0.14	0.08	0.12	0.09	0.11	0.11
CaO	11.90	11.78	11.68	11.88	12.10	12.30	11.86	11.40	12.36	6.94	11.59	11.00	10.86	11.19
TOTAL	98.66	99.24	99.33	100.40	99.96	100.02	99.17	99.54	99.53	99.67	99.36	99.53	99.92	99.49
AB	0.41	0.38	0.37	0.40	0.39	0.38	0.40	0.42	0.39	0.57	0.41	0.44	0.45	0.43
OR	0.01	0.02	0.01	0.01	0.01	0.01	0.01	0.01	0.01	0.08	0.02	0.01	0.01	0.01
AN	0.58	0.60	0.62	0.59	0.60	0.61	0.59	0.57	0.60	0.35	0.57	0.55	0.54	0.56

	fs4-08	fs5r08	fs5c08	fs6r08	fs6c08	fs7z08	fs7z08	fs7z08	fs7z08	fs7z08	fs7z08	fs7z08	fs8-08
Na2O	4.63	4.44	4.41	6.03	4.51	5.40	5.12	5.16	8.62	6.11	5.62	6.65	3.84
K2O	0.24	0.23	0.24	0.45	0.15	0.31	0.33	0.31	0.14	0.47	0.43	0.67	0.14
SiO2	54.83	56.05	54.18	59.14	54.22	57.37	53.94	55.66	63.12	58.90	57.54	60.21	51.46
Al2O3	27.80	15.00	28.17	25.90	27.90	26.48	26.72	26.43	22.72	25.25	26.51	24.57	28.35
FeO	0.84	14.52	0.90	0.95	1.00	0.81	0.76	0.75	0.90	0.60	0.67	0.71	0.90
MgO	0.10	2.64	0.12	0.07	0.13	0.08	0.10	0.08	-	0.07	0.08	-	0.17
CaO	11.58	9.10	11.87	9.07	11.94	10.22	10.49	10.53	4.66	8.51	9.69	7.40	12.89
TOTAL	100.02	101.98	99.89	101.61	99.85	100.67	97.46	98.92	100.16	99.91	100.54	100.21	97.75
AB	0.41	0.46	0.40	0.53	0.40	0.48	0.46	0.46	0.76	0.55	0.50	0.59	0.35
OR	0.02	0.02	0.01	0.03	0.01	0.02	0.02	0.02	0.01	0.03	0.03	0.04	0.01
AN	0.57	0.52	0.59	0.44	0.59	0.50	0.52	0.52	0.23	0.42	0.47	0.37	0.64

(a) **Feldspar Analyses** DM90.25 (centre); DM90.24 (chill) - AGE G'
DM90.8 (centre) - AGE G"

fs=feldspar; r=rim; c=core; z=zoning across a single grain
left hand number=number of mineral grain in slide
right hand number=sample number preceded by DM90.

DM90.24

All plagioclases analysed are slightly larger than the groundmass ones (phenocrysts in a cryptocrystalline groundmass). Matrix feldspars very difficult to isolate and analyse.

DM90.25
fs1,2 - groundmass
fs3,6,7 - 2nd generation
fs4,5 - phenocryst

DM90.8
fs1-6,8: groundmass
fs7: phenocryst

	fs1-20	fs2-20	fs3-20	fs4-20	fs5z20	fs5z20	fs5z20	fs5z20	fs5z20	fs5z20
Na2O	4.48	3.40	4.28	4.14	3.28	3.22	3.21	3.31	3.38	3.43
K2O	0.07	–	0.06	0.06	–	–	–	–	–	0.04
SiO2	54.26	52.16	53.07	53.45	50.55	51.50	51.13	51.16	51.61	51.65
Al2O3	28.17	29.77	28.06	28.70	29.61	29.82	30.00	29.51	29.77	29.12
FeO	0.74	0.49	0.69	0.74	0.54	0.55	0.50	0.53	0.44	0.50
MgO	0.16	0.19	0.15	0.17	0.22	0.19	0.18	0.16	0.18	0.17
CaO	12.10	14.11	12.33	12.79	14.08	14.04	14.30	14.02	13.91	13.68
TOTAL	99.98	100.12	98.64	100.05	98.28	99.32	99.32	98.69	99.29	98.59
AB	0.40	0.30	0.38	0.36	0.30	0.30	0.29	0.30	0.31	0.31
OR	0.01	–	0.01	0.01	–	–	–	–	–	0.01
AN	0.59	0.70	0.61	0.63	0.70	0.70	0.71	0.70	0.69	0.68

	fs1-19	fs2-19	fs3-19	fs4-19	fs5-19	fs6-19	fs7-19
Na2O	1.89	1.96	2.30	1.81	1.83	5.27	4.92
K2O	–	–	–	–	–	0.14	0.09
SiO2	47.72	47.56	47.61	47.30	46.85	53.83	53.03
Al2O3	31.45	31.10	30.15	30.93	30.64	25.32	26.21
FeO	0.46	0.41	0.55	0.38	0.46	0.87	0.88
MgO	0.16	0.20	0.22	0.21	0.19	0.13	0.15
CaO	16.71	16.58	15.29	16.56	16.38	10.43	11.32
TOTAL	98.39	97.81	96.12	97.19	96.35	95.99	96.60
AB	0.17	0.18	0.21	0.16	0.17	0.47	0.44
OR	–	–	–	–	–	0.01	0.01
AN	0.83	0.82	0.79	0.84	0.83	0.52	0.55

	fs1-27	fs2r27	fs2c27	fs3c27	fs4c27	fs5-27	fs6r27	fs6c27
Na2O	5.96	6.51	5.05	4.93	5.40	4.24	6.55	4.91
K2O	0.33	0.36	0.34	0.24	0.20	0.23	0.36	0.28
SiO2	56.50	56.39	52.63	53.04	54.96	53.92	56.98	52.54
Al2O3	25.81	24.93	24.76	26.24	24.58	27.12	23.75	25.42
FeO	0.53	0.69	2.15	0.98	1.55	0.70	1.07	0.76
MgO	0.07	–	0.23	0.08	0.14	0.08	–	0.07
CaO	9.12	8.36	9.96	10.74	9.13	11.36	7.33	10.02
TOTAL	98.32	97.24	95.12	96.25	95.96	97.65	96.04	94.00
AB	0.53	0.57	0.47	0.45	0.51	0.40	0.60	0.46
OR	0.02	0.02	0.02	0.01	0.01	0.01	0.02	0.02
AN	0.45	0.41	0.51	0.54	0.48	0.59	0.38	0.52

	fs1-09	fs2-09	fs3-09	fs4-09	fs5-09	fs6-09
Na2O	3.30	3.69	3.45	3.41	3.56	3.41
K2O	–	0.07	0.07	–	0.06	0.05
SiO2	51.96	52.48	52.61	51.92	52.33	51.95
Al2O3	30.28	29.14	29.73	29.74	28.94	29.85
FeO	0.85	0.96	0.89	0.71	0.78	0.75
MgO	0.24	0.26	0.23	0.23	0.28	0.22
CaO	14.00	13.49	13.65	13.65	13.45	13.92
TOTAL	100.63	100.09	100.63	99.66	99.40	100.15
AB	0.30	0.33	0.31	0.31	0.32	0.30
OR	–	0.01	0.01	–	0.01	0.01
AN	0.70	0.66	0.68	0.69	0.67	0.69

	fs1r11	fs1c11	fs2r11	fs2c11	fs3r11	fs3c11	fs4r11	fs4c11	fs5r11	fs5c11	fs6r11	fs6c11
Na2O	5.98	4.70	4.38	3.70	4.39	4.05	5.50	5.49	6.00	3.99	5.72	4.49
K2O	0.25	0.11	0.07	0.05	0.13	0.09	0.18	0.18	0.22	0.10	0.25	0.08
SiO2	58.23	54.39	53.39	51.80	54.01	52.72	56.06	55.75	57.67	53.06	58.70	53.63
Al2O3	25.42	27.47	28.40	29.22	27.89	28.50	26.38	26.22	25.57	28.36	25.82	27.83
FeO	0.60	1.01	0.89	0.68	0.87	0.63	0.80	0.71	0.85	0.69	0.70	0.75
MgO	0.05	0.11	0.12	0.20	0.10	0.13	0.08	0.07	0.06	0.11	0.06	0.15
CaO	8.23	11.30	11.96	13.40	11.66	12.58	9.97	9.77	8.63	12.06	8.33	11.83
TOTAL	98.76	99.10	99.21	99.06	99.04	98.69	98.97	98.19	98.99	98.38	99.58	98.78
AB	0.56	0.43	0.40	0.33	0.40	0.37	0.49	0.50	0.55	0.37	0.55	0.41
OR	0.02	0.01	0.00	0.00	0.01	0.01	0.01	0.01	0.01	0.01	0.02	0.00
AN	0.43	0.57	0.60	0.66	0.59	0.63	0.50	0.49	0.44	0.62	0.44	0.59

(a) Feldspar Analyses DM90.27 (centre) - AGE F
DM90.20 & 11 (centre); DM90.19 & 9 (chill) - AGE E

fs=feldspar; r=rim; c=core; z=zoning across a single grain
left hand number=number of mineral grain in slide
right hand number=sample number preceded by DM90.
All plagioclase groundmass unless otherwise stated.

DM90.19
fs1,2,4,5 : phenocryst
fs3,6,7 : groundmass

	fs1-18	fs2-18	fs3-18	fs4-18	fs5-18	fs6-18	fs7-18	fs1-17	fs2-17	fs3-17	fs4-17	fs5-17	fs6-17	fs7-17
Na2O	4.52	4.53	4.99	6.32	5.48	4.69	4.49	5.36	6.35	9.58	6.43	9.18	5.92	6.21
K2O	0.23	0.24	0.26	0.38	0.32	0.24	0.22	0.27	3.88	0.08	2.78	0.57	0.26	0.26
SiO2	55.10	54.13	54.96	58.07	56.13	54.97	54.30	56.57	59.27	64.79	67.16	64.48	56.04	57.86
Al2O3	28.04	27.46	27.08	25.25	26.23	27.30	27.67	24.46	19.93	21.09	19.39	21.49	25.32	25.71
FeO	0.95	0.96	0.94	0.73	0.83	0.91	0.89	2.79	2.59	0.47	1.16	0.61	1.23	1.12
MgO	0.10	0.09	0.07	0.06	-	0.12	0.10	1.02	0.47	0.10	0.08	0.08	0.18	0.12
CaO	11.91	11.75	10.93	8.81	9.97	11.33	11.94	10.28	5.83	3.17	4.04	3.48	9.65	8.78
TOTAL	100.85	99.16	99.23	99.62	98.96	99.56	99.61	100.75	98.32	99.28	101.04	99.89	98.60	100.06
AB	0.40	0.40	0.44	0.55	0.49	0.42	0.40	0.47	0.52	0.84	0.61	0.80	0.52	0.55
OR	0.01	0.02	0.02	0.02	0.02	0.02	0.01	0.02	0.21	0.01	0.18	0.03	0.02	0.02
AN	0.59	0.58	0.54	0.43	0.49	0.56	0.59	0.51	0.27	0.15	0.21	0.17	0.46	0.43

	fs1r11	fs1c11	fs2z11	fs2z11	fs2z11	fs2z11	fs2z11	fs2z11	fs2z11	fs2z11	fs2z11	fs2z11
Na2O	10.07	6.89	2.81	3.47	3.52	3.45	3.59	3.62	3.52	3.62	3.46	3.89
K2O	0.09	0.14	0.08	0.12	0.11	0.11	0.11	0.10	0.14	0.10	0.11	0.13
SiO2	67.09	68.63	49.74	51.60	51.90	51.71	51.95	51.55	51.94	52.06	51.08	52.59
Al2O3	21.82	21.59	30.39	29.17	29.10	29.11	29.21	29.17	29.27	29.17	29.15	28.92
FeO	0.21	-	0.90	0.68	0.68	0.71	0.70	0.69	0.69	0.68	0.69	0.90
MgO	-	-	0.15	0.19	0.17	0.19	0.17	0.16	0.18	0.19	0.19	0.17
CaO	1.72	1.28	14.81	13.56	13.27	13.49	13.46	13.66	13.50	13.36	13.55	12.90
TOTAL	101.00	98.53	98.88	98.79	98.76	98.77	99.19	98.95	99.22	99.18	98.23	99.51
AB	0.91	0.90	0.25	0.31	0.32	0.31	0.32	0.32	0.32	0.33	0.31	0.35
OR	0.01	0.01	0.00	0.01	0.01	0.01	0.01	0.01	0.01	0.01	0.01	0.01
AN	0.09	0.09	0.74	0.68	0.67	0.68	0.67	0.67	0.67	0.67	0.68	0.64

	fs3r11	fs3c11	fs4r11	fs4c11	fs5r11	fs5c11	fs6r11	fs6c11	fs7r11	fs7c11
Na2O	5.64	3.99	4.46	3.59	4.11	4.17	4.26	4.04	3.42	3.37
K2O	0.08	0.13	0.15	0.11	0.13	0.14	0.14	0.13	0.07	0.09
SiO2	70.01	53.92	54.17	51.71	53.31	53.59	53.65	53.81	51.12	51.16
Al2O3	21.78	29.03	27.81	29.12	28.29	28.49	28.13	28.53	29.37	29.20
FeO	0.33	0.90	0.92	0.78	1.20	1.05	0.99	1.05	0.91	0.83
MgO	-	0.16	0.18	0.18	0.21	0.17	0.22	0.19	0.20	0.18
CaO	0.99	12.82	11.90	13.22	12.47	12.26	12.40	12.54	13.90	13.57
TOTAL	98.83	100.95	99.59	98.70	99.72	99.86	99.79	100.28	98.99	98.40
AB	0.90	0.36	0.40	0.33	0.37	0.38	0.38	0.37	0.31	0.31
OR	0.01	0.01	0.01	0.01	0.01	0.01	0.01	0.01	0.00	0.01
AN	0.09	0.64	0.59	0.67	0.62	0.61	0.61	0.63	0.69	0.69

	fs1-10	fs2-10	fs3-10	fs4-10	fs5-10	fs6-10	fs7r10	fs7c10
Na2O	5.48	5.14	4.53	4.35	5.07	4.35	3.27	3.08
K2O	0.29	0.23	0.14	0.13	0.22	0.15	0.09	0.27
SiO2	57.33	56.63	55.17	52.99	55.20	54.34	50.78	50.96
Al2O3	26.43	26.75	28.07	28.06	27.17	28.19	30.21	29.23
FeO	0.99	1.08	1.14	0.98	1.14	1.03	0.70	0.75
MgO	0.11	0.13	0.15	0.20	0.11	0.17	0.17	0.16
CaO	10.39	10.94	12.18	12.64	11.33	12.15	14.41	15.16
TOTAL	101.02	100.90	101.38	99.35	100.24	100.38	99.63	99.61
AB	0.48	0.45	0.40	0.38	0.44	0.39	0.29	0.26
OR	0.02	0.02	0.01	0.01	0.01	0.01	0.01	0.02
AN	0.50	0.53	0.59	0.61	0.55	0.60	0.70	0.72

(a) **Feldspar Analyses** DM90.10 (centre); DM90.11 (chill) AGE D
DM90.18 (centre); DM90.17 (chill) AGE B

fs=feldspar; r=rim; c=core; z=zoning across a single grain
left hand number=number of mineral grain in slide
right hand number=sample number preceded by DM90.
All plagioclase groundmass unless otherwise stated.

DM90.10
fs1-fs6 : groundmass
fs7: phenocryst

DM90.11
fs1,2,7 : phenocryst
fs3,4,5,6 : microphenocryst

	fs1z04	fs1z04	fs1z04	fs1z04	fs1z04	fs1z04	fs1z04	fs1z04	fs1z04	fs2z04
Na2O	2.72	3.33	3.18	3.38	3.14	3.20	3.38	3.43	3.00	5.50
K2O	0.10	0.11	0.10	0.12	0.11	0.12	0.09	0.13	0.09	0.60
SiO2	49.65	51.01	51.02	50.61	50.51	50.42	52.22	51.93	50.44	57.99
Al2O3	30.53	29.45	29.81	29.71	29.91	29.63	29.93	29.43	30.07	25.72
FeO	0.64	0.65	0.48	0.50	0.49	0.53	0.50	0.52	0.63	1.05
MgO	0.14	0.18	0.16	0.18	0.19	0.17	0.19	0.18	0.16	0.08
CaO	14.87	13.45	13.75	13.45	14.01	13.77	13.88	13.49	14.28	8.49
TOTAL	98.65	98.18	98.50	97.94	98.36	97.83	100.19	99.12	98.68	99.43
AB	0.25	0.31	0.29	0.31	0.29	0.29	0.30	0.31	0.27	0.52
OR	0.01	0.01	0.01	0.01	0.01	0.01	0.01	0.01	0.01	0.04
AN	0.75	0.69	0.70	0.68	0.71	0.70	0.69	0.68	0.72	0.44

	fs2z04	fs2z04	fs2z04	fs2z04	fs3/04	fs4z04	fs4z04	fs4z04	fs5/04	fs1z05
Na2O	3.94	4.03	3.60	4.20	4.89	5.31	3.80	4.76	2.76	6.20
K2O	0.16	0.16	0.18	0.23	0.44	0.56	0.24	0.34	0.47	0.48
SiO2	53.14	53.36	52.68	53.52	56.17	57.26	51.46	55.03	56.33	59.58
Al2O3	28.55	28.13	27.74	27.73	27.02	25.86	26.59	27.16	27.32	26.06
FeO	0.80	0.65	2.08	1.14	1.07	1.10	4.94	1.12	1.08	0.71
MgO	0.17	0.20	0.71	0.35	0.09	0.09	1.03	0.13	0.10	0.04
CaO	12.66	12.02	11.70	11.60	9.96	9.10	10.07	10.73	10.62	8.15
TOTAL	99.42	98.55	98.70	98.75	99.65	99.28	98.12	99.27	98.68	101.23
AB	0.36	0.37	0.35	0.39	0.46	0.50	0.40	0.44	0.31	0.56
OR	0.01	0.01	0.01	0.01	0.03	0.03	0.02	0.02	0.03	0.03
AN	0.63	0.62	0.63	0.60	0.52	0.47	0.59	0.54	0.66	0.41

	fs1z05	fs1z05	fs1z05	fs1z05	fs1z05	fs1z05	fs1z05	fs1z05	fs1z05	fs1z05
Na2O	5.54	5.27	5.22	5.16	5.05	5.04	5.11	5.11	5.15	5.20
K2O	0.43	0.35	0.35	0.34	0.33	0.30	0.33	0.31	0.35	0.31
SiO2	58.10	56.28	56.14	55.71	55.37	55.37	55.21	55.66	55.53	55.88
Al2O3	26.53	26.97	26.94	27.20	27.25	27.17	27.19	27.06	27.07	26.85
FeO	0.68	0.87	0.61	0.69	0.62	0.70	0.62	0.63	0.64	0.69
MgO	0.09	0.10	0.08	0.08	0.09	0.09	0.08	0.09	0.10	0.08
CaO	9.17	9.98	10.26	10.55	10.80	10.69	10.53	10.44	10.40	10.29
TOTAL	100.53	99.82	99.60	99.74	99.50	99.35	99.06	99.30	99.23	99.30
AB	0.51	0.48	0.47	0.46	0.45	0.45	0.46	0.46	0.46	0.47
OR	0.03	0.02	0.02	0.02	0.02	0.02	0.02	0.02	0.02	0.02
AN	0.47	0.50	0.51	0.52	0.53	0.53	0.52	0.52	0.52	0.51

	fs1z05	fs1z05	fs1z05	fs1z05	fs2r05	fs2c05	fs3r05	fs3c05	fs4r05	fs4c05	fs5r05	fs5c05
Na2O	5.17	5.57	5.72	6.76	6.33	4.06	5.44	4.58	6.71	4.51	5.73	3.87
K2O	0.34	0.42	0.42	0.63	0.61	0.17	0.43	0.27	0.80	0.23	0.38	0.18
SiO2	55.94	57.07	56.77	59.19	59.21	53.08	57.41	55.07	61.06	54.53	57.76	53.22
Al2O3	26.85	26.54	26.39	24.73	25.43	28.83	26.58	27.93	24.51	28.17	26.22	28.94
FeO	0.62	0.68	0.84	0.73	0.63	0.58	0.71	0.69	0.50	0.58	0.58	0.61
MgO	0.07	0.05	0.04	–	–	0.16	0.07	0.11	–	0.11	0.07	0.11
CaO	10.15	9.61	9.23	7.03	7.57	12.61	9.43	11.50	6.45	11.61	9.15	12.83
TOTAL	99.15	99.94	99.41	99.07	99.78	99.49	100.07	100.14	100.02	99.73	99.89	99.75
AB	0.47	0.50	0.52	0.61	0.58	0.36	0.50	0.41	0.62	0.41	0.52	0.35
OR	0.02	0.02	0.03	0.04	0.04	0.01	0.03	0.02	0.05	0.01	0.02	0.01
AN	0.51	0.48	0.46	0.35	0.38	0.63	0.48	0.57	0.33	0.58	0.46	0.64

(a) Feldspar Analyses DM90.5 (centre); DM90.4 (chill) AGE A

fs=feldspar; r=rim; c=core; z=zoning across a single grain
left hand number=number of mineral grain in slide
right hand number=sample number preceded by DM90.
All plagioclase groundmass unless otherwise stated.

DM90.4
fs1 - phenocryst
fs2 - 2nd generation
fs3,4,5 - groundmass

	px1-30	px2-30	px3-30	px4-30	px5-30	px6-30	px7-30	px8-30	px1-29	px2-29
SiO2	50.01	49.87	49.60	50.17	49.39	50.31	50.28	49.41	47.19	48.14
TiO2	0.98	0.95	1.11	0.96	1.00	0.77	0.90	1.28	1.45	1.57
Al2O3	3.02	2.35	2.10	2.64	1.87	1.26	2.56	2.59	3.77	3.99
Cr2O3	0.27	–	–	0.19	–	–	0.21	–	0.17	–
FeO	12.57	16.30	16.65	12.40	20.48	21.47	13.23	16.48	14.07	14.92
MnO	0.30	0.30	0.34	0.31	0.37	0.43	0.27	0.30	0.21	0.28
MgO	14.96	15.09	12.04	14.25	12.35	12.30	14.90	12.12	13.31	12.50
CaO	17.08	13.75	16.82	16.76	12.60	13.30	15.93	16.61	16.88	17.22
Na2O	0.30	0.19	0.25	0.25	0.18	0.17	0.20	0.25	0.24	0.34
K2O	–	–	–	–	–	–	–	–	–	–
TOTAL	99.49	98.80	98.91	97.93	98.24	100.01	98.48	99.04	97.29	98.96
WO	0.36	0.29	0.36	0.36	0.27	0.28	0.34	0.36	0.36	0.37
EN	0.43	0.44	0.36	0.43	0.37	0.36	0.44	0.36	0.40	0.37
FS	0.21	0.27	0.28	0.21	0.36	0.36	0.22	0.28	0.24	0.26

	px3-29	px4-29
SiO2	47.06	48.31
TiO2	1.59	1.79
Al2O3	2.60	3.77
Cr2O3	–	0.08
FeO	21.65	16.10
MnO	0.50	0.31
MgO	10.88	12.58
CaO	13.76	16.58
Na2O	0.26	0.30
K2O	–	–
TOTAL	98.30	99.82
WO	0.30	0.35
EN	0.33	0.37
FS	0.37	0.28

	px1c25	px2c25	px3c25	px4c25	px5c25	px6c25	px7c25	px1c24	px2c24	px3c24	px4c24	px5c24	px6c24	px7c24
SiO2	50.83	51.54	51.37	51.04	50.55	50.93	51.43	49.38	49.06	48.93	50.22	48.19	48.26	49.33
TiO2	1.10	0.91	0.83	0.99	0.96	0.94	0.94	1.36	1.76	1.83	1.03	1.63	1.71	1.34
Al2O3	2.77	2.03	2.12	2.33	2.46	2.33	2.38	3.54	3.87	4.10	2.81	3.67	4.03	3.42
Cr2O3	0.11	–	–	–	–	–	–	0.31	0.25	0.10	0.21	–	0.35	0.10
FeO	11.49	15.30	12.07	12.74	13.98	12.04	12.82	10.54	12.30	13.77	10.59	17.36	12.90	12.51
MnO	0.21	0.31	0.33	0.22	0.30	0.23	0.29	0.17	0.25	0.32	0.14	0.35	0.30	0.26
MgO	15.07	16.15	15.51	15.09	14.92	15.29	15.66	14.71	15.07	15.24	15.03	14.38	14.61	14.69
CaO	18.66	14.39	17.19	17.42	16.25	17.51	16.80	18.73	17.21	15.20	18.36	13.25	16.62	17.30
Na2O	0.27	0.21	0.23	0.27	0.24	0.29	0.28	0.30	0.26	0.26	0.25	0.23	0.21	0.28
K2O	–	–	–	–	–	–	–	–	–	–	–	0.19	–	–
TOTAL	100.51	100.84	99.65	100.10	99.66	99.56	100.60	99.04	100.03	99.75	98.64	99.25	98.99	99.23
WO	0.38	0.29	0.35	0.36	0.34	0.36	0.34	0.39	0.36	0.32	0.38	0.28	0.35	0.36
EN	0.43	0.46	0.45	0.43	0.43	0.44	0.45	0.43	0.44	0.45	0.44	0.42	0.43	0.43
FS	0.19	0.25	0.20	0.21	0.23	0.20	0.21	0.18	0.20	0.23	0.18	0.30	0.22	0.21

(b) Pyroxene Analyses DM90.30 (centre); DM90.29 (chill) - AGE H
DM90.25 (centre); DM90.24 (chill) - AGE G'

px=pyroxene; r=rim; c=core
left hand number=number of mineral grain in slide
right hand number=sample number preceded by DM90.
All pyroxenes groundmass unless otherwise stated.

	px1r06	px1c06	px2r06	px2c06	px3r06	px3c06	px4r06	px4c06	px5r06	px5c06	px6r06	px6c06	px7r06
SiO2	49.97	51.17	51.03	51.19	51.10	50.94	50.95	51.40	50.84	51.33	51.73	52.09	50.93
TiO2	1.07	0.76	0.73	0.68	0.67	0.69	0.71	0.78	0.98	0.85	0.67	0.63	0.70
Al2O3	3.32	2.96	2.64	2.44	2.37	2.48	2.68	2.69	3.07	2.87	1.90	1.84	2.66
Cr2O3	0.17	0.58	0.40	0.44	0.47	0.45	0.50	0.49	0.25	0.33	0.11	0.34	0.41
FeO	10.60	9.20	8.84	8.90	8.82	8.61	8.84	8.76	12.23	11.01	10.67	9.52	9.51
MnO	0.25	0.20	0.22	0.19	0.18	0.21	0.24	0.19	0.29	0.19	0.25	0.19	0.25
MgO	15.09	16.06	15.87	15.78	15.78	15.77	15.56	16.05	14.95	14.85	16.66	16.17	15.58
CaO	18.68	18.95	19.52	19.48	19.53	19.73	19.52	19.83	17.34	18.33	17.26	18.89	19.49
Na2O	0.31	0.32	0.28	0.25	0.27	0.25	0.26	0.32	0.25	0.30	0.25	0.26	0.28
K2O	–	–	–	–	–	–	–	–	–	–	–	–	–
TOTAL	99.44	100.19	99.53	99.37	99.20	99.12	99.27	100.50	100.21	100.06	99.50	99.94	99.81
WO	0.39	0.39	0.40	0.40	0.40	0.41	0.40	0.40	0.36	0.38	0.35	0.39	0.40
EN	0.44	0.46	0.45	0.45	0.45	0.45	0.45	0.45	0.43	0.43	0.47	0.46	0.44
FS	0.18	0.15	0.15	0.15	0.14	0.14	0.15	0.14	0.20	0.18	0.17	0.15	0.16

	px7c06	px8r06	px8c06	px1r07	px1c07	px2r07	px2c07	px3r07	px3c07	px4r07
SiO2	50.08	50.47	51.61	49.74	49.84	50.52	50.22	50.45	50.35	49.82
TiO2	1.07	1.02	0.69	0.96	0.83	0.91	0.98	1.06	1.10	0.94
Al2O3	3.51	3.09	2.34	1.64	2.32	2.72	3.20	2.40	2.26	2.24
Cr2O3	0.41	0.12	0.14	–	–	–	0.36	–	–	–
FeO	10.13	11.07	12.31	21.80	16.84	11.73	9.99	17.72	18.17	16.83
MnO	0.27	0.28	0.34	0.48	0.34	0.31	0.21	0.43	0.44	0.34
MgO	15.22	15.41	16.80	12.24	15.63	15.64	15.61	15.10	14.47	14.17
CaO	18.77	17.87	15.27	13.83	13.51	17.13	18.72	13.58	13.64	15.04
Na2O	0.31	0.27	0.23	0.24	0.21	0.26	0.31	0.28	0.28	0.25
K2O	–	–	–	–	–	–	–	–	–	–
TOTAL	99.77	99.60	99.74	100.93	99.51	99.21	99.60	101.02	100.70	99.63
WO	0.39	0.37	0.31	0.29	0.28	0.35	0.39	0.28	0.28	0.31
EN	0.44	0.45	0.48	0.35	0.45	0.45	0.45	0.43	0.42	0.41
FS	0.17	0.18	0.20	0.36	0.28	0.19	0.16	0.29	0.30	0.28

	px4c07	px5r07	px5c07	px6z07	px6z07	px6z07	px6z07	px6z07	px6z07	px7t07
SiO2	50.88	50.69	51.21	51.09	51.07	50.71	51.28	50.45	50.05	50.45
TiO2	0.89	0.78	0.64	0.70	0.74	0.84	0.79	1.04	1.13	0.98
Al2O3	2.60	2.00	1.51	2.24	2.59	2.80	2.74	3.41	2.59	3.12
Cr2O3	0.08	–	–	0.44	0.48	0.52	0.46	0.29	–	0.23
FeO	11.99	18.10	21.42	8.90	8.88	8.98	8.73	9.98	14.64	10.87
MnO	0.26	0.48	0.43	0.20	0.19	0.24	0.20	0.25	0.31	0.28
MgO	15.46	16.78	18.58	16.35	16.01	15.79	15.89	15.64	14.47	15.60
CaO	17.64	11.50	5.91	19.62	19.69	20.01	19.80	18.68	16.98	17.96
Na2O	0.29	0.11	0.09	0.23	0.27	0.28	0.28	0.30	0.31	0.28
K2O	–	–	–	–	–	–	–	–	–	–
TOTAL	100.08	100.44	99.78	99.77	99.92	100.17	100.18	100.06	100.48	99.78
WO	0.36	0.23	0.12	0.40	0.40	0.41	0.41	0.39	0.35	0.37
EN	0.44	0.47	0.53	0.46	0.45	0.45	0.45	0.45	0.41	0.45
FS	0.20	0.29	0.35	0.14	0.14	0.15	0.14	0.17	0.24	0.18

	px7t07	px7t07	px7t07	px7t07	px7t07	px1-08	px2r08	px2c08	px3c08	px4c08	px5c08
SiO2	50.37	50.78	50.59	50.73	49.74	51.11	49.87	51.34	50.38	50.25	50.78
TiO2	0.91	0.84	0.92	0.95	1.17	0.81	1.05	0.85	1.15	1.10	0.98
Al2O3	3.17	2.64	2.84	2.81	2.52	1.82	1.87	1.71	1.96	2.28	1.84
Cr2O3	0.20	0.13	0.10	–	–	0.13	–	–	–	–	–
FeO	10.94	10.85	11.73	12.29	15.52	12.95	19.25	20.12	17.31	14.11	18.85
MnO	0.25	0.23	0.25	0.27	0.34	0.22	0.42	0.43	0.33	0.35	0.45
MgO	15.84	15.97	15.70	15.25	13.71	15.26	13.69	15.94	12.67	14.15	15.71
CaO	17.86	18.25	17.70	17.40	16.93	16.71	13.04	10.33	16.75	17.19	11.79
Na2O	0.28	0.30	0.30	0.28	0.31	0.21	0.18	0.16	0.26	0.25	0.19
K2O	–	–	–	–	–	–	–	–	–	–	–
TOTAL	99.82	99.98	100.12	99.98	100.24	99.22	99.37	100.88	100.81	99.68	100.59
WO	0.37	0.37	0.36	0.36	0.35	0.35	0.28	0.21	0.35	0.36	0.24
EN	0.45	0.45	0.45	0.44	0.39	0.44	0.40	0.46	0.37	0.41	0.45
FS	0.18	0.18	0.19	0.20	0.26	0.21	0.32	0.33	0.28	0.23	0.31

(b) <u>Pyroxene Analyses</u> DM90.6 & 7 (centre) - AGE G
DM90.8 (centre) - AGE G″

px=pyroxene; r=rim; c=core; z=zoning across a single grain
t=traverse across a crack system
left hand number=number of mineral grain in slide
right hand number=sample number preceded by DM90.
All pyroxenes groundmass unless otherwise stated.

DM90.6
px 1-4 : phenocryst
px 5-8 : groundmass

	px1-20	px2-20	px3-20	px4-20	px5-20	px1-19	px2-19	px3-19	px4-19	px5-19
SiO2	50.76	51.81	49.91	52.82	51.54	50.75	51.15	49.64	50.33	49.27
TiO2	0.40	0.41	0.55	0.39	0.67	0.38	0.49	0.42	0.46	0.95
Al2O3	3.72	3.24	1.94	1.59	1.20	3.94	3.25	3.96	2.64	3.58
Cr2O3	0.71	0.16	–	–	–	1.05	0.44	1.05	0.16	0.18
FeO	6.68	7.50	16.87	11.32	20.38	6.60	6.70	6.30	9.66	10.63
MnO	0.20	0.16	0.37	0.29	0.50	0.17	–	0.13	0.20	0.24
MgO	17.30	16.26	16.09	17.10	19.80	17.01	16.50	16.37	18.30	14.40
CaO	18.58	20.01	12.79	16.70	4.65	18.48	19.86	19.68	15.44	18.66
Na2O	0.25	0.25	0.23	0.26	–	0.25	0.20	0.22	0.19	0.20
K2O	–	–	–	–	–	–	–	–	–	–
TOTAL	98.60	99.80	98.75	100.47	98.74	98.63	98.59	97.77	97.38	98.11
WO	0.39	0.41	0.26	0.34	0.09	0.39	0.41	0.41	0.32	0.40
EN	0.50	0.47	0.46	0.48	0.57	0.50	0.48	0.48	0.52	0.42
FS	0.11	0.12	0.28	0.18	0.34	0.11	0.11	0.11	0.16	0.18

	px1-27	px2c27	px3c27	px4-27	px5-27	px1-09	px2-09	px3-09	px4-09	px5-09	px6-09
SiO2	49.06	48.19	47.04	47.80	47.73	50.03	50.58	49.09	51.44	52.85	50.49
TiO2	0.93	0.37	0.88	0.86	0.90	0.95	0.53	1.04	0.59	0.38	0.85
Al2O3	1.94	2.14	1.57	2.27	1.71	3.99	2.04	2.90	3.33	1.47	4.14
Cr2O3	–	–	–	–	–	–	–	–	0.26	–	0.23
FeO	15.42	13.37	17.90	13.00	16.86	11.61	17.34	16.49	10.81	15.26	11.14
MnO	0.37	0.31	0.45	0.30	0.37	0.26	0.42	0.32	0.27	0.35	0.27
MgO	11.40	12.50	10.40	12.69	11.41	15.25	15.90	13.73	18.09	19.94	15.76
CaO	17.57	17.77	16.65	17.78	16.71	16.48	11.50	14.68	15.03	10.23	16.53
Na2O	0.26	0.28	0.22	0.23	0.23	0.25	0.15	0.21	0.19	0.11	0.25
K2O	–	–	–	–	–	–	–	–	–	–	–
TOTAL	96.95	94.93	95.11	94.93	95.92	98.82	98.46	98.46	100.01	100.59	99.66
WO	0.38	0.39	0.37	0.39	0.36	0.35	0.24	0.31	0.30	0.20	0.35
EN	0.35	0.38	0.32	0.38	0.34	0.45	0.47	0.41	0.52	0.55	0.46
FS	0.27	0.23	0.31	0.23	0.30	0.20	0.29	0.28	0.18	0.25	0.19

	px1r11	px1c11	px2r11	px2c11	px3r11	px3c11	px4r11	px4c11	px5r11	px5c11
SiO2	52.04	51.74	50.44	50.61	51.64	50.77	51.12	52.48	50.16	50.60
TiO2	0.45	0.47	0.75	0.57	0.44	0.74	0.56	0.41	0.90	0.52
Al2O3	1.78	1.76	2.25	3.00	1.75	2.85	3.34	1.95	1.70	1.81
Cr2O3	–	–	–	0.18	–	–	0.23	0.27	–	–
FeO	9.82	9.04	15.20	9.09	9.21	10.23	7.95	7.58	18.24	11.70
MnO	0.29	0.27	0.35	0.16	0.28	0.28	0.19	0.21	0.43	0.31
MgO	17.13	16.68	15.90	16.87	17.11	15.91	16.15	17.28	12.91	15.22
CaO	18.05	19.24	14.60	18.18	18.49	18.44	19.53	19.38	15.61	17.82
Na2O	0.25	0.23	0.28	0.28	0.23	0.27	0.24	0.24	0.24	0.22
K2O	–	–	–	–	–	–	–	–	–	–
TOTAL	99.81	99.43	99.76	98.93	99.16	99.48	99.31	99.79	100.18	98.20
WO	0.36	0.39	0.30	0.37	0.37	0.38	0.40	0.39	0.32	0.37
EN	0.48	0.47	0.45	0.48	0.48	0.45	0.46	0.49	0.37	0.44
FS	0.16	0.15	0.25	0.15	0.15	0.17	0.13	0.12	0.30	0.19

(b) Pyroxene Analyses DM90.27 (centre) - AGE F
DM90.20 & 11 (centre); DM90.19 & 9 (chill) - AGE E

px=pyroxene; r=rim; c=core
left hand number=number of mineral grain in slide
right hand number=sample number preceded by DM90.
All pyroxenes groundmass unless otherwise stated.

DM90.19
px1,2,3 : phenocryst
px4,5 : groundmass

	px1r11	px1c11	px2/11	px3/11	px1-10	px2-10	px3c10	px3r10	px4c10	px4r10	px5-10	px6-10
SiO2	50.73	51.73	50.44	51.62	49.74	51.13	52.09	52.61	51.73	52.19	51.03	50.32
TiO2	0.86	0.50	0.88	0.64	1.17	0.77	0.54	0.54	0.66	0.63	0.94	1.18
Al2O3	3.48	2.20	3.57	2.45	3.08	3.04	2.65	2.08	2.66	2.39	3.08	2.51
Cr2O3	0.21	0.16	0.14	0.17	–	0.13	0.22	0.15	0.12	0.17	0.13	–
FeO	10.44	9.97	10.40	9.84	13.55	12.17	9.30	9.67	9.69	9.72	13.36	18.42
MnO	0.22	0.24	0.26	0.22	0.25	0.29	0.19	0.26	0.25	0.27	0.26	0.35
MgO	16.50	17.55	16.20	16.93	13.99	17.30	17.37	17.53	16.52	16.96	17.34	13.38
CaO	18.02	17.08	17.61	17.48	17.47	15.19	17.54	17.39	18.27	17.76	13.77	14.96
Na2O	0.29	0.25	0.29	0.28	0.31	0.24	0.23	0.22	0.25	0.26	0.26	0.28
K2O	–	–	–	–	–	–	–	–	–	–	–	–
TOTAL	100.75	99.68	99.78	99.63	99.56	100.26	100.13	100.45	100.15	100.35	100.17	101.40
WO	0.37	0.35	0.36	0.36	0.37	0.31	0.36	0.35	0.37	0.36	0.28	0.31
EN	0.47	0.49	0.46	0.48	0.41	0.49	0.49	0.49	0.47	0.48	0.50	0.39
FS	0.17	0.16	0.17	0.16	0.22	0.20	0.15	0.16	0.16	0.16	0.22	0.30

	px1-18	px2-18	px3-18	px4-18	px5-18	px6-18	px7-18	px1-17	px2-17	px3-17
SiO2	50.59	50.57	50.23	50.45	50.19	50.61	51.00	48.56	51.30	49.18
TiO2	0.58	0.68	0.67	0.84	0.74	0.64	0.61	0.88	–	0.96
Al2O3	2.04	2.13	3.12	2.93	2.66	2.31	1.63	3.54	0.37	4.17
Cr2O3	–	–	–	–	–	–	–	–	–	–
FeO	15.04	15.30	12.83	12.69	12.95	14.32	18.31	15.00	15.16	16.37
MnO	0.28	0.36	0.31	0.29	0.30	0.30	0.49	0.39	0.54	0.37
MgO	14.49	14.47	15.52	14.86	14.89	14.40	12.85	12.01	10.17	10.61
CaO	16.05	15.81	15.92	17.45	17.13	17.22	15.51	18.55	21.48	14.36
Na2O	0.21	0.25	0.26	0.31	0.26	0.23	0.20	0.24	0.17	0.74
K2O	–	–	–	–	–	–	–	–	–	0.29
TOTAL	99.28	99.57	98.86	99.82	99.12	100.03	100.60	99.17	99.19	97.05
WO	0.33	0.33	0.33	0.36	0.36	0.35	0.32	0.39	0.45	0.34
EN	0.42	0.42	0.45	0.43	0.43	0.41	0.37	0.35	0.30	0.35
FS	0.25	0.25	0.22	0.21	0.21	0.24	0.31	0.26	0.25	0.31

(b) <u>Pyroxene Analyses</u> DM90.10 (centre); DM90.11 (chill) - AGE D
DM90.18 (centre); DM90.17 (chill) - AGE B

px=pyroxene; r=rim; c=core
left hand number=number of mineral grain in slide
right hand number=sample number preceded by DM90.
All pyroxenes groundmass unless otherwise stated.

DM90.11
note: pyroxene occurs as microphenocrysts and phenocrysts in a glassy matrix.

DM90.10
px1,2,5,6 : groundmass
px3,4 : phenocrysts

	px1r04	px1c04	px2r04	px2c04	px3r04	px3c04	px4r04	px4c04	px5z04	px5z04
SiO2	51.02	51.80	50.88	51.01	51.98	51.26	52.47	51.36	51.08	50.93
TiO2	0.79	0.67	0.88	1.04	0.66	0.67	0.48	0.70	0.74	0.63
Al2O3	2.90	2.53	2.93	3.19	2.24	2.54	1.81	2.90	3.19	2.50
Cr2O3	0.09	0.31	0.17	0.15	0.16	0.26	0.18	0.35	0.45	0.39
FeO	10.45	9.52	10.81	10.91	9.54	9.46	9.61	8.70	8.95	8.89
MnO	0.31	0.22	0.26	0.31	0.16	0.20	0.24	0.25	0.21	0.24
MgO	16.26	17.20	16.50	16.38	16.90	16.58	17.63	16.40	16.62	16.82
CaO	18.17	17.95	17.25	17.31	18.50	18.67	17.54	19.30	18.39	18.41
Na2O	0.23	0.19	0.23	0.22	0.18	0.22	0.22	0.25	0.21	0.21
K2O	–	–	–	–	–	–	–	–	–	–
TOTAL	100.22	100.39	99.92	100.53	100.31	99.85	100.17	100.21	99.84	99.02
WO	0.37	0.36	0.35	0.35	0.37	0.38	0.35	0.39	0.38	0.38
EN	0.46	0.48	0.47	0.47	0.47	0.47	0.49	0.46	0.47	0.48
FS	0.17	0.15	0.18	0.18	0.15	0.15	0.15	0.14	0.15	0.14

	px5z04	px5z04	px5z04	px5z04	px5z04	px1r05	px1c05	px2r05	px2c05	px3r05
SiO2	50.22	49.66	51.58	50.57	51.17	51.72	51.43	51.01	50.65	51.78
TiO2	0.92	1.45	0.65	0.79	0.57	0.70	0.70	0.96	0.89	0.70
Al2O3	3.37	4.16	2.25	3.48	2.10	1.86	2.74	2.03	2.15	2.42
Cr2O3	0.28	0.29	0.28	0.45	0.23	–	0.28	–	–	0.13
FeO	10.02	11.09	9.55	9.05	9.31	14.56	9.04	15.92	13.43	9.85
MnO	0.23	0.28	0.23	0.17	0.28	0.29	0.20	0.36	0.32	0.29
MgO	15.62	16.17	17.27	16.32	17.18	15.92	16.63	13.91	15.12	16.55
CaO	18.45	16.42	17.59	18.67	18.03	15.52	19.02	16.73	17.05	18.76
Na2O	0.26	0.22	0.19	0.24	0.19	0.22	0.22	0.28	0.27	0.23
K2O	–	–	–	–	–	–	–	–	–	–
TOTAL	99.37	99.74	99.59	99.74	99.06	100.79	100.28	101.22	99.87	100.69
WO	0.38	0.34	0.36	0.38	0.37	0.32	0.39	0.34	0.35	0.38
EN	0.45	0.47	0.49	0.47	0.48	0.45	0.47	0.40	0.43	0.46
FS	0.17	0.19	0.15	0.15	0.15	0.24	0.15	0.26	0.22	0.16

	px3c05	px4r05	px4c05	px5r05	px5c05	px6z05	px6z05	px6z05	px6z05	px6z05
SiO2	51.08	51.85	52.26	51.43	51.58	49.78	50.96	50.93	50.79	51.17
TiO2	0.92	0.58	0.56	0.66	0.85	0.76	0.92	0.98	0.97	0.88
Al2O3	3.10	2.27	1.89	2.30	2.63	1.24	1.59	1.72	1.85	2.04
Cr2O3	0.28	0.09	0.13	0.11	0.23	–	–	–	–	–
FeO	9.85	10.37	9.36	9.40	9.76	21.22	18.52	17.50	16.29	14.26
MnO	0.24	0.26	0.28	0.21	0.22	0.45	0.46	0.41	0.37	0.32
MgO	16.49	17.06	16.93	16.79	16.61	10.95	12.98	13.38	13.72	14.98
CaO	18.45	17.77	18.03	18.85	18.14	15.64	15.95	16.33	16.50	16.75
Na2O	0.22	0.21	0.27	0.23	0.22	0.22	0.21	0.26	0.25	0.23
K2O	–	–	–	–	–	–	–	–	–	–
TOTAL	100.64	100.45	99.72	99.98	100.25	100.25	101.59	101.52	100.74	100.63
WO	0.37	0.36	0.37	0.38	0.37	0.33	0.33	0.33	0.34	0.34
EN	0.47	0.48	0.48	0.47	0.47	0.32	0.37	0.38	0.39	0.43
FS	0.16	0.17	0.15	0.15	0.16	0.35	0.30	0.29	0.27	0.23

	px6z05	px6z05	px6z05	px6z05	px6z05	px6z05	px6z05
SiO2	51.49	52.35	52.45	52.62	52.05	52.49	52.14
TiO2	0.74	0.58	0.53	0.55	0.60	0.55	0.58
Al2O3	2.02	1.77	1.71	1.94	2.11	1.90	2.15
Cr2O3	–	–	–	0.11	–	0.11	0.11
FeO	12.05	12.11	11.73	10.25	10.47	10.30	10.65
MnO	0.29	0.31	0.34	0.25	0.27	0.28	0.17
MgO	15.98	17.08	17.45	17.16	16.89	17.21	16.50
CaO	17.36	16.27	16.18	17.66	17.84	17.81	17.91
Na2O	0.24	0.23	0.22	0.23	0.24	0.20	0.20
K2O	–	–	–	–	–	–	–
TOTAL	100.17	100.70	100.60	100.77	100.46	100.86	100.41
WO	0.35	0.33	0.32	0.36	0.36	0.36	0.36
EN	0.45	0.48	0.49	0.48	0.47	0.48	0.47
FS	0.20	0.19	0.19	0.16	0.17	0.17	0.17

(b) Pyroxene Analyses DM90.5 (centre); DM90.4 (chill) - AGE A

px=pyroxene; r=rim; c=core; z=zoning across a single grain
left hand number=number of mineral grain in slide
right hand number=sample number preceded by DM90.
All pyroxenes groundmass unless otherwise stated.

	ol1-20	ol2-20	ol3-20	ol4-20	ol5-20
SiO2	38.70	39.05	38.96	38.65	38.83
TiO2	-	-	-	-	-
Al2O3	-	-	-	-	-
Cr2O3	-	-	-	-	-
FeO	19.76	19.66	21.47	21.83	20.53
MnO	0.23	0.21	0.31	0.26	0.24
MgO	41.13	41.38	39.73	39.73	41.45
CaO	0.35	0.34	0.39	0.41	0.34
NiO	-	-	-	-	-
TOTAL	100.17	100.64	100.86	100.88	101.39

(c) **Olivine Analyses** DM90.20 (centre) - Age E

ol = olivine

left hand number = number of mineral grain in slide

right hand number = sample number preceded by DM90.

	ilm30	ilm29	ilm25	ilm25	ilm25	ilm25	ilm24	ilm08	ilm08	ilm08
SiO2	0.15	1.90	0.12	-	-	-	1.91	-	-	0.08
TiO2	49.13	47.23	49.74	50.60	51.26	50.73	47.24	52.00	51.44	51.56
Al2O3	0.13	0.62	0.12	-	-	-	0.78	-	-	-
Cr2O3	-	-	-	-	-	-	-	-	-	-
FeO	43.31	41.39	43.96	44.36	45.28	44.85	43.01	45.46	45.19	45.41
Fe2O3	6.16	5.33	4.79	4.36	2.29	3.79	4.66	-	1.79	1.59
MnO	1.03	1.21	0.72	0.95	0.80	0.53	0.85	0.67	1.05	0.88
MgO	-	0.33	0.10	0.10	-	0.13	0.09	0.13	-	0.09
CaO	-	1.20	-	-	-	-	0.57	0.08	-	-
TOTAL	99.92	99.21	99.55	100.36	99.63	100.03	99.11	98.34	99.47	99.61

	ilm08	ilm08	ilm08	ilm27	ilm27	ilm27	ilm09	ilm09	ilm09	ilm19
SiO2	0.12	0.10	-	-	-	-	0.31	0.51	0.17	-
TiO2	52.25	51.87	52.36	50.98	50.96	52.18	50.38	50.05	49.96	50.72
Al2O3	-	0.08	-	-	0.14	-	0.15	0.25	-	-
Cr2O3	-	-	-	-	-	-	-	-	-	-
FeO	45.60	45.54	46.09	44.26	44.15	45.24	43.71	43.85	43.79	43.15
Fe2O3	-	1.00	0.67	1.07	2.49	0.87	3.10	3.11	4.78	2.45
MnO	1.26	1.21	0.98	1.57	1.65	1.66	1.37	1.17	0.79	2.04
MgO	-	-	-	-	-	-	-	-	0.17	-
CaO	0.17	-	-	-	-	-	0.45	0.45	0.18	0.31
TOTAL	99.40	99.80	100.10	97.88	99.38	99.95	99.47	99.39	99.85	98.67

	ilm20	ilm20	ilm11	ilm11	ilm11	ilm11	ilm11	ilm18	ilm18	ilm17
SiO2	0.08	0.10	-	-	0.12	0.12	0.16	0.30	0.19	0.42
TiO2	51.39	52.07	51.45	52.81	50.71	50.91	51.59	50.49	42.17	48.93
Al2O3	-	-	-	-	-	0.08	0.11	-	0.47	0.09
Cr2O3	-	-	-	-	-	-	-	-	-	-
FeO	44.25	45.10	44.30	45.01	43.45	43.76	44.33	43.53	36.63	40.94
Fe2O3	2.11	1.07	0.99	-	1.17	1.61	-	3.46	19.55	5.44
MnO	1.88	1.82	1.72	1.70	1.72	1.79	1.91	1.68	1.32	3.07
MgO	-	-	-	-	-	-	0.06	-	-	-
CaO	0.12	-	0.17	-	0.43	0.27	0.14	0.41	0.14	0.35
TOTAL	99.83	100.16	98.64	99.52	97.60	98.54	98.30	99.88	100.47	99.25

	ilm05	ilm05	ilm05	ilm05	ilm05	ilm04	ilm04	ilm04
SiO2	-	0.08	-	-	0.12	0.34	0.25	0.12
TiO2	50.65	50.98	50.67	50.74	51.12	48.30	48.81	48.54
Al2O3	0.10	-	-	0.08	-	0.14	0.07	-
Cr2O3	-	-	-	-	-	-	-	-
FeO	43.72	44.12	43.99	44.18	44.05	41.08	41.18	41.40
Fe2O3	2.95	3.02	2.61	2.93	2.23	5.51	5.34	5.50
MnO	1.64	1.58	1.31	1.31	1.64	2.41	2.43	1.89
MgO	-	-	-	-	-	-	-	-
CaO	0.13	0.17	0.19	0.09	0.31	0.25	0.43	0.37
TOTAL	99.18	99.95	98.77	99.33	99.47	98.03	98.50	97.82

(d) Opaque Mineral Analyses - Ilmenite

ilm = ilmenite

right hand number = sample number preceded by DM90.

Fe_2O_3 calculated using the method of Stormer (1983) and Hugo (1993).

	ilm05	ilm05	ilm05	ilm05	ilm05	ilm05	ilm05	ilm05	ilm05	ilm05
SiO2	0.02	0.02	-	-	0.28	-	-	0.02	0.01	-
TiO2	50.45	50.10	49.68	49.82	47.66	49.04	49.72	49.56	48.82	49.44
Al2O3	0.03	0.03	0.03	0.02	0.55	-	0.01	0.01	0.03	0.01
Cr2O3	0.06	0.01	-	-	-	0.03	-	-	-	-
FeO	44.29	43.82	43.49	43.61	40.37	42.81	43.61	42.62	42.87	43.26
Fe2O3	3.63	3.95	5.10	5.01	7.96	5.75	4.66	4.53	5.91	5.19
MnO	0.48	0.78	0.82	0.45	1.56	1.05	0.50	1.92	0.49	0.48
MgO	0.35	0.26	0.20	0.41	0.69	0.13	0.33	0.02	0.31	0.40
TOTAL	99.31	98.97	99.32	99.32	99.07	98.81	98.83	98.68	98.44	98.78

	ilm05	ilm05	ilm05	ilm05	ilm05	ilm05	ilm05	ilm05	ilm05	ilm05
SiO2	0.02	-	-	-	-	-.	0.06	0.01	-	0.08
TiO2	50.72	50.46	51.15	52.00	52.09	50.88	50.88	50.93	50.65	50.98
Al2O3	0.03	0.03	0.03	0.03	0.03	0.04	0.04	0.02	0.10	-
Cr2O3	0.05	0.03	0.05	0.03	-	-	-	-	-	-
FeO	44.57	44.21	44.57	45.60	45.72	44.59	44.43	44.45	43.89	44.24
Fe2O3	2.63	3.24	3.32	1.92	1.03	2.95	3.33	3.62	2.76	2.89
MnO	0.52	0.71	1.16	0.50	0.46	0.49	0.90	1.29	1.64	1.58
MgO	0.30	0.26	0.14	0.37	0.37	0.38	0.27	0.02	-	-
TOTAL	98.84	98.94	100.42	100.45	99.70	99.33	99.91	100.34	99.04	99.77

	ilm05	ilm05	ilm05	ilm04	ilm04	ilm04	ilm25	ilm25	ilm25	ilm25
SiO2	-	-	0.12	0.25	0.34	0.12	0.06	0.03	0.03	0.02
TiO2	50.67	50.74	51.12	48.81	48.30	48.54	52.54	51.99	51.98	51.76
Al2O3	-	0.08	-	0.07	0.14	-	0.04	0.02	0.10	0.03
Cr2O3	-	-	-	-	-	-	0.03	0.04	0.03	0.02
FeO	44.24	44.30	44.31	41.43	40.99	41.74	46.57	46.05	45.89	45.84
Fe2O3	2.34	2.80	1.95	5.05	5.61	5.13	0.10	1.27	1.67	1.21
MnO	1.31	1.31	1.64	2.43	2.41	1.89	0.63	0.69	0.43	0.61
MgO	-	-	-	-	-	-	0.06	0.03	0.26	0.06
TOTAL	98.56	99.23	99.14	98.04	97.79	97.42	100.03	100.12	100.39	99.55

	ilm25	ilm25	ilm25	ilm25	ilm25	ilm25	ilm25	ilm25	ilm25	ilm25
SiO2	0.04	0.02	0.08	0.04	0.04	0.08	0.14	0.05	0.05	0.06
TiO2	50.25	51.98	51.05	51.17	51.55	51.17	48.31	50.29	52.35	51.58
Al2O3	0.16	0.03	0.13	0.04	0.04	0.03	0.64	0.03	0.02	0.03
Cr2O3	0.03	0.03	0.07	-	-	-	0.08	-	-	-
FeO	44.54	46.10	45.11	45.39	45.35	45.29	42.67	44.55	46.30	45.66
Fe2O3	3.81	1.16	3.03	1.90	1.71	2.56	6.71	3.10	0.70	1.91
MnO	0.61	0.52	0.67	0.54	1.02	0.72	0.80	0.67	0.77	0.70
MgO	0.04	0.08	0.12	0.07	0.01	0.05	0.07	0.03	0.03	0.05
TOTAL	99.48	99.92	100.26	99.15	99.72	99.90	99.42	98.72	100.22	99.99

(d) Additional Opaque Mineral Analyses - Ilmenite

ilm=ilmenite

right hand number=sample number preceded by DM90.

from Hugo (1993)

Fe_2O_3 calculated using the method of Stormer (1983) and Hugo (1993).

	ilm25	ilm08	ilm08	ilm08	ilm08	ilm08	ilm08	ilm08	ilm08	ilm08
SiO2	0.06	0.04	0.27	0.04	0.02	0.10	0.02	0.02	0.54	0.03
TiO2	51.59	51.26	51.83	50.87	51.85	49.72	51.41	51.04	51.60	52.16
Al2O3	0.03	0.14	0.03	0.04	0.04	0.41	0.04	0.05	0.32	0.03
Cr2O3	-	0.03	0.02	0.05	-	0.04	0.01	0.03	-	-
FeO	45.35	45.15	45.94	44.75	45.69	43.70	45.29	44.94	45.58	46.01
Fe2O3	1.99	1.13	0.34	1.90	0.71	3.53	1.17	1.36	0.06	0.79
MnO	1.09	0.90	0.86	0.94	0.68	1.00	0.71	0.91	0.74	0.76
MgO	0.01	0.04	0.07	0.05	0.16	0.07	0.13	0.03	0.40	0.09
TOTAL	100.12	98.69	99.36	98.64	99.15	98.57	98.78	98.38	99.24	99.87

	ilm08	ilm08	ilm06	ilm06	ilm06	ilm06	ilm06	ilm06	ilm06	ilm06
SiO2	0.42	0.04	0.03	0.05	0.08	0.05	0.06	0.03	0.01	0.16
TiO2	51.07	50.88	52.01	50.46	51.70	51.85	51.97	52.10	52.34	48.33
Al2O3	0.29	0.02	0.02	0.04	0.04	0.04	0.03	0.01	0.01	0.25
Cr2O3	-	-	0.07	0.09	0.11	0.10	0.04	-	0.01	0.03
FeO	44.97	44.76	45.11	43.70	44.89	44.97	45.17	45.84	45.88	42.36
Fe2O3	2.04	2.72	1.51	2.64	1.09	1.68	0.57	1.17	0.55	7.55
MnO	1.06	0.80	1.21	1.72	1.67	1.69	1.60	0.94	1.00	1.25
MgO	0.21	0.13	0.27	-	-	-	0.01	0.06	0.10	0.01
TOTAL	100.06	99.35	100.23	98.70	99.58	100.38	99.45	100.15	99.90	99.94

	ilm06	ilm06	ilm06	ilm06	ilm06	ilm11	ilm11	ilm11	ilm11
SiO2	0.31	0.01	0.02	0.02	0.06	0.12	-	0.12	-
TiO2	49.91	52.68	52.49	52.07	52.00	50.91	51.45	50.71	52.81
Al2O3	0.74	0.05	0.05	0.04	0.06	0.08	-	-	-
Cr2O3	0.02	0.02	-	0.01	0.02	-	-	-	-
FeO	43.69	46.22	45.48	45.44	45.18	43.97	44.52	43.86	45.01
Fe2O3	3.62	0.12	0.54	0.65	1.43	1.38	0.75	0.71	-
MnO	1.22	0.95	1.64	1.06	1.60	1.79	1.72	1.72	1.70
MgO	0.18	0.11	0.05	0.18	0.02	-	-	-	-
TOTAL	99.69	100.16	100.27	99.47	100.37	98.25	98.44	97.12	99.52

(d) Additional Opaque Mineral Analyses - Ilmenite

ilm = ilmenite

right hand number = sample number preceded by DM90.

from Hugo (1993)

Fe_2O_3 calculated using the method of Stormer (1983) and Hugo (1993).

	mt30	mt30	mt30	mt30	mt30	mt30	mt06	mt06	mt06	mt06
SiO2	0.89	0.10	0.43	0.70	3.27	-	0.11	0.23	0.14	0.11
TiO2	24.52	23.46	22.10	31.30	10.35	25.69	29.57	32.99	23.49	25.74
Al2O3	0.56	0.83	0.43	0.33	1.61	0.30	1.23	0.78	2.00	1.44
Cr2O3	-	-	-	-	0.10	-	-	-	-	0.10
FeO	53.30	51.82	50.73	59.10	42.67	53.70	57.16	59.40	50.43	52.53
Fe2O3	16.64	21.12	22.83	3.82	38.05	17.63	8.78	0.20	17.93	13.91
MnO	0.33	0.40	0.46	0.59	0.16	0.53	0.66	0.69	0.56	0.63
MgO	0.09	-	-	-	0.58	-	-	0.08	0.20	0.10
CaO	0.09	-	-	0.08	0.22	-	-	-	-	-
TOTAL	96.42	97.74	96.98	95.92	97.01	97.85	97.51	94.37	94.75	94.56

	mt07	mt07	mt07	mt25	mt25	mt24	mt24	mt27	mt27	mt09
SiO2	0.09	0.10	0.11	0.12	1.45	0.24	0.30	0.11	0.11	0.16
TiO2	32.92	24.17	11.24	10.81	7.18	7.34	4.42	2.20	3.85	21.04
Al2O3	0.31	0.46	0.89	2.00	1.23	1.12	0.69	0.71	0.64	0.23
Cr2O3	-	-	-	-	0.15	0.14	0.09	0.09	0.09	-
FeO	59.33	51.92	40.88	40.17	37.66	35.84	34.20	32.47	34.08	48.93
Fe2O3	1.62	19.04	45.07	44.36	49.06	50.44	56.70	62.22	59.24	25.82
MnO	0.92	0.51	0.19	0.22	0.25	-	-	-	-	0.60
MgO	-	-	-	-	0.51	-	-	-	-	-
CaO	-	-	-	-	0.08	0.82	0.19	-	-	0.30
TOTAL	95.19	96.20	98.37	97.67	97.56	95.94	96.59	97.79	98.01	97.08

	mt09	mt09	mt19	mt20	mt20	mt20	mt11	mt11	mt10	mt18
SiO2	0.16	0.25	0.12	0.55	0.42	0.19	0.14	0.10	4.11	0.12
TiO2	17.34	5.30	1.61	6.27	1.45	1.00	2.06	2.04	25.65	23.43
Al2O3	0.39	0.22	0.76	2.44	0.54	0.64	0.85	0.41	1.62	1.63
Cr2O3	-	-	-	0.19	0.22	0.13	-	-	-	-
FeO	45.67	35.22	32.02	35.87	31.52	31.02	31.00	31.93	55.00	50.91
Fe2O3	33.22	56.44	63.79	51.02	62.32	63.66	59.63	61.97	6.73	19.18
MnO	0.73	0.20	-	0.22	-	-	-	-	0.70	0.71
MgO	-	-	-	0.15	0.15	-	-	-	0.55	-
CaO	0.19	0.14	0.10	0.07	0.08	0.10	0.13	-	2.24	-
TOTAL	97.70	97.77	98.40	96.78	96.70	96.75	93.81	96.46	96.59	95.98

	mt18	mt18	mt18	mt18	mt17
SiO2	0.12	0.28	0.14	0.18	0.25
TiO2	23.43	16.97	20.04	24.77	5.83
Al2O3	1.63	2.41	2.23	1.57	0.51
Cr2O3	-	0.11	-	-	-
FeO	50.91	45.52	47.77	52.35	35.40
Fe2O3	19.18	31.31	25.14	16.93	55.16
MnO	0.71	0.52	0.69	0.79	0.34
MgO	-	-	-	-	-
CaO	-	0.08	-	-	0.26
TOTAL	95.98	97.21	96.01	96.59	97.76

(d) Opaque Mineral Analyses - Titanomagnetite

mt=titanomagnetite

right hand number=sample number preceded by DM90.

Fe_2O_3 calculated using the method of Stormer (1983) and Hugo (1993).

	mt05	mt05	mt05	mt05	mt05	mt05	mt05	mt25	mt25	mt25
SiO2	0.66	0.69	0.38	0.14	0.84	1.88	0.45	0.59	0.36	0.30
TiO2	20.22	20.29	23.31	29.07	18.06	21.69	23.61	6.63	22.18	28.98
Al2O3	0.80	1.00	0.60	0.77	1.10	0.68	0.78	1.89	1.13	2.09
Cr2O3	-	0.02	0.04	0.04	0.01	0.06	0.09	0.16	0.12	0.13
FeO	46.99	47.18	50.02	55.72	44.77	52.44	51.14	37.58	51.62	57.25
Fe2O3	25.62	24.80	19.58	8.52	27.90	19.73	20.40	51.56	23.89	8.24
MnO	1.48	1.16	1.20	1.18	1.02	0.32	1.27	0.22	0.60	0.71
MgO	0.87	0.92	0.47	0.06	1.13	0.08	0.48	0.08	0.06	0.07
TOTAL	96.64	96.06	95.60	95.50	94.83	96.88	98.22	98.71	99.96	97.77

	mt25	mt25	mt25	mt25	mt25	mt25	mt25	mt25	mt25	mt25
SiO2	1.09	0.15	1.58	1.54	0.12	0.67	0.12	0.19	0.14	0.16
TiO2	5.88	6.69	12.57	9.29	31.45	9.53	5.81	26.77	32.27	9.86
Al2O3	1.02	6.73	3.02	1.42	2.34	2.59	2.55	1.94	1.17	4.08
Cr2O3	0.19	0.21	0.14	0.23	0.04	0.23	0.18	0.11	0.08	0.15
FeO	36.69	37.53	43.24	40.20	59.36	40.11	35.78	55.40	59.63	40.11
Fe2O3	51.32	45.73	35.15	43.07	3.17	44.35	51.93	13.06	2.52	43.10
MnO	0.16	0.13	0.21	0.27	0.42	0.23	0.10	0.35	0.59	0.22
MgO	0.12	0.09	0.53	0.23	0.09	0.16	0.06	0.08	0.08	0.08
TOTAL	96.47	97.26	96.44	96.25	96.99	97.87	96.53	97.90	96.48	97.76

	mt25	mt25	mt08	mt08	mt08	mt08	mt08	mt08	mt08	mt08
SiO2	0.15	1.50	0.15	0.25	0.56	0.17	0.19	0.50	0.12	0.56
TiO2	6.62	10.13	4.51	27.06	4.70	4.17	19.73	6.40	3.39	6.27
Al2O3	4.94	1.19	1.86	0.96	2.68	2.29	3.11	2.22	1.95	2.53
Cr2O3	0.25	0.15	0.18	0.10	0.25	0.28	0.16	0.11	0.15	0.17
FeO	37.17	41.24	34.61	55.97	35.69	33.96	48.67	36.41	33.85	37.06
Fe2O3	48.37	43.01	55.45	14.85	53.67	54.55	24.88	49.59	58.22	50.86
MnO	0.17	0.36	0.16	0.61	0.17	0.15	0.44	0.16	0.13	0.21
MgO	0.17	0.26	0.03	0.04	0.04	0.04	0.15	0.04	0.02	0.06
TOTAL	97.84	97.84	96.95	99.84	97.76	95.61	97.33	95.43	97.83	97.72

	mt08	mt06	mt06	mt06	mt06	mt06	mt06	mt18	mt18	mt18
SiO2	0.17	2.62	6.31	0.91	4.12	0.85	0.47	0.22	0.17	0.17
TiO2	3.47	21.65	9.68	32.45	28.24	8.40	31.78	21.41	21.09	21.30
Al2O3	2.21	1.65	1.71	0.91	1.86	1.22	0.92	2.83	3.01	2.90
Cr2O3	0.24	0.14	0.11	0.06	0.05	0.11	0.09	0.13	0.13	0.13
FeO	33.39	53.77	46.75	61.13	60.99	38.75	60.05	50.03	49.51	49.16
Fe2O3	56.18	17.95	32.46	2.23	1.80	46.55	3.87	21.71	21.89	20.75
MnO	0.12	0.48	0.17	0.87	0.67	0.22	0.65	0.75	0.72	0.75
MgO	0.04	0.14	0.80	0.12	0.63	0.02	0.01	0.03	0.06	0.14
TOTAL	95.82	98.40	97.99	98.68	98.36	96.12	97.84	97.11	96.58	95.30

	mt18	mt18	mt18	mt18	mt18	mt18	mt18	mt18	mt18	mt18
SiO2	0.14	0.15	0.13	0.13	0.28	0.15	0.10	0.21	0.16	0.13
TiO2	22.31	20.87	16.39	33.31	16.57	14.22	20.95	28.92	17.51	23.73
Al2O3	2.64	2.74	2.84	1.33	1.92	3.40	2.41	1.63	2.80	2.21
Cr2O3	0.14	0.12	0.12	0.08	0.14	0.14	0.12	0.14	0.11	0.13
FeO	50.05	48.83	44.92	59.89	44.99	43.16	49.34	56.95	46.25	52.22
Fe2O3	19.03	21.73	30.57	0.15	30.66	34.21	23.50	9.33	29.05	18.70
MnO	0.70	0.75	0.60	1.23	0.58	0.55	0.82	0.88	0.62	0.74
MgO	0.10	0.03	0.04	0.07	0.06	0.04	0.03	0.06	0.04	0.04
TOTAL	95.11	95.22	95.61	96.19	95.20	95.87	97.27	98.12	96.54	97.90

(d) Additional Opaque Mineral Analyses - Titanomagnetite

mt = titanomagnetite

right hand number = sample number preceded by DM90.

from Hugo (1993)

Fe_2O_3 calculated using the method of Stormer (1983) and Hugo (1993).

APPENDIX 3

WHOLE-ROCK ANALYSIS

Appendix 3a X-Ray Fluorescence (XRF) Analysis

Preparation of Samples for XRF analysis
Laboratory facilities at the erstwhile Department of Geology and Mineralogy, University of Natal, Pietermaritzburg were used for sample preparation.

Weathered edges must be removed from the sample. This may be done manually using a hammer and chisel, or using the rock-splitter. The sample must be broken down to fist-sized pieces before being placed in the jaw-crusher. After every sample has been crushed, the splinters of rock must be bagged and sealed carefully. Great care must be taken to ensure that no contamination of the sample takes place. The jaw-crusher, and its various components must be scrubbed with a wire brush and washed down with acetone after each sample has been crushed.

Remaining sample preparation was done at the Department of Geology and Applied Geology, University of Natal, Durban. The splinter-sized samples were placed in a jaw-crusher for further breaking down in size. Samples were then milled down to a fine powder, in an agate mill.

Whole-rock analyses were conducted by the technical staff at the erstwhile Department of Geochemistry, University of Cape Town. All analyses were conducted by X-Ray fluorescence procedures adopted and devised by the above Department and described in Duncan *et al.* (1984a).

Table I Precision, "accuracy" and detection limits for major oxide analysis by XRF (from Duncan *et al.*, 1984a).

Oxide	% Concentration	Precision	"Accuracy"	L.L.D.
SiO_2	50.0	0.140	0.264	0.04
TiO_2	1.0	0.008	0.008	0.005
Al_2O_3	15.0	0.080	0.079	0.02
Fe_2O_3	9.0	0.038	0.064	0.014
MnO	0.15	0.008	0.003	0.008
MgO	8.0	0.148	0.086	0.07
CaO	12.0	0.028	0.030	0.008
Na_2O	2.5	0.032	0.067	0.08
K_2O	0.20	0.002	0.022	0.002
P_2O_5	0.20	0.012	0.018	0.011

Precision is expressed as an absolute error in % oxide (2 sigma counting error) on the given concentration. "Accuracy" is the average absolute difference (in % oxide) between the recommended values for standards on the calibration line and their calculated values. L.L.D. is the lower limit of detection (in % oxide) at the 99 % confidence level.

Table II Precision, "accuracy" and detection limits for trace element analysis by XRF (from Duncan *et al.*, 1984a).

Element	Concentration Range (ppm)	Precision	L.L.D.
Nb	4*–150	1.0–1.2	1.8
Zr	40–400	0.9–1.4	1.4
Y	20–40	0.8–1.0	1.3
Rb	3*–90	0.8–1.1	1.5
U	4–10	2.0–2.5	3.5
Sr	80–800	1.0–1.7	1.5
Th	5–30	2.3–3.1	4.0
Pb	5–100	2.3–3.2	4.5
Zn	8–150	0.9–1.7	1.4
Cu	5–90	1.8–2.1	2.9
Ni	10–210	0.7–1.0	1.2
Ga	15–20	0.38–0.46	0.45
Ba	10–800	2.1–6.0	3.7
Sc	25–40	1.0–1.2	1.2
Co	15–100	1.9–2.5	4.5
Cr	25–350	1.5–2.1	2.2
V	50–350	2.4–3.7	5.5
S	20–5000	10–40	20

Precision is expressed as an absolute error in ppm (2 sigma counting error) in the given concentration range. L.L.D. is the lower limit of detection (in ppm) at the 99 % confidence level.

* For many samples at or approaching the detection limit for Nb and Rb, samples were re-analysed using longer counting times in order to attain lower detection limits and better precision.

Table III X-Ray Fluorescence Whole-Rock Analyses (Data)

Major Elements (wt%), all Fe as Fe_2O_3; Trace Elements (ppm); < implies below detection limit

	DM90.4	DM90.5	DM90.6	DM90.7	DM90.8	DM90.9	DM90.10
	AGE $A_{(chill)}$	AGE A	AGE G	AGE G	AGE G"	AGE E	AGE D
SiO_2	50.70	50.63	49.43	49.89	48.88	49.38	49.81
TiO_2	2.01	1.83	2.54	2.54	3.31	1.45	2.12
Al_2O_3	13.62	13.97	13.01	13.18	12.32	14.25	13.88
Fe_2O_3	14.60	13.93	15.82	15.88	18.32	13.72	15.04
MnO	0.22	0.22	0.22	0.22	0.25	0.21	0.22
MgO	5.91	6.27	5.63	5.69	5.00	7.32	5.85
CaO	10.53	10.86	10.03	10.33	9.83	11.68	10.47
Na_2O	2.50	2.28	2.55	2.51	2.31	2.28	2.35
K_2O	0.49	0.51	0.58	0.55	0.53	0.17	0.40
P_2O_5	0.25	0.23	0.29	0.29	0.34	0.13	0.25
H_2O-	0.28	0.30	0.27	0.26	0.28	0.15	0.15
LOI	<0.05	0.13	0.33	<0.13	<0.21	0.14	0.14
TOTAL	101.11	101.17	100.69	101.33	101.37	100.90	100.67
Mo	1.1	<0.6	0.7	1.1	1.3	<0.6	<0.6
Nb	9.9	8.4	9.3	10.0	14.6	2.9	9.0
Zr	148	132	165	167	233	82	136
Y	40	38	41	41	53	30	39
Sr	193	197	227	204	195	138	181
U	<1.8	<1.8	1.9	<1.9	<2.0	<1.8	<1.8
Rb	11.5	12.6	20	17.1	14.6	4.5	11.0
Th	<2.4	<2.4	3.6	3.3	<2.5	<2.3	<2.4
Pb	<2.7	<2.7	<2.8	<2.8	<2.9	<2.7	<2.7
Ba	182	181	169	178	158	33	110
Sc	39	37	34	35	33	36	39
S	630	602	635	580	495	512	201
La	16.7	15.3	13.0	13.6	21	6.8	8.8
Ce	33	33	35	32	46	14.4	26
Nd	23	20	23	23	34	11.9	14.7
Cs	<6.0	8.1	<6.0	<6.0	<6.3	<6.0	<6.0
Co	49	48	51	50	48	54	50
Mn	1632	1526	1571	1556	1752	1516	1643
Cr	101	117	131	131	69	236	69
V	313	311	385	372	396	315	386
Ga	18.7	19.3	22	23	25	19.2	21
Zn	115	105	119	118	149	97	118
Cu	206	195	318	324	397	203	268
Ni	59	67	62	62	53	118	62

Table III X-Ray Fluorescence Whole-Rock Analyses continued

Major Elements (wt%), all Fe as Fe_2O_3; Trace Elements (ppm); < implies below detection limit

	DM90.18	DM90.19	DM90.20	DM90.25	DM90.27	DM90.30
	AGE B	AGE $E_{(chill)}$	AGE E	AGE G'	AGE F	AGE H
SiO_2	51.49	49.90	49.78	49.21	50.95	49.02
TiO_2	1.98	0.95	1.05	3.07	2.61	2.95
Al_2O_3	13.29	16.03	15.40	12.77	12.62	12.48
Fe_2O_3	15.74	11.88	12.66	16.82	16.97	18.83
MnO	0.23	0.19	0.20	0.24	0.24	0.26
MgO	4.67	7.32	7.25	5.42	4.32	5.38
CaO	8.93	12.54	12.08	10.19	8.81	9.94
Na_2O	2.61	2.28	2.08	2.46	2.58	2.24
K_2O	0.81	0.12	0.16	0.49	0.75	0.33
P_2O_5	0.40	0.06	0.06	0.28	0.28	0.28
H_2O-	0.35	0.17	0.21	0.18	0.23	0.14
LOI	0.23	0.05	0.50	<0.12	0.29	<0.39
TOTAL	100.74	101.48	101.44	101.12	100.66	101.86
Mo	1.3	<0.6	<0.6	<0.7	1.3	0.8
Nb	15.1	1.6	1.6	12.7	14.6	8.4
Zr	243	41	41	191	238	172
Y	44	18.3	18.9	45	49	53
Sr	298	149	154	219	213	158
U	<1.8	<1.7	2.0	<1.9	<1.9	<2.0
Rb	18.1	2.1	5.0	12.0	21	9.5
Th	3.9	<2.3	<2.3	<2.5	3.4	<2.5
Pb	3.7	<2.6	<2.6	<2.8	4.5	<2.9
Ba	363	16.8	43	141	226	59
Sc	35	35	36	36	30	39
S	395	328	176	447	543	95
La	30	4.3	<2.7	15.7	21	11.8
Ce	64	<6.1	<6.2	39	50	30
Nd	38	4.0	5.2	28	33	19.9
Cs	<6.0	<5.6	<5.8	<6.3	<6.0	<6.3
Co	48	56	55	50	50	53
Mn	1623	1369	1436	1696	1658	1860
Cr	18.4	250	195	91	41	92
V	325	256	286	410	380	446
Ga	21	17.9	18.6	22	24	24
Zn	110	76	80	128	129	150
Cu	228	111	138	335	299	365
Ni	35	91	88	55	38	61

Appendix 3b ICP-MS Analysis

Rare earth element (REE) and selected trace element compositions were determined for eight Rooi Rand dolerite samples by Inductively Coupled Plasma Mass Spectrometry, using the unit available at the Department of Geology and Applied Geology, University of Natal, Durban. The analytical technique and ICP-MS operating conditions for solution analysis followed are outlined in Jarvis (1989).

Samples were prepared initially in the same manner as those for X-Ray fluorescence analysis, up to the fine powder stage. To obtain the sample in an aqueous form, the standard preparation steps were carried out in the clean laboratory as follows:

Weigh powder and flux (anhydrous lithium metaborate) into a weighing boat in a ratio of 1:3. Place this in a Au/Pt crucible and place in a 1000°C oven for 3 hours. This allows trace minerals such as zircon which are not very soluble, to dissolve. After 3 hours, take sample out and chill it in a glass of water. The sample should come away from the crucible with ease. Transfer the glass sample to a bottle with a stirrer. Add 98ml 2% Nitric Acid, then stir for approximately 4 hours to dissolve the glass in the acid. 98ml assumes a sample volume of 1ml, and 1ml of internal standard is added (this adds up to 100ml) with a concentration of 100ppb of Indium. The stirrer is then removed from the bottle with a magnet. The sample is now ready for use.

Table IV Detection limits for ICP-MS (from Jarvis, 1989).

Element	Detection limit/ ng ml^{-1}	Quantification limit*/ µg g^{-1}	Quantification limit†/ µg g^{-1}
^{139}La	0.075	0.125	0.00125
^{140}Ce	0.1	0.17	0.0017
^{141}Pr	0.09	0.15	0.0015
^{146}Nd	0.2	0.35	0.0035
^{147}Sm	0.2	0.25	0.0025
^{153}Eu	0.06	0.10	0.001
^{157}Gd	0.1	0.15	0.0015
^{159}Tb	0.03	0.05	0.0005
^{163}Dy	0.1	0.20	0.002
^{165}Ho	0.04	0.05	0.0005
^{167}Er	0.06	0.10	0.001
^{169}Tm	0.01	0.02	0.0002
^{172}Yb	0.06	0.10	0.001
^{175}Lu	0.05	0.10	0.001
^{89}Y	0.10	0.20	0.002

* 500× dilution.
† 5× dilution.

Values for those rare earth and trace elements analysed by both XRF and ICP methods compare well. For Rb, Sr and Y, values fall within a few ppm of each other for almost every analysis, the XRF values being almost consistently the higher of the two. The same may be said for the remainder of those elements analysed by both methods, although many concentrations fall below the XRF detection limits, making comparison of data impossible. As stated in Chapter 4, for the sake of consistency, only the REE values from the ICP analysis have been plotted and used. All trace element values used are thus from the XRF analysis.

Table V ICP-MS Analysis (Data)

Concentrations in parts per million

	DM90.30	DM90.25	DM90.8	DM90.27	DM90.20	DM90.10	DM90.18	DM90.5
	AGE H	AGE G'	AGE G"	AGE F	AGE E	AGE D	AGE B	AGE A
Rb	9.05	11.80	13.37	19.36	4.30	9.45	15.91	11.93
Sr	148.62	232.45	186.99	204.42	151.94	171.67	282.57	190.43
Y	48.16	40.28	50.53	46.94	17.72	35.82	42.33	33.59
Cs	0.95	0.30	0.49	0.37	0.24	0.16	0.32	0.13
La	8.93	13.60	16.49	18.44	2.02	9.17	25.95	12.00
Ce	23.17	32.78	39.17	41.54	5.37	22.33	56.46	27.33
Pr	3.67	5.03	5.75	5.98	0.92	3.26	7.61	3.85
Nd	18.75	23.98	27.54	27.51	5.08	16.21	33.32	17.46
Sm	6.54	7.21	8.11	8.24	1.96	5.32	8.94	5.22
Eu	2.08	2.04	2.31	2.24	0.79	1.60	2.52	1.53
Gd	7.35	7.21	8.61	8.21	2.40	5.76	8.41	5.25
Tb	1.47	1.36	1.68	1.53	0.46	1.07	1.44	0.97
Dy	7.79	7.25	8.78	7.59	2.83	5.84	7.73	5.57
Ho	1.39	1.32	1.58	1.38	0.55	1.06	1.38	1.03
Er	4.45	3.97	4.71	4.25	1.69	3.39	4.36	3.43
Tm	0.67	0.59	0.76	0.68	0.26	0.56	0.69	0.54
Yb	4.52	3.79	4.49	4.13	1.69	3.37	4.39	3.34
Lu	0.65	0.53	0.63	0.56	0.22	0.47	0.64	0.47
Pb	6.37	4.96	5.90	6.26	3.76	5.31	5.96	5.12
Th	0.82	1.45	1.76	2.39	0.18	0.89	2.92	1.31
U	0.25	0.35	0.49	0.59	0.14	0.23	0.69	0.35

Table VI Chondritic REE abundances used in REE normalization (Evensen *et al.*, 1978).
(ppm)

La	0.2446
Ce	0.6379
Pr	0.09637
Nd	0.4738
Sm	0.1540
Eu	0.05802
Gd	0.2043
Tb	0.03745
Dy	0.2541
Ho	0.05670
Er	0.1660
Tm	0.02561
Yb	0.1651
Lu	0.02539

Appendix 3c Electron Microprobe analysis across a micro-scale dyke

Whole-rock major element analysis of a micro-scale dyke was done using electron microprobe analytical procedures outlined in Appendix 2, the only exception being that the electron beam was defocussed on the glassy dyke. Instrumental operating conditions, precision and detection limits are outlined in Duncan *et al.* (1984a) and Appendix 2.

	dyke00	dyke03	dyke06	dyke09	dyke12	dyke15	dyke18	dyke21	dyke26	dyke31
SiO2	50.54	52.18	48.70	53.50	51.73	50.36	48.37	49.06	49.65	49.37
TiO2	0.25	0.24	4.14	1.26	1.68	2.30	3.48	2.23	2.54	2.95
Al2O3	5.34	8.58	5.99	13.58	16.98	14.17	12.01	12.41	14.40	12.12
Cr2O3	-	-	-	-	-	-	-	-	-	-
FeO	19.91	15.34	16.80	11.67	9.89	12.52	16.44	14.72	13.15	16.29
MnO	0.27	0.23	0.15	0.18	0.18	0.22	0.28	0.22	0.18	0.28
MgO	9.99	7.76	8.59	5.13	4.23	4.94	5.43	6.68	4.48	5.42
CaO	9.73	10.55	12.63	9.22	10.64	10.05	9.92	10.62	9.67	9.48
Na2O	0.69	2.19	1.05	4.23	3.85	3.72	3.27	2.81	3.79	3.10
K2O	0.09	0.08	0.06	0.06	0.07	0.12	0.19	0.15	0.25	0.08
TOTAL	96.82	97.15	98.11	98.83	99.24	98.41	99.39	98.89	98.10	99.11

	dyke36	dyke41	dyke46	dyke51	dyke56	dyke61	dyke64	dyke67	dyke70	dyke73
SiO2	46.60	50.92	50.43	48.89	48.58	48.13	49.82	48.46	48.04	49.33
TiO2	3.96	1.67	1.44	3.52	2.52	2.52	1.54	3.16	2.87	2.50
Al2O3	9.49	13.17	13.69	13.04	11.86	10.70	14.34	12.58	11.59	11.42
Cr2O3	-	-	-	-	-	-	-	-	-	-
FeO	19.13	14.33	13.89	15.25	17.03	17.23	13.75	16.43	16.25	15.42
MnO	0.31	0.24	0.19	0.27	0.24	0.24	0.18	0.23	0.28	0.23
MgO	7.19	5.49	5.53	5.28	5.84	6.87	4.97	5.18	7.50	6.41
CaO	10.17	9.63	10.31	9.38	9.42	10.94	10.30	9.41	10.32	10.55
Na2O	2.08	3.27	3.18	3.37	2.90	2.35	3.24	3.15	2.46	2.78
K2O	0.15	0.09	0.13	0.10	0.52	0.24	0.33	0.47	0.20	0.10
TOTAL	99.10	98.81	98.80	99.12	98.89	99.21	98.47	99.07	99.51	98.73

	dyke76	dyke79	dyke81
SiO2	49.50	52.13	49.41
TiO2	2.29	5.74	2.28
Al2O3	11.48	14.84	5.70
Cr2O3	-	-	-
FeO	14.80	7.29	18.19
MnO	0.23	-	0.24
MgO	6.44	2.81	9.07
CaO	10.76	10.54	12.34
Na2O	2.77	5.07	0.97
K2O	0.08	0.09	0.05
TOTAL	98.36	98.51	98.25

Dyke Whole-rock Analyses DM90.11 - AGE D (chill margin)

APPENDIX 4

PETROLOGICAL MODELLING RESULTS

Appendix 4a Fractional crystallization major element modelling

G* from E

INPUT DATA

	DAUGHTER AGE G*	OLIV-1	CPX-1	PLAG-1	ILMEN	TIMGT	PARENT AGE E
SiO2	48.88	38.96	51.81	52.16	0.10	0.54	49.78
TiO2	3.31	0.01	0.41	0.01	52.07	6.27	1.05
AL2O3	12.32	0.01	3.24	29.77	0.01	2.44	15.40
FeO	16.46	21.47	7.50	0.49	46.06	81.78	11.39
MnO	0.25	0.31	0.16	0.01	1.82	0.22	0.20
MgO	5.00	39.73	16.26	0.19	0.01	0.15	7.25
CaO	9.83	0.39	20.01	14.11	0.01	0.06	12.08
Na2O	2.31	0.01	0.25	3.40	0.01	0.01	2.08
K2O	0.53	0.01	0.01	0.01	0.01	0.01	0.16

LEAST SQUARES APPROXIMATION

	OBS.	PARENT CALC.	DIFF.	VECTOR	MIX COEFF.	STD-DEV.
SiO2	49.78	49.66	-0.12	DAUGHTE	0.5003	0.0138
TiO2	1.05	1.05	0.00	OLIV-1	0.0561	0.0034
AL2O3	15.40	15.36	-0.04	CPX-1	0.1509	0.0076
FeO	11.39	11.36	-0.03	PLAG-1	0.2912	0.0071
MnO	0.20	0.15	-0.05	ILMEN	-0.0149	0.0021
MgO	7.25	7.24	-0.01	TIMGT	0.0163	0.0025
CaO	12.08	12.07	-0.01			
Na2O	2.08	2.18	0.10	TOTALS	1.0000	0.0180
K2O	0.16	0.27	0.11			
				F=0.5003		

SUM OF SQUARES OF RESIDUALS = 0.04

B from (C)

INPUT DATA

	DAUGHTER AGE B	CPX-2	PLAG-2	OLIV-1	ILMEN	PARENT TIMGT	AGE (C)
SiO2	51.49	50.65	56.28	38.96	0.10	0.54	49.21
TiO2	1.98	0.89	0.01	0.01	52.07	6.27	3.07
AL2O3	13.29	2.15	26.97	0.01	0.01	2.44	12.77
FeO	14.14	13.43	0.87	21.47	46.06	81.78	15.13
MnO	0.23	0.32	0.01	0.31	1.82	0.22	0.24
MgO	4.67	15.12	0.10	39.73	0.01	0.15	5.42
CaO	6.93	17.05	9.98	0.39	0.01	0.06	10.19
Na2O	2.61	0.27	5.27	0.01	0.01	0.01	2.46
K2O	0.81	0.01	0.35	0.01	0.01	0.01	0.49

LEAST SQUARES APPROXIMATION

	OBS.	PARENT CALC.	DIFF.	VECTOR	MIX COEFF.	STD-DEV.
SiO2	49.21	48.96	-0.25	DAUGHTE	0.5919	0.0073
TiO2	3.07	3.05	-0.02	CPX-2	0.1906	0.0034
AL2O3	12.77	12.71	-0.06	PLAG-2	0.1613	0.0040
FeO	15.13	15.05	-0.08	OLIV-1	-0.0068	0.0011
MnO	0.24	0.26	0.02	ILMEN	0.0287	0.0007
MgO	5.42	5.40	-0.02	TIMGT	0.0344	0.0009
CaO	10.19	10.14	-0.05			
Na2O	2.46	2.45	-0.01	TOTALS	1.0000	0.0091
K2O	0.49	0.54	0.05			

SUM OF SQUARES OF RESIDUALS = 0.08

(a) Results obtained from major element mixing in fractional crystallization modelling. F-values given by daughter mix coefficients. Mineral input data from Appendix 2. OLIV-1 =ol3-20, CPX-1=px2-20, CPX-2=px2c05, PLAG-1=fs2-20, PLAG-2=fs1z05, ILMEN=ilm20, TIMGT=mt20.

G' from E

INPUT DATA

	DAUGHTER AGE G'	OLIV-1	CPX-1	PLAG-1	ILMEN	TIMGT	PARENT AGE E
SiO2	49.21	38.96	51.81	52.16	0.10	0.54	49.78
TiO2	3.07	0.01	0.41	0.01	52.07	6.27	1.05
AL2O3	12.77	0.01	3.24	29.77	0.01	2.44	15.40
FeO	15.13	21.47	7.50	0.49	46.06	81.78	11.39
MnO	0.24	0.31	0.16	0.01	1.82	0.22	0.20
MgO	5.42	39.73	16.26	0.19	0.01	0.15	7.25
CaO	10.19	0.39	20.01	14.11	0.01	0.06	12.08
Na2O	2.46	0.01	0.25	3.40	0.01	0.01	2.08
K2O	0.49	0.01	0.01	0.01	0.01	0.01	0.16

LEAST SQUARES APPROXIMATION

	OBS.	PARENT CALC.	DIFF.
SiO2	49.78	49.59	-0.19
TiO2	1.05	1.05	0.00
AL2O3	15.40	15.34	-0.06
FeO	11.39	11.35	-0.04
MnO	0.20	0.15	-0.05
MgO	7.25	7.24	-0.01
CaO	12.08	12.07	-0.01
Na2O	2.08	2.27	0.19
K2O	0.16	0.27	0.11

VECTOR	MIX COEFF.	STD-DEV.
DAUGHTE	0.5353	0.0207
OLIV-1	0.0506	0.0048
CPX-1	0.1399	0.0110
PLAG-1	0.2687	0.0107
ILMEN	-0.0151	0.0029
TIMGT	0.0205	0.0034
TOTALS	1.0000	0.0266

F=0.5353

SUM OF SQUARES OF RESIDUALS = 0.09

F from E

INPUT DATA

	DAUGHTER AGE F	OLIV-1	CPX-1	PLAG-1	ILMEN	TIMGT	PARENT AGE E
SiO2	50.95	38.96	51.81	52.16	0.10	0.54	49.78
TiO2	2.61	0.01	0.41	0.01	52.07	6.27	1.05
AL2O3	12.62	0.01	3.24	29.77	0.01	2.44	15.40
FeO	15.25	21.47	7.50	0.49	46.06	81.78	11.39
MnO	0.24	0.31	0.16	0.01	1.82	0.22	0.20
MgO	4.32	39.73	16.26	0.19	0.01	0.15	7.25
CaO	8.81	0.39	20.01	14.11	0.01	0.06	12.08
Na2O	2.58	0.01	0.25	3.40	0.01	0.01	2.08
K2O	0.75	0.01	0.01	0.01	0.01	0.01	0.16

LEAST SQUARES APPROXIMATION

	OBS.	PARENT CALC.	DIFF.
SiO2	49.78	49.47	-0.31
TiO2	1.05	1.05	0.00
AL2O3	15.40	15.31	-0.09
FeO	11.39	11.32	-0.07
MnO	0.20	0.14	-0.06
MgO	7.25	7.22	-0.03
CaO	12.08	12.03	-0.05
Na2O	2.08	2.17	0.09
K2O	0.16	0.30	0.14

VECTOR	MIX COEFF.	STD-DEV.
DAUGHTE	0.3975	0.0125
OLIV-1	0.0557	0.0039
CPX-1	0.1982	0.0076
PLAG-1	0.3214	0.0072
ILMEN	-0.0054	0.0023
TIMGT	0.0326	0.0025
TOTALS	1.0000	0.0171

F=0.3975

SUM OF SQUARES OF RESIDUALS = 0.14

(a) (contd.) Results obtained from major element mixing in fractional crystallization modelling. F-values given by daughter mix coefficients. Mineral input data from Appendix 2. OLIV-1=ol3-20, CPX-1=px2-20, CPX-2=px2c05, PLAG-1=fs2-20, PLAG-2=fs1z05, ILMEN=ilm20, TIMGT=mt20.

A from E

INPUT DATA

	DAUGHTER AGE A	OLIV-1	CPX-1	PLAG-1	ILMEN	TIMGT	PARENT AGE E
SiO2	50.93	38.96	51.81	52.16	0.10	0.54	49.78
TiO2	1.83	0.01	0.41	0.01	52.07	6.27	1.05
AL2O3	13.97	0.01	3.24	29.77	0.01	2.44	15.40
FeO	12.54	21.47	7.50	0.49	46.06	81.78	11.39
MnO	0.22	0.31	0.16	0.01	1.82	0.22	0.20
MgO	6.27	39.73	16.26	0.19	0.01	0.15	7.25
CaO	10.86	0.39	20.01	14.11	0.01	0.06	12.08
Na2O	2.28	0.01	0.25	3.40	0.01	0.01	2.08
K2O	0.51	0.01	0.01	0.01	0.01	0.01	0.16

LEAST SQUARES APPROXIMATION

	OBS.	PARENT CALC.	DIFF.
SiO2	49.78	49.70	-0.08
TiO2	1.05	1.05	0.00
AL2O3	15.40	15.38	-0.02
FeO	11.39	11.37	-0.02
MnO	0.20	0.16	-0.04
MgO	7.25	7.25	0.00
CaO	12.08	12.08	0.00
Na2O	2.08	2.14	0.06
K2O	0.16	0.31	0.15

VECTOR	MIX COEFF.	STD-DEV.
DAUGHTE	0.5941	0.0165
OLIV-1	0.0368	0.0035
CPX-1	0.1238	0.0082
PLAG-1	0.2219	0.0089
ILMEN	-0.0052	0.0020
TIMGT	0.0285	0.0023
TOTALS	1.0000	0.0210

F=0.5941

SUM OF SQUARES OF RESIDUALS = 0.03

B from E

INPUT DATA

	DAUGHTER AGE B	OLIV-1	CPX-1	PLAG-1	ILMEN	TIMGT	PARENT AGE E
SiO2	51.49	38.96	51.81	52.16	0.10	0.54	49.78
TiO2	1.98	0.01	0.41	0.01	52.07	6.27	1.05
AL2O3	13.29	0.01	3.24	29.77	0.01	2.44	15.40
FeO	14.14	21.47	7.50	0.49	46.06	81.78	11.39
MnO	0.23	0.31	0.16	0.01	1.82	0.22	0.20
MgO	4.67	39.73	16.26	0.19	0.01	0.15	7.25
CaO	8.93	0.39	20.01	14.11	0.01	0.06	12.08
Na2O	2.61	0.01	0.25	3.40	0.01	0.01	2.08
K2O	0.81	0.01	0.01	0.01	0.01	0.01	0.16

LEAST SQUARES APPROXIMATION

	OBS.	PARENT CALC.	DIFF.
SiO2	49.78	49.43	-0.35
TiO2	1.05	1.04	-0.01
AL2O3	15.40	15.30	-0.10
FeO	11.39	11.31	-0.08
MnO	0.20	0.15	-0.05
MgO	7.25	7.21	-0.04
CaO	12.08	12.02	-0.06
Na2O	2.08	2.16	0.08
K2O	0.16	0.34	0.18

VECTOR	MIX COEFF.	STD-DEV.
DAUGHTE	0.4100	0.0146
OLIV-1	0.0496	0.0044
CPX-1	0.2008	0.0085
PLAG-1	0.3060	0.0086
ILMEN	-0.0014	0.0026
TIMGT	0.0350	0.0028
TOTALS	1.0000	0.0198

F=0.4100

SUM OF SQUARES OF RESIDUALS = 0.19

(a) (contd.) Results obtained from major element mixing in fractional crystallization modelling. F-values given by daughter mix coefficients. Mineral input data from Appendix 2. OLIV-1=ol3-20, CPX-1=px2-20, CPX-2=px2c05, PLAG-1=fs2-20, PLAG-2=fs1z05, ILMEN=ilm20, TIMGT=mt20.

D from E

INPUT DATA

	DAUGHTER AGE D	OLIV-1	CPX-1	PLAG-1	ILMEN	TIMGT	PARENT AGE E
SiO2	49.81	38.96	51.81	52.16	0.10	0.54	49.78
TiO2	2.12	0.01	0.41	0.01	52.07	6.27	1.05
AL2O3	13.88	0.01	3.24	29.77	0.01	2.44	15.40
FeO	13.53	21.47	7.50	0.49	46.06	81.78	11.39
MnO	0.22	0.31	0.16	0.01	1.82	0.22	0.20
MgO	5.85	39.73	16.26	0.19	0.01	0.15	7.25
CaO	10.47	0.39	20.01	14.11	0.01	0.06	12.08
Na2O	2.35	0.01	0.25	3.40	0.01	0.01	2.08
K2O	0.40	0.01	0.01	0.01	0.01	0.01	0.16

LEAST SQUARES APPROXIMATION

	OBS.	PARENT CALC.	DIFF.	VECTOR	MIX COEFF.	STD-DEV.
SiO2	49.78	49.51	-0.27	DAUGHT	0.5905	0.0143
TiO2	1.05	1.05	0.00	OLIV-1	0.0386	0.0031
AL2O3	15.40	15.31	-0.09	CPX-1	0.1345	0.0070
FeO	11.39	11.33	-0.06	PLAG-1	0.2227	0.0077
MnO	0.20	0.16	-0.04	ILMEN	-0.0076	0.0018
MgO	7.25	7.22	-0.03	TIMGT	0.0214	0.0021
CaO	12.08	12.03	-0.05			
Na2O	2.08	2.18	0.10	TOTALS	1.0000	0.0182
K2O	0.16	0.24	0.08			
				F=0.5905		

SUM OF SQUARES OF RESIDUALS = 0.10

H from E

INPUT DATA

	DAUGHTER AGE H	OLIV-1	CPX-1	PLAG-1	ILMEN	TIMGT	PARENT AGE E
SiO2	49.02	38.96	51.81	52.16	0.10	0.54	49.78
TiO2	2.95	0.01	0.41	0.01	52.07	6.27	1.05
AL2O3	12.48	0.01	3.24	29.77	0.01	2.44	15.40
FeO	16.94	21.47	7.50	0.49	46.06	81.78	11.39
MnO	0.26	0.31	0.16	0.01	1.82	0.22	0.20
MgO	5.38	39.73	16.26	0.19	0.01	0.15	7.25
CaO	9.94	0.39	20.01	14.11	0.01	0.06	12.08
Na2O	2.24	0.01	0.25	3.40	0.01	0.01	2.08
K2O	0.33	0.01	0.01	0.01	0.01	0.01	0.16

LEAST SQUARES APPROXIMATION

	OBS.	PARENT CALC.	DIFF.	VECTOR	MIX COEFF.	STD-DEV.
SiO2	49.78	49.91	0.13	DAUGHT	0.5219	0.0082
TiO2	1.05	1.05	0.00	OLIV-1	0.0513	0.0020
AL2O3	15.40	15.44	0.04	CPX-1	0.1459	0.0044
FeO	11.39	11.42	0.03	PLAG-1	0.2830	0.0042
MnO	0.20	0.16	-0.04	ILMEN	-0.0117	0.0012
MgO	7.25	7.27	0.02	TIMGT	0.0096	0.0015
CaO	12.08	12.12	0.04			
Na2O	2.08	2.17	0.09	TOTALS	1.0000	0.0106
K2O	0.16	0.18	0.02			
				F=0.5219		

SUM OF SQUARES OF RESIDUALS = 0.03

(a) (contd.) Results obtained from major element mixing in fractional crystallization modelling. F-values given by daughter mix coefficients. Mineral input data from Appendix 2. OLIV-1=ol3-20, CPX-1=px2-20, CPX-2=px2c05, PLAG-1=fs2-20, PLAG-2=fs1z05, ILMEN=ilm20, TIMGT=mt20.

Appendix 4b Mantle and MORB values used in fractional crystallization major element calculations

	(1)	(2)	(3)	(4)
	"Manhot"	"Mancold"	N-MORB	E-MORB
SiO_2	44.57	45.46	50.40	51.18
TiO_2	0.18	0.06	1.36	1.69
Al_2O_3	1.76	1.37	15.19	16.01
Fe_2O_3	8.05	6.77	10.01	9.40
MnO	0.00	0.00	0.18	0.16
MgO	43.56	43.9	8.96	6.90
CaO	1.26	1.35	11.43	11.49
Na_2O	0.07	0.16	2.30	2.74
K_2O	0.08	0.16	0.09	0.43

Sources:
(1) & (2) from Table 9.1 Sweeney (1988)
(3) & (4) from Humphris *et al.* (1985)

(1) "Hot" mantle peroditite xenoliths. Mineral chemistry implies high P, T conditions of formation relative to "cold". Most likely from asthenosphere or base of lithosphere.

(2) "Cold" garnet-bearing peridotite xenoliths. Mineral chemistry implies relatively low P, T conditions of equilibration. Most likely representative of sub-cratonic lithospheric mantle.

Appendix 4c Fractional crystallization trace element modelling

	AGE E OBS.	AGE G" OBS.	CALC.
Rb	5.0	14.6	9.9
Ba	43.0	158.0	84.3
Sr	154.0	195.0	167.5
Y	18.9	53.0	31.4
Zr	41.0	233.0	79.8
Nb	1.6	14.6	3.0
Ni	88.0	53.0	19.6
Cu	138.0	397.0	261.6
Zn	80.0	149.0	121.5
Sc	36.0	33.0	40.0
Cr	195.0	69.0	84.9
Co	55.0	48.0	54.2
V	286.0	396.0	437.7

	AGE (C) OBS.	AGE B OBS.	CALC.
Rb	12.0	18.1	20.18
Ba	141.0	363.0	235.71
Sr	219.0	298.0	265.94
Y	45.0	44.0	64.15
Zr	191.0	243.0	309.62
Nb	12.7	15.1	18.54
Ni	55.0	35.0	34.39
Cu	335.0	228.0	501.87
Zn	128.0	110.0	151.04
Sc	36.0	35.0	24.82
Cr	91.0	18.4	17.04
Co	50.0	48.0	42.04
V	410.0	325.0	302.49

(c) Predicted and observed trace element contents (ppm), obtained using results of the least squares major element approximation. Left hand analysis is the parent, and right hand analysis, the daughter.

	AGE E OBS.	AGE G' OBS.	CALC.
Rb	5.0	12.0	9.3
Ba	43.0	141.0	78.9
Sr	154.0	219.0	167.1
Y	18.9	45.0	29.9
Zr	41.0	191.0	74.7
Nb	1.6	12.7	2.8
Ni	88.0	55.0	21.9
Cu	138.0	335.0	245.1
Zn	80.0	128.0	114.9
Sc	36.0	36.0	39.5
Cr	195.0	91.0	80.1
Co	55.0	50.0	53.5
V	286.0	410.0	406.0

	AGE E OBS.	AGE F OBS.	CALC.
Rb	5.0	21.0	12.5
Ba	43.0	226.0	105.6
Sr	154.0	213.0	180.9
Y	18.9	49.0	36.7
Zr	41.0	238.0	99.0
Nb	1.6	14.6	3.5
Ni	88.0	38.0	12.1
Cu	138.0	299.0	319.0
Zn	80.0	129.0	132.9
Sc	36.0	30.0	38.4
Cr	195.0	41.0	36.5
Co	55.0	50.0	49.7
V	286.0	380.0	446.4

(c) (contd.) Predicted and observed trace element contents (ppm), obtained using results of the least squares major element approximation. Left hand analysis is the parent, and right hand analysis, the daughter.

	AGE E OBS.	AGE A OBS.	CALC.
Rb	5.0	12.6	8.4
Ba	43.0	181.0	71.4
Sr	154.0	197.0	167.0
Y	18.9	38.0	27.6
Zr	41.0	132.0	67.5
Nb	1.6	8.4	2.4
Ni	88.0	67.0	27.3
Cu	138.0	195.0	221.3
Zn	80.0	105.0	105.0
Sc	36.0	37.0	38.2
Cr	195.0	117.0	68.0
Co	55.0	48.0	52.0
V	286.0	311.0	356.4

	AGE E OBS.	AGE B OBS.	CALC.
Rb	5.0	18.1	12.08
Ba	43.0	363.0	102.48
Sr	154.0	298.0	182.41
Y	18.9	44.0	35.72
Zr	41.0	243.0	95.99
Nb	1.6	15.1	3.36
Ni	88.0	35.0	13.66
Cu	138.0	228.0	308
Zn	80.0	110.0	129.12
Sc	36.0	35.0	37.19
Cr	195.0	18.4	32.86
Co	55.0	48.0	48.89
V	286.0	325	425.34

(c) (contd.) Predicted and observed trace element contents (ppm), obtained using results of the least squares major element approximation. Left hand analysis is the parent, and right hand analysis, the daughter.

	AGE E	AGE D	
	OBS.	OBS.	CALC.
Rb	5.0	11.0	8.4
Ba	43.0	110.0	71.8
Sr	154.0	181.0	168.0
Y	18.9	39.0	27.6
Zr	41.0	136.0	67.9
Nb	1.6	9.0	2.5
Ni	88.0	62.0	28.0
Cu	138.0	268.0	222.9
Zn	80.0	118.0	107.3
Sc	36.0	39.0	37.5
Cr	195.0	69.0	77.0
Co	55.0	50.0	52.3
V	286.0	386.0	371.5

	AGE E	AGE H	
	OBS.	OBS.	CALC.
Rb	5.0	9.5	9.5
Ba	43.0	59.0	80.9
Sr	154.0	158.0	164.0
Y	18.9	53.0	30.4
Zr	41.0	172.0	76.6
Nb	1.6	8.4	2.9
Ni	88.0	61.0	24.9
Cu	138.0	365.0	252.3
Zn	80.0	150.0	120.9
Sc	36.0	39.0	39.6
Cr	195.0	92.0	104.0
Co	55.0	53.0	55.8
V	286.0	446.0	442.8

(c) (contd.) Predicted and observed trace element contents (ppm), obtained using results of the least Squares major element approximation. Left hand analysis is the parent, and right hand analysis, the daughter.

Appendix 4d Fractional crystallization rare earth element modelling

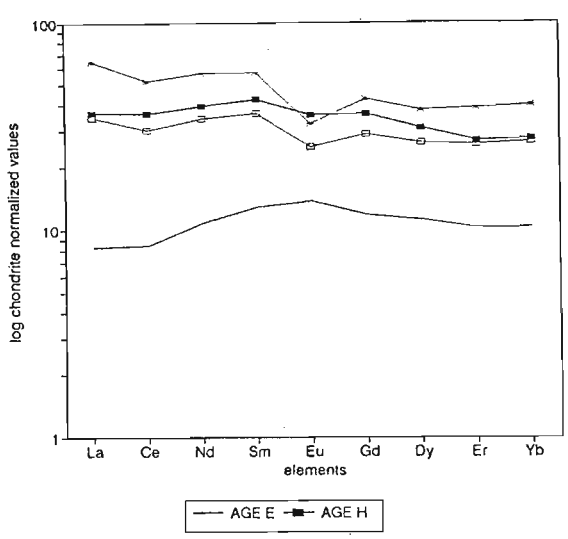

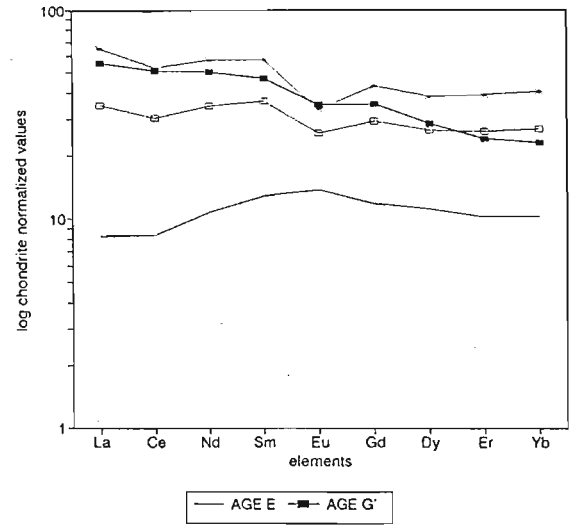

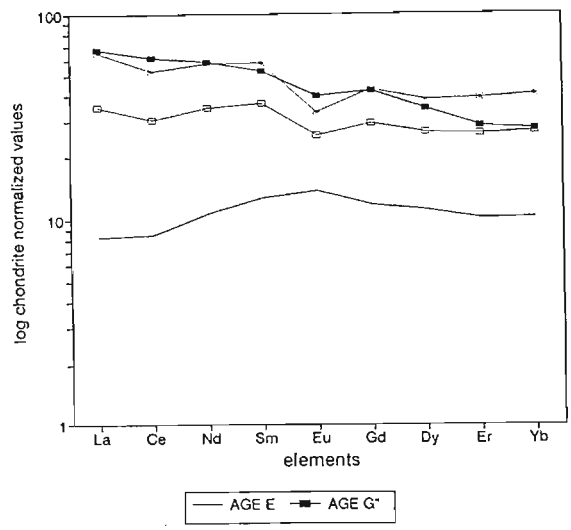

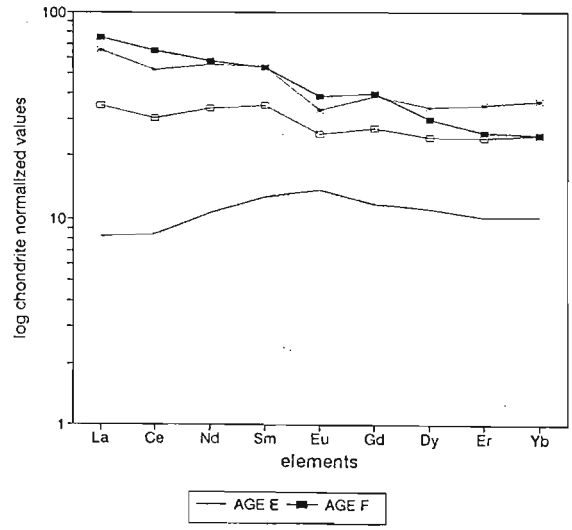

(d) Chondrite normalized REE profiles for fractional crystallization of the Rooi Rand dolerites from an Age E-like source. (solid line=parent; ■=daughter; +,□,*=70,80 and 90% fractional crystallization respectively).

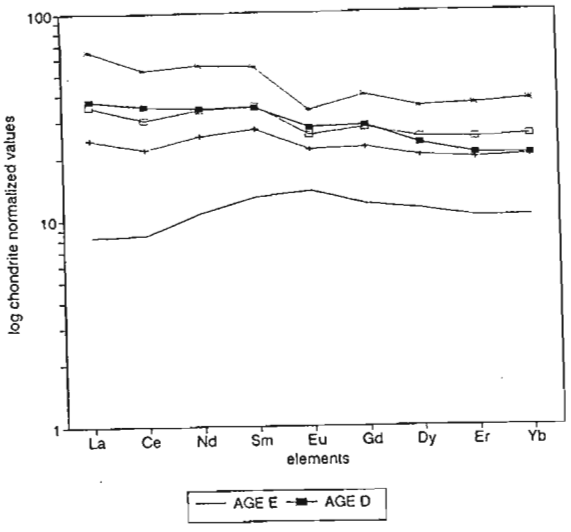

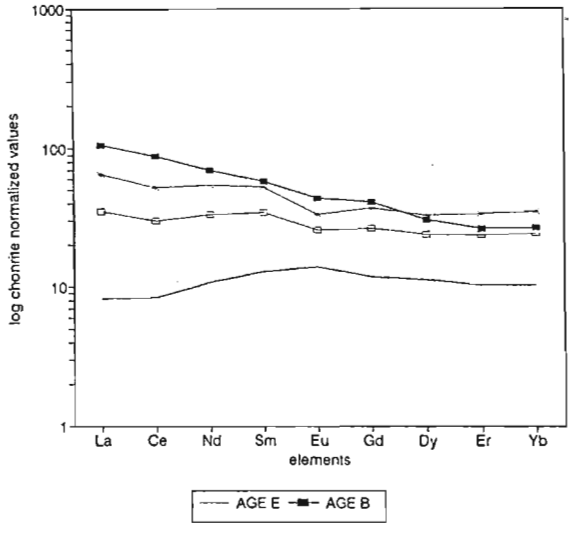

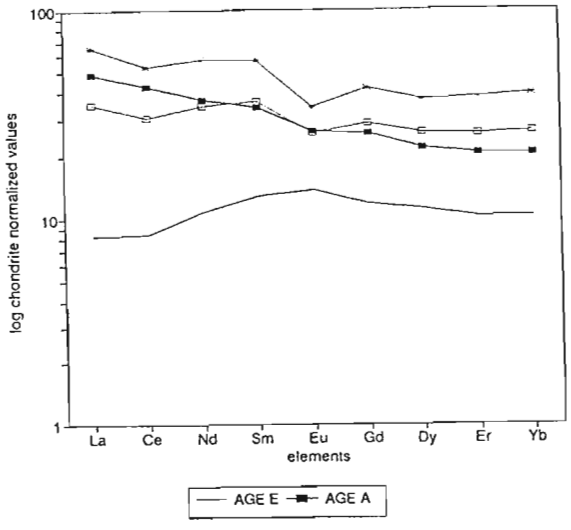

(d) (contd.) Chondrite normalized REE profiles for fractional crystallization of the Rooi Rand dolerites from an Age E-like source. (solid line=parent; ■=daughter; +,□,*=70,80 and 90% fractional crystallization respectively).